University College London

Catalytic Processes in Porous Transition Metal Silicates

By

Carolyn Marie Barker

A thesis submitted for the degree of Doctor of Philosophy

Department of Chemistry

February 2002

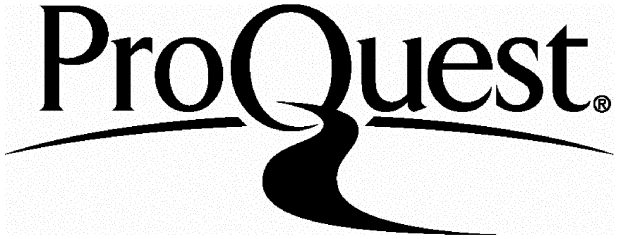

Abstract

Quantum mechanical cluster calculations on the mechanism of alkene epoxidations within peroxide saturated titanium molecular sieve catalysts are reported. This thesis addresses three major themes; the first is the nature of the titanium active sites, in dehydrated and hydrated titanium molecular sieves. Secondly the nature and formation mechanism of the oxygen-donating species for oxidation catalysis is presented. Finally, elucidation of the complete mechanistic catalytic cycle for the titanium molecular sieve mediated oxidation of alkenes to epoxides, in the presence of peroxide, is reported. A focal point of this work is the relationship between reaction energetics and the structure and electronic properties of varied ligands and alkenes.

Highlights include the elucidation of a new, stable oxygen-donating species, $(\equiv SiO)_3Ti\text{-}\eta^1[O(H)OH](OH_2)$, isolated for the first time by this work, which has a low activation barrier of formation (< 20 $kJmol^{-1}$) and shows favourable reaction energetics for the epoxidation of alkenes.

Furthermore, the first experimental evidence for the existence of two particular oxygen-donating structures in the catalyst, $(\equiv SiO)_3Ti\text{-}\eta^2(OOR).H_2O$ and $(\equiv SiO)_3Ti\text{-}\eta^1(OOR)(OH_2).H_2O$, which were predicted to exist by quantum mechanical calculations by this work, is reported. One of the oxidation agents is shown to provide an energetically favourable route to epoxide formation and the other is proposed as the oxygen-donor for diol formation, one of the major by-products in epoxidation catalysis.

Contents

Acknowledgements

Firstly, I would like to thank my supervisors, Prof. Richard Catlow and Dr. Nik Kaltsoyannis for their guidance, dedication and invaluable suggestions to this work. Many thanks to Richard Catlow and Molecular Simulations Inc., San Diego for the opportunity to further my research in America for two summers; a fantastic and unforgettable experience.

I am particular grateful to the Engineering and Physical Sciences Research Council (EPSRC) for funding me throughout my PhD. Much appreciation goes to MSI for allowing me access to β versions of their quantum mechanical code Dmol$^{4.2}$.

Thank you to all those members of the Davy Faraday Research Laboratory who have given me invaluable help and assistance and who have contributed to this work. In particular Dr. Martin Attfield, Dr. Spencer Braithwaite, Dr. Stefan Bromley, Dr. Furio Corá, Mr. Martin Foster, Dr. Sam French, Dr. David Gleeson, Dr. Mark Green, Dr. Gopinathan Sankar, Dr. Phil Sinclair, Dr. Ben Slater, Dr. Alex Simperler, Dr. Alexei Sokol, Dr. John Turner and Mr. Lee Whitmore. I would also like to acknowledge Dr. George Fitzgerald and Dr. Jan Andzelm at MSI, San Diego for their assistance and helpful suggestions during my stay.

I would like to acknowledge the members of the Computational Chemistry group at Pfizer Global Research and Development, especially Dr. Mike Snarey and Dr. Alex Alex, who have been so supportive of me whilst writing this thesis.

Finally, a huge thank you to Ben for his unparalleled support, understanding, assistance and inspiration.

Conventions

All pictorial representations of molecules in this thesis follow the convention shown below, unless otherwise stated.

Titanium

Oxygen

Silicon

Carbon

Hydrogen

Chapter 1

Molecular Sieves and Catalysis

1.1 Molecular Sieves

Molecular sieves, of which zeolites are the most well-known example, are ordered, porous, inorganic solids with void channels running through their frameworks in one, two or three dimensions.

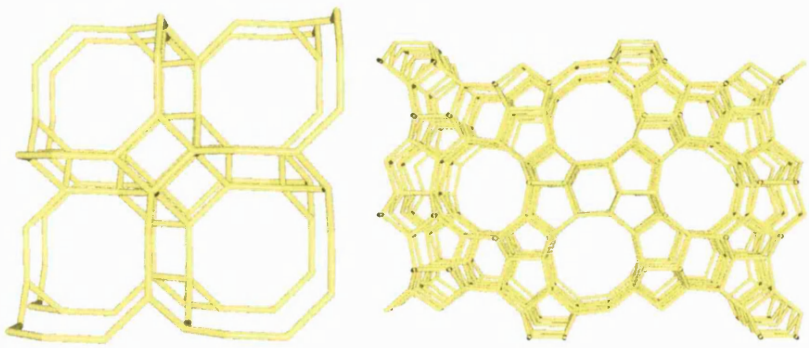

Figure 1.1 Microporous inorganic frameworks, chabasite (left) and silicalite (right).

Discrete organic molecules, which are sufficiently small to fit into the framework space-filled pores, can diffuse through the solid. Larger molecules cannot gain

access to the crystal interior and are therefore absorbed on the exterior of the crystal, thus playing no role in the reactive chemistry of the absorbed species. The selective diffusion of small molecules gives rise to many important industrial applications [1,2,3] and subsequently molecular sieve chemistry is the focus of many research groups around the world.

1.2 Industrial Applications

The commercial uses of molecular sieves are wide-ranging and include:

- Ion exchange.
  - Exchange of radioactive ions with harmless cations.
  - Water softening.
- Gas separation.
  - Production of pure oxygen and nitrogen from air.
  - Separation of para-xylene from a mixed para-xylene/meta-xylene stream.
- Shape-selective heterogeneous catalysis.
  - Hydrocarbon cracking.
  - Hydroquinone synthesis from phenol.
  - Methanol to gasoline conversion.

In addition, zeolites have numerous domestic applications such as in washing powder, cat litter and air purifiers.

Today, more than 100 zeolite and molecular sieve structures are recorded in the Atlas of Zeolite Structure Types issued by the International Zeolite Committee [4]. The number has increased steadily over the last thirty years. The number of patents (US) issued regarding these materials is also growing accordingly. However, despite the industrial relevance and high academic research interest, only a small number of molecular sieves are used in commercial processes or products. It should be noted that many of these molecular sieves are used for more than one application, however. Table 1.1 is taken from the work of

Schoonover and Cohn in their recent appraisal of the industrial applications of molecular sieves [3].

Decade	Known Structure Types	US Patents (composition or use)	Commercial Structure types
1950 – 1969	27	2900	3
1970 – 1979	11	4900	1
1980 – 1989	26	7400	2
1990 – 1999	61	8200	5
Total	125	23400	11

Table 1.1 Zeolite discovery and use by decade

There are many constraints to achieving commercial success and even though molecular sieves are highly researched there are still many questions that need to be addressed regarding structure and in particular reactivity. Computer modelling is now a key tool for gaining insight into these highly useful materials and enabling the acceleration of laboratory chemistry to a commercial scale.

1.3 Structure

Molecular sieves typically have low densities (relative to quartz SiO_2) due to the large space-filled channels running the length of the framework, which are of sufficient size (3Å to in excess of 100Å) to permit diffusion of organic molecules. In some instances when these empty channels meet, large cavities known as supercages form which are ideal for chemical reactions to take place in. Of course reaction can and does take place in the pores themselves but this is more dependent on substrate size constraints.

The frameworks of molecular sieves consist of TO_4 tetrahedra, where T can be silicon, aluminium or phosphorus. For purely siliceous zeolites such as zeolite β, T is silicon. In aluminosilicate zeolites, the tetrahedral T sites are a mixture of silicon and aluminium atoms. An important development in the 1980s

was the advent of aluminophosphates, known as ALPOs [4,5]; here T is a mixture of aluminium and phosphorus.

The tetrahedra combine at corners, linking the T atoms together through oxygen bridges, to yield three dimensional, ordered frameworks. The tetrahedral primary building units can be arranged in an infinite number of ways to generate an infinite number of possible three-dimensional frameworks with channel structures extending throughout the crystal. A number of particular arrangements of linking tetrahedra occur regularly in zeolites which are generally known as secondary building units (SBU) [1,6]. Much work in theoretical chemistry has focused on manipulating these geometrical shapes to form new hypothetical structures [7]. To gain a clearer idea of how SBUs piece together to form very complex frameworks the classic example of the aluminosilicate zeolite Faujasite, also known as zeolite X or Y depending on the Si/Al ratio, is discussed. Zeolite Y is the more siliceous form and is used commercially as a catalyst for hydrocarbon cracking.

The Faujasite structure is built up of sodalite units which are comprised of four- and six- ring SBUs linked together to form a cubo-octahedron, bridged together *via* six-rings. Six-rings consist of six T atoms held together by oxygen bridges, so in fact six-rings contain 12 atoms and four-rings contain eight atoms and so on. Sodalite cages feature in many other zeolites but in Faujasite this arrangement creates three orthogonal 7.4Å diameter channel systems, which intersect in large supercages, of 13Å in diameter, figure 1.2.

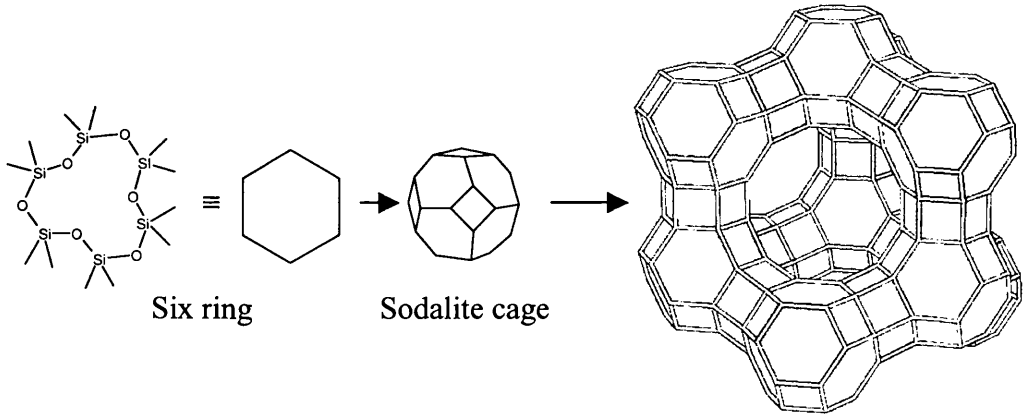

Figure 1.2 Construction of the Faujasite structure from sodalite cages, which are, in turn built from 6-rings and 4-rings. The vertices represent a Si or Al T atom and the lines oxygen bridges.

Molecular sieves in general can be characterised in terms of their pore size, as shown in table 1.2.

Classification	Pore Diameter / Å	Structure Type	Example
Microporous, *Small*	4.1	LTA	Zeolite A
Microporous, *Medium*	5.3 by 5.6 and 5.1 by 5.5	MFI	Silicalite, ZSM-5
	5.3 by 5.4	MEL	TS-2, ZSM-11
Microporous, *Large*	6.5 by 7.0 and 2.6 by 5.7	MOR	Mordenite
	7.6 by 6.4 and 5.5 by 5.5	BEA	Zeolite β
Microporous, *Extra Large*	7.4	FAU	Zeolite X and Y
Mesoporous	30 – 100	-	MCM-41

Table 1.2 Structure types and pore diameters of a selection of molecular sieves

The reader will note the three-letter code in the *structure type* column in table 1.2. This code is assigned by the International Zeolite Committee (IZC) and describes a characteristic and specific topology or arrangement of primary building units. The IZC code is only applied to crystalline frameworks, which by definition have regular repeat units. However, the term molecular sieve has been applied to any ordered, porous structure that can selectively absorb molecules on the basis of size and shape. MCM-41, developed by Mobil does indeed fit this remit, but its pore walls are not crystalline [8,9].

MCM-41 consists of an amorphous silica framework with a regular array of uniform pores running in one dimension. The pores are much larger than any natural or synthetic zeolite, around 30Å to 100Å in diameter, and thus the material is termed mesoporous. It has been postulated that the large diameter of the channels could allow for applications in the highly lucrative production of pharmaceuticals or fine chemicals, where bulkier substrates are generally a requirement. The large inner channels are lined with hydroxyl groups, a feature which has proven to be particular useful for the grafting of redox transition metals, such as titanium onto the surface walls, figure 1.3.

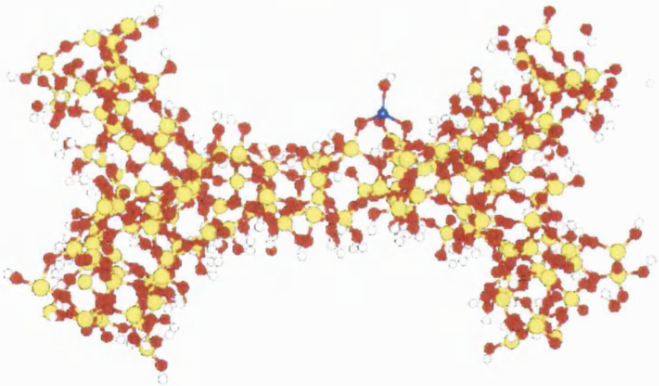

Figure 1.3 Ti grafted onto mesoporous MCM-41.

Probably one of the most notable advancements in molecular sieve chemistry since the field was first created, is the introduction of metals into the frameworks; this will be discussed in the following section.

1.4 Incorporation of metals

The use of zeolites has dramatically increased due to the incorporation of elements other than silicon and aluminium into the frameworks. Pure aluminium and silicon oxides are catalytically virtually inert. Siliceous solids can be functionalised for catalysis applications by incorporation of variable oxidation state metals. The metals can either be incorporated into the silica frameworks or grafted onto the surface silanols of mesoporous silicas, post-synthesis. The position of transition metals incorporated into molecular sieves depends on the particular silica framework and they can either directly substitute for Si in tetrahedral positions or can reside in extra-framework sites.

1.4.1 Framework substitution

Direct framework substitution of metals into molecular sieves is extensive. Ti^{4+} [10-19], V^{4+}, Cr^{3+}, Mn^{2+}, Fe^{3+}, Co^{2+}, Cu^{2+}, Zn^{2+}, As^{5+}, Zr^{4+}, Ge^{4+} [20] and Sn^{4+} have all been incorporated into microporous zeolites [2]. Probably the most reported example of direct framework incorporation of transition metals into zeolites is Titanium Silicalite-1 (TS-1), where a small ratio of Si ions in the zeolite silicalite are directly substituted for Ti.

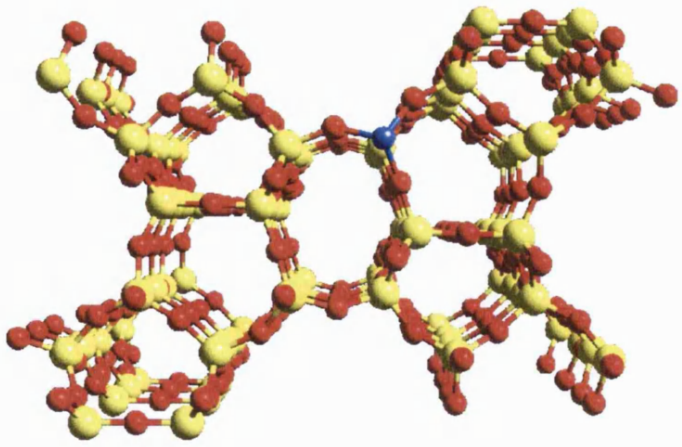

Figure 1.4 TS-1. A small amount of Ti is substituted directly into the silica framework.

The inclusion of Ti into silicalite confers catalytic activity for the oxidation of phenol with 100% selectivity and desired product yields. The pure silica material is by way of contrast, completely catalytically inert.

1.4.2 Extra-framework metal exchange

A feature of many zeolites, and one that gives rise to many unique properties, is the presence of Al in the framework. The different formal valancies of Si (tetravalent) and Al (trivalent) produce an overall negative charge for each Al incorporated into the framework which are typically balanced by extra-framework alkali, alkaline earth or rare earth metal cations. Exchange of these metal ions can readily occur, either with protons resulting in a Brønsted acidic material, or with transition metals such as Ni^{2+} [21-24], Co^{2+} [25] and Cr^{3+}, resulting (in the most part) in active catalysts for a variety of organic transformations. Ni exchanged zeolite Y, figure 1.5, is an active catalyst for the trimerisation of acetylene to benzene [26-28] and is prepared by direct ion exchange of Na or Li zeolite Y by treatment with aqueous $NiNO_3$. However, the resultant material is inert, so far as the trimerisation of acetylene to benzene is concerned and activation requires prolonged exposure to e.g. N_2 gas saturated with acetylene. The acetylene draws the Ni ions out of the space-restricted double six-rings shown in figure 1.5 into the 13Å diameter Faujasite supercages where reaction can take place. Na exchanged zeolite Y is also used in industry for hydrocarbon cracking, where heavy hydrocarbons are broken down into smaller units associated with the gasolines.

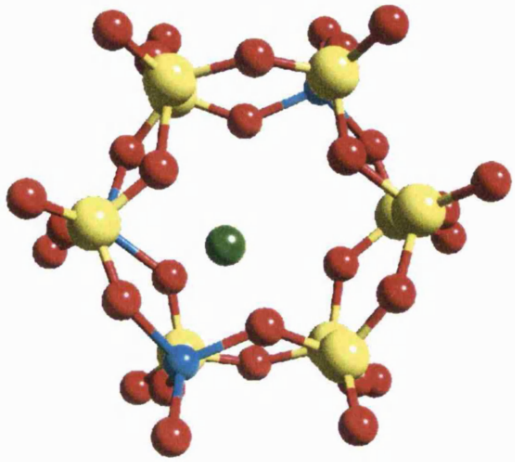

Figure 1.5 Double six-ring of Nickel exchanged zeolite Y. Si is yellow, O is red, Al is turquoise and Ni^{2+} is green.

Focus is now turned to the reactivity of molecular sieves. Molecular sieves play an important role in ion exchange and gas separation but by far the most lucrative industrial application is in heterogeneous catalysis.

1.5 Catalysis

A catalyst lowers the activation energy of a reaction (often by providing an alternative pathway that avoids the slow, rate-determining step of the uncatalysed reaction) and results in a higher reaction rate at the same temperature [29]. A homogeneous catalyst is a catalyst that is in the same phase as the reaction mixture and a heterogeneous catalyst is in a different phase, e.g. a solid-state catalyst for the reaction of gases. Heterogeneous catalysis normally depends on at least one reactant being absorbed (usually chemisorbed) and modified to a form in which it readily undergoes reaction. There are two fundamental considerations in zeolite catalysis: the first is the basic reaction mechanism, and the second is the way in which the reaction is controlled due to the space constraints of the porous framework. There are two general reaction mechanisms that molecular sieves can engage in, acid-base catalysis and redox catalysis.

1.5.1 Acid-Base Catalysis

The inherent catalytic activity of aluminosilicates is attributable to the presence of acidic sites due to aluminium ions on their internal surfaces [30], i.e. the Al^{3+} charge balancing protons can be donated to a base. These acidic protons can be of Lewis or Brønsted acid character and are generally accepted to be firmly bonded to the lone pair of the bridging oxygen species, figure 1.6.

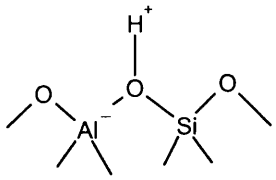

Figure 1.6 Acidic sites in zeolites

The acid strength and number of acid centres can be adjusted in a controlled manner during synthesis and/or by subsequent ion exchange or de-alumination. The acid-base catalysis of zeolites has been the focus of many publications and the reader is directed to references [2,31,32] for further information. Acid-base reactions are not, however, the only type of catalysis that molecular sieves engage in. The presence of transition metals has extended the catalytic potential of molecular sieves to redox catalysis, an area of science that this thesis is concerned with.

1.5.2 Redox Catalysis

The catalytic properties of redox molecular sieves are greatly dependent on the individual nature of the metal site, the structure and the sorption properties of the molecular sieve. In Ti- and V substituted zeolites, which have similar compositions and structural features, their catalytic properties are quite different due to distinct redox sites under analogous conditions. Aside from the dimensions of the pores, the hydrophilic/hydrophobic properties of the pores also have a

major effect on the course of the reaction. To date, redox molecular sieves have been applied to the epoxidation of double bonds, the hydroxylation of aromatic and aliphatic C-H bonds and the oxidation of O, N and S functionalities.

In section 1.3 the grafting of transition metals onto the pore walls of mesoporous MCM-41 was discussed. This synthetic technique allows for the tailored incorporation of ligands with the metal (in framework substituted molecular sieves, calcination of the material, necessary as part of the synthesis removes any metal ligands present). This is of importance as the choice of ligands can accelerate catalysis substantially [33].

As noted earlier, it is not only the chemical composition of molecular sieves that dictates catalytic activity. An equally important factor in directing the course of catalysis is the geometry and topology of the porous framework. This is known as shape-selectivity.

1.6 Shape Selectivity

Shape selectivity makes it possible to orient molecular transformations in a direction other than would be taken if there were no steric constraints [34]. Mobil research workers mentioned the role of shape selectivity in catalysis for the first time at the beginning of the 1960s. Since then, four main categories of shape selectivity have been identified and described in the literature:

1. Reactant shape selectivity.

When only a fraction of the reactants can easily reach the active sites of the solid due to the narrowness of its pore openings.

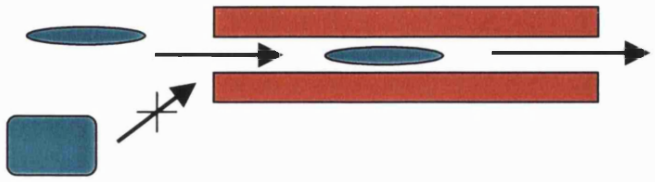

2. Product shape selectivity.

Only products small enough in relation to the pore size can easily diffuse out of the zeolite structure.

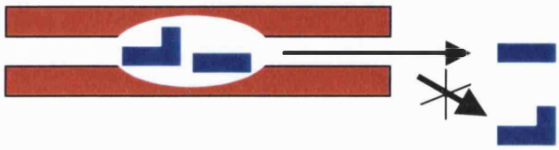

3. Transition state selectivity.

When the space available in the pores of the zeolite strongly inhibits or prevents the formation of the reaction intermediate or transition species that precedes that of a product.

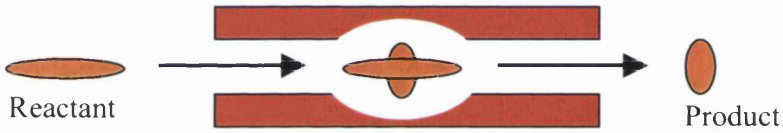

4. Molecular traffic control.

This phenomenon can occur in a zeolite that has at least two different sized channels in its pore system. The reactants may circulate preferentially in one class of pores, while the products tend to diffuse through another.

A number of factors have been outlined that need to be considered when investigating one of the most industrially relevant areas of solid-state chemistry, molecular sieve catalysis. As with most catalytic systems there is a lack of information regarding the mechanisms of reactions, which is the focus of this thesis. Theoretical methods have become a fundamental tool in the search for the reaction mechanisms of many systems, a technique that we have indeed employed to gain insight into the catalytic activity of molecular sieves. However, before I turn to chapter 2, which discusses molecular modelling techniques, a number of experimental methods that have been applied to the study of molecular sieves are outlined.

1.7 Experimental Techniques

X-ray diffraction is the primary tool used by the chemist to investigate the structure of complex inorganic materials. Unfortunately X-rays suffer from the fact that the intensity of scattering is proportional to the atomic number of the scattering atoms. Thus, light nuclei in the presence of heavy nuclei, e.g. H and similar nuclei e.g. Al and Si, cannot be easily distinguished. X-ray diffraction will thus give averaged structures over Al-O-Si and Si-O-Si units and therefore, other techniques that give information on short-range order, such as X-ray absorption spectroscopy (EXAFS and XANES) neutron diffraction and/or nuclear magnetic resonance spectroscopy, NMR, are required.

1.7.1 EXAFS

EXAFS (Extended X-ray Absorption Fine Structure), one such local environment analysis technique, has been applied to the problem of defect/active-site characterisation in molecular sieves. Indeed in Chapter 4, EXAFS analysis of a Ti grafted molecular sieve is able to confirm the structure of oxygen-donating species in Ti molecular sieve redox catalysts, predicted to exist by quantum mechanical calculations [35,36]. A brief description of EXAFS now follows.

When the energy of a beam of X-rays passing through a solid becomes greater than the binding energy of a core electron in a specific atom, the electron is emitted from the core to a continuum state. At this point there is a sharp increase in the observed absorption coefficient known as the absorption edge. As the photon energy increases, the absorption coefficient becomes oscillatory due to interference between the outgoing electron wave and the same wave after it is backscattered from the surrounding atoms. The region of oscillatory behaviour is known as the EXAFS region. The oscillatory behaviour of the measured absorption contains information about the local structure around the excited atom and is dependent upon the type of backscattering atom and its distance from the central atom. Extraction of a physical model for the local structure around the

absorbing centre is then performed by fitting a calculated EXAFS spectrum of a 3D model to the data observed.

1.7.2 Neutron Diffraction

X-ray diffraction and X-ray absorption spectroscopy have been successfully used to give detailed and quantitative information about the heavy atoms in molecular sieve catalysts. However, if one requires information regarding the light atoms in a system, neutron diffraction is an essential technique. Although neutron diffraction is not a method used often in zeolite chemistry, in combination with quantum mechanical studies it has been used to good effect in revealing the geometrical change undergone by acetylene as it binds to a Ni exchanged zeolite Y catalyst [37] (Ni zeolite Y is an efficient catalyst for the trimerisation of acetylene to benzene).

1.7.3 Other Experimental Techniques

Infra-red and Raman vibrational spectroscopies have also been used extensively to probe the local structure of molecular sieves [38] and magic angle spinning (MAS) nuclear magnetic resonance (NMR) has had a major impact on zeolite chemistry. NMR depends on the local environment of the nucleus in question and the coordination of Si in molecular sieves can be efficiently probed using this technique [39]. However, the inherent difficulty of probing molecular sieves by experimental techniques, especially with regard to reaction mechanisms (femto-second pulsed laser spectroscopy is the only techique that can directly examine mechanisms and even then it only yields vibrational information rather than actual geometries), means that computational techniques are a fundamental tool in the search for answers regarding the reactivity of these solids.

1.8 Summary

Almost the whole of the modern chemical industry depends on the development, selection and application of catalysts. The discovery of microporous and mesoporous molecular sieves has revolutionised the field of heterogeneous catalysis. Numerous reactions of potential interest, hitherto not feasible because of low activity, selectivity and/or the service life of the catalyst can now be commercially explored using molecular sieves. The inclusion of metals into crystalline aluminosilicates is of huge industrial and academic interest as the search for new molecular sieves, greater reactivity and insight into reaction mechanisms continues.

Of growing importance is the science of stereoselective zeolite catalysts, which are capable of producing an enantiomeric excess of a given species from a prochiral precursor [40]. Chirality is clearly of enormous relevance in the quest for catalysts for use in the pharmaceutical and fine chemical industry. Focus is already on Ti substituted molecular sieves, as they are known stereoselective catalysts for the epoxidation of alkenes, with retention of the alkene double bond configuration.

In this chapter the industrial importance of molecular sieves, in particular transition metal doped frameworks has been outlined, especially with regard to heterogeneous catalysis. However, the understanding of catalytic mechanisms is still poor and the aim of this thesis is to employ computational techniques to enhance our understanding of one of the most commercially and academically important catalytic systems, titanium substituted molecular sieves. An appraisal of modern computational modelling techniques and its application to molecular sieve science now follows.

1.9 References

(1) Kerr, G. T. *Scientific American* **1989**, *July*, 82.

(2) Arends, I. W. C. E.; Sheldon, R. A.; Wallau, M.; Schuchardt, U. *Angew. Chem. Int. Ed. Engl.* **1997**, *36*, 1144-1163.

(3) Schoonover, M. W.; Cohn, M. J. *Topics in Catalysis* **2000**, *13*, 367-372.

(4) Meier, W. M.; Olson, D. H. *Atlas of Zeolite Structure Types*; 4th ed., 1996.

(5) Wilson, S. T.; Lok, B. M.; Messina, C. A.; Cannon, T. R.; Flanigen, E. M. *J. Am. Chem. Soc.* **1982**, *104*, 1146.

(6) Catlow, C. R. A. In *Modelling of Structure and Reactivity in Zeolites*; Catlow, C. R. A., Ed.; Academic Press: London, 1991.

(7) Price, G. D.; Wood, I. G.; Akporiaye, D. E. In *Modelling of Structure and Reactivity of Zeolites*; Catlow, C. R. A., Ed.; Academic Press Ltd: London, 1991.

(8) Beck, J. *J. Am. Chem. Soc.* **1992**, *114*, 10834.

(9) Kresge, C.; Leonowicz, M.; Roth, W.; Vartuli, J.; Beck, J. *Nature* **1992**, *359*, 710.

(10) Bellussi, G.; Rigutto, M. S. *Stud. Surf. Sci. Catal.* **1994**, *85*, 177-213.

(11) Kumar, R.; Pais, G. C. G.; Pandey, B.; Kumar, P. *J. Chem. Soc., Chem. Commun.*, **1995**, 1315-1316.

(12) Corma, A.; Navarro, M. T.; Pariente, J. P. *J. Chem. Soc., Chem. Commun.*, **1994**, 147-148.

(13) Corma, A.; Navarro, M. T.; Pariente, J. P.; Sanchez, F. *Stud. Surf. Sci. Catal.* **1994**, *84*, 69-75.

(14) Franke, O.; Rathousky, J.; Schulzekloff, G.; Starek, J.; Zukal, A. *Stud. Surf. Sci. Catal.* **1994**, *84*, 77-84.

(15) Maschmeyer, T.; Rey, F.; Sankar, G.; Thomas, J. M. *Nature* **1995**, *378*, 159-162.

(16) Tanev, P. T.; Chibwe, M.; Pinnavaia, T. J. *Nature* **1994**, *368*, 321-323.

(17) Tuel, A.; Taarit, B. *J. Chem. Soc., Chem. Commun.* **1994**, 1667-1668.

(18) Tuel, A. *Zeolites* **1995**, *15*, 236-242.

(19) Zahedi-Niaki, M. H.; Kapoor, M. H.; Kaliaguine, S. *J. Catal.* **1998**, *177*, 231-239.

(20) Zicovich-Wilson, C. M.; Corma, A. *J. Phys. Chem. B* **2000**, *104*, 4134-4140.

(21) Ouden, C. J. J. d.; Jackson, R. A.; Catlow, C. R. A.; Post, M. F. M. *P. Phys. Chem. B.* **1990**, *94*, 5286 - 5290.

(22) Dooryhee, E.; Catlow, C. R. A.; Couves, J. W.; Maddox, P. J.; Thomas, J. M.; Greaves, G. N.; Steel, A. T.; Townsend, R. P. *J. Phys. Chem.* **1991**, *95*, 4514 - 4521.

(23) Thomas, J. M.; Williams, C.; Rayment, T. *J. Chem. Soc., Faraday Trans. I* **1988**, *84*, 2915 - 2931.

(24) George, A. R.; Catlow, C. R. A.; Thomas, J. M. *Catal. Lett.* **1991**, *8*, 193 - 200.

(25) Pierloot, K.; Delabie, A.; Ribbing, C.; Verberckmoes, A. A.; Schoonheydt, R. A. *J. Phys. Chem. B* **1998**, *102*, 10789 - 10798.

(26) Pichat, P.; Vedrine, J. C.; Gallezot, P.; Imelik, B. *J. Catal.* **1974**, *32*, 190.

(27) Maddox, P. J.; Stachviski, J.; Thomas, J. M. *Catal. Lett.* **1988**, *1*, 191.

(28) George, A. R.; Catlow, C. R. A.; Thomas, J. M. *J. Chem. Soc., Faraday Trans.* **1995**, *91*, 3975.

(29) Atkins, P. W. *Physical Chemistry*; Oxford University Press: Oxford, 1992.

(30) Whan, D. A.,, 532.

(31) Karge, H. *Stud. Surf. Sci. Catal.* **1991**, *65*, 133.

(32) Holderich, W.; Hesse, M.; Naumann, F. *Angew. Chem. Int. Ed. Engl.* **1988**, *27*, 226-246.

(33) Berrisford, D. J.; Bolm, C.; Sharpless, K. B. *Angew. Chem. Int. Ed. Engl.* **1995**, *34*, 1059-1070.

(34) Csicsery, S. M. *Chemistry in Britain* **1985**, *May*, 473-477.

(35) Barker, C. M.; D.Gleeson; Sankar, G.; Kaltsoyannis, N.; Catlow, C. R. A.; Thomas, J. M. *Accepted in Phys. Chem. Chem. Phys.* **2001**.

(36) Sankar, G.; Thomas, J. M.; Catlow, C. R. A.; Barker, C. M.; Glesson, D.; Kaltsoyannis, N. *J. Phys. Chem. B* **2001**, *105*, 9028 - 9030.

(37) Turner, J. F. C.; Benmore, C. J.; Barker, C. M.; Kaltsoyannis, N.; Thomas, J. M.; David, W. I. F.; Catlow, C. R. A. *J. Phys. Chem. B* **2000**, *104*, 7570-7573.

(38) Cheetham, A.; Day, P. *Solid State Chemistry: Techniques*; Oxford Science Publications: Oxford, 1987.

(39) Thomas, J. M.; Klinowski, J.; Anderson, M. W. *J. Chem. Soc., Faraday Trans. I* **1986**, *82*, 2851.

(40) Thomas, J. M. *Angew. Chem. Int. Ed. Engl.* **1988**, *27*, 1673-1691.

Chapter 2

Molecular Modelling

2.1 Introduction

One of the fundamental goals of theoretical chemistry is to accurately model and predict macroscopic properties of matter on a microscopic scale. Broadly speaking, this equates to determining the energy of particles, a molecule, atom or ion at a given geometry, temperature, pressure at an instance of time. Two distinct yet complementary methodologies are typically at the disposal of the computational chemist who wishes to elucidate physical or electronic properties of molecules, namely, classical mechanics and quantum mechanics [1,2].

Before describing the theoretical basis of these techniques, it is worth outlining the problems that can now be addressed to microporous and mesoporous inorganic materials. In order to address the accuracy of a given theoretical model, one must reproduce the physical properties of known molecular sieves. Given satisfactory correlation with experiment and provided the model is transferable, one can predict known zeolite structures and propose new, stable molecular sieves that have yet to be synthesised. Indeed notable successes of predictive modelling in recent years are:

- Experimental confirmation [3] of the existence of a new stable phase of zeolite β, type C, initially proposed and supported by theoretical work [4,5].
- Negative thermal expansion in purely siliceous zeolite Y, predicted by Parker *et al.* [6] using free-energy minimisation methods and confirmed by experimental methods [7].
- Prediction of a new chabasite template by *de novo* design [8], which was confirmed through successful synthesis of the said zeolite.

One can use classical mechanical based methods to reproduce structures and vibrational properties of microporous and mesoporous materials, simulate gas separation processes and to chart the pathways of sorbed molecules within molecular sieve pores. However, quantum mechanical techniques are the primary method for modelling reactivity of sorbed molecules (which clearly involves charge transfer and the breakage and/or formation of bonds), usually in catalysis [9]. Catalysis is an area that is notoriously difficult to gain insight into *via* experiment, see section 1.7. Some of the key points relevant to classical and quantum mechanical approaches are now outlined.

2.2 Classical Mechanics

One of the simplest views one can have of a chemical system is of a collection of solid spheres (the atoms) held together by springs (the bonds). This is obviously a gross simplification since molecules are more accurately described as a collection of atomic nuclei surrounded by an electron cloud. For ionic systems the concept of the covalent bond is, of course, redundant, however the idea of atoms being essentially solid spherical entities is still valid. In fact it is possible to represent a partially covalent system such as a zeolite using a purely ionic approach supplemented by appropriate covalent terms [10].

In modelling a chemical system, one seeks the geometrical arrangements of atoms that correspond to stable molecules, and the energy of that particular configuration. In classical mechanics, the electronic motions are ignored and the energy of a system is calculated as a function of the nuclear positions only.

Quantum mechanics, discussed later in this chapter, does include electrons in the description of the system but this is a more computationally demanding method. Classical mechanics is thus often used to perform calculations on systems containing a significant number of atoms and large-length scales. Ignoring electrons does seem a little drastic but when used for appropriate problems the method work exceptionally well, with in some cases answers that are as accurate as even the highest level quantum mechanical calculation, in a fraction of the computer time.

For molecules, the simple interatomic potential model can be extended to the 'molecular mechanics' strategy in which, the total energy, $E_{TOT,}$ of a molecule is constructed from a number of individual component energy terms as shown in equation 2.1.

$$E_{TOT} = E_{str} + E_{bend} + E_{tors} + E_{vdw} + E_{el} \qquad 2.1$$

Each of these terms has a particular functional form that describes a physical process such as bond stretching or bond bending. The validity of this description of the total energy depends on a number of assumptions; the most important being that the individual energy terms are independent of each other and that they are transferable from one molecule to another.

For convenience the energy terms are often subdivided into two classes, bonded and non-bonded. In some simple molecular mechanics calculations, notably conformational analysis, the bonded energy terms are assumed to be constant and only the effect of the non-bonded terms are taken into account. The component terms are described as follows:

Bonded terms

- E_{str} The energy penalty incurred when bonds are distorted from their *ideal* (equilibrium) values.
- E_{bend} The energy penalty incurred when distorting bond angles away from their *ideal* values.
- E_{tor} The change in energy caused by rotating a bond.

Non-bonded terms

- E_{vdw} The van der Waal's energy.
- E_{el} The energy arising from Coulombic interactions.

Equation 2.1 is the form of a simple force field. Some force fields also include additional (cross) terms that take into account the fact that these individual terms are not strictly independent. For instance, as a bond angle decreases the corresponding bond lengths increase slightly.

The above terms constitute an equation that is analytically differentiable, so that standard numerical optimisation techniques can be used to minimise the energy of the system. Each of the terms are calculated as follows:

2.2.1 Bond stretching

$$E_{str} = \sum K_s (d - d_0)^2 \qquad 2.2$$

K_s is the force constant for bond stretching.

d_0 is the equilibrium bond length for a given pair of atoms.

d is the actual bond length.

Σ Signifies that this equation is summed for all bonds in the molecule.

This simple harmonic form is often inadequate, particularly when bonds deviate significantly from the equilibrium distance. A more accurate representation is the Morse potential:

$$E_{str} = \sum D_e \{1 - \exp[-c(d - d_0)]\}^2 \qquad 2.3$$

D_e is the bond dissociation energy.

c is a constant.

The value of this function approaches the value of bond dissociation energy as the bond is stretched.

2.2.2 Angle bending

$$E_{bend} = \sum K_{\Theta}(\Theta - \Theta_0)^2$$

2.4

This form of the equation is again harmonic in nature.

K_{Θ} is the angle deformation constant.

Θ_0 is the equilibrium bond angle

Θ is the actual angle

2.2.3 Torsion angle

This term describes the deviation in energy upon rotation about a given bond, and is essential to differentiate between *cis* and *trans* conformations. For example a torsional term would be used between each carbon atom in a benzene ring in order to insure planarity.

$$E_{tors} = \sum V_n \cos(n\omega)$$

2.5

The form of the equation is that of a Fourier series.

V_n is a constant, which determines the rotational barrier around a given bond.

ω is the torsional angle.

2.2.4 Van der Waals Interactions

The van der Waals interaction is essentially composed of two parts and is shown schematically in figure 2.1.

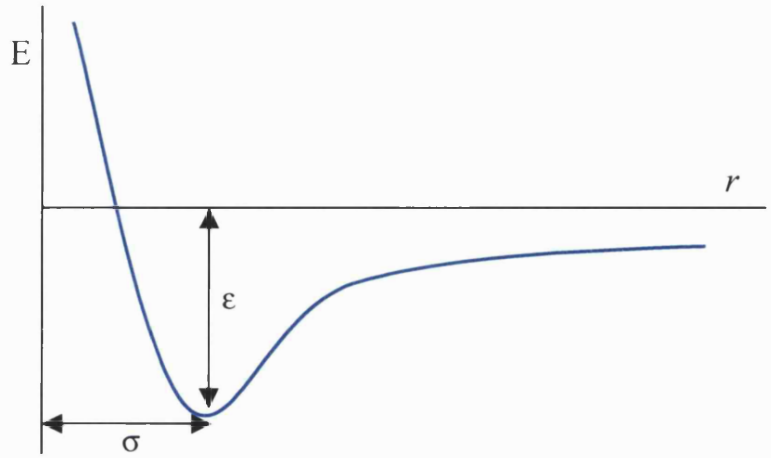

Figure 2.1: Van der Waals energy as a function bond distance, *r*.

The potential energy curve above shows two distinct regions: repulsion at short distances with a longer-ranged attractive part. The short-range repulsion originates from the electron clouds overlapping unfavourably. The longer ranged attractive section arises from the instantaneous static polarisation of neighbouring electron clouds, the London forces.

A number of expressions have been used to account for the van der Waals (VDW) attraction or repulsion between atoms. A common form is the Lennard-Jones potential.

$$E_{vdw} = \sum \frac{B}{r^{12}} - \frac{A}{r^{6}} \qquad 2.6$$

r is the distance between the two atoms.

A and *B* are parameters that depend on the nature of the two atoms.

An alternative, but equivalent equation is:

$$E_{vdw} = \sum E\left[\left(\frac{r_m}{r}\right)^{12} - 2\left(\frac{r_m}{r}\right)^{6}\right] \qquad 2.7$$

r_m is the minimum energy distance.

E is the depth of the well at r_m.

2.2.5 Electrostatics

$$E_{ele} = \sum \frac{Q_1 Q_2}{\varepsilon r} \qquad 2.8$$

Q_1 and Q_2 are the charges on the two atoms.

R is the distance between the atoms.

ε is the dielectric constant of the medium between the two charges.

The dependence of the energy as the inverse of distance between the charges means the E_{el} term converges very slowly as a function of distance, particularly in solids. This term causes more problems than any other in the energy equation.

2.2.6 Other terms

Numerous other terms can also be added to the basic equation. These can deal with solvent effects, cross terms, constraints from NMR experiments etc. The form of the energy equation makes such additions quite easy. The form of the force field outlined above is sufficient for most purposes as it can deal with both geometric and thermodynamic properties. It is usually sufficient for reproducing spectroscopic data as the equations ignore any couplings between the terms. A simple example of coupling is when a bond angle is compressed. As the two extreme atoms move together so there is a corresponding increase in the two bond lengths in order to compensate for the energy increase due to van der Waals repulsion.

2.2.7 Parameterisation

The forcefield consists of a number of simple functions, with relatively few parameters, but determining the optimal values for the parameters is one of the most problematic aspects of this technique. An example of a popular forcefield is

CFF91 embodied in the Cerius^{2} [11] visualisation package, which was derived by carrying out large numbers of quantum mechanical calculations on varied organic and inorganic molecules, and a fitting procedure was used to determine the optimum values.

Typically an atom is 'typed' by recognising the chemical environment of the atom. For example, an oxygen atom double bonded to a carbon atom in a ketone is somewhat different from that of an oxygen atom in the water molecule. This typing procedure obviously seeks to generalise the properties of an atom or molecule, and this is both the strength and the weakness of this approach.

Atomistic modelling techniques have proved extremely valuable in the prediction of crystal structure. For example, lattice energy minimisation calculations demonstrated that the monoclinic phase of the zeolite silicalite was the minimum energy form [12], both orthorhombic and monoclinic symmetries had been observed by experiment. Furthermore molecular mechanics has been used to good effect in determining the optimum positions of cations in zeolites. Among the zeolites that have been studied in this way are Ni Mordenite [13], Ni zeolite Y [14,15], K zeolite X [10] and Sr zeolite A [16]. Molecular mechanics simulations can also assist in determining the location of organic moieties absorbed in zeolite channels [17]. The reader is directed to the articles of Catlow for further information on the application of molecular mechanics in the field of zeolites [18-20].

However, the molecular mechanics approach is weakest when there is any form of charge transfer or when the chemical environment of the atom deviates significantly from that which the forcefield has been parameterised upon. For this reason, it is often imperative, as in the study of catalytic processes within porous materials, to use electronic structure methods based upon quantum mechanics to investigate problems more realistically [21].

2.3 Quantum Mechanics

The powerful equations of classical physics break down when considering systems at the atomic level because electrons display both particle and wave characteristics. To model electronic effects the analogous quantum mechanical expression of Newton's second law, the Schrödinger equation, can be employed. The time-dependent Schrödinger equation is shown below.

$$\mathbf{H}\Psi(\mathbf{r},t) = i\hbar\frac{\partial\Psi(\mathbf{r},t)}{\partial t} \qquad 2.9$$

Here the dual particle-wave nature of an electron is interpreted by a wave function, Ψ which is related to the total energy of the system. It is from the wavefunction that various properties of an electron can be derived. The electron is travelling through space given by a position vector $\mathbf{r}$ and at time t. Planck's constant divided by 2π is denoted by $\hbar$. $\mathbf{H}$ is the Hamiltonian operator, which will be discussed later in this section.

In reality the majority of problems and subsequently the Schrödinger equation can be simplified firstly, by separating Ψ into a spatial function, ψ and a time function, τ

$$\Psi(\mathbf{r},t) = \Psi(\mathbf{r})\tau(t) \qquad 2.10$$

and secondly, by incorporating the resultant equation (2.10) into equation 2.9 to yield the familiar time-independent Schrödinger equation:

$$\mathbf{H}\Psi(\mathbf{r}) = E\,\Psi(\mathbf{r}) \qquad 2.11$$

The Hamiltonian operator $\mathbf{H}$ of an N particle system comprises both kinetic and potential energy terms:

$$\mathbf{H} = \mathbf{H}_{kin} + \mathbf{H}_{pot} \qquad 2.12$$

where the kinetic energy component is defined as:

$$\mathbf{H}_{kin} = -\frac{\hbar^2}{2m}\nabla^2$$

2.13

The potential energy component is a simple coulomb repulsion between pairs of charged entities:

$$\mathbf{H}_{pot} = \frac{1}{4\pi\varepsilon_0}\sum \frac{q_i q_j}{r_{ij}^2}$$

2.14

The time-independent Schrödinger equation, 2.11 is an example of an eigenvalue equation, where a linear operator, i.e. the Hamiltonian operator acts on a function to give the function back again.

The Schrödinger equation is so complex that it can only be solved exactly for the hydrogen atom and thus many approximations have to be employed to extend its use to real and interesting systems. The first and most important is the Born-Oppenheimer approximation.

2.3.1 Born-Oppenheimer approximation

The Schrödinger equation is so complex that it can only be solved exactly for the hydrogen atom. However in 1927, Born and Oppenheimer [22] showed that, to a very good approximation, the motions of the nuclei and the electrons in a system could be considered separately. It states that, as the masses of the nuclei are so much greater than the masses of the electrons, the electrons can adjust almost instantaneously to any changes in the positions of the nuclei. The electronic wavefunction then only depends on the positions of the nuclei and not on their momenta. With this approximation two separate Schrödinger equations can be written. The first describes the electronic motion, where E_{el} is the electronic energy.

$$H_{el}\Psi_{el}(r) = E_{el}\Psi_{el}(r)$$

2.15

The second describes the motion of the nuclei on the potential energy surface. The total energy E_T, therefore, is defined as,

$$E_T = E_{el} + \frac{e^2}{4\pi\varepsilon_0 |R_1 - R_2|} \qquad 2.16$$

where the nuclei are fixed at positions R_1 and R_2 for the purpose of calculating the electronic wavefunction, ε_0 is the vacuum permitivity and e is the charge of an electron.

Solution of the electronic wave-equation at various points on the potential energy surface is required in order to describe phenomena such as electronic transitions, electron and proton transfer processes and bond breakage and formation. Using this approximation it is possible to solve the equation exactly for the simplest of molecular species, H_2^+ and isotopically equivalent species such as HD^+. For the majority of chemical phenomena the Born-Oppenheimer approximation is a useful one, but breaks down for heavy atoms where relativistic interactions must be considered [23].

For polyelectronic systems, an exact solution to the Schrödinger equation cannot be found because the interactions *between* electrons can not be accounted for exactly. An electron can have either α or β spin ("spin up" or "spin down"). These two states are characterised by the spin quantum number m_s, that can take the value +1/2 or -1/2. Spin is incorporated into the solutions of the Schrödinger equation by describing each one-electron wavefunction as the product of a spatial part and a spin part. In accordance with the Pauli exclusion principle each spatial orbital can contain two electrons with paired spins. Since these electrons are indistinguishable they can be exchanged with no change in electron density. Since the electron density is equal to the square of the wavefunction the wavefunction must either not change when there is an exchange in electron density or change sign. For electrons, the sign of the wavefunction must change and this is known as the antisymmetry principle.

2.3.2 Slater determinants

A Slater determinant [24] is an elegant expression for the orbital wavefunction that satisfies the antisymmetry principle. The many-electron wave function, ψ can be defined as:

$$\Psi = \frac{1}{\sqrt{N!}} \begin{vmatrix} \chi_1(x_1) & \chi_2(x_1) & \cdots & \chi_n(x_1) \\ \chi_1(x_2) & \chi_2(x_2) & & \chi_n(x_2) \\ \vdots & \vdots & & \vdots \\ \chi_1(x_N) & \chi_2(x_N) & \cdots & \chi_n(x_N) \end{vmatrix} \qquad 2.17$$

Where N is the number of electrons and $\chi_i(x)$ is the orthonormal one-electron functions containing spin orbital terms where x contains the three spatial coordinates and the spin coordinate. Inspection of equation 2.17 shows that exchanging any two rows of a determinant (a process that corresponds to exchanging two electrons) changes the sign of the determinant and therefore leads directly to the antisymmetry property.

The othonormal one-electron functions $\chi_i(x)$, can be represented by, for example Gaussian type orbitals or Slater type orbitals (section 2.3.4), and the variation theorem is a mechanism for assessing whether one wavefunction is *more correct* than the other. The theorem states that the energy of an approximate wavefunction is always too high. Thus, the lower the energy the better the wavefunction.

2.3.3 Self Consistent Fields (SCF)

SCF formally includes the effect of electron repulsion by assuming that each electron moves in an average field due to the nuclei and the remaining electrons. For example, in a two-electron atom, the potential, V, experienced by a single electron (el_1) would be defined as:

$$V = -\frac{Ze^2}{4\pi\varepsilon_0|R-r_2|} + \frac{e^2}{4\pi\varepsilon_0}\int \frac{\phi_1(r_1)}{|r_1-r_2|}d\tau_1$$

2.18

where, r_1 is the position of the el_1, r_2 is the position of the other electron, el_2, ϕ_1 is the orbital occupied by el_1, R is the position of the nucleus and Ze is the total electron charge. Equation 2.18 can be formally written as a one-electron eigenvalue equation for el_2, where ϕ_2 is the orbital occupied by el_2.

$$\left\{-\frac{\hbar^2}{2m}\nabla_2^2 + V\right\}\phi_2 = E\phi_2$$

2.19

Equation 2.19 shows that an iterative scheme is required to determine both ϕ_1 and ϕ_2 since ϕ_1 must be known in order to calculate ϕ_2. This expression does not take into account spin or antisymmetry, however, an eigenvalue equation which incorporates the variational principle can be defined as:

$$\hat{h}\phi_i = e_i\phi_i$$

2.20

where, e_i are the orbital energies and $\hat{h}$ is known as the Hartree-Fock operator, defined in terms of the electron density. The form of all the orbitals is varied simultaneously in order to attain the lowest possible energy. Each SCF orbital can be written as a linear combination of fixed atomic orbitals $\phi 1$, $\phi 2$, ... ϕn (LCAO).

$$\Psi_{MO} = \sum C_K\phi_K$$

2.21

ϕ_K represents k atomic orbitals, C_K is the LCAO expansion coefficient and Ψ_{MO} is the molecular orbital. These orbitals are known as basis functions and from n basis functions, n LCAO functions are generated. Because the basis functions do not change during the iterative cycles it is usual to calculate all the integrals at the start of an SCF calculation and store them.

Given an appropriate form of the many-electron wavefunction, a method of determining the coefficients in the LCAO expansion is required. This can be achieved using perturbation theory but it is more common to use variational procedures based on the wavefunction, such as Hartree Fock theory (section 2.3.5), or the charge density, i.e., Kohn-Sham density functional theory (section 2.3.7).

2.3.4 Basis sets

Two common forms are used to define a basis set, Slater type orbitals (STOs) and Gaussian type orbitals (GTOs). STOs have the general form:

$$\phi(r) = r^{n-1} e^{-\zeta r} \qquad 2.22$$

where r is an instantaneous electron position, ζ is a parameter determining the radial extent of the orbital and n is the principle quantum number. These orbitals may be combined in a linear fashion, for example to form double ζ functions. However, use of these functions is limited because one has to resort to numerical (as opposed to analytical) integration of these equations in practical applications.

Gaussian type orbitals (GTOs), suggested by Boys [25] have the advantage that they can be solved analytically, thereby being less computationally expensive. They have the form:

$$\phi(\zeta, r) = x^a y^b z^c e^{-\zeta r^2} \qquad 2.23$$

where $a+b+c = l-1$ where l is the angular quantum number. Both equations 2.22 and 2.23 refer to the radial part of the orbital only and have to be multiplied by an angular part (the spherical harmonics).

Like STOs, the primitive Gaussians may be combined in order to form a linear set and increase the degrees of freedom. Gaussian orbitals are widely used in molecular structure calculations, but have serious defects. Long range overlap

is underestimated, charge density at the nucleus is underestimated and spin density at the nucleus is underestimated.

The simplest type of basis set is a minimal basis set where each atom is represented by a single orbital of each type as in descriptive organic chemistry. Thus a carbon atom would need 2 s-orbitals and 1 p-orbital of each type. The basis functions would normally be a linear combination of primitive Gaussian functions, known as a contracted Gaussian. A double ζ basis set comprises exactly double the number of functions than a minimal basis set. A polarization function is an atomic orbital with angular momentum quantum number higher than the maximum necessary to describe the ground state of the neutral atom. Thus, a d-orbital for carbon is a polarization function. They are required to accurately describe the electron density in a molecule, where the symmetry is much lower than in an atom and to describe the response of the electron density to an external field. For an excellent discussion of basis sets the reader is directed to reference [26].

2.3.5 Hartree-Fock theory (HF)

Hartree-Fock theory [27] is concerned with finding a single determinant wavefunction that is the best approximation to the ground state of the system described by the Hamiltonian. The Hamiltonian is defined as:

$$H = \sum \hat{h}_i + \sum_{i>j} \frac{1}{r_{ij}} \qquad 2.24$$

where $\hat{h}_i$ is a one electron *Hartree-Fock* operator for the i^{th} electron moving in a field of nuclear charge (Z_A), r_{ij} denotes the distance between electrons i and j and r_{iA} is the electron-nucleus distance.

$$\hat{h}_i = -\frac{1}{2}\nabla_i^2 + \sum_{A}^{nuclei} \frac{Z_A}{r_{iA}} \qquad 2.25$$

An estimate of the energy of the system described by a normalised antisymmetry wavefunction ψ can therefore be define as,

$$\tilde{E} = \int \tilde{\psi}^* H \psi d\tau$$

2.26

It can be shown that $\tilde{E} \geq E_{exact}$, i.e. the variational principle. Determination of the energy of the system is achieved by finding a set of spin orbitals that minimises the electronic energy, in accordance with the variational principle. Total spin is accounted for by the form of the wavefunction, not by spin dependencies in the Hamiltonian. Varying the molecular orbitals under orthonormality constraints leads to an expression for the variation in the energy of the system, which when set to zero leads to a set of *Hartree Fock* equations, which the *best* molecular orbitals must satisfy.

$$\hat{f}\psi_i = \varepsilon_i \psi_i$$

2.27

The Hartree Fock molecular orbitals are denoted ε_i and the $\hat{f}$ is the Fock operator.

In all but the simplest of cases numerical solution of the Hartree-Fock equations is extremely difficult and approximations for the best description of molecular orbitals are introduced. One widely used approach is to use LCAO, equation 2.21. The problem of finding the best LCAO molecular orbitals is then one of varying the coefficients until the energy reaches a minimum (equation 2.28), with the only constraint being that the atomic orbitals must remain orthonormal. The energy is minimised when the following matrix equation is satisfied:

$$\mathbf{Fc} = \varepsilon \mathbf{Sc}$$

2.28

The *Hamiltonian matrix* **F** has elements $(H)_{ij} = \int \phi_i^* H \phi_j d\tau$, the *overlap matrix* **S** has elements $(S)_{ij} = \int \phi_i^* \phi_j d\tau$, ε is the matrix of orbital energies and **c** is the

matrix of expansion coefficients. These equations were simultaneously proposed by Roothan [28] and Hall [29] and form the basis of modern Hartree-Fock quantum chemistry procedures. Because the wavefunction and energies depend on the matrices **S** and **F**, the Roothan-Hall equations are usually solved iteratively.

2.3.5.1 Open shell systems

Discussion so far has been limited to closed shell systems, i.e. where the ground state of an atom or molecule contains no unpaired electrons. However, there are obviously many systems whose ground state electronic configuration contains unpaired electrons and these cases are typically treated by two main methods. The first is a simple extension to closed shell SCF theory, where some of the orbitals are singly occupied with all spins parallel, known as restricted Hartree Fock (RHF). It is possible to treat certain more general electronic states of atoms and molecules by the RHF technique. The most common method for describing the ground state of a system with unpaired electrons, however, is unrestricted Hartree-Fock theory (UHF). This method permits the spatial distributions of electrons with α and β spins to vary independently. Formally the UHF wavefunction ψ_{UHF} can be written as a sum of different spin states,

$$\Psi_{UHF} = C_{2s+1}\Psi_{2s+1} + C_{2s+3}\Psi_{2S+3} + \ldots \qquad 2.29$$

where $s = \frac{1}{2}(n_\alpha - n_\beta)$ with n_α and n_β being the number of α-spin and β-spin electrons. Thus, if $n_\beta = n_\alpha + 1$, the UHF wavefunction will contain contributions from a doublet, a quartet etc., and the highest contribution will have multiplicity $n_\alpha + n_\beta + 1$. The UHF technique is widely used for investigating open-shell species. However, one of the problems of UHF is that it is not strictly variational an therefore, in principle, calculated energies can be lower than true energies. The UHF has the added disadvantage that the wave function is normally not an eigenfunction of the S^2 operator, where the S^2 operator evaluates the value of the total electron spin squared. This means that a singlet UHF wave function may

also contain contributions from higher-lying triplet, quintet etc. states. Thus, when using UHF, the expectation value of S^2 must be checked.

2.3.6 Electron Correlation

The most significant drawback of Hartree Fock theory is the inadequate representation of electron correlation. In the self-consistent field method the electrons are assumed to be moving in an average potential of the other electrons, and so the instantaneous position of an electron is not influenced by the presence of a neighbouring electron. There are a number of ways the correlation effects can be incorporated into the Hartree Fock approach. Two of the main methods are configuration interaction (CI) and Møller-Plesset Perturbation Theory (MP2).

2.3.6.1. Configuration Interaction

Configuration Interaction includes the excited states in the description of an electronic state. Constructing other determinants by replacing one or more of the occupied spin orbitals with a virtual spin orbital can generate an excited state. The full CI method forms the wavefunction ψ as a linear combination of the Hartree-Fock determinant and all possible substituted determinants. Full CI is the most complete non-relativistic treatment of the molecular system possible, within the limitations imposed by the chosen basis set. However, it is very computationally expensive and impractical for all but the very smallest systems.

2.3.6.2 Møller-Plesset Perturbation Theory

Another approach to electron correlation is Møller-Plesset perturbation theory, which adds higher excitations to the Hartee-Fock theory as a non-iterative correction. This approach is based upon many-body perturbation theory. Perturbation is based upon dividing the Hamiltonian into two parts:

$$H = H_0 + \lambda V$$

2.30

such that H_0 is solvable exactly. λV is a perturbation applied to the H_0, a correction that is assumed to be small in comparison to it (note V is not the Potential Energy). The assumption that V is a small perturbation to H_0 means that the perturbed wavefunction and energy can be expressed as a power series in V

$$E_i = E_i^{(0)} + \lambda E_i^{(1)} + \lambda^2 E_i^{(2)} + \ldots$$

2.31

To obtain an improvement on the Hartree-Fock energy it is necessary to use Møller-Plesset Perturbation theory to at least the second order, hence MP2. The advantage of MP2 is that it is size independent, unlike CI. However, Møller-Plesset is not variational and can sometimes give energies that are lower than the true energy. MP2 calculations are also computationally intensive and so their use is often restricted to single-point calculations of energy minimised geometries.

An alternative quantum mechanical technique available to the chemist that implicitly includes electron correlation is that of Density Functional Theory.

2.3.7 Density functional theory (DFT)

Hohenberg and Kohn [30] proved that the total ground state electronic energy can be described solely by functionals (a function of a function) of the charge density, thus:

$$E[\rho] = T[\rho] + V_{ee}[\rho] + V_{ne}[\rho]$$

2.32

where E is the charge density, T the kinetic energy, V_{ee} is the electron-electron repulsion and V_{ne} the nucleus-electron attraction energy. This is to be compared with the Hartree-Fock many-electron wavefunction;

$$E = \int \Psi^* \mathrm{H} \Psi d\tau$$

2.33

Hence, the DFT expression is determined by the charge density, a function of three coordinates whereas the analogous HF expression is a function of many coordinates. Similarly, it has been shown that to satisfy the variational principle $E_0 \leq E[\tilde{\rho}]$ whereas for HF $E_0 \leq E[\tilde{\Psi}]$.

Kohn and Sham [31] modified this approach to incorporate orbitals into this formalism. This leads to an analogous set of expressions to those produced by Roothan-Hall, which can be duly solved self-consistently. Thus, the ground state properties are computed in a similar fashion to those due to the single determinant HF theory.

Kohn and Sham showed that by considering an artificial state where an electronic system experiences an external potential, and an artificial state with an identical potential but where the electrons are *non-interacting*, one could define a single determinant wavefunction. This wavefunction can be written in terms of non-interacting orbitals that may be conveniently expressed as LCAO's. Thus, the electron density can be expressed as:

$$\rho(r) = \sum \left| \Psi_i(r) \right|^2$$

2.34

which is to be contrasted with HF formalism [32] shown below.

$$\Psi = \left| \Psi_1(1), \Psi_2(2) \ldots \Psi_n(n) \right|$$

2.35

By manipulating the non-interacting kinetic energy operator, they were able to show that:

$$\varepsilon_i \phi_i = \left(-\frac{1}{2} \nabla^2 + v_{ks} \right) \phi_i$$

2.36

where v_{KS} is the Kohn-Sham effective potential.

$$v_{ks} = v(r) + \int \frac{\rho(r')}{|r - r'|} dr' + v_{xc}(r)$$

2.37

v_{XC} is the exchange correlation potential and is derived from $E_{XC}(\rho)$, the exchange-correlation energy, and is therefore a functional.

$$v_{xc} = \frac{\delta E_{xc}[\rho]}{\delta \rho}$$

2.38

The exchange-correlation potential and therefore the energy functional underpin the focus of current density functional research. Essentially, electron-exchange arises from the antisymmetry of the quantum mechanical wavefunction whilst correlation is concerned with the motions of the individual electrons. Remembering that single determinant HF theory means that exchange is dealt with exactly but correlation is explicitly absent, this contrasts markedly with DFT where both exchange and correlation may be included but are inexact. Therefore, the derivation of E_{XC} is critical. An exact E_{XC} implies exact knowledge of the charge density provided we have a *complete* basis set.

Slater formulated a simple expression of v_{XC} based solely on the example of a homogenous electron gas. The resulting equations define v_{XC} in terms of a pure exchange energy E_X, where E_X is a function of $\rho(r)$ at r. Such expressions are termed *local density functionals* and v_{XC} is an example of the *local density approximation* (LDA).

In an analogous extension of RHF to UHF the LDA formalism can be extended to incorporate spin; the resulting expressions are embodied in the LSDA (local spin density approximation). As in the case of UHF theory, LSDA leads to an improved solution to the total energy, but in the case of LSDA, one can also consider spins of different spatial densities.

One of the most important developments in DFT, which is a logical extension of the LSDA methods, is to consider the non-local regions of electron density. Typically, these *generalised gradient approximation* (GGA) methods evaluate E_{XC} from both the electron density and the gradient of the density at a

point r. An example of such a method is the PWY86 (Perdew, Wang, Yue) GGA approximation, which generally results in a 1% error in the exchange energy. Gradient corrected methods have been employed throughout the work presented in this thesis. The paper of Perdew et al. provides a good description of the origins and chemical consequences of the non-local approach [33]. An example of the differences in the local density functional approximation and the non-local density functional theory approach in calculations of metal-ligand distances in organometallic systems is presented in reference [34]. The authors found that gradient corrected functionals generally over-estimated metal-ligand bond-lengths by between 0.02Å and 0.09Å, whilst the LDA approach underestimated bond-lengths by < 0.1Å. On the whole the gradient corrected density functionals were found tosystematically give the closest agreement with known experimental values.

2.4 Advantages and Disadvantages of DFT and HF

DFT gives a quantum chemical description of a system at far less computational expense than more traditional methods such as HF. For example, HF scales formally as N^4 where N is the number of basis functions, and DFT can be efficiently implemented as an N^3 algorithm. Because DFT (generally) implicitly includes electron correlation (albeit approximately) it typically outperforms HF with comparable basis sets with respect to geometries. Very approximately it is often necessary to carry out a HF calculation at the MP2 level (which typically scale as N^6) to get similar reproduction of bond-lengths and angles as DFT. Inclusion of electron correlation in DFT ultimately gives a more correct description of the ground state of a system resulting in more experimentally faithful binding energies and charge densities. DFT is a particularly useful tool in describing transition states as correlation is more important in these systems. In most cases LDA is less accurate at calculating geometries, energies and electronic structure than GGA density functional theory, an example is in solid NiO. However, LDA can provide accurate energies for specific systems with the benefit of much less computational expense. It is well known that DFT consistently

underestimates activation energies, however, the accuracy of HF is system specific with energy barriers overestimated in some cases and underestimated in others.

2.5 Transition States

Molecular modelling is often used to locate the global minimum on an energy surface, as this corresponds to the most thermodynamically stable, lowest energy arrangement of the atoms in the molecular system in question. Any movement away from a minimum gives a configuration with higher energy. When following a reaction pathway, the maximum is also of great importance on the potential energy surface. The arrangement of atoms at the highest point lying on the *lowest energy pathway* between two minima is the transition structure. Transition states are crucial in determining reaction mechanisms, activation energies and reaction rates. Figure 2.2 shows the energy profile for a simple one-dimensional unimolecular reaction for reactant A going to product B, *via* transition state AB.

Figure 2.2 One dimensional reaction coordinate for a simple reaction of substrate A to product B *via* transition state AB.

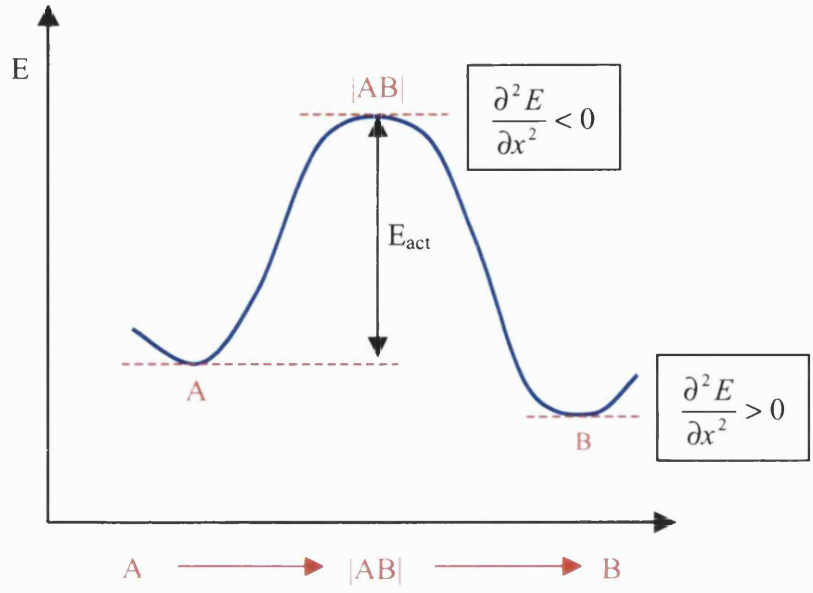

One can see from figure 2.2 that at a maximum and a minimum, the gradient and thus the first derivative of the energy (with respect to the nuclear coordinates) will be zero. Calculation of the first derivatives, or forces as they are often known, therefore affords location of a minimum, i.e. the reactant structure A and the product structure B and the maximum (the transition structure AB) in the example shown above. Figure 2.2 also indicates that the minima and maximum can be distinguished from each other through the 2^{nd} derivatives of the energy (with respect to the nuclear coordinates). For a maximum the 2^{nd} derivative is always < 0 and for a minimum it is > 0. The 2^{nd} derivatives in a quantum mechanical calculation are stored in a matrix called a Hessian.

In reality, for polymolecular systems, the energy profile of a reaction is more complex than the one-dimensional figure shown above, as there are many degrees of freedom and thus the simple ideas aforementioned need to be extended to a multi-dimensional energy hypersurface, figure 2.3.

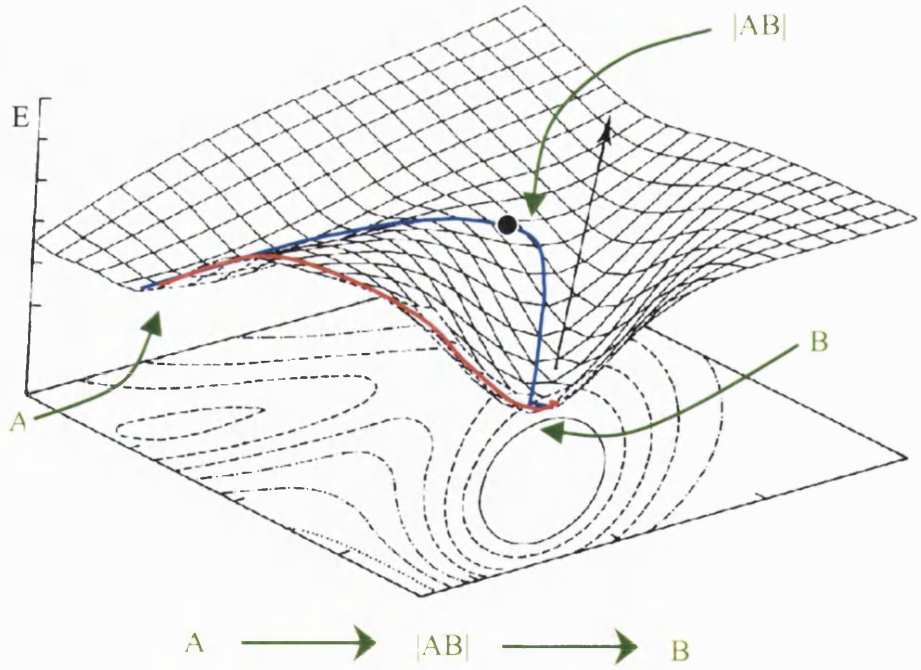

Figure 2.3 Energy surface for the reaction of reactant A to product B *via* transition state AB. The Red line indicates the most direct route between the reactant and the product and the blue line indicates the actual reaction pathway.

Figure 2.3 shows that the reaction pathway is *not* necessarily the most direct route between a reactant and product, shown by the red line. It is, however, *always* the route with the smallest activation barrier. Thus, by definition the transition structure must be a maximum along the direction of the reaction path and a minimum for all displacements perpendicular to the path. In practice one assesses the eigenvalues of a calculation, which are directly related to the vibrational frequencies, in order to characterise minima (reactants and products) and transition states. A minimum is characterised by zero negative eigenvalues and a saddle point is characterised by one negative eigenvalue.

2.5.1 Methods for finding transition states

Minima and maxima are located using either analytical or numerical methods which gradually change the coordinates of the system to produce configurations with lower and lower energies (or the reverse for a maximum) until the minimum is reached. A variety of algorithms are available, however the most common second derivative methods, essential when requiring curvature information, are the Newton-Raphson and the Quasi Newton approaches [35]. These techniques assume that the potential energy surface is close to quadratic and thus for a purely quadratic function the transition state will be found in a single step; in real systems more steps are generally required. Both the Newton-Raphson and the Quasi-Newton methods require the inverse of the Hessian (2nd derivative) matrix. The Quasi-Newton algorithm builds up the inverse Hessian in successive geometry steps, however, the Newton-Raphson method requires the inverse Hessian at every point in the geometry search and is therefore more computationally expensive.

For transition state searches in particular, a fairly accurate estimate of the inverse Hessian is required at each step since the potential energy surface around the transition structure is often much more flat than the surface around a minima. Methods for finding saddle points (especially transition states) are usually more effective when the initial geometry is as close as possible to the transition structure. A number of methods have been developed that seek to aid in obtaining

this initial guess, for example, the linear (LST) and quadratic synchronous transit (QST) techniques which find a guess to the transition state structure that lie between the two supplied structures [36,37].

The LST method essentially draws a line between the reactant and product minima on the potential energy hypersurface and locates the highest point along this line. The QST method refines this starting at the LST maxima and minimising the energy perpendicular to the LST line. Both LST and QST procedures can generate reasonably good initial guesses for a transition state structure providing that the reaction path is not too complex.

Once the transition state has been found, the whole reaction path may be located by tracing the *intrinisc reaction coordinate*, which corresponds to the steepest decent path in mass-weighted coordinates, from the transition state to the reactant and product. At the transition state the vibrational normal coordinate associated with the imaginary frequency (indicated by the single negative eigenvalue) is the reaction coordinate. All reaction pathways with associated transition states discussed in this thesis have been rigourously checked by calculating the intrinsic reaction coordinate. For an excellent discussion of intrinsic reaction coordinates and transition state methods in general the reader is directed to reference [38].

2.6 Discussion

Describing molecules using interatomic potentials, under the influence of classical Newtonian forces is obviously a simplification, as it ignores most electronic effects. However, as long as the parameters on which the method is based are accurate, reliable geometries and relative energies can be routinely obtained. Computer time requirements increase roughly as the square of the number of atoms which when contrasted with molecular orbital methods, where this figure can be from N^3 to N^6 if N is the number of orbitals, is very efficient.

The quantum mechanical approach involves attempts to solve the Schrödinger equation for the molecular system in question. In theory this equation can yield a description of all chemistry but, in practice, solutions to the

Schrödinger equation for most molecules have to be approximate. Quantum mechanics is a theory rather than a model and rests firmly on theoretical foundation. The only thing preventing its use for most molecular systems is that, unlike molecular mechanics, it requires very large computer resources.

The majority of the calculations reported in this thesis were performed on a Silicon Graphics Origin 2000 R12000 based multiprocessor machine, which at the time of writing is considered to be a relatively high performing computer. Some typical timings for calculations described in this thesis are given in table 2.1.

Model	# Heavy atoms	# atoms	# Constrained atoms	DFT Recipe	CPU time for SCF convergence	CPU time for Hessian calculation
$(H_3SiO)Ti(OH)(H_2O_2)$[a,c]	10	22	3	BP86/DZVP[n]	8 mins	-
$(H_3SiO)Ti(OH)(H_2O_2)$[a,d,t]	10	22	3	BP86/DZVP[n]	8 mins	5½ hours
$(H_3SiO)Ti(Otert\text{-}butyl)(H_2O_2)$[a,e]	14	34	3	BP86/DZVP[n]	16 mins	-
$(H_3SiO)Ti(Otert\text{-}butyl)(H_2O_2)$[a,t]	14	34	3	BP86/DZVP[n]	16 mins	11 hours
Benzene on a Ni exchanged 6 ring of faujasite[b,f]	31	49	12	VWN/DNP[l]	4 hours	-
	31	49	12	BLYP/DNP[n]	13½ hours	-

Table 2.1 CPU timings of a number of DFT cluster calculations on zeolite fragments, all otimisations use 'high' energy and gradient convergence criteria and a 'fine' integration grid.. [a]SG R12000. [b]SG Multi processor Origin. [c] Figure 4.13, *Reactant*. [d] Figure 4.13, *TS*. [e] Figure 4.23, right. [f] Figure 2.4. [l] local DFT. [n] Non-local DFT [t] transition state.

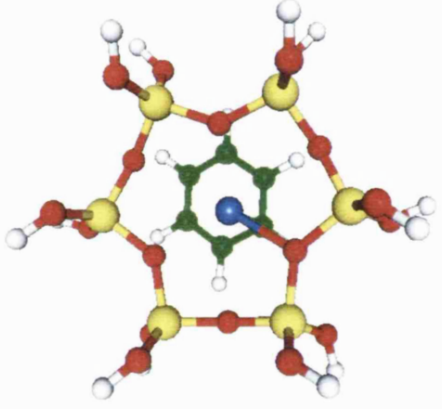

Figure 2.4 Benzene bound to a 6 ring of the Ni exchanged zeolite Faujasite. Nickel is blue.

Clearly, the most computationally intensive individual calculations reported here are the calculation of the Hessian matrix required for transition state searches and non-local geometry optimisation of a large, forty-nine atom cluster. The CPU timings shown in table 2.1 merely serve as an indication of how the size of the model, the type of calculation and the particular DFT recipe are all fundamental factors in the computational expense of a calculation. Furthermore, the data also indicate the length-scale involved in modelling the reaction mechanisms presented in this thesis. Several hundred separate clusters have been modelled in this work, the majority of which require many hundreds of optimisation cycles to achieve the very strict energy and gradient criteria imposed, a strategy that in my experience is necessary for reliable reaction energies.

Important considerations when embarking on a new calculation are; what methodology and accuracy is appropriate and is it possible to use the desired strategy with the available computer resources? For the class of materials discussed in this thesis, a topical question is how important are long-range forces upon the reactivity of the site? One needs to establish whether it is necessary to simulate the 'active site' with a fully periodic unit cell, or with a bare or with an embedded cluster. Recently, periodic DFT geometry optimisation and molecular dynamics calculations have been reported on zeolites with relatively small cells [39], but because of the size of the cell and number of constituent atoms, this approach was and is not feasible with the available resources. Currently, performing a geometry optimisation on even 100 atoms using the periodic DFT approach is far from routine. Even with the emergence of so called *order N* methods, which scale linearly with the number of atoms [40], it will be a number of years before it is possible to carry out geometry optimisations on a mesoporous cell.

At the time this work was started the quantum mechanics/molecular mechanics (QM/MM) or embedded cluster approach [41-46] was evaluated but found to be too computationally demanding. At the present time QM/MM techniques are now becoming more accessible to the average modeller. Quantum mechanics has been applied to numerous problems in zeolite science, a number of which will be discussed in the following chapter, however, the reader is directed to references [19,47] for further information.

The most expensive part of the calculations described are geometry optimisation and transition state searches, where I found it was necessary to use very high precision basis sets to obtain reliable energetics. Therefore, the cluster approach is the only appropriate computational model for the problems described here, but in chapter 4, I also show that the model has the essential chemistry described at a high level of accuracy.

2.7 References

(1) Leach, A. R. *Molecular Modelling Principles and Applications*; Addison Wesley Longman Limited: Edinburgh, 1996.

(2) Jensen, F. *Introduction to Computational Chemistry*; John Wiley & Sons: Chichester, 1999.

(3) Liu, Z.; Ohsuma, T.; Terasaki, O.; Camblor, M. A.; Diaz-Cabanas, M.; Hiraga, K. *J. Am. Chem. Soc.* **2001**, 132.

(4) Tomlinson, S. M.; Jackson, R. A.; Catlow, C. R. A. *J. Chem. Soc., Chem. Commun.* **1990**, 813 - 816.

(5) Treacy, M. M. J.; Vaughan, D. E. W.; Strohmaier, K. G.; Newsam, J. M. *Proc. R. Soc. London, Ser. A* **1996**, *452*, 813 - 840.

(6) Couves, J. W.; Jones, R. H.; Parker, S. C.; Tschaufeser, P.; Catlow, C. R. A. *J. Phys.: Condens. Matter* **1993**, *5*, L329-L332.

(7) Attfield, P.; Sleight, A. W. *Chem. Commun.* **1998**, 601 - 602.

(8) Lewis, D. W.; Willock, D. J.; Catlow, C. R. A.; Thomas, J. M.; Hutchings, G. J. *Nature* **1996**, *382*, 604 - 606.

(9) Catlow, C. R. A.; Barker, C. M.; Bell, R. G.; Bromley, S. T.; Coombes, D. S.; Cora, F.; French, S.; Slater, B.; Sokol, A. A.; Whitmore, L.; Woodley, S. M. *Nato ASI series* **2000**, *560*, 3 - 60.

(10) Sanders, M. J.; Catlow, C. R. A. In *Proceedings of the 6th International Zeolite Conference*; Olson, D., Bisio, A., Eds.; Butterworths, 1984.

(11) Molecular Simulations Inc. In; 4.2 ed.: San Diego.

(12) Bell, R. G.; Jackson, R. A.; Catlow, C. R. A. *J. Chem. Soc., Chem. Commun.* **1990**, 782.

(13) Ouden, C. J. J. d.; Jackson, R. A.; Catlow, C. R. A.; Post, M. F. M. *P. Phys. Chem. B.* **1990**, *94*, 5286 - 5290.

(14) George, A. G.; Sanderson, J. S.; Catlow, C. R. A. *J. Computer-Aided Materials Design* **1993**, *1*, 169 - 176.

(15) George, A. R.; Catlow, C. R. A.; Thomas, J. M. *Catal. Lett.* **1991**, *8*, 193 - 200.

(16) Sanders, M. J.; Catlow, C. R. A.; Smith, J. V. *J. Phys. Chem.* **1984**, *88*, 2796.

(17) Wright, P. A.; Thomas, J. M.; Cheetham, A. K.; Nowak, A. K. *Nature* **1985**, *318*, 611 - 614.

(18) Catlow, C. R. A. In *Modelling of Structure and Reactivity in Zeolites*; Catlow, C. R. A., Ed.; Academic Press: London, 1991.

(19) Catlow, C. R. A.; Bell, R. G.; Gale, J. D. *J. Mater. Chem.* **1994**, *4*, 781 - 792.

(20) Jackson, R. A.; Catlow, C. R. A. *Molecular Simulations* **1988**, *1*, 207 - 224.

(21) Bader, R. F. W. *Chem. Rev.* **1991**, *91*, 893 - 928.

(22) Born, M.; Oppenheimer, R. *Ann. Phys.* **1927**, *84*, 457.

(23) Kaltsoyannis, N. *J. Chem. Soc., Dalton Trans* **1997**, 1 - 11.

(24) Slater, J. C. *Phys. Rev.* **1929**, *34*, 1293.

(25) Boys, S. F. *Rev. Mod. Phys.* **1960**, *32*, 306.

(26) Feller, D.; Davidson, E. R. In *Reviews in Computational Chemistry*; Lipkowitz, K. B., Boyd, D. B., Eds.: New York, 1990; Vol. Chapter 1.

(27) Hartree, D. R. *The Calculation of Atomic Structures*; John Wiley & Sons: New York, 1957.

(28) Roothan, C. C. J. *Rev. Mod. Phys.* **1951**, *23*, 69.

(29) Hall, G. C. *Proc. Roy. Soc.* **1951**, *A205*, 541.

(30) Hohenberg, P.; Kohn, W. *Phys. Rev. B* **1964**, 864.

(31) Kohn, W.; Sham, L. J. *Phys. Rev. A* **1965**, 11377.

(32) Labanoswki, L. J. K.; Andzelm, J. W. *Density Functional Methods in Chemistry*; Springer-Verlag: New York, 1990.

(33) Perdew, J. P.; Ernzerhof, M.; Zupan, A.; Burke, K. *J. Chem. Phys.* **1997**, *108*, 1522.

(34) Bray, M. R.; Deeth, R. J.; Paget, V. J.; Sheen, P. D. *Int. J. Quant. Chem.* **1997**, *61*, 85 - 91.

(35) Dewar, M. J. S.; Healy, E. F.; Stewart, J. J. P. *J. Chem. Soc., Faraday Trans. II* **1984**, *80*, 227.

(36) Jensen, A. *Theoret. Chim. Acta.* **1983**, *63*, 269 - 290.

(37) Halgren, T. A.; Lipscomb, W. N. *Chem. Phys. Lett.* **1977**, *49*, 225 - 231.

(38) Schlegel, H. B. In *Ab Initio Methods in Quantum Chemistry I*; Lawley, K. P., Ed.; John wiley & Sons Ltd., 1987; pp 249 - 285.

(39) Rozanska, X.; vanSanten, R. A.; Hutschka, F.; Hafner, J. *J. Am. Chem. Soc.* **2001**, *123*, 7655 - 7667.

(40) Bowler, D. R.; Gillan, M. J. *Mol. Simul* **2000**, *25*, 239 - 255.

(41) Hill, J. R.; Sauer, J. *J. Phys. Chem.* **1994**, *98*, 1238 - 1244.

(42) Pisani, C.; Birkenheuer, U. *Int. J. Quant. Chem.* **1995**, *29*, 221 - 234.

(43) Svensson, M.; Humbel, S.; Froese, R. D. J.; Matsubara, T.; Sieber, S.; Morokuma, K. *J. Phys. Chem.* **1996**, *100*, 19357 - 19363.

(44) Gao, J. *Acc. Chem. Res* **1996**, *29*, 298 - 305.

(45) Eichler, U.; Kolmer, C. M.; Sauer, J. *J. Comp. Chem.* **1997**, *18*, 463 - 477.

(46) Pisani, C.; Orlando, R.; Cora, F. *J. Chem. Phys.* **1992**, *97*, 4195 - 4204.

(47) Sauer, J.; Ugliengo, P.; Garrone, E.; Saunders, V. R. *Chem. Rev.* **1994**, *94*, 2095 - 2160.

Titanium Molecular Sieves

Chapter 3

Titanium Molecular Sieves Literature Review

3.1 Introduction

Ti supported or embedded in silica is a powerful heterogeneous catalyst for the oxidation of olefins with hydroperoxides. Ever since the late 1960's Shell has utilised non-zeolite titanium/silica mixtures as an industrial catalyst for the epoxidation of propylene with organo hydroperoxides [1], figure 3.1.

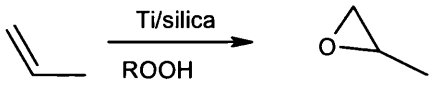

Figure 3.1 Industrial utilisation of non-zeolite Ti-silica catalysts. R signifies an organic moiety such as tertiary butyl.

The Shell catalyst is highly selective of propylene oxide and is completely insoluble in the reaction medium, making it eminently suitable for industrial application. However, the hydrophilicity of silica limits the use of simple and

cheap oxidising agents such as aqueous hydrogen peroxide. Thus, non-porous titanium catalytic oxidations are performed with hazardous and corrosive concentrated H_2O_2 or more expensive organoperoxides, which can give rise to toxic by-products. There has been pressure on chemical industries to clean up their technologies, so the need to find catalysts that are efficient and selective with environmentally friendly water-soluble oxidising agents is high.

Since the 1960's, scientists have realised the catalytic potential of introducing titanium ions into *zeolitic* structures [2]. However, it wasn't until 1983 that Taramasso, Perego and Notari from the Enichem laboratory in Italy synthesised the first Ti zeolite. Hydrothermal treatment of the microporous zeolite silicalite (IZC code MFI) with homoleptic TiR_4 molecules resulted in titanium silicalite-1, also known as TS-1 [3].

3.2 TS-1

Taramasso, *et al.* showed that this new zeolitic-transition metal composite was composed of $(TiO_2)_x(SiO_2)_{1-X}$ ($\leq$0.04M) units, indicating that a low concentration of Ti^{IV} ions had been introduced into the *framework* positions of the microporous siliceous zeolite framework [4].

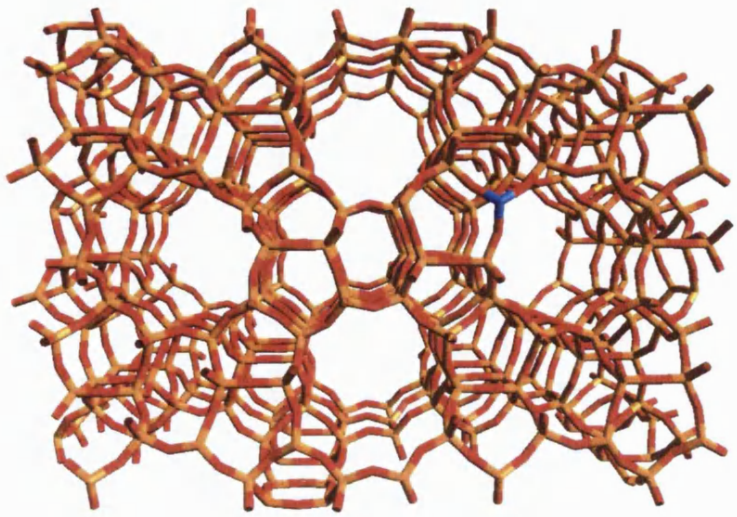

Figure 3.2 TS-1, Si (orange) and Ti (blue) tetrahedra connected via oxygen bridges (red)

As observed for non-porous Ti-silicas, TS-1 was found to be an extremely active redox catalyst with H_2O_2, owing to the high propensity of titanium to change its coordination number under the action of oxygen donating reagents. However, unlike homogeneous Ti-silica systems, such as the Shell catalyst, TS-1 was found to be efficient with *aqueous* H_2O_2, a property that is extremely important in modern industry today.

TS-1 is unique in its class as a transition metal heterogeneous catalyst to be active with aqueous hydrogen peroxide. It exhibits unique catalytic activity and selectivity in the oxidation of a large number of organic substrates, such as alkenes, alcohols, aromatics, phenols and alkanes, using H_2O_2 as oxidant under mild conditions [5-9]. The ability of TS-1 to be active in aqueous media is attributed to the hydrophobic silica framework of silicalite. The hydrophobic micropores (6Å in diameter) of the catalyst are assumed to exclude water from its internal voids and thus protect the active sites from deactivation. In redox reactions with hydrogen peroxide, TS-1 displays the following characteristics [10].

- High efficiency.
- High selectivity (typically ~ 100%).
- High desired product yields.
- Minimal decomposition of the sacrificial oxidant (a common problem associated with hydrogen peroxide, i.e. $H_2O_2 \rightarrow O_2 + H_2$).
- Minimal deactivation of the catalyst through titanium leaching.

Furthermore, only low temperatures of ~300K need to be employed for activity. By far the largest contribution to the literature has concerned the microporous titanosilicate TS-1 as this material has been developed for industrial application and has been available for the longest period.

3.3 Industrial Applications

In 1987, the successful start-up of a new process was announced for the production of 10,000 tons per annum of catechol and hydroquinone by the selective oxidation of phenol with H_2O_2 catalyzed by TS-1 at the Enichem plant in Italy, figure 3.3.

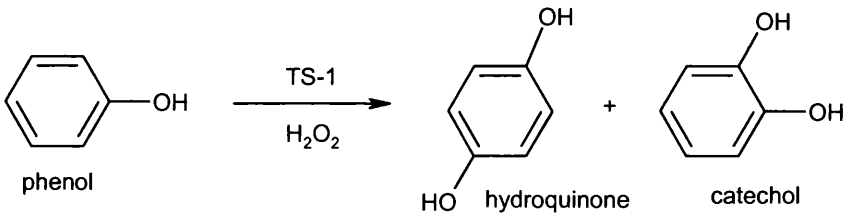

Figure 3.3 Industrial application of TS-1.

The process concerts 100% of phenol to catechol and hydroquinone with 94% selectivity and 84% yield on H_2O_2. A plant was also planned in 1993 for the TS-1 catalysed oxidation of cyclohexanone to cyclohexanone oxime, a reaction that occurs with 98% product selectivity and 93% H_2O_2 selectivity [11].

The ultimate goal of Ti molecular sieve research, however is to employ TS-1 for the commercially lucrative epoxidation of alkenes. So far this potential application has not come to fruition for reasons of which are discussed in the papers of Marcilly [12], Clerici [13]and Notari [14]. Even though there have been numerous experimental studies of TS-1 and other titanium molecular sieves, it is still uncertain how these powerful catalysts operate. Elucidation of the catalytic active species and oxidation mechanism could lead to enhancements for further industrial applications.

3.4 Epoxidation of alkenes

The potential wider industrial application of Ti molecular sieves has lead to a vast body of work in the literature. However, this thesis is dedicated to just one

catalytic process, the epoxidation of alkenes with peroxide. Epoxides are important intermediates in organic synthesis of fine chemicals and pharmaceuticals, both extremely lucrative industries. The direct epoxidation of alkene has been the main process for preparing the epoxides. Epoxidation has traditionally been carried out by peracids and the procedures are costly and produce pollutants. It is highly desirable to replace the conventional process with a more environmentally friendly procedure and one of the most promising possibilities is TS-1.

In chapter 4, quantum mechanical calculations, at the Density Functional level of theory, on the nature of Titanium sites in molecular sieves and the mechanism of oxidation with hydroperoxides are presented. In chapter 5 Density Functional Theory calculations regarding the *mechanism* of ethene and propene epoxidations catalysed by Ti molecular sieves with H_2O_2 as the sacrificial oxidant are presented. These areas of interest are displayed schematically in figure 3.4.

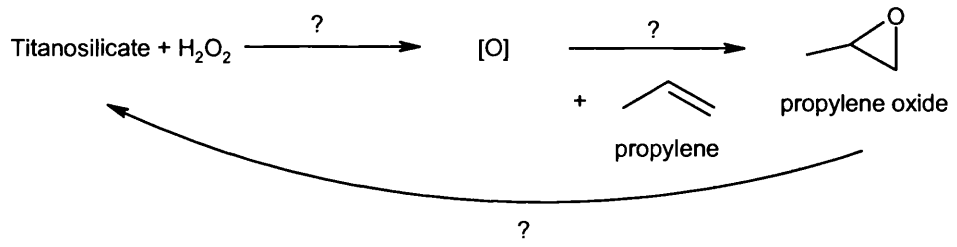

Figure 3.4 Reaction scheme for Titanosilicate lead propylene epoxidation with hydrogen peroxide.

Hence, this chapter will focus on the three most relevant areas of Ti molecular sieve literature.

1. Structure of the titanium active centres (the catalytic activity of titanosilicates must be ascribed to Ti sites because pure crystalline silicas are totally inactive).
2. Structure and chemistry of the *oxygen donating species* formed by the interaction of peroxide with the Ti sites in molecular sieve cavities.

3. Mechanism of Ti molecular sieve mediated alkene epoxidations with peroxide.

For comprehensive reviews on the synthesis of microporous titanosilicates and reactivity other then epoxidation transformations, the reader is referred to the work of Notari [10].

3.5 The Ti molecular sieve family

Following the unique catalytic properties and commercial success of TS-1 many other microporous titanosilicates such as TS-2 [15,16] and Ti-β [17] have been developed. TS-2 is a ZSM-11 type molecular sieve (IZC code MEL) with pore size and activity similar to that of TS-1. Ti-β is of particular interest since the zeolite β framework is hydrophilic and subsequently shows high oxidation reactivity in aprotic solvents such as acetonitrile. Zeolite β is a highly siliceous crystal with little or no aluminium present. The framework consists of three-dimensional pores of diameter 7Å by 7Å, which can be entered into via twelve membered ring apertures. The larger pore size allows this material to be used for the epoxidation of branched and cyclic alkenes [18].

3.5.1 Ti-MCM41

The need for catalysts with even larger pore sizes, for oxidation of very bulky reactants common in the fine chemical and pharmaceutical industries, has lead to the synthesis of *mesoporous* Ti molecular sieves such as Ti-MCM41[19]. Consistent with TS-1 and other microporous titanosilicates, MCM41 has an ordered porous aluminosilicate structure, with 30Å to 100Å diameter channels running in one dimension only. Unlike crystalline microporous zeolites, the internal walls of MCM-41 are amorphous with silanol groups lining the channel surfaces. A diagram of a single pore of MCM-41 is displayed in figure 3.5.

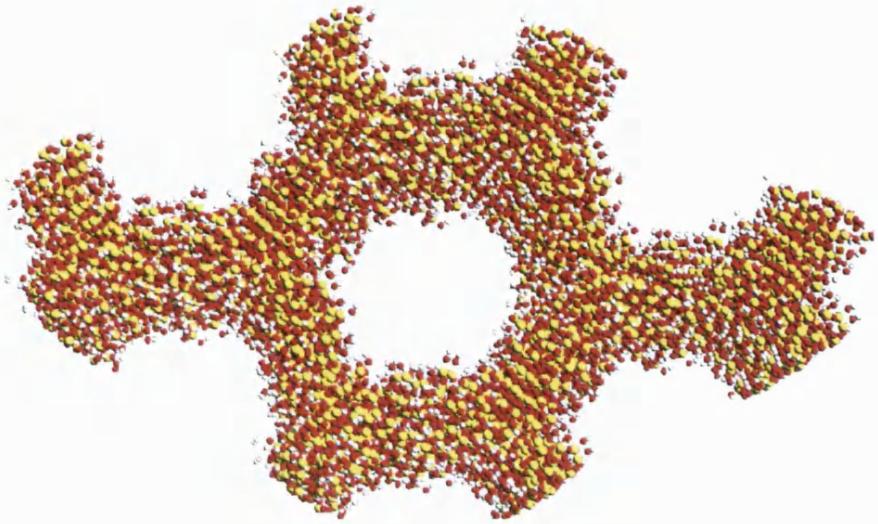

Figure 3.5 A single pore of MCM-41 viewed in cross-section.

The amorphous walls and large pore size allow for the grafting of Ti atoms, via titanocene dichloride ($TiCl_2Cp_2$, where Cp = cyclopentadiene), onto the surface silanol groups, in a site separated fashion [20,21]. This process is shown schematically in figure 3.6 (highlighted in red) alongside the usual titanium molecular sieve synthetic procedure; embedding the metal atoms into the framework by substituting for a number of the silicon atoms. Ti atoms can be substituted into the framework of molecular sieves during initial synthesis of the zeolite (shown in white) or post zeolite synthesis (indicated in blue).

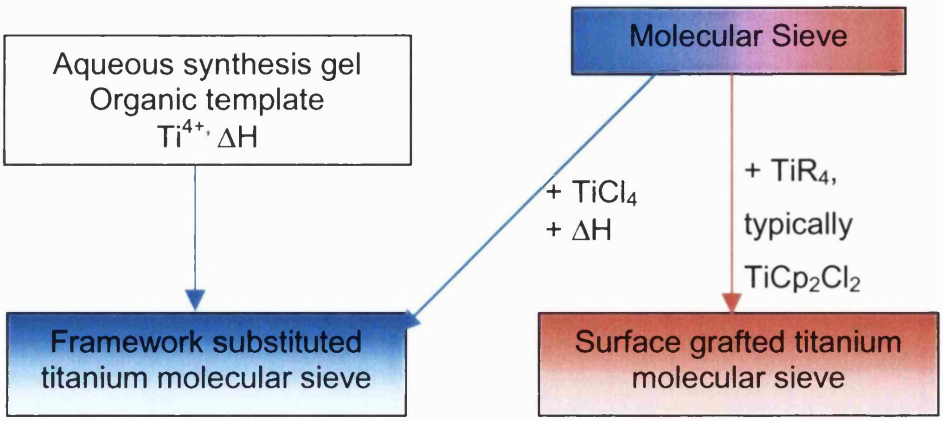

Figure 3.6 Synthesis of Ti molecular sieves.

The ability of chemists to graft titanium ions onto the walls of Ti-MCM41 also allows for the design of specific ligands, which could enhance the catalytic activity. The effect that ligands can have on epoxidation reaction kinetics will be discussed further in section 3.8.4.

3.6 Structure

The high activity and selectivity of TS-1 and other titanium molecular sieves are attributed to the presence of Ti in monoatomic *framework* sites in the silicate lattice. Evidence for the substitution of Ti directly into the framework T sites is extensive.

- An increase in the unit cell parameters upon heating with homoleptic $TiOR_4$ compounds which is in accordance with the isomorphous substitution of Si with Ti (Si bonds ~1.6Å, Ti-O bonds ~1.8Å) [4,10,14,22,23]
- The diffuse reflectance UV-vis spectra of TS-1 shows a strong transition at 48,000 – 50,000cm^{-1} that is absent from silicalite and must therefore correspond to a charge transfer process localised on Ti^{IV} [14,24,25].
- The *absence* of an UV-vis band at 30,000cm^{-1} which is characteristic of non-framework anatase (TiO_2) [24,25].
- Appearance of an infrared band at 960cm^{-1} attributed one of the vibrational modes of a Ti centre surrounded by four [SiO_4] tetrahedra, such as in TiO_2-SiO_2 glasses [26].

It should be noted that the last point is, however, a tentative assignment and the 960cm^{-1} IR fingerprint of Ti molecular sieves has also been attributed to Ti=O stretching vibrations. This is covered in detail in section 3.3.1.

Titanium ions in purely ionic Ti oxides such as anatase and rutile are in octahedral coordination with an average Ti-O bond length of ~1.94Å, table 3.1. The Ti-O bond length is found to decrease with an increase in the amount of silica. The decrease in Ti-O bond length from ~1.9Å – ~1.8Å is consistent with a change in octahedral geometry to tetrahedral.

Table 3:1. Experimentally derived structural parameters for Ti-(silicate) oxides.

	Species	Method	Ti-O
Octahedral	TiO_2 [27]	XAS	1.94
	$Ti(Opropyl)_4$ on silica [28]		1.88
	TiO_2/SiO_2 (Ti:Si, 6:1) [27]	XAS	1.91
	TiO_2/SiO_2 (Ti:Si, 1:1) [27]	XAS	1.88
Tetrahedral	TiO_2/SiO_2 (Ti:Si, 1:8)[27]	XAS	1.82
	TS-1 [29]	XANES	1.79
	TS-1	XRD	1.79
	TS-1	EXAFS	1.80-1.81

The 1.8Å Ti-O bond length in TS-1 and other titanium molecular sieves is yet further evidence for the *direct* substitution of titanium for silicon since the tetrahedral coordination is preserved, table 3.1. The tetrahedral nature of titanium sites was originally met with much scepticism, since Ti generally prefers to be in octahedral coordination, however the four-fold structure of the discrete metal sites in the dry-state is now almost universally accepted.

In addition, UV-vis spectroscopy has also indicated that the Ti atoms are highly dispersed, more so than in any other type of material [14,24,25,30]. The catalytic efficiency is found to be severely impaired when more that a few percent of titanium atoms are incorporated into the frameworks. The excess Ti atoms adopt extra framework positions by direct exchange of the aluminium charge balancing cations. The extra-framework titanium is thought to form TiO_2 units, which poison the framework catalytically active framework Ti sites.

Most of the derivation of the tetrahedral nature of titanium sites has been through experiment, where X-ray absorption spectroscopy has probably been the most extensively applied technique [14,20,21,30-33].

Classical potential models and quantum mechanics cluster calculations of monoclinic TS-1 showed that, substitution at just three of the 12 non-equivalent crystallographic sites in silicalite were favourable [34]. The study progressed by suggesting that the substitution of titanium in the silicalite lattice is preferred over the formation of species with tetrahedral coordinated titanium atoms in edge sharing or bridging positions, figure 3.7. Calculations carried out at the Ab initio level of theory have since confirmed these findings [33].

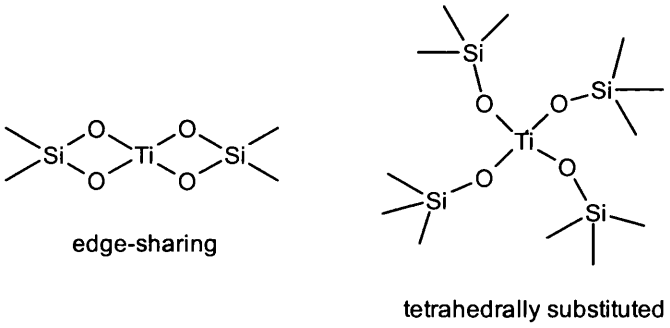

Figure 3.7 Suggested representation of edge sharing and framework substituted Ti sites in TS-1

3.6.1. Hydration

EXAFS and other spectroscopic techniques have characterised the structure of dehydrated titanium sites in substituted molecular sieves, however less is known about the partially hydrated form, which resembles more the synthesis and the operating environment of the catalyst.

Upon addition of H_2O the 48,000 – 50,000cm^{-1} UV-vis band, a fingerprint for Ti^{IV}, progressively shifts to 42,000cm^{-1}; the effect is reversible. The lower wavenumber indicates an increase in the coordination of the metal. The ability of Ti^{4+} to change its coordination number between 4 and 6 is well known, but how this happens in the molecular sieve framework is not certain. It has been assumed that the coordination expansion takes place with hydrolysis of the Ti-O-Si bridges. *Tripodal*, *bipodal* and *monopodal* structures have all been suggested as representative of the active sites in titanium molecular sieves, arising from the progressive hydrolysis of a tetrapodal Ti site, shown in figure 3.8. The term

tripodal indicates three Ti-O-Si bridges anchoring the metal to the silica framework, bipodal signifies that there are two anchoring Ti-O-Si bridges and monopodal intuitively denotes a structure with a single anchoring Ti-O-Si bridge. Due to the steric restrictions imposed on the local structure of the metal centres by the fairly rigid molecular sieve framework, hydrogen bonds between the cleaved and hydrolysed Ti-O-Si bridges are thought probable. This is indicated in figure 3.8 on the tripodal model.

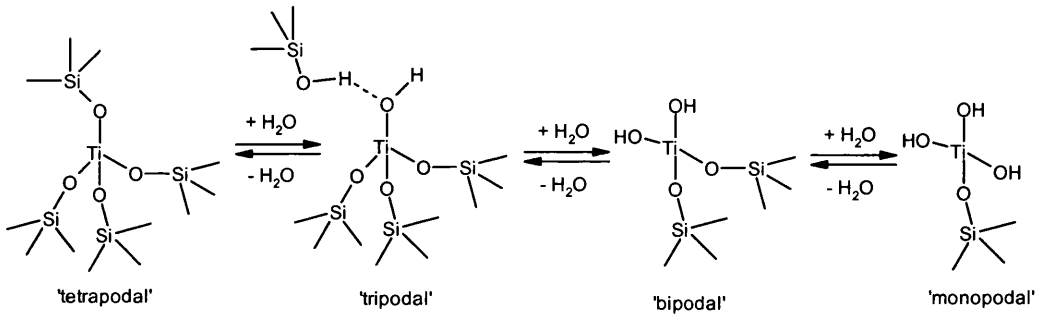

Figure 3.8: Suggested models of the metal sites in Ti molecular sieves.

Experimental evidence for the formation of TiOH species in TS-1 has been obtained from IR and ^{17}O NMR studies of TS-1 treated with labelled water [26]. Density Functional Theory calculations have suggested that after calcination, the dominant surface titanium species of grafted Ti-MCM41 is the tripodal $(\equiv SiO)_3TiOH$ complex and that an appreciable concentration of $(=SiO)_2Ti(OH)_2$ complexes (figure 3.8) would also be present [35].

An alternative view is that titanyl (Ti=O) groups are representative of the active sites in titanosilicates [36], figure 3.9.

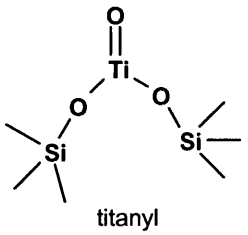

Figure 3.9: Suggested representation of Ti sites in molecular sieves

The 960cm^{-1} IR band observed for titanosilicates has also been explained by titanyl groups which show a stretching band in the same region as Ti=O vibrations (by reference to fresonite [37] and JDFL-1 [38]). However, lack of UV-vis confirmation has lead many commentators to dismiss this notion [24]. Density Functional Theory calculations of $(H_3SiO)_3Ti{=}O$ small molecule clusters have suggested that titanyl groups can form by relatively low energy pathways [36], with an activation barrier of < 70 kJmol^{-1}. Note that these energies have been corrected in the manner described in reference [39] and are scaled by 130%.

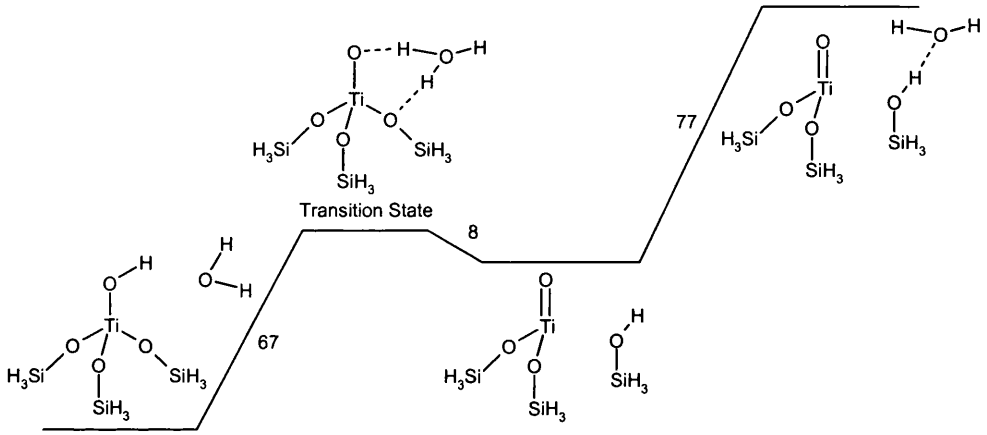

Figure 3.10 Suggested pathway for titanyl formation. Density functional theory calculated energies are in kJmol^{-1} taken from the paper of Sinclair and Catlow [36].

Sinclair and Catlow propose that if titanyl species do exist they would probably be in dynamic equilibrium with hydroxide forms of tetrahedral Ti sites but their short lifetime could be a route to the oxygen-donating species in peroxide doped Ti molecular sieves.

Recent periodic calculations on the model system Ti-chabasite [40] and combined quantum mechanics/molecular mechanics embedding procedures on Ti sites in silicalite [41] have also indicated that the formation of bis-aquo complexes of Ti might occur in hydrated molecular sieves, figure 3.11.

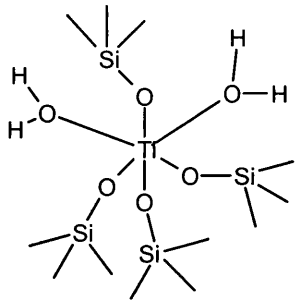

bis-aquo, tetrapodal Ti site

Figure 3.11 Example of a bis-aquo Ti site where two molecules of water are weakly coordinated to the metal centre.

Sauer *et al.*, noted that the absorption energies of water to tetrahedral Ti clusters were indicative of a medium strong hydrogen bond and suggested that the effect of hydration must be taken into account when discussing Ti sitings in zeolites [41].

3.7 Summary

Clearly there is still confusion over the nature of titanium sites in molecular sieve catalysts at operating conditions. The structure and energetic stability of all five literature models of Ti sites discussed in the preceding section; titanyl groups, monopodal, bipodal and tripodal Ti-OH structures and tetrapodal groups will be presented in Chapter 4 with the focal point being the effect of hydration.

3.8 Oxidation activity

Ti molecular sieve catalysts have been applied to the epoxidation of double bonds [11,29,42-60], the oxidation of alkanes [8,9,17,42,45,50,61-65], the hydroxylation of aliphatics and aromatics [64,66-68] and the oxidation of sulphur [48,64,69,70] and nitrogen functionalities [71-73], in relatively simple molecules. However, as aforementioned, due to the vast body of literature regarding Ti molecular sieve oxidations and given the focus of this thesis, here we will only review activity targeted towards alkene epoxidations.

TS-1 and Ti-β catalyse the epoxidation of small-chain alkenes, in dilute solutions of hydrogen peroxide, at below 80°c [59,74]. Consistent with a heterolytic mechanism, the reaction occurs with the full retention of double bond configuration [29]. Preferred solvents for fast kinetics tend to be methanol and acetone for TS-1 whilst acetonitrile and methanol with Ti-β and epoxide selectivity can be higher than 90%. Table 3.2 gives a flavour of the epoxidation activity exhibited by Ti molecular sieves. The reader will note that doping TS-1 with gold severely retards epoxide product yields, in comparison to pure TS-1. Additives, solvents, peroxides, alkene conformations and the presence of acids/bases are all highly influential on the oxidation activity of Ti molecular sieves. The following sections review the relationship that activity has with the reactant environment.

Catalyst	Alkene	Peroxide	Solvent	Reaction conditions	% Epoxide conversion	% Epoxide Selectivity
TS –1 [14]	Propene	H_2O_2	Methanol	320 K	99	98
Au doped TS-1 [56]	Propene	H_2O_2	Methanol	343-473 K	< 1	99
TS –1 [49]	C_3 & C_4 allylic alcohols	H_2O_2	Methanol	303 K	18 - 98	0 - 74
TS-1 [58]	Cyclic hydroxy alkenes	H_2O_2	Acetone	323 K	80 – 86	75 - 90
Ti-β [48]	Cyclohexene	H_2O_2	Methanol	333K	100	3
Ti-β [52]	Oct-1-ene	TBHP	MeCN	363K / 100 min	14	80
Ti↑MCM41 [53]	Cyclohexene	TBHP	Acetonitrile	298K	21	-

Table 3.2 Epoxidation activity of Ti molecular sieves, taken from the literature.

3.8.1 Solvent Effects

The nature of the solvents has been shown to influence the reaction kinetics and selectivities of epoxidations in Ti-silicates. Clerici and other groups have published a number of studies on the effects of solvent and the results are collated in table 3.3. Two explanations of the solvent dependence on reaction rates have been given. The first is that the solvent is an integral part of the oxygen-donating species. Protic solvents are found to give higher epoxidation activities than aprotic solvents for both TS-1 [59] and Ti-β [48] (row 4 and row 1, table 3.3 respectively).

Sheldon *et al.* [75,76] suggested that polar solvents such as acetone or methanol are preferable because they can create a single liquid phase but are not strongly absorbed on the molecular sieve. Clerici and Ingallina argued that the ascribed positive effect of protic solvents must be due to the formation of five-membered ring cyclic Ti-peroxo species whose formation is stabilised by the solvent and which donate an oxygen to the alkene, figure 3.12.

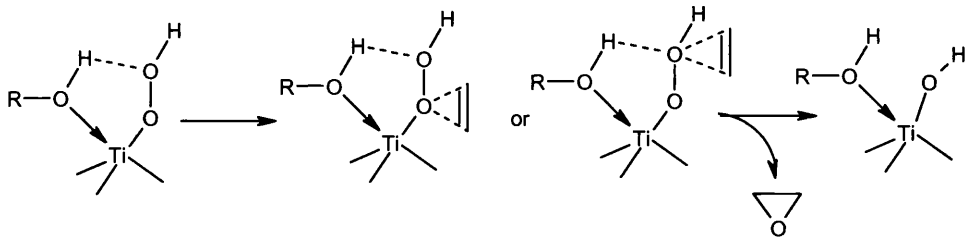

Figure 3.12. Proposed involvement of solvents (ROH) in alkene epoxidations[59].

However, TS-1 is active for alkene epoxidation in the absence of solvents, although with reduced activity [42], and thus the five-membered ring shown on the far left of figure 3.12 would not be necessary for this mode of reaction.

The second argument put forward to explain the solvent effects on epoxidation reaction rates is that the molecular sieve acts as a second solvent, extracting the alkenes from the bulk solvent. The size and the hydrophobicity/hydrophilicity of the molecular sieve pores and the solvent determine which alkenes are selectively extracted. This second rationale is discussed in detail in reference [76].

Catalyst	Alkene	Epoxidation Conditions	Solvent Effects on % epoxide conversion	Solvent Effects on % epoxide selectivity
Ti-β [48]	Cyclohexene	H_2O_2, 333K	methanol > ethanol >> t-butanol ≈ MeCOEt > MeCOMe > MeCN	
Ti-β [77]	1-hexene		MeCN > MeCOMe > MeCOEt	
Ti-β [52]	oct-1-ene	TBHP, 90°	CF_3CH_2OH >> H_2O = MeCN(H_2O free) > MeCN ≈ MeOH/H_2O = MeOH > MeOH(H_2O free) ≈ oct-1-ene > t-butanol ≈ PHCl	CF_3CH_2OH >> H_2O = MeCN(H_2O free) > MeCN ≈ MeOH/H_2O = MeOH > MeCN = MeCN(H_2O free) >> MeOH(H_2O free) > CF_3CH_2OH > t-butanol >>H_2O, MeOH/H_2O, MeOH, PhCl, oct-1-ene
TS-1 [59]	Various small, linear alkenes		methanol > ethanol > t-butanol	
TS-1 [57]	propylene	H_2O_2 293-343K	methanol (92 wt%) > methanol (52 wt%) > ethanol > methyl acetate > acetonitrile > t-butyl alcohol	
TS-1 [49]	Various allylic alcohols	H_2O_2 30°	Methanol, ethanol and H_2O are all good solvents	
Ti-MCM41 [53]	cyclohexene		acetonitrile > isooctane >>2-propanol > pyridine > methanol	
Ti-MCM41 [11]	cyclohexene	TBHP and MPPH 25°	MPPH > TBHP	MPPH > TBHP

Table 3.3 Solvent effects on epoxdation reaction kinetics, selected from the literature

3.8.2 Alkene effects

There are two general trends regarding how the structure of alkenes affects catalytic activity. The first is that a decrease in reactivity is observed with increasing alkene chain length. This is nicely demonstrated by the work of Corma *et al.*, who presented the kinetics of oxidation of a number of linear alkenes with hydrogen peroxide and tert-butyl hydroperoxide on Ti-β catalyst [60], summarised in row 1 of table 3.4. A decrease in the reactivity was observed in the order, 1-decene > 1-octene > 1-hexene. The authors commented that the intrinisic reactivity of the double bond is expected to be very similar for the three linear chain alkenes and, in any case, should increase with increasing chain length. They suggested that the observed order of reactivity could be explained in terms of increasing diffusion limitation through the zeolite channels with increasing chain length. A decrease in reactivity due to increasing chain length is also observed for Ti-β cyclohexene epoxidation (row 2) and due to shape-selectivity effects in TS-1 (rows 3 and 4), i.e. the cis-crotyl alcohol has faster oxidation kinetics than the trans-crotyl alcohol in TS-1.

The second trend regarding how the structure of alkenes affects catalytic activity is that reactivity increases with higher alkyl substitutions of the alkene. Again the work of Corma *et al.* will be used to demonstrate this effect (row 1, table 3.5). The order of reactivity observed for the Ti-β catalyst is 2-hexene > 1-hexene ≥ 3-hexene. Epoxidation of olefins on Ti-zeolite catalysts is thought to occur through an electrophilic attack by the Ti species [59] and consequently, the reactivity would increase with the number of alkyl substituents, due to induction of electron density into the double bond. On this basis, 3-hexene would react even faster than 2-hexene, however this is not observed experimentally and can be rationalised by steric arguments.

It is evident that the reaction kinetics of titanosilicate mediated epoxidations can be dependent on the number, position and the nature of substituent groups (row 3, table 3.4) and steric configuration of the alkene.

Catalyst	Reaction Conditions	Reactivity Trends
TS-β [60]	Oxidation of linear and branched alkenes H_2O_2 & TBHP / methanol / 50°c	1-hexene > 1-octene > 1-docene 2-hexene > 1-hexene ≥ 3-hexene
Ti-β [48]	Epoxidation of cyclohexene H_2O_2 / methanol / 333K	cyclohexene > cycloheptene > cis-3-heptene ≈ cyclooctene > cis-2-heptene > 1-heptene > 1-dodecene > cyclododecene
TS-1 [59]	Varoous linear and branched alkyl alkenes H_2O_2 Methanol	1-hexene >> cyclohexene 1-butene > allyl chloride ($ClCH_2CH{=}CH_2$) > allyl alcohol
TS-1 [49]	Epoxidation of C_3 & C_4 allylic alcohols H_2O_2 / methanol / 30°	cis-crotyl alcohol > trans-crotyl alcohol > allyl alcohol >> 2-methylalcohol
TS-1 [58]	Epoxidation of (cyclic) hydroxy alkenes H_2O_2 / acetone	allylic alcohols selectively form the epoxide at the 6 position and not the 2. (stereospecificity is retained in the epoxide products).

Table 3.4 Alkene structure dependencies on epoxidation reaction kinetics, selected from the literature.

3.8.3 Acids, bases and additives

In order to gain insight into the oxidation pathways over titanium molecular sieves, a number of authors have studied the effect of adding acids, bases and flourides to the reaction mixture [42,59,76]. Basic compounds at low concentrations do not slow the epoxidation kinetics of TS-1, but do improve significantly the yields, up to 97% in the epoxidation of butene [59]. But at higher concentrations, Ti molecular sieve activity is decreased and eventually inhibited by bases. However, pre-treatment of the catalyst with neutral or acidic salts improves epoxidation selectivity without affecting the catalytic activity [47]. Introduction of flourides significantly retards oxidation kinetics, which is thought to be due to inhibition of the active sites by strong Ti-F binding.

3.8.4 R group effects

In the review of Ligand Accelerated Catalysis by Sharpless *et al.* [78], the discovery of non-zeolite titanium-catalysed asymmetric epoxidation was suggested to be dependent on ligand acceleration or R group effects where the ligand is -OR. A comparison of the epoxidation rates of different titanium alkoxides showed that the reaction rate with a mixture of $Ti(Oiso\text{-}propyl)_4$ and 50% tartrate (forming the $[Ti_2(DIPT)(Oiso\text{-}propyl)_6]$ complex as the major species) was significantly *lower* than that of the free $Ti(Oiso\text{-}propyl)_4$ alone; an example of R group deceleration. The ability of a specific ligand to lead to a faster, "ligand accelerated" reaction of an existing catalytic process is exhibited in both homogeneous and heterogeneous catalysts. The concept is most valuable in reactions catalysed by early transition metals, such as titanium, where dynamic ligand exchange processes can give rise to many molecular configurations which, at least for significant selectivity in organic reactions, must be self-controlled for the formation of highly organised transition states. Of course, the formation of very specific transition state configurations is assisted in titanium molecular sieves due to the rigidity of the anchoring silica support and confines of the pores.

Ti-silsesquioxanes, which are soluble molecular analogues of Ti molecular sieves, have been used by a number of groups to model the active sites of

titanosilicate catalysts [79-84]. For Ti-silsesquioxanes with different R groups, figure 3.13, the reaction rates for the epoxidation of cyclohexene with TBHP decreases in the following order R = CH_3 > Butyl > Propyl [80]. Steric inhibition of the Ti active sites and not electronic properties was considered the reason for such trends.

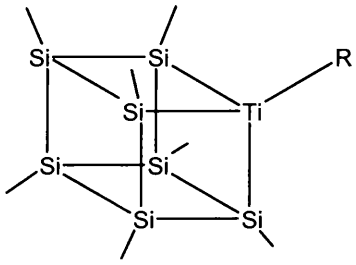

Figure 3.13 The cube-like Ti-silsesquioxane structure. The lines represent oxygen bridges.

Other studies, however, have reported that it is the electron-withdrawing/electron-donating capabilities of the R groups that affect the oxidation kinetics with electron-withdrawing functionalities are found to retard epoxidation rates.

It is known that R groups are known to affect the catalytic activity of non-zeolite titanium mediated epoxidations and that the Ti-OR bonds are stable in Ti-silsesquioxanes, where the silica environment is analogous to molecular sieve frameworks. Evidently, R group chemistry could be very important in tailoring the activity of these catalysts for future industrial applications. To the best of my knowledge, Ti-OR functionalities have still not been synthesised in molecular sieves. The closest achievements have been in the direct incorporation of other elements other than silicon or aluminium into the frameworks, such as germanium and tin, which are directly bonded to titanium centres through oxygen bridges [85-87]. Framework substitution of Ge has been found to increase activity whereas Sn retards epoxidation rates. Oldroyd *et al.* reported that the turnover frequency of cyclohexene epoxidation in a Ti-MCM41 catalyst is increased by 140% with Ti ions anchored by two –OSi bonds and one -OGe bonds compared to Ti sites anchored by three -OSi bonds [85]. Recent advances in synthesis of Ti-OR groups have been made through the ability to graft the Ti metal onto the surface of MCM41 (section 3.5.1). Previously, R groups that are incorporated during

framework substitution of the Ti ions into zeolites are always removed during calcination.

The effect that electron withdrawing and sterically bulky R groups, as well as Ge and Sn, have on the reaction kinetics of epoxidation will be examined in this thesis.

3.9 The oxygen-donating species in epoxidation reactions

The high selectivities observed for a wide range of olefins and the stereospecifity of the reaction are consistent only with a *heterolytic* mechanism. In early studies, two types of mechanism have been considered [75],

1. Formation of Ti-peroxides.

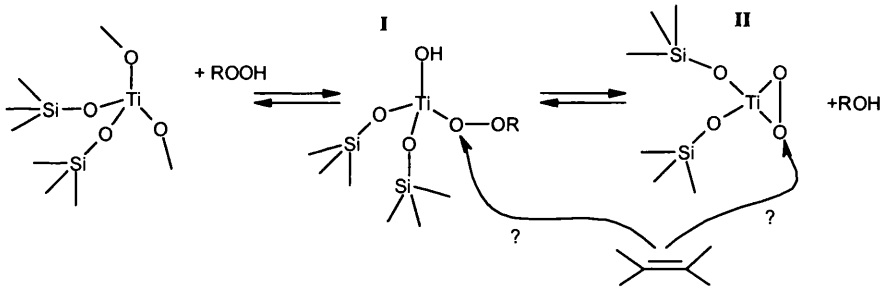

Figure 3.14 Suggested epoxidation mechanism *via* a Ti-peroxide species [75]

2. Formation of Ti-hydroperoxides.

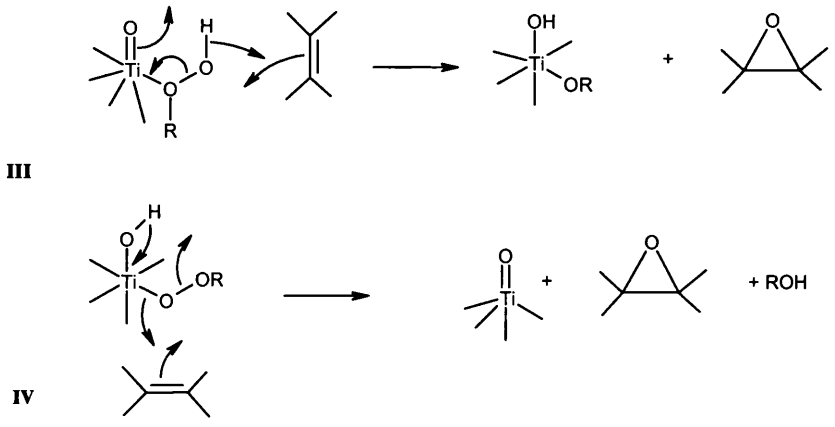

Figure 3.15 Suggested epoxidation mechanism *via* a Ti-hydroperoxide species [75]

The formation of a peroxo complex between H_2O_2 and the titanium atoms in titanium molecular sieves is certain. UV-Vis [25] studies of Titanosilicate/H_2O_2 systems confirm the presence of side-bonded (species II, figure 3.12) otherwise known as η^2 peroxo species, with an absorption band at 26,000cm^{-1} attributed to ligand to metal charge transfer of $O_2^{2-} \rightarrow Ti^4$. This assignment is based on a band at the same frequency for $[TiF_5(O_2)]^{-3}$ complexes. However, UV-vis cannot determine the exact structure of η^2 Ti-peroxo complexes. The strong repulsion between formally unshared electrons in planar H_2O_2 can be reduced by transition-metal ions such as titanium, as they accept electron density from the filled anti-bonding orbitals of H_2O_2 interacting with the empty metal d orbitals of appropriate symmetry. It is for this reason that even *hydroperoxo* (-OOH) complexes may prefer the side-on configuration that can provide added stability.

Thus, three types of Ti-η_2(OO) complex have been suggested as the oxygen-donating species in titanium molecular sieves. 1) Formation of Ti-$\eta^2(O_2)$ complexes [33,88] that are readily formed in aqueous TiR_4/peroxide mixtures (species (a), figure 3.16). 2) Binding of hydroperoxo or organoperoxo ligands (with H_2O_2 or ROOH respectively) in an η^2 fashion to the titanium centre [39,89], (species (b) figure 3.16) and 3) the anionic analogue of the aforementioned complex (species (c), figure 3.16) [90,91].

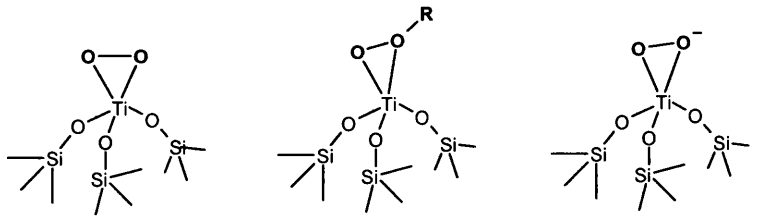

Figure 3.16 Suggested structures for the Ti-peroxo species in titanium molecular sieves with hydroperoxide.

Since discrete Ti-$\eta^2(O_2)$ complexes are known to readily form and be very stable in the liquid phase a number of authors have assumed species (a) to be the oxygen-donating group in titanium molecular sieve catalysts. However, density functional theory cluster calculations indicate that in alkene epoxidation reactions,

Ti-$\eta^2(O_2)$ complexes will indeed form, but only in the *absence* of the alkene and therefore cannot be the catalytic mediating species [39]. Furthermore, Ti-$\eta^2(-O_2)$ complexes do not explain the observed influence of varied peroxide substituents on the reaction kinetics of porous titanosilicate catalysts [42,48,53]. In addition, the acidic properties of TS-1/H_2O_2 mixtures are thought to be due to the presence of Ti-peroxo complexes and thus, Ti-$\eta^2(-O_2)$ type complexes cannot directly account for this phenomenon.

A number of quantum chemical studies have suggested that Ti-η^2(OOR) species are stable [39,92] and energetically accessible and that they provide an explanation for the aforementioned peroxide and acid-base effects [14,59,91] observed for titanosilicate/peroxide mixtures. Density functional theory calculations also suggest that Ti-η^2(OOH) are the key catalytic species, donating an oxygen to a weakly bound alkene molecule [39]. An activation barrier of < 60 kJmol^{-1} has been quoted for the formation of Ti-η^2(OOH) species.

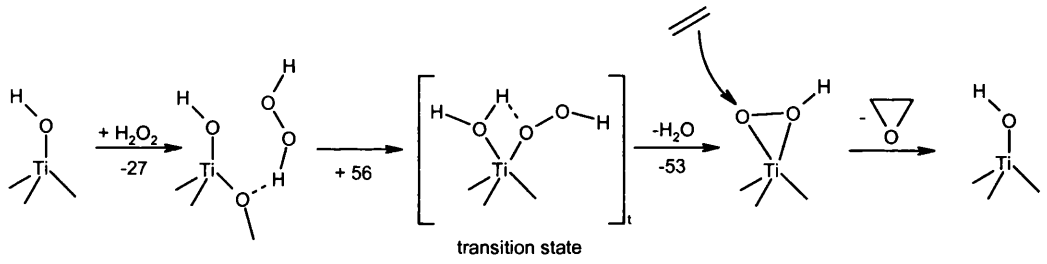

Figure 3.17 Suggested mechanism for the formation of Ti-η^2(OOH) complexes and their role as oxygen donors to alkenes [39]. Energies are in kJmol^{-1}.

Transfer of electron density from the partially filled π^* O-O anti-bonding orbitals of the peroxidic oxygen(s) to the Ti^{IV} centre is thought to stabilise η^2-OOH species.

Hartree Fock cluster calculations on a number of Ti-peroxo models found the Ti-$\eta^2(O_2^-)$ ion pair model to be the most stable [91]. The authors characterised the complex by a calculated O-O vibration which was in good agreement with an IR and Raman analysis of a hydrogen peroxide doped TS-1 catalyst.

However, all of the Ti-η^2(peroxo) species have one major failing; they do not explain the well-documented dependence of solvents on the catalytic

reactivity of titanium molecular sieve systems with peroxide [14,47,48,52,53,59,65,77]. Thus, many workers champion a Ti-η^1(OOR) complex or a 5-membered ring intermediate [26,42,44,51,59,92-96] where the solvent or adsorbate is an integral part of the compound, offering stabilisation of the peroxide moiety through hydrogen bonding (species (a) and (b), figure 3.18). The five-membered ring complex was introduced in section 3.8.1.

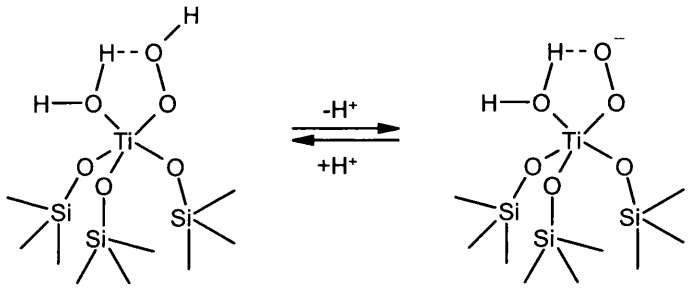

(a) (b)

Figure 3.18 Suggested structures of the Ti-peroxo complexes in peroxide doped titanium molecular sieves.

Species (a), in the figure above is also consistent with the known tendency of titanium to expand its coordination shell above 4 and has several organic analogues [26]. However, quantum mechanical simulations of small model $Ti(OH)_4$ clusters found the Ti-η^1(OOH) complex to be 33 $kJmol^{-1}$ less stable than the Ti-η^2(OOH) complex [92].

Alkyl hydroperoxides (ROOH) are known to form both η^2(OOR) and η^1(OOR) complexes with transition metals depending on the binding strength of other ligands. The observation that different peroxides lead to variations on the regioselectivity of epoxidations has also been considered to indicate that the whole –OOR group is involved in the active oxygen donating species [97]. Furthermore, Sheldon *et al.* have demonstrated that the structure of the ROOH hydroperoxide can play an important role in determining the selectivities in Ti-O_2-SiO_2 mixed oxide catalysed epoxidations [98], another indication that the peroxide R substituents must be part of the Ti-peroxo catalytic species. If this is the case, electron withdrawing substituents in the hydroperoxide are likely to increase the

rate of epoxidation by enhancing the electrophilic nature of the Ti-peroxo complex.

3.10 Summary

UV-vis and ESR experimental techniques have shown that Ti-peroxo complexes definitely do form but give very limited information on the structure of such species. Although a large number of theoretical studies have been undertaken, the nature of the oxygen-donating species is still unclear. No one study has presented a thorough, systematic and quantitative interrogation of the formation, structure and coordination of all Ti-peroxo complexes suggested in the literature, until now. This thesis reports the energetics and structure of all of the literature postulated Ti-peroxo complexes described in the preceding section in a detailed and systematic manner. The effect of hydration and proton transfer mechanisms is also explored which lead to a new Ti-peroxo species, not previously reported in the literature. This work also shows for the first time, evidence that particular Ti-peroxo complexes, predicted though quantum mechanical calculations, do exist in titanium molecular sieves through excellent agreement with EXAFS spectroscopy. Identifying the nature of Ti-peroxo complexes in titanium molecular sieves is crucial in elucidating the mechanism of epoxidations.

3.11 Epoxidation mechanisms

Tailored studies [11] and the high epoxide yields and stereospecificity [42,59] observed in epoxidation reactions strongly indicate that titanium molecular sieves catalysts function in a non-radical manner. For epoxidations, it is generally considered that the mechanism is heterolytic mechanism (for the oxidation of alkanes a homolytic mechanism has been suggested [42,59]).

Initial binding of the alkene to the titanium centre before Ti-peroxo formation has been suggested [11]. However, Sinclair and Catlow found no evidence of initial ethene binding to tetrahedral Ti sites in their quantum mechanical cluster calculations. Optimisation of a tripodal cluster with ethene in

bonding distance to the titanium resulted in the alkene being expelled from the coordination sphere. All other studies have reported alkene binding to the O-O functionality in the Ti-peroxo complex. There are two main areas of focus in the literature concerning the mechanism of epoxidation reactions, the first is the nature of the Ti-peroxo complex and the second is which peroxidic oxygen will be donated to the alkene.

A number of mechanisms mediated by side-bonded Ti-$\eta^2(O_2)$ species have been reported [8,14,58,61,69,88]. The direct mechanism of Notari is shown in figure 3.19. In this mechanism either of the peroxidic oxygen atoms could equally be targeted.

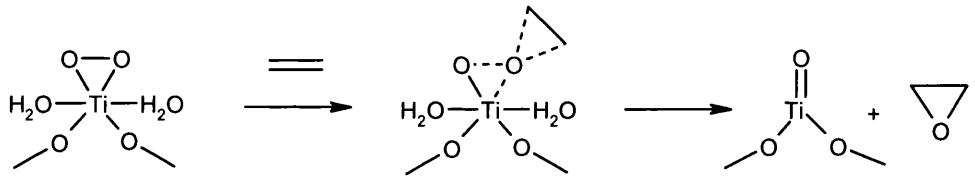

Figure 3.19 Suggested mechanism for the epoxidation of alkenes by a Ti-$\eta^2(O_2)$ complex, taken from the work of Notari.

An epoxidation mechanism involving the side-bonded Ti-η^2(OOH) complex is presented in figure 3.17, taken from the work of Sinclair *et al.* Other studies that favour a Ti-η^2(OOH) mediated epoxidation mechanism can be found in the literature [92,95].

A mechanism favoured by some for the epoxidation of alkenes *via* five-membered ring Ti-η^1(OOH) complexes is shown in figure 3.12 and is taken from the work of Cerici *et al.* [59]. It has been postulated that the alkene will preferentially attack the peroxidic oxygen directly bound to the titanium atom because it will be the most electrophilic and thus will minimise the repulsion with the electron-rich alkene double bond. Density Functional theory calculations have shown that ethene interaction at the peroxidic oxygen furthest away from the metal centre is repulsive, regardless of the direction of attack. Geometry optimisation leads to positioning of the ethene molecule distance > 3.5Å away from the targeted oxygen. However, attack of the oxygen bound to the titanium

on the other hand, was found to be attractive and resulted in the formation of the epoxide [94], figure 3.20.

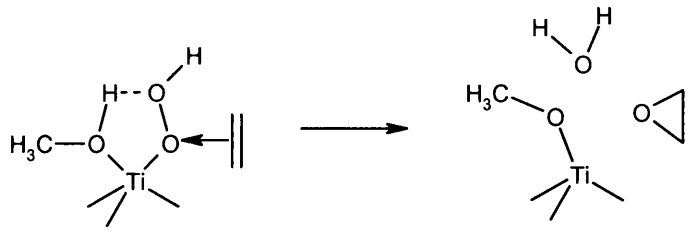

Figure 3.20 Result of Density Functional Theory calculations, by Neurock and Manzer, on the attack of ethene to a methyl derivatised five-membered ring Ti-η^1(OOH) complex.

The overall epoxidation reaction step was calculated to be –220 kJmol^{-1}. Adam *et al.* [93] meanwhile, has proposed that donation of the peroxidic oxygen furthest from the titanium centre in a five-membered ring complex will occur in alkene epoxidations, figure 3.21. Comparing diastereoselectivities with those observed for dioxiranes was used as the basis for the mechanistic proposal.

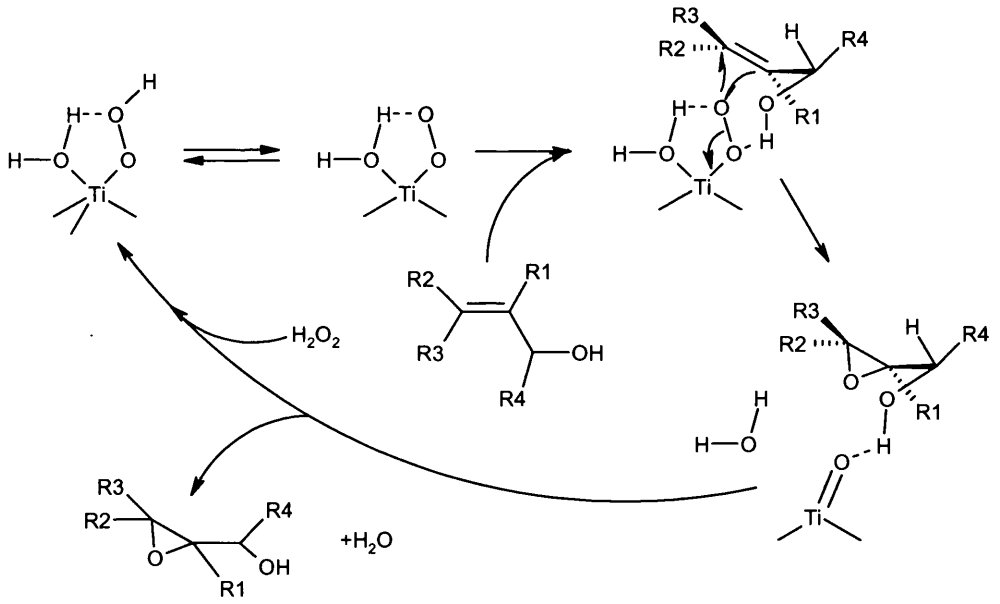

Figure 3.21. Suggested epoxidation mechanism by donation of the peroxidic oxyegn furthest from the titanium centre in a five-membered ring Ti-peroxo complex taken from the work of Adam *et al.*

Other suggested mechanisms involving five-membered ring η^1 complexes are reported in references [42,67].

Clearly, despite the large number of experimental and theoretical studies reported in the literature the mechanism of the titanium molecular sieve catalysed epoxidation of alkenes is still not fully understood. The reader will notice that the mechanisms presented in this section contain different titanium active site structures and diverse Ti-peroxo oxygen-donating species. If the mechanism of epoxidation is elucidated, surely the structure of both the titanium active site and the Ti-peroxo complex must be determined. There have been numerous experimental and quantum mechanical studies concerning the nature of titanium active sites, however, very few have examined the effect of hydration and yet the reaction of titanium molecular sieve catalysts are carried out in a protic medium.

Thus, in order to elucidate the mechanism of alkene epoxidations within the pores of titanium molecular sieves with peroxide the following chapter presents detailed quantum mechanical calculations on, firstly the nature of titanium active sites in dehydrated and hydrated catalysts. A systematic investigation of all structures discussed in section 3.6.1 is reported.

Secondly, quantum mechanical calculations on the nature of Ti-peroxo complexes are analysed, with discussion centred on full reaction profiles of formation of a number of the literature postulated structures, presented in section 3.9. In addition the transition states have been unequivocally determined. All literature proposed Ti-peroxo structures are used as models for the interpretation of EXAFS data of a tert-butyl hydroperoxide doped Ti-MCM41 catalyst where the simulated spectra of two of the complexes exhibit striking similarity to the experimental analysis. This is the first time direct evidence of the existence of specific Ti-peroxo complexes has been obtained. In addition the effect that R groups have on the reaction profiles of the formation of Ti-peroxo is also examined with any trends compared to previous activity studies reported in the literature.

Finally, employing the insight gained into the key catalytic species in Chapter four, the mechanism of alkene epoxidations is explored in chapter five. A systematic approach is employed using frontier orbital theory to investigate

HOMO-LUMO and LUMO-HOMO mechanisms. Furthermore, the interaction of ethene and propene with each of the peroxidic oxygens, in all of the Ti-peroxo complexes, in turn, is examined. Finally, in Chapter six I present a complete catalytic cycle for the titanium molecular sieve catalysed epoxidation of alkenes with peroxide with the structure of the oxygen-donating species verified by EXAFS. The cycle includes mechanisms for by-product formation and regeneration of the catalyst. This is the first systematic and quantitative study of the complete catalytic process with all plausible literature proposed active sites, Ti-peroxo complexes and mechanisms explored. Furthermore, I will also report a new, stable Ti-peroxo complex, which has the lowest activation barrier of formation of all the oxygen-donating species studied and that readily donates an oxygen atom to alkenes to form epoxides.

Of particular importance to the mechanistic studies presented in the forthcoming chapters is the effect of varying R groups and alkene structure.

3.12 Summary

There is a huge body of literature available regarding the synthesis, structure, and reactivity of titanium molecular sieves. I have focused on the areas that are relevant to this thesis. For further information, the review of Notari [10] is by far the most comprehensive, however, the reader is also referred to reference [76] for an excellent introduction to the field of transition metal substituted molecular sieves, which includes titanium systems. For a discussion of the fundamentals of metal-catalysed epoxidations with peroxide, the work of Sheldon is particularly insightful [75,98] and for a review of transition metals in catalysis the reader is referred to reference [78]. Finally, Clerici systematically covers the vast area of titanium molecular sieve activity (not just in oxidations) in his recent paper in Topics in Catalysis; an issue dedicated to the industrial applications of zeolites [13].

3. 13 References

(1) Wulff, H. In *3,642,833; 3,923,843; 4,021,454; 4,367,342*: U.S. Patent, 1971.

(2) Young, D. A. In *3,329,481*: U.S. Patent, 1967.

(3) Taramasso, M.; Perego, G.; Notari, B. In *4,410,501*: U.S. Patent, 1983.

(4) Taramasso, M.; Perego, G.; Notari, B. In *Proceedings of the 5th international Conference on Zeolites*; Heydon and Sons, London: Naples, 1980.

(5) Epsosito, A.; Taramasso, M.; Buonomo, F. In *2,116,974*: U.S. Patent, 1985.

(6) Esposito, A.; Neri, C.; Buonomo, F. In *4,480,135*: U.S. Patent, 1984.

(7) Neri, C.; Esposito, A.; Anfossi, B.; Buonomo, F. In *100,119*: European Patent Appl, 1984.

(8) Huybrechts, D. R. C.; Bruycker, L. D.; Jacobs, P. A. *Nature* **1990**, *345*, 240-242.

(9) Tatsumi, T.; Nakamura, M.; Negishi, S.; Tominage, H. *J. Chem. Soc., Chem. Commun.* **1990**, 476.

(10) Notari, B. *Advances in Catalysis* **1996**, *41*, 253-334.

(11) Oldroyd, R. D.; M.Thomas, J.; Maschmeyer, T.; MacFaul, P. A.; Snelgrove, D. W.; Ingold, K. U.; Wayner, D. D. M. *Angew. Chem. Int. Ed. Engl.* **1996**, *35*, 2787-2790.

(12) Marcilly, C. R. *Topics in Catalysis* **2000**, *13*, 357 - 366.

(13) Clerici, M. G. *Topics in Catalysis* **2000**, *13*, 373 - 386.

(14) Notari, B. *Catalysis Today* **1993**, *18*, 163-172.

(15) Reddy, J. S.; Kumar, R. *J. Catal.* **1991**, *130*, 440.

(16) Reddy, J. S.; Kumar, R.; Ratnasamy, P. *Appl. Catal.* **1990**, *58*, L1.

(17) Camblor, M. A.; Corma, A.; Perez-Pariente, J. *Zeolites* **1993**, *13*, 82-87.

(18) Corma A., C. M. A., Esteve P., Martinez A., Perez-Pariente J., *journal of Catalyss* **1994**, *145*, 151-158.

(19) Corma, A.; Navarro, M. T.; Pariente, J. P. *J. Chem. Soc., Chem. Commun.*, **1994**, 147-148.

(20) Maschmeyer, T.; Rey, F.; Sankar, G.; Thomas, J. M. *Nature* **1995**, *378*, 159-162.

(21) Sankar, G.; Rey, F.; Thomas, J. M.; Greaves, G. N.; Corma, A.; Dobson, B. R.; Dent, A. J. *J. Chem. Soc., Chem. Commun.* **1994**, 2279-2280.

(22) Man, A. J. M. d.; Sauer, J. *J. Phys. Chem.* **1996**, *100*, 5025-5034.

(23) Millini, R.; Passara, E. P.; Perego, G.; Bellussi, G. *Journal of Catalysis* **1992**, *137*, 497-503.

(24) Boccuti, M.; Rao, K.; Zeccina, A.; Leofanti, G.; Petrini, G. *Stud. Surf. Sci. Catal* **1989**, *48*, 133.

(25) Geobaldo, F.; Bordiga, S.; Zeccina, A.; Giamello, E.; Leofanti, G.; Petrini, G. *Catalysis Letters* **1992**, *16*, 109-115.

(26) Bellussi, G.; Carati, A.; Clerici, M. G.; Maddinelli, G.; Millini, R. *Journal of Catalysis* **1992**, *133*, 220-230.

(27) Liu, Z.; Davis, R. J. *J. Phys. Chem* **1994**, *98*, 1253-1261.

(28) Fraile, J. M.; Garcia, J.; Mayoral, J. A.; Proietti, M. G.; Sanchez, M. *J. Phys. Chem.* **1996**, *100*, 19484-19488.

(29) Lamberti, C.; Bordiga, S.; Arduino, D.; Zecchina, A.; Spano, G.; Genoni, F.; Petrini, G.; Carati, A.; Villain, F.; Vlaic, G. *J. Phys. Chem. B* **1998**, *102*, 6382-6390.

(30) Blasco, T.; Corma, A.; Navarro, M. T.; Pariente, J. P. *Journal of Catalysis* **1995**, *156*, 65-74.

(31) Alba, M.; Luan, Z.; Klinowski, J. *J. Phys. Chem.* **1996**, *100*.

(32) Pei, S.; Zajak, G. W.; Kaduck, J. A.; Faber, J.; Boyanov, B. I.; Duck, D.; Fazzini, D.; Morrison, T. I.; Yang, D. S. *Catal. Lett.* **1993**, *21*, 333.

(33) Trong-On, D.; Bittar, A.; Sayari, A.; Kaliaguine, S.; Boneviot, L. *Catalysis Letters* **1992**, *16*, 85-95.

(34) Jentys, A.; Catlow, C. R. A. *Catal. Lett.* **1993**, *22*, 251.

(35) Sinclair, P. E.; Sankar, G.; Catlow, C. R. A.; Thomas, J. M.; Maschmeyer, T. *J. Phys. Chem. B* **1997**, *101*, 4232-4237.

(36) Sinclair, P. E.; Catlow, C. R. A. *J. Chem. Soc., Chem. Commun* **1997**, 1881-1882.

(37) Markgraf, S. A.; Halliyal, A.; Bhalla, A. S.; Newnham, R. E.; Prewitt, C. T. *Ferroelectrics* **1985**, *62*, 17.

(38) Roberts, M. A.; Sankar, G.; Thomas, J. M.; Jones, R. H.; Du, H.; Chen, J.; Pang, W.; Xu, R. *Nature* **1996**, *381*, 401-404.

(39) Sinclair, P. E.; Catlow, C. R. A. *J. Phys. Chem. B.* **1999**, *103*, 1084-1095.

(40) Zicovich-Wilson, C. M.; Dovesi, R.; Corma, A. *J. Phys. Chem. B* **1999**, *103*, 988.

(41) Ricchiardi, G.; Andres, d. M.; Sauer, J. *Phys. Chem. Chem. Phys* **2000**, *2*, 2195-2204.

(42) Khouw, C. B.; Dartt, C. B.; Labinger, J. A.; Davis, M. E. *Journal of Catalysis* **1994**, *149*, 195-205.

(43) Adam, W.; Peters, K.; Renz, M. *Journal of Organic Chemistry* **1997**, *62*, 3183-3189.

(44) Bhaumik, A.; Tatsumi, T. *Chem. Commun.* **1998**, 463.

(45) Tatsumi, T.; Koyano, K. A.; Igarashi, N. *J. Chem. Soc., Chem. Commun.* **1998**, 325-326.

(46) Yang, Q.; Li, C.; Yuan, S.; Li, J.; Ying, P.; Xin, Q.; Shi, W. *Journal of Catalysis* **1999**, *183*, 128-130.

(47) Thiele, G. F.; Roland, E. *J. Mol. Catal.A: Chemical* **1997**, *117*, 351 - 356.

(48) Jappar, N.; Xia, Q.; Tatsumi, T. *Journal of Catalysis* **1998**, *180*, 132-141.

(49) Hutchings, G. J.; Firth, P. G.; Lee, D. F.; McMorn, P.; Bethell, D.; Page, P. C. B.; King, F.; Hancock, F. In *£rd World Congree on Oxidation Catalysis*; Grasselli R.K., O. S. T., Gaffney A.M., Lyons J.E.,, Ed.; Elsevier Science B.V., 1997; pp 535-544.

(50) Corma, A.; Camblor, M. A.; Esteve, P.; Martinez, A.; Perez-Pariente, J. *J. Catal.* **1994**, *145*, 151 - 158.

(51) Bhaumik, A.; Tatsumi, T. *Jouranl of Catalysis* **1999**, *182*, 349-356.

(52) Sato, T.; Dakka, J.; Sheldon, R. A. *J. Chem. Soc., Chem. Commun.* **1994**, 1887-1888.

(53) Ingold, K. U.; Snelgrove, D. W.; MacFaul, P. A.; Oldroyd, R. D.; Thomas, J. M. *Catalysis Letters* **1997**, *48*, 21-24.

(54) Corma, A.; Iglesias, M.; Sanchez, F. *J. Chem. Soc., Chem. Commun.* **1995**, 1635.

(55) Laufer, W.; Meiers, R.; Holderich, W. *Journal of Molecular catalysis A: Chemical* **1999**, *141*, 215-221.

(56) Nijhuis, T. A.; Huizinga, B. J.; Makkee, M.; Moulijin, J. A. *Ind. Eng. Chem. Res* **1999**, *38*, 884-891.

(57) Clerici, M. G.; Bellussi, G.; Romano, U. *Journal of Catalysis* **1991**, *129*, 159-167.

(58) Kumar, R.; Pais, G. C. G.; Pandey, B.; Kumar, P. *J. Chem. Soc., Chem. Commun.*, **1995**, 1315-1316.

(59) Clerici, M. G.; Ingallina, P. *J. Catal* **1993**, *140*, 71-83.

(60) Corma, A.; Esteve, P.; Martinez, A.; Valencia, S. *J. Catal.* **1995**, *152*, 18 - 24.

(61) Fujiwara, M.; Xu, Q.; Souma, Y.; Kobayashi, T. *J. Mol. Catal. A: Chemical* **1999**, *142*, 77-84.

(62) Tanev, P. T.; Chibwe, M.; Pinnavaia, T. J. *Nature* **1994**, *368*, 321-323.

(63) Hayashi, T.; Tanaka, K.; Haruta, M. *Journal of Catalysis* **1998**, *178*, 566-575.

(64) Ramaswamy, A. V.; Sivasanker, S. *Catal. Lett.* **1993**, *22*, 239.

(65) Clerici, M. G. *Applied Catalysis* **1991**, *68*, 249-261.

(66) Adam, W.; Nestler, B. *J. Am. Chem. Soc* **1993**, *115*, 7226-7231.

(67) Bhaumik, A.; Tatsumi, T. *Journal of Catalysis* **1998**, *176*, 305-309.

(68) Pol, A. J. H. P. v. d.; Verduyn, A. J.; Hooff, J. H. C. v. *Applied Catalysis A: General* **1992**, *92*, 113-130.

(69) Reddy, R. S.; Reddy, J. S.; Kumar, R.; Kumar, P. *J. Chem. Soc., Chem. Commun.* **1992**, 84.

(70) Robinson, D. J.; Davies, L.; McGuire, N.; Lee, D. F.; McMorn, P.; Willock, D. J.; Watson, G. W.; Page, P. C. B.; Bethall, D.; Hutchings, G. J. *Phys. Chem. Chem. Phys.* **2000**, *2*, 1523 - 1529.

(71) Reddy, S. J.; Jacobs, P. A. *J. Chem. Soc., Faraday Trans.* **1993**, *1*, 2665.

(72) Selvam, T.; Ramaswamy, A. V. *Chem. Commun.* **1996**, 1215.

(73) Tatsumi, T.; Jappar, N. *Journal of Catalysis* **1996**, *161*, 570-576.

(74) Waal, J. C. v. d.; Rigutto, M. S.; Bekkum, H. v. *Appl. Catal. A* **1998**, *167*, 331.

(75) Sheldon, R. A. *J. Mol. Catal.* **1980**, *7*, 107-126.

(76) Arends, I. W. C. E.; Sheldon, R. A.; Wallau, M.; Schuchardt, U. *Angew. Chem. Int. Ed. Engl.* **1997**, *36*, 1144-1163.

(77) Corma, A.; Esteve, P.; Martinez, A. *J. Catal* **1996**, *161*, 11.

(78) Berrisford, D. J.; Bolm, C.; Sharpless, K. B. *Angew. Chem. Int. Ed. Engl.* **1995**, *34*, 1059-1070.

(79) Crocker, M.; Herold, R. H. M.; Orpen, A. G. *Chem. Commun.* **1997**, 2411 - 4212.

(80) Maschmeyer, T.; Klunduk, M. C.; Martin, C. M.; Shephard, D. S.; Thomas, J. M.; Johnson, B. F. G. *Chem. Commun.* **1997**, 1847 - 1848.

(81) Krijnen, S.; Abbenhuis, H. C. L.; Hanssen, R. W. J. M.; Hooff, J. H. C. v.; Santen, R. A. v. *Angew. Chem. Int. Ed. Engl.* **1998**, *37*, 356 - 358.

(82) Krijnen, S.; Mojet, B. L.; Abbenhuis, H. C. L.; Hooff, H. H. C. v.; Santen, R. A. v. *Phys. Chem. Chem. Phys.* **1999**, *1*, 361 - 365.

(83) Abbenhuis, H. C. L.; Krijnen, S.; Santen, R. A. v. *Chem. Commun.* **1997**, 331 - 332.

(84) Feher, F. J.; Budzichowski, T. A.; Rahimian, K.; Ziller, J. W. *J. Am. Chem. Soc.* **1992**, *114*, 3859 - 3866.

(85) Oldroyd, R. D.; Sankar, G.; Thomas, J. M.; Ozkaya, D. *J. Phys. Chem. B* **1998**, *102*, 1849-1855.

(86) Zicovich-Wilson, C. M.; Corma, A. *J. Phys. Chem. B* **2000**, *104*, 4134-4140.

(87) Attfield, M. P. *Private Communication* **2000**.

(88) Huybrechts, D. R. C.; Vaesen, I.; Li, H. X.; Jacobs, P. A. *Catalysis Letters* **1991**, *8*, 237-244.

(89) Tantanak, D.; Vincent, M. A.; Hillier, I. H. *J. Chem. Soc., Chem. Commun.* **1998**, 1031-1032.

(90) Zecchina, A.; Bordiga, S.; Lamberti, C.; Ricchiardi, G.; Scarano, D.; Petrini, G.; Leofanti, G.; Mantegazza, M. *Catalysis Today* **1996**, *32*, 97-106.

(91) Tozzola, G.; Antegazza, M. A.; Ranghino, G.; Petrini, G.; Bordiga, S.; Ricchiardi, G.; Lamberti, C.; Zulian, R.; Zecchina, A. *Journal of Catalysis* **1998**, *179*, 64-71.

(92) Karlsen, E.; Schoffel, K. *Catalysis Today* **1996**, *32*, 107-114.

(93) Adam, W.; Corma, A.; Reddy, I.; Renz, M. *J. Org. Chem.* **1997**, *62*, 3631-3637.

(94) Neurock, M.; Manzer, L. E. *J. Chem. Soc., Chem. Commun.* **1996**, 1133-1134.

(95) Wu, Y.; Lai, D. *J. Org. Chem.* **1995**, *60*.

(96) Vayssilov, G. N.; Santen, R. A. v. *Journal of Catalysis* **1998**, *175*, 170-174.

(97) Ledon, H. J.; Varescon, F. *Inorg. Chem.* **1984**, *23*, 2735.

(98) Sheldon, R. A.; Doorn, J. v.; Schram, C.; Jong, A. d. *J. Catal.* **1973**, *31*, 438.

Chapter 4

Hydration and Oxidation of Titanium Molecular Sieves

4.1 Introduction

This chapter reports gradient corrected density functional theory calculations, within the cluster approximation, on the structure, hydration and oxidation of derivatised, tetrahedral framework Ti^{4+} centres in molecular sieves.

Firstly, the structure and coordination of Ti atoms embedded or grafted in molecular sieves is examined. Focus is centred on the effect that water has on the geometry and stability of Ti sites. Calculated geometries are compared to experiment where possible to assess the accuracy of the model and DFT recipe. Thus, allowing a consistent strategy to be developed for use in assessing the geometry of undocumented and hypothetical structures.

Secondly, the oxidation of Ti sites with peroxide is rigorously explored. The geometry and stability of a number of different Ti-peroxo species (many of which have been postulated in the literature, see section 3.9) is presented, including reaction profiles of formation and transition state determination. Indeed a highlight of this work is the accurate prediction of the structure of Ti-peroxo complexes, which has been corroborated through EXAFS experiments of tert-

butyl peroxide/Ti↑MCM-41 catalysts by Dr. G. Sankar and Dr. D. Gleeson of the Royal Institution of Great Britain [1,2].

Throughout this work emphasis is placed on interpreting the strong relationship that structure, i.e. metal ligand sterics and peroxide conformation, and electronic properties have on reaction pathways.

4.2 Methodological Details

Non-local Density Functional Theory (DFT), a rigorous quantum mechanical technique (see section 2.3.7), was implemented for all geometry and energy calculations. Due to the computationally demanding nature of quantum mechanical calculations, a finite molecular cluster approximation was employed, which involves extracting a small part, the most reactive part, of the material of interest, here TS-1, and using this as our cluster. Two clusters have been chosen, one extending two coordination shells (left, figure 4.1) from the reactive titanium centre and the other extending three coordination spheres from the metal ion (right, figure 4.1). DGauss [3], a pure density functional code was used for optimisation of the smaller cluster containing 21 atoms. This code was chosen due to its exploitation of analytical second derivatives which, compared to numerical second derivatives, are much faster for transition state calculations. The density functional theory code DMol [4], available as part of the Cerius2 [5] suite was employed for all geometry and energy calculations of the 'extended' cluster. The latter, with over 30 atoms, is far more computationally expensive than the small cluster and DMol was chosen due to its superior efficiency in treating large molecular systems.

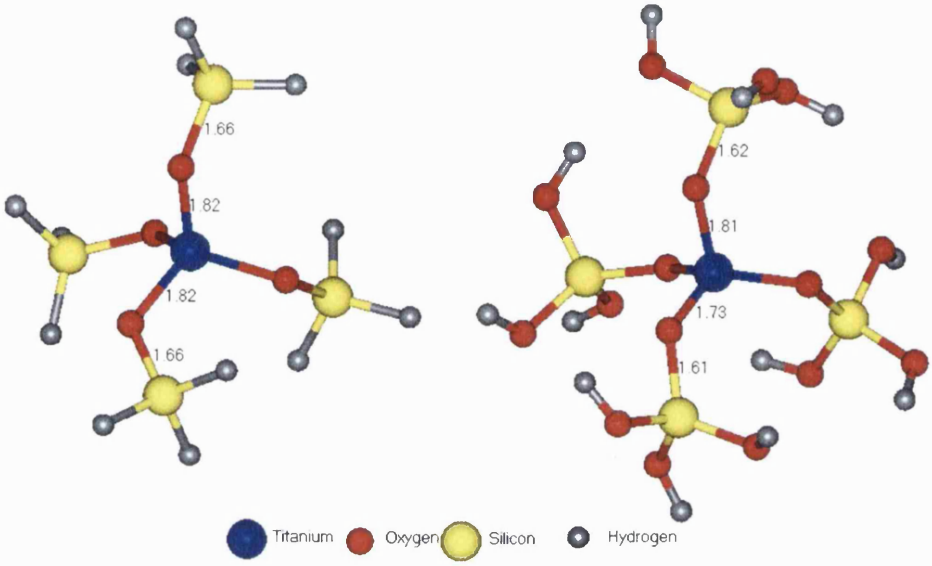

Figure 4.1 DFT optimised Ti clusters extracted from the crystallographic structure of silicalite, the zeolite in TS-1.

The extended cluster will only be used for select calculations where the 3rd coordination shell is necessary for accurate comparison with EXAFS data. The majority of results presented in this chapter will be on the smaller cluster and subsequent derived models.

The cluster model is, of course, a gross simplification of the real system. A more complete treatment of titanium molecular sieves would naturally take into account the steric, polarising and long-range electrostatic effects of the molecular sieve lattice. However, the numerous studies on titanosilicate materials quite clearly show that reactivity is very local to the metal ions extending, essentially to only the first coordination shell. There is very little perturbation of the surrounding silicate framework observed either when the metal ions are embedded into the crystalline lattice during synthesis or whilst reacting in catalysis, for example. Given the additional computational expense incurred in extending the cluster, the need to include the non-reactive silica framework in our model is not justified. Furthermore, the metal cations are highly dispersed within the silicate sieve, in well-prepared titanosilicates; thus Ti-O-Ti and Ti-O-Si-O-Ti interactions are extremely unlikely and do not need to be included in the model. Both of these factors allow the cluster approximation to be implemented with confidence since

one is modelling discrete reactive sites that are essentially isolated from neighbouring active centres and whose structural changes are highly localised.

All severed bonds have been capped with protons in order to retain charge neutrality, as shown in figure 4.1. In an attempt to represent the rigidity of the zeolite framework, all silicon ions have been fixed in space during optimisation. However, in order to relieve undue strain caused by this confinement both the small and extended clusters have been fully energy minimised first, with no constraints and the Si ions fixed at their energy minimised positions. For the smaller cluster, this procedure was performed by a previous group of this laboratory and the protocol is outlined in more detail in reference [6]. Partial optimisation (minimisation of all atoms bar the Si ions) of both the small and extended clusters was performed employing the gradient corrected functional of Becke [7] and Perdew [8] (BP86), in addition to the local parameterisation of Vosko Wilk and Nusair [9]. An all electron double ξ basis with polarisation on all non-hydrogen atoms (DZVP), specifically optimised for DGauss was used for minimisation of the smaller clusters. The DZVP basis is not available in DMol and thus the closely related all electron double numerical precision (DNP) basis set was used for minimisation of the extended clusters. The DNP basis also has polarisation on all non-hydrogen atoms.

Validation of the BP86/DZVP DFT recipe will not be discussed in detail here since a thorough appraisal of DFT methodologies for mechanistic studies using clusters can be found in reference [6]. Table 4.1 is taken from the work of Sinclair and shows calculated and experimental properties of isolated methanol and a methanol dimer for a number of DFT recipes. It can be seen that the BP86/DZVP and BLYP/TZVP approaches hold up particularly well when compared to experiments (highlighted in blue). However, since the DZVP basis is less computationally expensive than its triple zeta (TZVP) counterpart and crucially, when coupled with the BP86 functional gives accurate energies (ΔE), vital when exploring reaction pathways, the BP86/DZVP recipe was chosen for this work. It should be stressed, as with all computational modelling techniques, that there is a degree of error in all geometries, energies and other physical properties calculated. For the DFT calculations, the bond lengths are

overestimated by around 0.01 Å [10-14] and reaction energies are underestimated by ~ 30%.

No symmetry constraints were used throughout this work and all optimisations were performed in Cartesian coordinates. A spin unrestricted wave function was employed in modelling the Ti-$\eta^2(O_2)$ and H_3O radical species. The maximum deviation from ideal expectation value $\mathbf{S}^2$ (i.e $\langle \mathbf{S}^2 \rangle$ where **S** is the spin quantum number) was 0.0046, thus showing there to be minimal spin contamination when employing the spin unrestricted wave function. All minimum energy structures have zero (approximate) Hessian eigenvalues and all transition states have a single, dominant negative (approximate) Hessian eigenvalue.

Property	DFT					HF//MP2[a]	MP2[c 15]		Observed
	DZVP[dg] (BLYP)	TZVP[dg] (BLYP)	DZVP[cp] (BLYP)	DZVP[cp] (BLYP)	DZVP[dg] (BP86)	6-31G**	DZP	VTZ(2df,2p)	
$-\Delta E$	17.3	12.4	15.8	15.4	13.8	16.1	14.1	15.8	13.2 ± 0.4 [15]
ν_{OH} dimer; dimer	3518	3517	3489	3483	3507	3664	3576	3537	3528[d], 3541 [d], 3547 [e]
$-\Delta\nu_{OH}$ dimerisation	133	150	160	160	182	67	131	177	126 [d], 139 [d], 107 [e]
r_{OH} monomer	0.979	0.974	0.980	0.979	0.977	0.942		0.969	0.963 [16]
r_{CO} monomer	1.445	1.448	1.447	1.446	1.435	1.398			1.421 [16]
r_{CH} monomer	1.102	1.098	1.101	1.100	1.102	1.082			1.094 [16]
	1.110	1.105	1.108	1.108	1.109	1.088			
	1.110	1.105	1.108	1.108	1.109	1.088			
∠monomer	107.5	108.1	107.5	107.5	107.4	109.7			108.0 [16]
μ monomer	1.819	1.831	1.824	1.819	1.818	1.834			1.70 [16]
ν_{OH} monomer	3651	3667	3649	3643	3689	3731	3707	3714	3667[d], 3682[f]
ν_{CH} monomer	3053	3024	3064	3062	3067	2917			3005[d], 2999[f]
	2972	2958	2983	2977	2987	2853			2962[d], 2970[f]
	2919	2919	2925	2919	2929	2810			2847[d], 2844[f]
δ_{COH} monomer	1358	1345	1342	1334	1366	1327			1335[d], 1336[f]
νmonomer	988	962	995	990	1021	1058			1034[d], 1034[f]

a: HF frequencies scaled by the factor 0.89 [16]. b: SCF convergence of 10^{-6}on elements of the density matrix, gradient convergence of 10^{-6} Hartree $bohr^{-1}$ and a 'high' integration grid quality. c; Frequencies were corrected for anharmonicity. Their final estimate for $\Delta\nu_{OH}$, after higher correlation and BSSE corrections, is $126cm^{-1}$.
d: Ar matrix [17,18]. e: gas-phase [19]. f: gas-phase [17,19]. g: force constant calculation [19].

Table 4.1: Calculated and experimental properties of isolated methanol and a methanol dimer [6]. Energies (ΔE) are in $kJmol^{-1}$, distance (r) in Å, dipole moments (μ) in Debye, angles in ° and frequencies (ν,δ) in cm^{-1}.

4.3 Structure of the titanium centres

In this section the following problems are considered,

- What is the most accurate model of Ti centres in zeolites, within the BP86/DZVP cluster approximation?
- What is the effect of hydration on the geometry and energies of Ti centres?

The aim of this work is not to engage in an exhaustive search of all possible Ti site conformations, but to provide a valid and robust model of Ti sites in molecular sieves, which can be used as the basis for all further mechanistic work. The energetics of formation of Ti sites in zeolites is not discussed here as this problem has been explored elsewhere [20]. All titanium models chosen for this work contain the metal in a 4+ oxidation state, with all but the titanyl model in tetrahedral coordination. Formation of such sites has been shown to be energetically viable elsewhere (see section 3.6).

In order to investigate the geometry and energetic stability of Ti sites in molecular sieves five structurally distinct Ti^{4+} clusters, proposed in the literature, have been modelled using the BP86/DZVP recipe. The first, a titanyl cluster ('=Ti=O') is considered to form in TiO_2-SiO_2 mixed oxides [21], during calcination. The Ti=O group, shown in figure 4.2 was suggested on the basis of comparisons with other transition metal oxide systems.

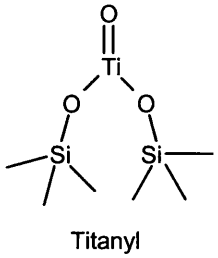

Figure 4.2: Suggested model of Ti sites in Ti zeolites

IR and NMR studies of TS-1 treated with labelled water show the formation of TiOH species [22]. It is thought that the Ti-O-Si(framework) bonds could reversibly

hydrolyse in the presence of water to form the TiOH groups. Thus, all possible combinations of the presence of TiOH groups have been studied, through calculation of a *monopodal* species with one anchoring Si-O-Ti linkage, a *bipodal* model with two anchoring Ti-O-Si linkages and a *tripodal* cluster with three anchoring Ti-O-Si linkages, figure 4.3.

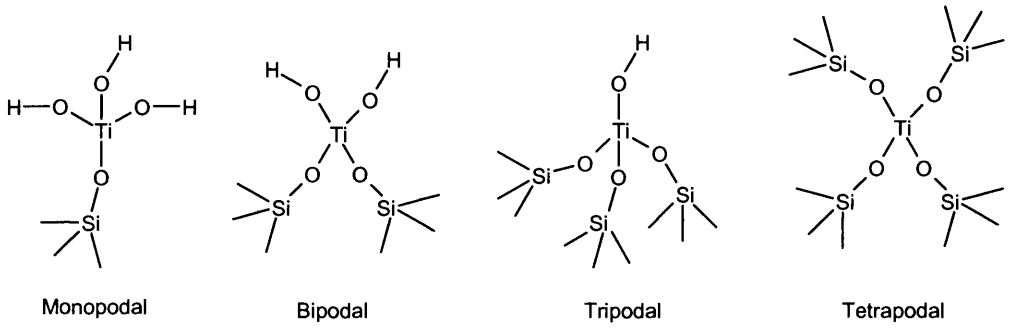

Figure 4.3: Models of Ti sites in Ti zeolites.

The final model to be studied is simply a tetrahedral Ti surrounded by four silanol groups, which is referred to as tetrapodal. This model is the initial configuration originally extracted from TS-1, as shown in figure 4.1. The tetrahedral coordination of Ti centres in dehydrated titanosilicates is unquestionable (see section 3.6, chapter 3), however the coordination of hydrated Ti centres in molecular sieves is uncertain.

A recent theoretical study by Sauer *et al.* [23] concluded that the relative stability of different Ti sites in microporous titanosilicates is substantially affected by the presence of water; suggesting that hydration should be taken into account when discussing Ti siting in zeolites. Considering historically, that most theoretical approaches and many experimental studies of titanosilicates have been on the dehydrated material, the hydration of Ti sites deserved consideration. All five clusters, shown in figure 4.2 and 4.3, have been optimised in the absence of water, with one molecule of water (referred to as *mono-aquo*) and with two molecules of water (*bis-aquo*). The water molecules were positioned so as to test the sensitivity of Ti to the presence of H_2O; i.e. the water oxygens were brought to a 2Å bonding distance of the metal with the protons pointing away from the centre of the pre-optimised cluster. Using chemical intuition, the water molecules were then rotated to

eliminate all hydrogen bonding interactions with surrounding ligands in the starting configuration, figure 4.4.

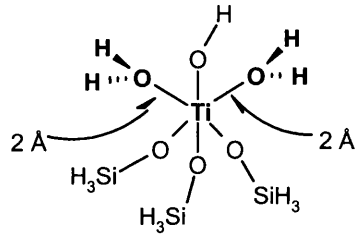

Figure 4.4: Positioning water molecules around a tetrahedral tripodal Ti site before relaxation of the resultant cluster.

The metal-ligand cluster and water molecules were then fully relaxed, apart from geometrical constraints placed on the xyz cartesian coordinates of the Si ions.

By using an interatomic potential based approach, such as Monte Carlo or molecular dynamics simulation, the Ti cluster could be completely immersed in water, with many spheres of hydration. In principle this could be a more computationally consistent way of exploring water coordination to the titanosilicate active sites. However, modelling such complex hydrogen bonding and proton transfer processes by potential models would require an extremely specialised forcefield and is outside the scope of this thesis. For more information on interatomic potential simulations of liquids the reader is referred to reference [24].

Figure 4.5 shows the BP86/DZVP optimised geometries, calculated energy differences and H_2O binding energies of the five clusters chosen as representative of Ti sites in porous titanosilicates. The optimised geometries of the hydrated structures shown in figure 4.5 are unlikely to be global energy minima due to the numerous conformations H_2O can adopt around a discrete cluster. However, the optimised geometries do compare well with experiment and other theoretical studies reported in table 4.2.

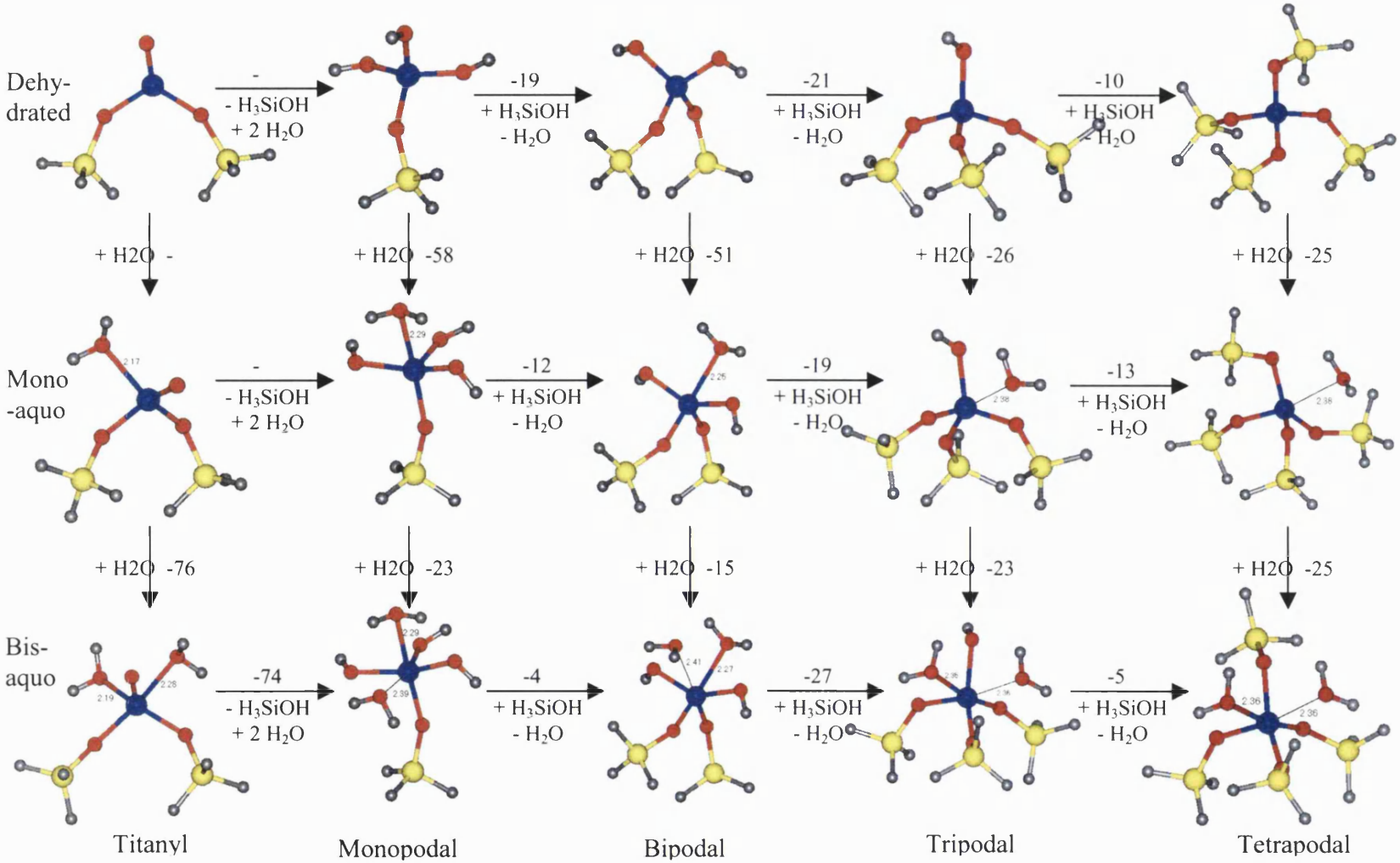

Figure 4.5 BP86/DZVP calculated geometries and Δ energies in $kJmol^{-1}$ for 5 different clusters representative of Ti active sites, with and without one and two molecules of water.

Reference	Species	Method	Coordination Number	Ti-O / Å	Ti-Si / Å	O-Si / Å	Ti-OH* / Å	Ti-O-Si / °
This work	$Ti(OSiH_3)_4$	DFT	4	1.81 - 1.82	3.20 - 3.41	1.68 - 1.69	N/A	131 - 155
	$Ti(OSiH_3)_3OH$		4	1.81 - 1.82	3.28 - 3.45	1.67 - 1.68	1.83	140 - 164
	$Ti(OSiH_2)_3(OH)_2$		4	1.81 - 1.82	3.26, 3.42	1.68, 1.68	1.82, 1.82	138, 157
	$Ti(OSiH_3)(OH)_3$		4	1.81	3.42	1.68	1.82 - 1.83	157
	$Ti(OSiH_3)(=O)$		3	1.84	3.35, 3.41	1.67, 1.68	1.64	145, 152
22	$H_8Ti_4Si_4O_{12}$	HF	4	1.79		1.65		150.8
	$Ti[Osi(OH)_3]_4$		4	1.79		1.63		146.5
	$Ti[OSi(OH)_3](HO)_3$		4	1.78 - 1.80		1.62 - 1.64		177
	$H_{12}TiSi_4O_{16}$ (ETS-10 model)		4	1.87 - 2.15		1.60-1.65		129 - 143
25	$Ti(OH)_4$	HF	4	1.81				
26	$Ti(OH)_4$	HF	4	1.83				
	$Ti[Osi(OH)_3]_4$		4	1.80				
27	TS-1 (Ti=1.47 wt %)	EXAFS	4.4 ± 0.6					
	TS-1 (Ti=2.03 wt %)		4.44 ± 0.25	1.79 ± 0.007				
28	$Ti(H_3SiO)_3(OH)$	DFT	4	1.81 - 1.82	3.35-3.42	1.67 - 1.68	1.82	148 - 158
	$Ti(H_3SiO)_2(OH)_2$		4	1.82		1.67 - 1.68	123-125	137 - 158
	$Ti(H_3SiO)_2(=O)$		3	1.85		1.66	1.65	
	$Ti(H_3SiO)_4$		4	1.81		1.68		144-153
29	Ti↑MCM41 (...SiO)$_3$TiOH	EXAFS		1.81	3.30			
30	Ti↑MCM41	EXAFS	4.1	1.82	3.19 - 3.37			138 - 160
	Ti↑Ge↑MCM41		3.8	1.81	3.19 - 3.34			139 - 158

Reference	Species	Method	Coordination Number	Ti-O / Å	Ti-Si / Å	O-Si / Å	Ti-OH* / Å	Ti-O-Si / °
31	Ti↑MCM41 (as prepared)	EXAFS	4.5	1.87				
	Ti↑MCM41 (calcined)		3.7	1.80				
	Ti↑MCM41 (during epoxidation)		4.6	1.82				
32	$Ti↑SiO_2$	EXAFS	4.1	1.83	3.18 - 3.34			134 - 152
	Ti↑MCM41		4.1	1.82	3.19 - 3.37			138 - 160
	Ti↑Ge↑MCM41		3.8	1.81	3.19 - 3.34			139 - 158
	Ti↑Sn↑MCM41		3.8	1.79	3.20 - 3.34			142 - 161
33	TS-1	XRD		1.79				
34-36	TS-1	EXAFS		1.80 - 1.81 ± 0.01				
37	TS-1	DFT		1.83		1.69 - 1.70		
38	$Ti(OSi)_4$	DFT	4	1.81				
	$Ti(OSi)_5$		5	1.84				
	$Ti(OSi)_4(=O)$		5	1.96 (ave.)			1.68	
	$Ti(OSi)_6$		6	1.96				
	SiO_4		4	1.65				
[Trong, 1992 #76]	TS-2 (Ti/Si=1.6%)	EXAFS/XANES	3.9	1.87	2.19			
	TS-2 (Ti/Si=4.2%)		3.6	1.89	2.19			
39	TS-1	EXAFS		1.81 ± 0.01				
40	Ti-JDF-L1	EXAFS	5	1.95 (Ti-OSi)			1.63	

Table 4.2 BP86/DZVP structural parameters of dehydrated Ti clusters, compared to literature values. *For the Ti=O models, this value inidicated is the Ti=O bond length

The total energy of each cluster with respect to the most stable configuration, the bis-aquo tetrapodal species (bottom right, figure 4.5), was calculated, so as to afford comparison of every configuration with each other; i.e the energy of the mono-aquo bipodal cluster was calculated to be $E = E_{mono\text{-}aquo\_bipodal} + 2E_{H3SiOH} - E_{H2O}$ (see figure 4.5). The normalised energy of all fifteen Ti-silicate clusters calculated is shown in figure 4.6, as an energy surface.

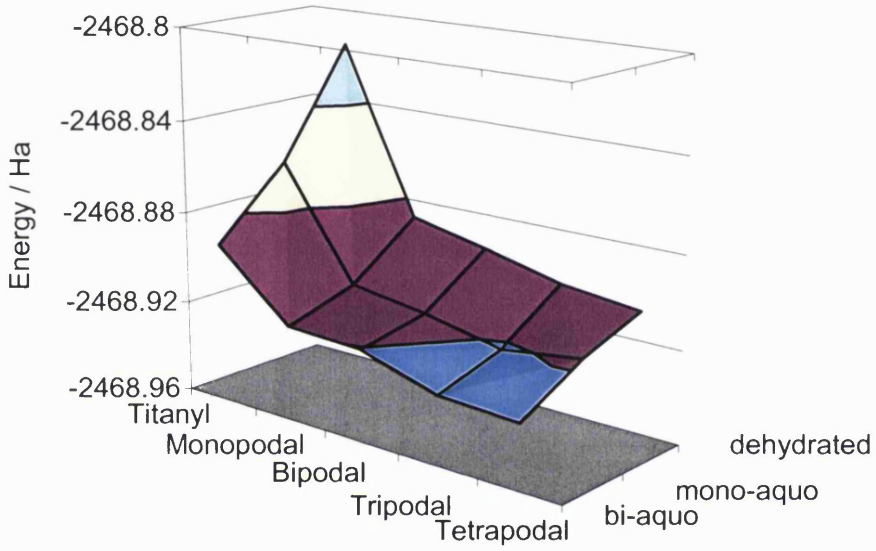

Figure 4.6 BP86/DZVP calculated energies of a number of dehydrated, mono-aquo and bis-aquo Ti clusters representative of the active sites in titanosilicates.

There are a number of points of interest of figure 4.6.

- For all five cluster types their energetic stability increases with the degree of hydration (dehydrated → bis-aquo).
- Regardless of the degree of hydration the titanyl cluster is markedly more unstable than all other configurations considered.
- The order of stability of Ti sites decreases: tetrapodal > tripodal > bipodal > monopodal >> titanyl for the dehydrated and bis-aquo series. For the mono-aquo series the order is altered slightly, in decreasing energetic stability: tripodal > tetrapodal > bipodal > monopodal >> titanyl.

- The most stable configurations are the bis-aquo tetrapodal cluster and the bis-aquo tripodal cluster (only 4kJmol^{-1} separates them).

4.3.1 Stability of Ti sites

The titanyl cluster is markedly less stable than the other four models considered, by between 74 - 191 kJmol^{-1}, depending on the degree of hydration. Thus, coupled with the fact that there is no UV-vis evidence for the existence of Ti=O groups in titanosilicates, I conclude that it is highly unlikely that titanyl groups will exist in Ti containing molecular sieves. If indeed titanyl species do exist, I suggest, in accordance with Sinclair *et al.*[41], that they will only form in hydrated media; the bis-aquo titanyl cluster was 117 kJmol^{-1} more stable than the dehydrated analogue. Moving on to the remaining four cluster models, we find that their energetic stability is reasonably similar, i.e. within 51 kJmol^{-1} for the dehydrated set, within 31 kJmol^{-1} for the mono-aquo set and within 35 kJmol^{-1} for the bis-aquo set. Of course, the Ti-O-Si bond breakage processes shown in figure 4.5 (from right to left, in rows) have been modelled using *isolated* silanol species (H_3SiOH); in an actual molecular sieve, these silanols would probably be stabilised by hydrogen bonds, figure 4.7.

Assuming that in the real system each silanol is involved in only one hydrogen bond and using the estimate of an H-bond as ~20 kJmol^{-1}, there is little difference in energy between the monopodal bipodal, tripodal and tetrapodal complexes.

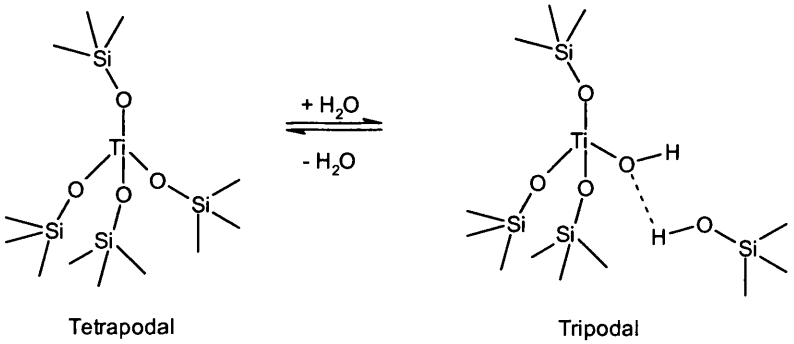

Figure 4.7: Potential hydrogen bonding (shown in red) between a broken and subsequently hydolysed Ti-O-Si bond in titanosilicates.

Considering the lack of metal leaching observed during catalysis, there is doubt over the viability of the monopodal model. Even though monopodal sites may well form in titanosilicates it is an unconvincing model of the catalytic active sites, since Ti-O-Si bonds are known to hydrolyse and breakage of the one anchoring Ti-O-Si bond would cause the metal to leach from the system. The bipodal, tripodal and tetrapodal species are therefore proposed to be stable in Ti embedded zeolites, in either a dehydrated or hydrated medium.

4.3.2 Hydration of Ti sites

In agreement with the work of Sauer[23] and others[42,43], hydration of tetrahedral Ti sites is found to be energetically favourable. Little can be inferred from the actual calculated binding energies of water, shown in figure 4.6, in different configurations, given the errors implicit in the cluster model. However, the calculated binding energies are of comparable magnitude to previous theoretically based estimates in the literature, table 4.3.

Model	Method	H_2O Binding energy / $kJmol^{-1}$	Ti-O^W / Å
This work	BP86/DZVP	15 - 59	2.25 – 2.41
$Ti(OSi\ldots)_4$[23]	QM/MM	6 – 62	2.26 – 2.40
Ti-chabasite[42]	Periodic HF	35	2.21 – 2.25
Various T4 Ti clusters[41]	BP86/DZVP	12 - 40	2.24 – 2.47

Table 4.3 Estimated binding energies of water to theoretical representations of Ti sites in molecular sieves. O^w indicates the oxygen atom in water.

The favourable comparison of our calculated binding energies of water to other theoretical studies shows that the cluster approach holds up well compared to the results of a periodic Hartree-Fock (HF) approach and a more computationally expensive QM/MM method. Considering the numerous conformations that H_2O

could adopt in this system, our clusters perform particularly well when comparing Ti-water bond lengths with the other theoretical studies aforementioned.

The binding energies of water to the tetrapodal, tripodal, bipodal and monopodal clusters are of a magnitude indicative of physisorption (< 60 $kJmol^{-1}$); and indicate that water is probably relatively mobile. Conversely, the binding energy of water to the titanyl complex is >120 $kJmol^{-1}$, suggestive of chemisorption. Since the titanyl cluster is so much higher in energy than the other complexes considered, the nature of the adsorption of H_2O on titanyl complexes will not be discussed here.

The calculations show that the addition of water causes the Ti coordination shell to expand. However, the relatively small binding energies of water to the metal suggest that the inclusion of water in titanosilicate studies is not essential. However, considering the kinetics of propene epoxidation have been reported to be retarded in the presence of water, the effect that water has on the geometry and electronic properties of Ti sites clearly needs to be examined.

4.3.2.1 Geometrical Considerations

The absorption of water on the titanium sites causes minimal change in the Ti-OSi bond lengths and an elongation of 0.05Å - 0.1Å in the Ti-OH bonds, figure 4.8.

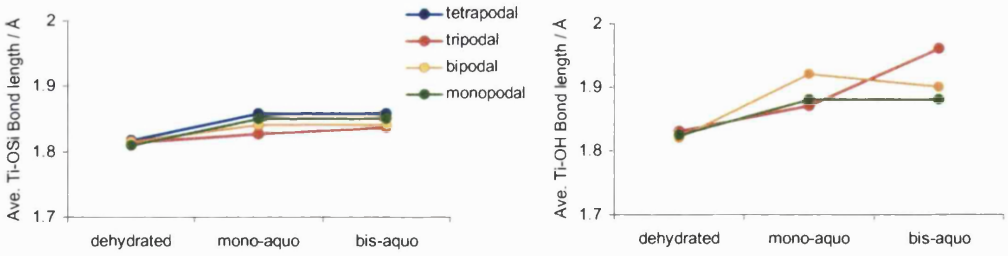

(a) (b

Figure 4.8 BP86/DZVP calculated (a) Ti-OSi and (b) Ti-OH bond lengths in Å for a number of tetrahedral Ti clusters during hydration with one and then two molecules of water (mono-aquo and bis-aquo respectively).

The lengthening of the Ti-OH bonds can be explained by hydrogen bonding between the water molecules and the hydroxyl ligand(s), figure 4.9. The Ti-OH bond in the

bis-aquo tripodal cluster (right, figure 4.9) is weakened by more than the bipodal (left, figure 4.9) and monopodal analogues due to two medium/strong H-bonding interactions on the same hydroxyl oxygen. The hydroxyl oxygens in the bis-aquo bipodal and monopodal complexes only engage in one hydrogen-bonding interaction with water each.

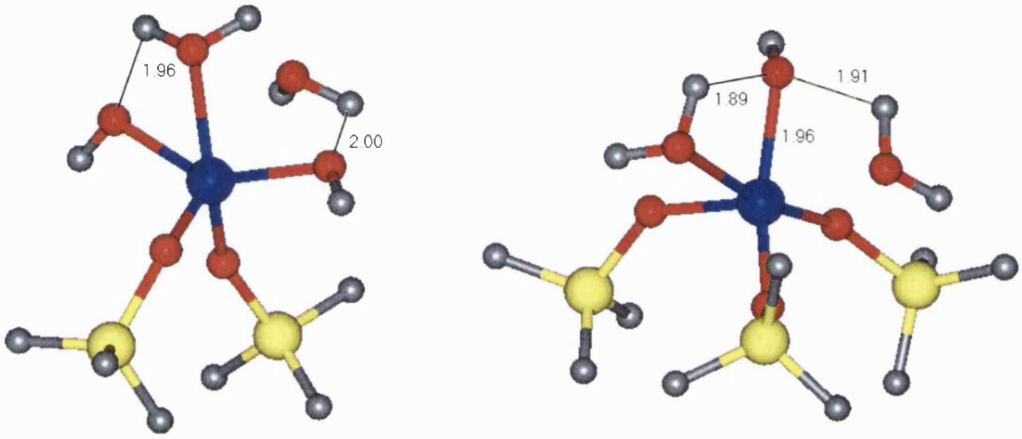

Figure 4.9 BP86/DZVP optimised geometries of bis-aquo bipodal (left) and bis-aquo tripodal (right) clusters, showing H-bonding between the water molecules and the hydroxyl ligand.

As was commented upon previously, the optimised geometries shown in figure 4.9 are unlikely to be global energy minima due to the numerous conformations H_2O can adopt around a discrete cluster. However, the calculations do suggest that TiOH groups will form hydrogen bonding interactions with H_2O, but considering the mobility of water we surmise that these bonds will break and form relatively easily. The calculations suggest that the TiOH bonds will fluctuate between ~ 1.8Å and 2.0Å but that the anchoring silanol bonds will remain stable under the mild reaction conditions employed in catalysis. I would like to stress, that if the tripodal and bipodal species were both to exist in a titanosilicate, the Ti-hydoxyl bond length would not necessarily be longer than in the bipodal active site. That observation holds for this study only and is relevant because the presence of water causes such an elongation in the TiOH bond lengths, the magnitude of which could be rationalised due to hydrogen bonding.

4.3.2.2 Electronic Considerations

Finally, the effect of the coordination of water on the electronic configuration of the different Ti cluster models is explored. Indeed figure 4.10 shows there to be little change in the partial charge of key ions, such as the metal (c) and its surrounding oxygen atoms (graphs a and b)

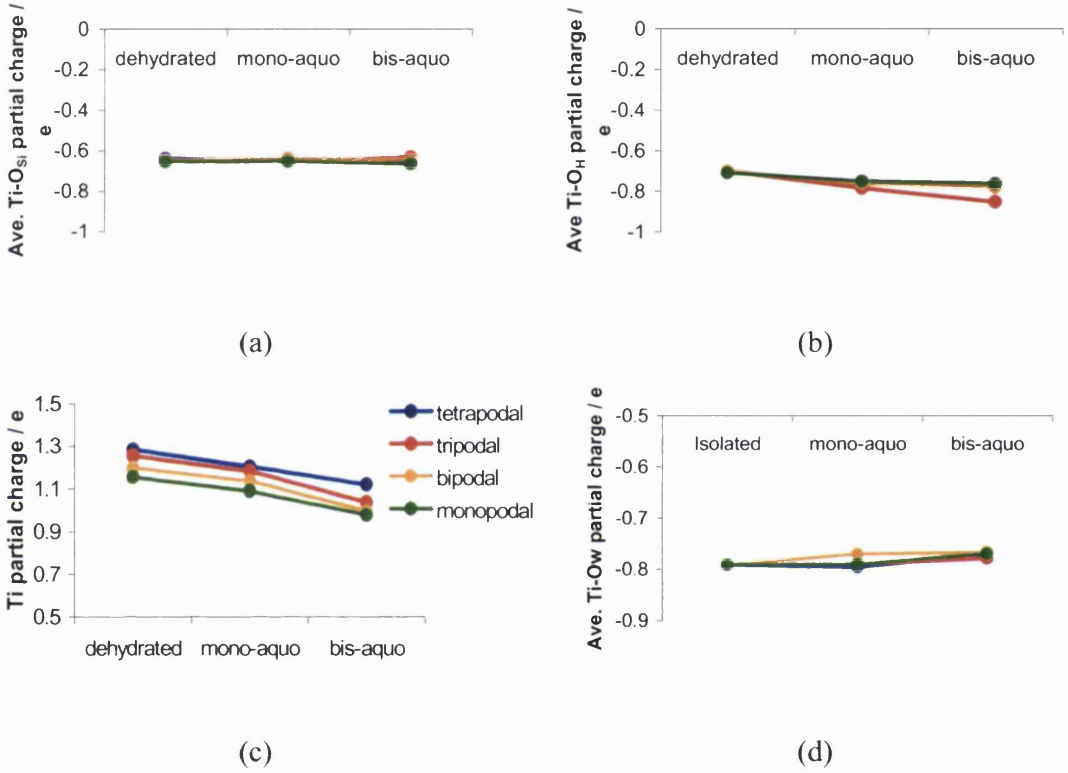

Figure 4.10 Average Mulliken partial charge of Ti-OSi oxygens (a), Ti-OH oxygens (b) Ti ions (c) and water oxygens (d) in Ti sites during hydration.

Each data point in graph *a* (except for the monopodal series), in graph *b* (except for the tripodal series) and the bis-aquo points in graph *d* is an average value. For example, there are three Ti-O-Si bonds in the tripodal cluster whose oxygen Mulliken charges are averaged to one point in chart (a). The approach is valid because the maximum deviation between the smallest and largest value for a single point is small, < 0.1electrons (e). The partial charge of the Ti ions is more positive as more water molecules are introduced. This deviation is ~ 0.1 e for all cluster types. Similarly the Mulliken partial charge of the TiOH oxygens becomes more

negative upon hydration, by ~ 0.1 e, which represents the decrease in electron donation from the hydroxyl oxygen to the metal's d orbitals upon interaction with water due to the weakening of the Ti-OH bond through $H_2O...HO$ hydrogen bonds.

In essence, the minimal change in the electronic configuration of the metal centre, the oxygen atoms of the metal ligands and the water oxygen atoms upon hydration supports the proposal that water binds relatively weakly to Ti sites in zeolites.

4.3.4 Conclusions

Optimised geometries and reaction energies for a number of clusters representative of Ti sites in zeolites, proposed in the literature have been calculated. The first question, which I have set out to address, is what is the most accurate model of Ti centres in zeolites, within the BP86/DZVP cluster approximation?

The titanyl model, which has been suggested as a representation of Ti sites in zeolites, is between 74 $kJmol^{-1}$ and 191 $kJmol^{-1}$ higher in energy than the monopodal, bipodal, tripodal and tetrapodal clusters. The latter four clusters, when taking into account probable hydrogen bonding between framework silanol groups and the Ti-OH ligands, are of similar energy, within 25 $kJmol^{-1}$ regardless of the degree of hydration. The BP86/DZVP calculated geometries for all the Ti clusters compare well with experiment and other theoretical studies where a larger portion of the silica zeolite framework has been included; thus the accuracy of our model holds up well. It is noted that the optimised cluster models, which include water, are unlikely to be global energy minima. In consideration of the fact that water does not bind tightly to the metal centre and has little effect on the geometry and electronic configuration of the metal complex I consider that the quoted energy differences between the five hydrated cluster types are still valid.

Given that the monopodal species has only one bond anchoring it to the zeolite framework and minimal metal leaching is observed in catalysis, this model is an unlikely representation of the active site. Thus, the bipodal, tripodal and tetrapodal clusters could all be stable and be the catalytically active sites in titanosilicates. Sinclair *et al.* have noted that it is unlikely that tetrapodal sites could

exist in surface grafted molecular sieves [28], thus in order to make this study applicable to all titanosilicates this cluster model will not be employed in further studies. Thus, we have chosen to employ the tripodal model for all future mechanistic work, as its three anchoring bonds would suggest the metal centre to be more stable than the bipodal species during catalysis. The stability of metal sites, shown by the abnormally low levels of Ti leaching during reaction, is one of the characteristic properties of Ti containing molecular sieve catalysts.

The second question I have sought to address, is what is the effect of hydration on the geometry and energies of Ti centres? In the presence of water, the expansion of tetrahedral sites to a coordination of 5 or 6 is found to be an energetically favourable process. The binding energies of water to the monopodal, bipodal, tripodal and tetrapodal species are of a magnitude indicative of physisorption (< 60 $kJmol^{-1}$). The preferential siting of water in order to create a distorted geometry has in fact no effect and I conclude that water only weakly binds to the active sites in Ti zeolites and does not need to be explicitly included in titanosilicate studies. Indeed the inclusion of water, in electronic structure calculations would incur an order of magnitude increase in the cost of the calculation, and may introduce a systematic error in a reaction energy profile due to the unrealistic static hydrogen bonds provided by a discrete number of water molecules.

Thus, all mechanistic studies reported here use the dehydrated tripodal cluster as the model of pre-reacted titanium centres in zeolites, figure 4.11.

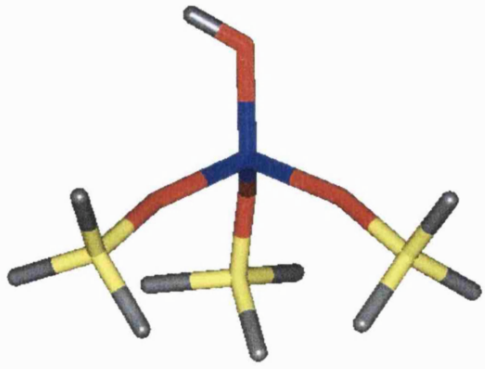

Figure 4.11. BP86/DZVP optimised geometry of a dehydrated tripodal cluster which we suggest to be representative of the active sites in Ti molecular sieves

4.4 Interaction with peroxide

The mechanism by which Ti containing molecular sieves reacting with hydroperoxide promote olefin oxidations such as the epoxidation of alkenes has been explained by the formation of titanium peroxo complexes. These Ti-peroxo species are stable intermediates with the ability to donate an oxygen ion to the alkene (or other small molecule organic substrate) thus facilitating epoxide formation

The formation of 'η^2' or side-bonded Ti-peroxo complexes in hydrogen peroxide doped TS-1 unquestionably occurs and has been observed through UV-Vis and ESR spectroscopy [44]. However, the exact nature, preferred coordination and role, as oxygen-donors, are unclear. By applying gradient corrected Density Functional Theory the formation of a number of structurally distinct Ti-peroxo complexes have been examined, starting with the η^2 and η^1 Ti-peroxo species shown in figure 4.12; both of which are extensively discussed in the titanosilicate literature (see section 3.9).

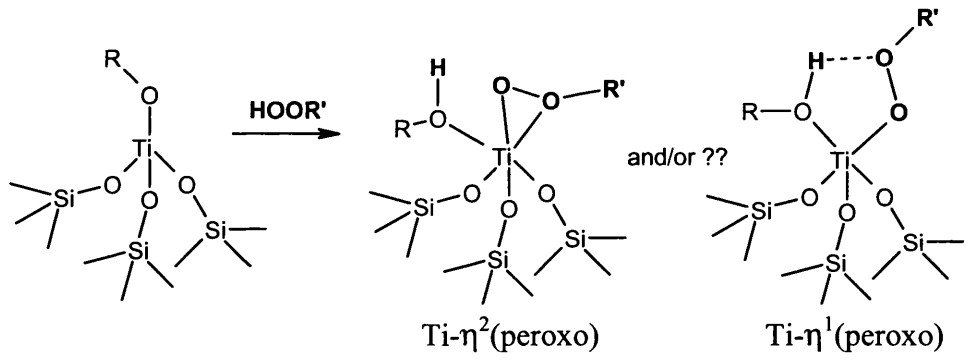

Figure 4.12: Literature proposed geometries of Ti-peroxo species in hydroperoxide doped Ti molecular sieves.

4.4.1. R groups

The reader will note the presence of R groups in figure 4.12 (not R', which represent the peroxide substituent). To date, derivatised porous titanosilicates (i.e. tetrahedral Ti-OR sites) can only be directly synthesised through grafting of Ti-OR species onto MCM-41. In hydrothermally *substituted* Ti-silicas the R groups are removed during calcination. However, is also thought highly likely that in metal substituted

microporous crystals, the Ti-OH or Ti-Si-O ligands will exchange for solvent species, i.e. if the solvent is methanol, the Ti-OH ligand would be replaced by Ti-OMe, forming of course Ti-OR species. Considering the unquestionable influence that the solvent has over reaction kinetics this proposal of direct solvent involvement with the catalytically active site is very plausible. Maschmeyer *et al.* showed that the nature of the R group in Ti-silisesquioxane/H_2O_2 mixtures has a direct effect on reaction kinetics for the epoxidation of alkenes (Ti-silsesquioxanes are molecular analogues of Ti containing molecular sieves). Thus, examining the effects of the R groups on titanosilicate energetics may provide valuable mechanistic insight and is therefore an integral part of this study.

The R groups used in this work have been chosen so as to examine any electronic or steric effects of these functional groups on the reaction pathways studied. Similar sized organic moieties, CH_3, CH_2F and CF_3 have been selected in order to examine electronic effects, with CH_3 in this case considered as neutral, CH_2F as electron withdrawing and CF_3 as highly electron withdrawing (electron withdrawing ligands are thought to retard the rates of epoxidation reactions). Furthermore, iso-butyl and tert-butyl groups have been selected to study the effect of sterically bulky ligands on reaction kinetics. Tert-butyl hydroperoxide (TBHP) is the most effective oxidant in Ti-mesoporous but is not reactive at all in Ti-microporous catalysts, such as TS-1. This is thought to be due to Ti active site inhibition by the presence of bulky peroxide in the sterically confined microporous silica. Finally, SiH_3, GeH_3 and SnH_3 ligands have been studied to see how reaction energetics may alter on descending group 14. Doping titanosilicates with germanium has been shown to increase reactivity, but, conversely, doping with tin is known to severely retard catalytic activity. The size and electron withdrawing nature of the R groups chosen are shown in table 4.4. The approximate size of the R group is measured by the Connolly surface area and the strength of the Ti-OR bond is indicated by the Ti-O bond length.

R group	Ti-OR Bond Length / Å	Connolly Surface Area / Å^2
H	1.827	23.08
CH_3	1.803	41.9
CH_2F	1.83	49.71
CF_3	1.88	61.56
iso-butyl	1.808	100.64
tert-butyl	1.793	99.05
SiH_3	1.82	59.26
GeH3	1.802	74.27
SnH_3	1.788	55.1

Table 4.4: Size and electron withdrawing/electron donating properties of a number of R groups.

4.4.2 η^2 Ti-peroxo complexes

Figure 4.13 shows the BP86/DZVP calculated reaction profile for the formation of the η^2 Ti-peroxo intermediate from the reaction between H_2O_2 and a 'Ti-OR' tetrahedral cluster.

4.4.2.1 The η^2 transition State

The most difficult part of calculating any reaction pathway is the determination of the transition state. The transition state associated with the Ti-η^2(OOH) product (with R = H incidentally) has been proposed previously [41]. However, verification of whether the transition state proposed was actually that associated with the Ti-η^2(OOH) product and the suggested reactant was outside the scope of that particular study. In this section this uncertainty is addressed directly. At the saddle point, the intrinsic reaction coordinate (IRC) is coincident with the dominant negative eigenvalue of the Hessian matrix. On either side of the saddle point is the steepest-

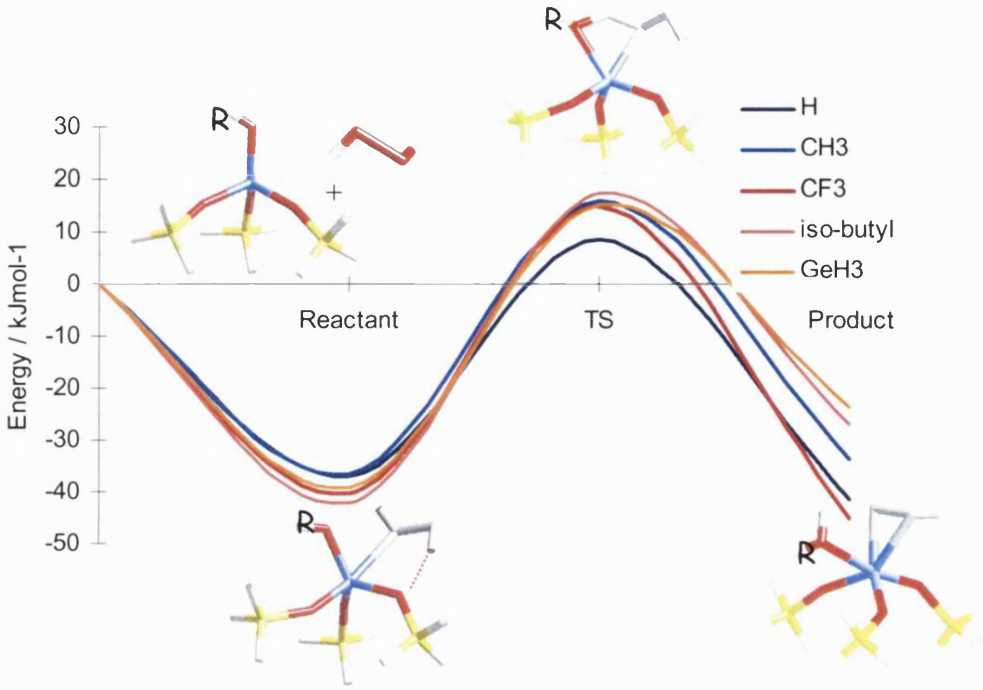

Figure 4.13 BP86/DZVP calculated reaction profiles for the formation of derivatised Ti-η^2(peroxo species) from the reaction between H_2O_2 and a 'Ti-OR' tetrahedral cluster. After reaction, the peroxide is highlighted in grey.

descent path from the saddle point to the reactants and products, see section 2.5.1, Chapter 2 for more details on IRCs. Thus, if the transition state for a reaction is known, one can trace the associated reactant and product by sliding from the maximum down the appropriate side of the potential energy surface in the direction given by the single dominant imaginary vibrational mode.

Thus, firstly the η^2 transition state has been calculated from coordinates provided to us by Dr Phil Sinclair of the Royal Institution of Great Britain. Modelling of transition states is slightly more complicated than usual in this work due to the presence of geometric constraints imposed on the Si ions. Constraints also give rise to negative eigenvalues in a 2nd derivative calculation. However, these should be minor compared to the imaginary wavenumbers associated with the transition state. Thus, all transition states characterised in this work have a single *dominant* negative eigenvalue. The BP86/DZVP calculated vibrational wavenumbers for the Ti-η^2(peroxo) TS (where R=H, incidentally) are shown below.

Vibrational Intensities

Mode	Freq	Intens-au
1	-875.21	0.4708
2	-101.13	0.0001
3	-62.84	0.0002
4	-55.28	0.0001
5	-39.82	0.0027
12	10.74	0.0005
13	33.65	0.0014
14	49.88	0.0004
15	60.21	0.0008

The reader will clearly see that one negative frequency is dominant, over eight times larger, than any of the others. Note that the intensity also clearly indicates the presence of one dominant vibration, reflected by the fact that the lowest frequency vibration is over 170 times more intense than any other vibration.

Now that the transition state has been determined, the all important direction in which one slides down the potential energy surface to the associated reactant and product well can be resolved. Most visualisation modelling packages allow vibrational modes to be viewed in three dimensions and we have used Oxford Molecular's UniChem [45] software, the dedicated viewer for DGauss output, to animate the dominant negative vibrational eigenmode. The negative eigenvalue is found to be a peroxidic hydrogen atom stretch from the peroxide fragment to the Ti-OR functionality and vice versa, figure 4.14.

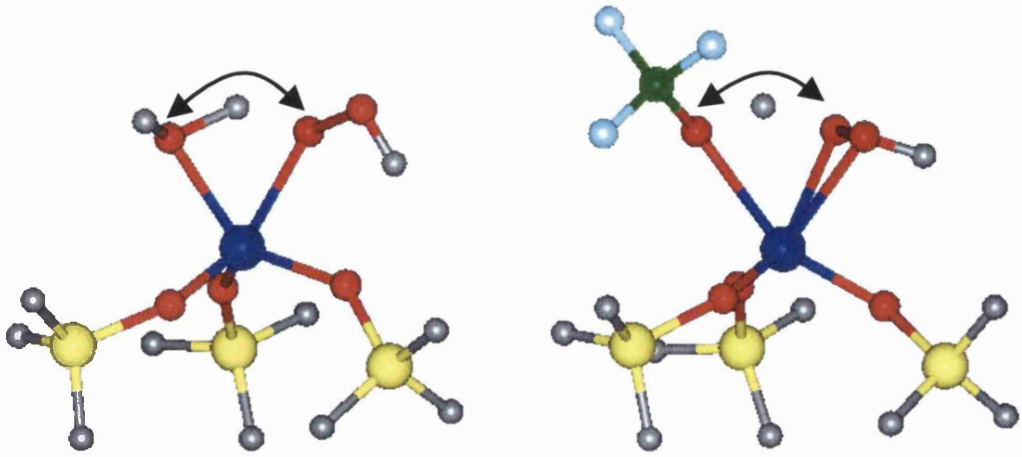

Figure 4.14 BP68/DZVP optimised η^2 transition states for R = H (left) and R = CF_3 (right). The arrow shows the direction of the single dominant imaginary vibrational eigenvalue, which is associated with hydrogen atom vibration.

This result is chemically sensible as the reaction process is the binding of a peroxide molecule to the metal cluster which the transition state represents. Animating the other negative eigenvalues allows one to check that the remaining imaginary frequencies are undeniably due to the constraints imposed on the Si ions. Indeed, they are found to be due to O-Si twists.

Given that the vibrational mode indicative of the reaction pathway has been found (the peroxidic hydrogen atom vibration), this information can be used to form starting geometries for associated reactant and product determination. If the hydrogen atom (figure 4.14) is moved manually towards the peroxide and the resultant structure minimised, the associated reactant should be found and likewise if the hydrogen atom is moved towards the Ti-OR ligand the corresponding product structure should be found. It is important not to move the hydrogen atom too far from the TS position, otherwise the wrong pathway could be taken during optimisation (because of the highly complex nature of the potential energy surface). This procedure was used to verify the reaction profile shown in figure 4.13 and all subsequent mechanistic pathways presented in this chapter. We did indeed find that the transition state presented by Sinclair *et al.* was that associated with the Ti-

η^2(OOH) product. However, our work indicates a different reactant conformation from that found in their work, notably in the orientation of the peroxide.

4.4.2.2 The η^2 reactant

Initial attack of the peroxide on the central Ti cation involves formation of a strong hydrogen bond between the peroxidic hydrogen atom and an oxygen atom of one of the anchoring silanol groups, shown by a red dotted line in figure 4.13. The second peroxidic hydrogen atom then forms a hydrogen bond with the Ti-OR oxygen. The binding energy of peroxide to the tetrahedral Ti-OR complex, for all R groups, is ~40 kJmol^{-1} directly accountable by the fact that two hydrogen bonds are formed; the energy of a hydrogen bond is assumed to be ~ 20 kJmol^{-1}, figure 4.15.

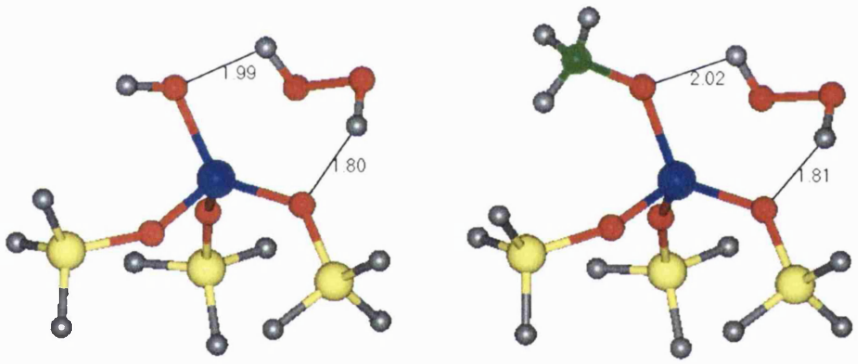

Figure 4.15 η^2 reactant for R = H (left) and R = CH_3 (right) clusters, showing the presence of 2 stabilising hydrogen bonds.

4.4.2.3 Reaction energetics

The similarity in the binding energies for all the R groups suggests that the nature of the R functionality has little effect on the ability of peroxide to bind to the metal cluster, which is of interest since there is a question over the ability of peroxide to gain access to the Ti sites when bulky ligands, such as iso-butyl are present. The iso-butyl and tert-butyl moieties are found to bend back away from the peroxide as it binds to the cluster causing no interference with this process.

Figure 4.14 shows that the transition state for R = CF_3 is much closer to the product than the R = H transition state is, and indeed all of the R groups which strongly resemble the R=H TS in their geometry. This is to be expected since the strongly electron withdrawing CF_3 functionality substantially weakens the Ti-OR bond, a weakening that is observed for all of the Ti-OR bonds and is most pronounced in the formation of the product, figure 4.16.

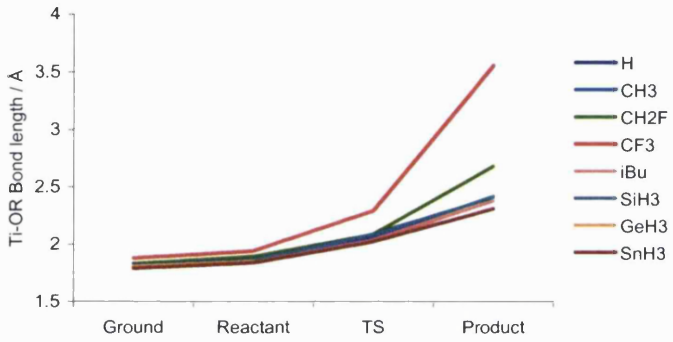

Figure 4.16 Changes in the Ti-OR bond length along the η^2 Ti-peroxo formation pathway, for a number of different R groups.

The activation barrier is less than 60 $kJmol^{-1}$ for all R groups studied which is comparable to previous theoretical studies of R = H clusters by a number of other groups. However, the reaction profile for all R groups, which include a sterically bulky and a highly electron withdrawing ligand, are very similar. Thus, the nature of the R group does not seem to have a considerable effect on the accessibility of the η^2 metal-peroxo intermediate, which could indicate that either,

- η^2 Ti-peroxo species are not the oxygen donating species
- η^2 Ti-peroxo species are the oxygen donating species but their formation is not the rate determining step
- The model is failing.

4.4.3 Ti-η^1(OOR) Formation

Figure 4.17 shows the calculated reaction profile for the formation of the η^1 Ti-peroxo intermediate.

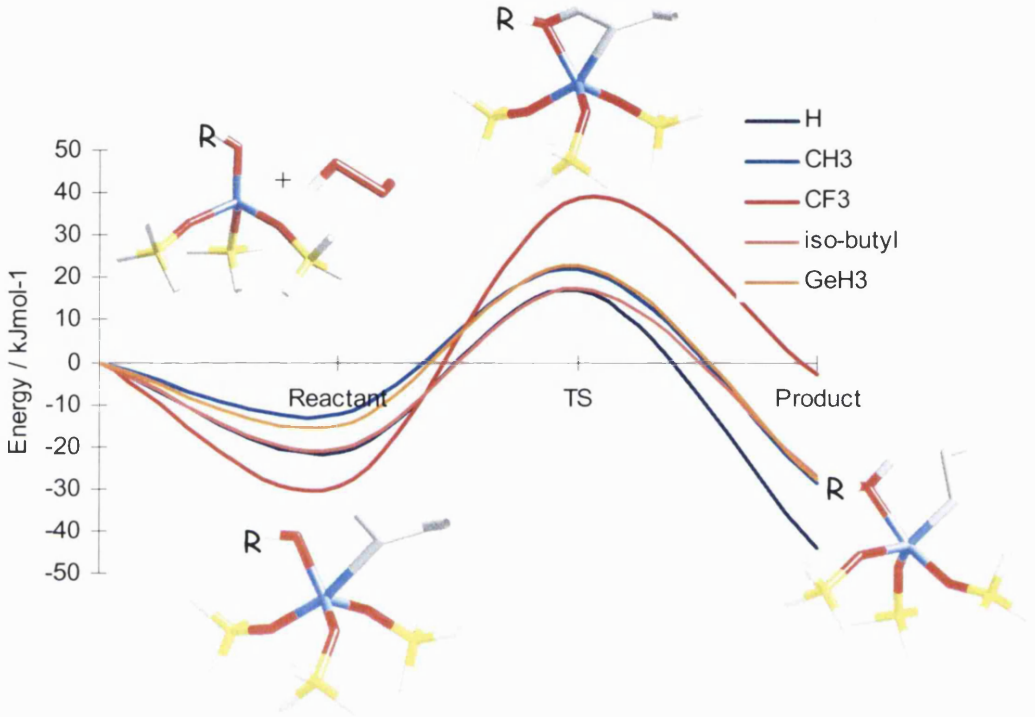

Figure 4.17: BP86/DZVP calculated reaction pathway for the formation of a Ti-η^1(peroxo) cluster from the interaction between H_2O_2 and a 'Ti-OR' complex, for a number of different R groups.

Again a primary aim of this work was to determine the transition state of the 5 membered ring η^1 Ti-peroxo complex proposed in the literature, which to the best of our knowledge has not been reported elsewhere. There are a number of automated techniques for finding transition states, however due to the complexity of the problem, chemical intuition is often the most efficient. In this instance, the 5 membered ring *product* was initially optimised (shown in figure 4.17). Since the η^1 reactant geometry is unlikely to differ substantially from the η^2 analogue, a model was manually constructed that was approximately a mid-point between the known η^2 reactant and the optimised 5 membered ring product. The geometry of the starting

structure was verified to be chemically reasonable by insuring that the bond lengths and angles were within the range typical for a titanosilicate system.

Using the same criteria as used in the previous section, the η^1 transition state was located and again verified by the presence of a single dominant negative eigenvalue. Considering the striking difference in the geometry of the η^2 and η^1 products it is notable that their transition states are remarkably similar, differing only in the orientation of the peroxide, as is shown in figure 4.18.

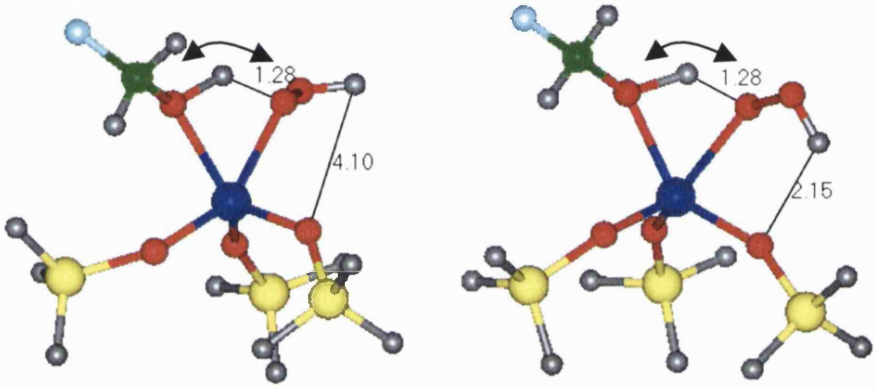

η^1 TS η^2 TS

Figure 4.18. DZVP/BP86 optimised geometries of the η^1 and η^2 transition states, with R = CH_2F. The double arrow indicates the direction of the single dominant negative eigenvalue. The nearest neighbour peroxide hydrogen atom and the silanol group are 4.10Å and 2.15Å apart for the η^1 and η^2 respectively.

It is clear that there is no hydrogen bonding between the peroxidic hydrogen atom and one of the silanol bonds in the η^1 transition state. As found in the previous mechanism, the dominant negative eigenvalue is associated with the hydrogen atom vibration between the peroxide and OR ligand.

Again, the activation barrier for the formation of the Ti-η^1(peroxo) intermediate is low, less than 50kJmol^{-1} for all R groups, except for the CF_3 functionality. Previous estimates in the literature for R = H clusters have put the activation barrier for η^1 Ti-peroxo formation in excess of 100 kJmol^{-1}. Indeed, this fact has been used by a number of commentators as reasoning to dismiss the Ti-η^1(peroxo) as a viable oxygen donating species. However our calculations clearly

suggest that the transition state could easily be overcome under the reaction conditions used.

As in the previous section, the transition state has been used to calculate the intrinsic reaction coordinate for the η^1 mechanism. Using this technique has confirmed that the transition state shown in figure 4.17 is that associated with the 5 membered ring product and the reactant for this particular reaction pathway. The interaction of the peroxide with the metal centre is not as strong as the corresponding interaction for the η^2 mechanism, shown by the smaller binding energies, between 8 $kJmol^{-1}$ and 29 $kJmol^{-1}$ (figure 4.17). This can be attributed to the loss of a hydrogen bond between the peroxide hydrogen atom and the silanol oxygen atom in the η^1 reactant in comparison to the η^2 reactant.

4.4.3.1 R-group effects

The reader will note that contrary to the effects noted in the η^2 mechanism the R-group does influence the η^1 reaction pathway energetics, which is underlined by the disparity in the product energies, shown in figure 4.17.

Figure 4.19 shows the difference in geometry between the less energetically stable R = CF_3 η^1 product and the more stable R = CH_3 η^1 product. The highly electron withdrawing CF_3 group moves away from the central Ti ion and forms the alcohol which remains in the coordination sphere due to hydrogen bonding between the alcohol oxygen and the peroxidic hydrogen atom.

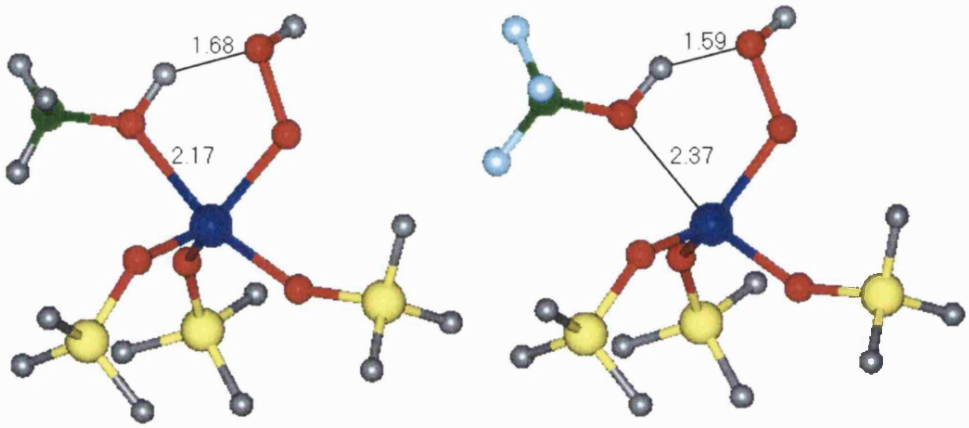

Figure 4.19 BP86/DZVP optimised R = CH_3 (left) and R = CF_3 (right) η^1 Ti-peroxo products.

Unlike the η^2 mechanism, figure 4.17 shows that R groups *do* influence the reaction energies for the formation of the η^1 Ti-peroxo product. This observation is highly significant since a large number of studies have documented the effect that R groups have on catalytic kinetics and any viable mechanism must account for these experimental observations. It is also clear from experiment that electron withdrawing substituents retard the catalytic activity in epoxidation reactions and the high activation barrier in the η^1 mechanism for R = CF_3 is consistent with this observation. It is difficult to rationalise how an electron withdrawing group would retard the catalytic reactivity in the η^2 mechanism considering the minimal effect that all the R groups have been demonstrated to have on the reaction pathway energetics. Furthermore, considering the activation barrier is < 50 $kJmol^{-1}$ for all R groups studied, except the CF_3 functionality of course, the Ti-η^1(peroxo) complex is a plausible model for the oxygen donating species in Ti containing molecular sieves.

For both mechanisms there are two further points of interest. Firstly, at no point in either of the R = iso-butyl or R = tert-butyl reaction pathways did the C_4 organic functionality inhibit access to the metal active site. Secondly, entirely consistent with experimental observations there is no titanium leaching, i.e. the Ti-

OSi bonds are not substantially weakened upon interaction with peroxide, with an average Ti-OSi fluctuation of 0.05Å and maximum fluctuation of 0.1Å.

4.4.4 Proton Transfer Processes

Of course the η^1 and η^2 Ti-peroxo complexes presented are modelled in vacuum and in reality they would be immersed in a medium of H_2O and peroxide; an environment where proton transfer can easily occur. In order to investigate the energetics of H-transfer the hydrogen acceptor (see figure 4.20) has been manually moved to the adjacent peroxidic oxygen donor, and the resultant structure relaxed.

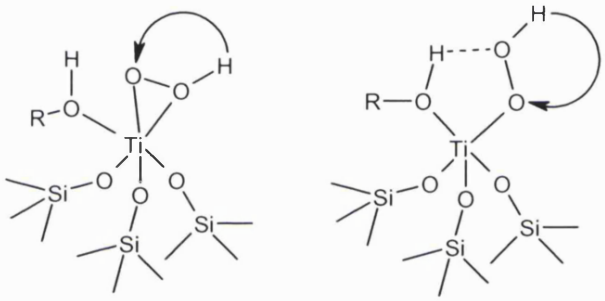

Figure 4.20 Modelling the effects of an H_2O/H_2O_2 medium through proton transfer.

For the η^2 species manual proton transfer resulted in rotation of the side-bonded –OOH fragment back to the original structure, indicating the η^2 complex would be stable in a polar medium. However, for the η^1 case, movement of the hydrogen acceptor resulted in a new stable Ti-peroxo intermediate (figure 4.21), which to the best of our knowledge is not documented elsewhere.

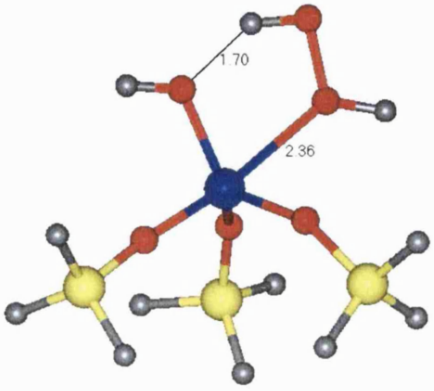

Figure 4.21: Optimised geometry of a new, stable Ti-peroxo structure.

The reader will note that, contrary to the two mechanisms discussed previously, here the peroxide remains intact when binding to the metal cluster. The geometry is stabilised by a hydrogen bond between the peroxide and the OR group, of length 1.70Å. The Ti-peroxo species in figure 4.21. is referred to as 'Ti-η^1[O(H)OH]'. The energetics of proton transfer from the peroxidic oxygen furthest from the metal (i.e. the η^1 complex) to the peroxidic oxygen closest to the Ti, thus forming the Ti-η^1[O(H)OH] complex can be easily charted. Constructing the starting geometry of the transition state of such a simple process, such as proton transfer, is relatively straightforward and the optimised transition state, characterised by one dominant negative vibrational frequency, is shown in figure 4.22, along with the corresponding reactant and product species.

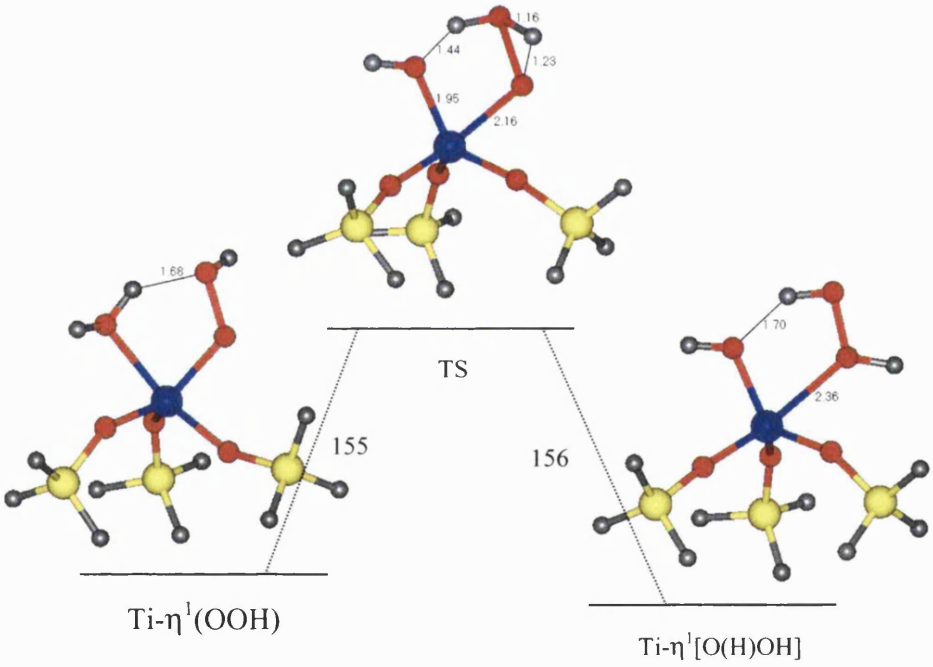

Figure 4.22: BP86/DZVP calculated reaction pathway and optimised geometries for the proton transfer between two peroxidic oxygens on an η^1 Ti-peroxo complex.

The activation barrier of 155 kJmol^{-1} clearly cannot be surmounted under the mild reaction conditions employed for catalysis and I hypothesise that if indeed this process occurs then it must be mediated by H_2O, H_2O_2 or ^-OOH species. However,

the Ti-η^1[O(H)OH] may indeed form from the interaction of peroxide with Ti sites and may not be just a facet of proton transfer within the η^1 species. We will now explore the activation energy and mechanism for the formation of Ti-η^1[O(H)OH] species for a number of R groups.

4.4.5 Ti-η^1[O(H)OH] formation

Figure 4.23 shows the formation of the Ti-η^1[O(H)OH] intermediate from the interaction of H_2O_2 with a 'Ti-OR' cluster for a number of different R groups.

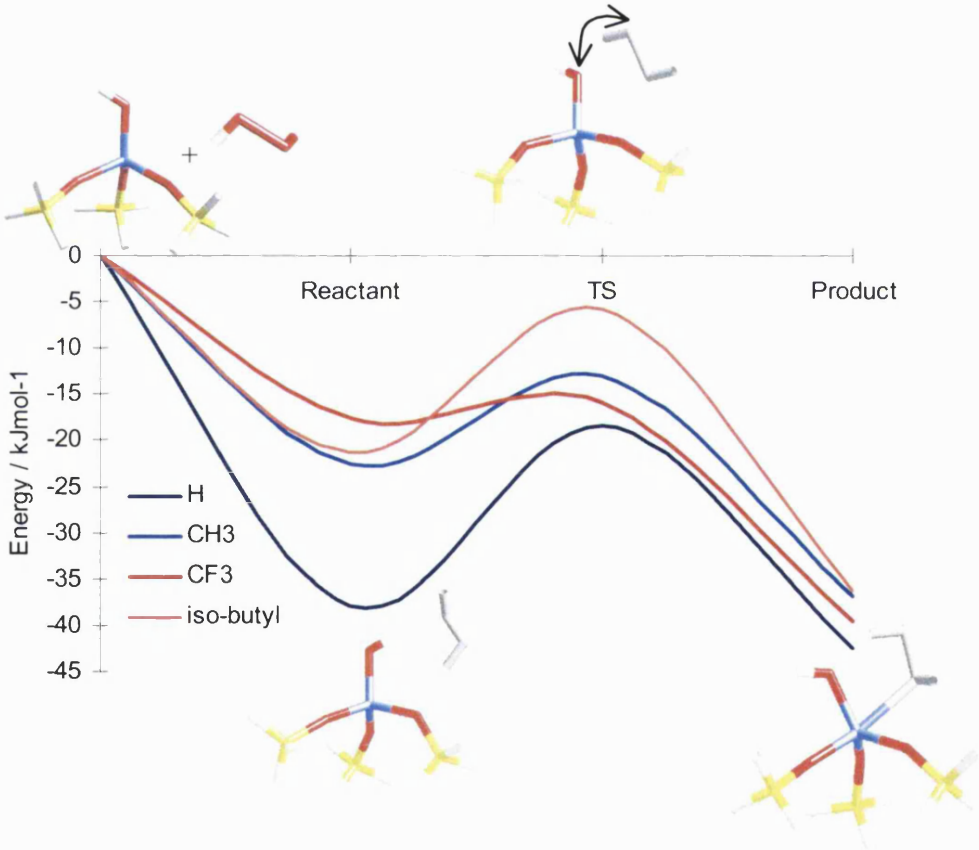

Figure 4.22 BP86/DZVP calculated reaction pathway for the formation of a number of R derivatised Ti-η^1[O(H)OH] complexes. The peroxide is emphasised in grey after it has reacted. The arrow indicates the direction of the single dominant eigenmode characterising the transition state.

Firstly, the binding energy of the peroxide to the Ti cluster when R=H is ~20 kJmol^{-1} greater than for the other R functionalities. Figure 4.23 shows the two

closest points of interaction between the peroxide and the Ti cluster. The additional H-bond between the Ti-OR ligand and peroxide for the R = H cluster is signified by the binding energy being ~20 $kJmol^{-1}$ greater than for all other R groups considered. There is little conformational or chemical change in the peroxide throughout the reaction pathway and the activation barrier for each R group is < 20 $kJmol^{-1}$. This energy barrier is easily surmountable under the reaction conditions employed for catalysis.

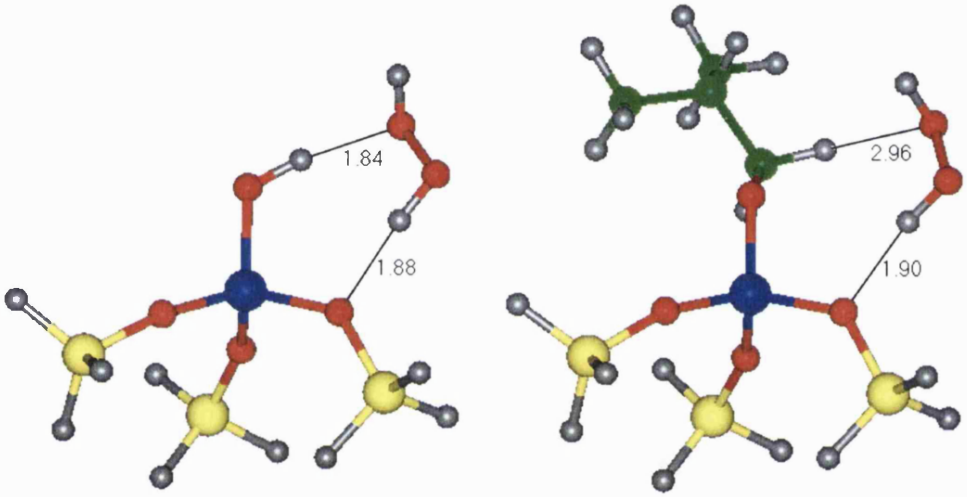

Figure 4.24 BP86/DZVP optimised Ti-η^1[O(H)OH] reactant for R = H (left) and R = iso-butyl (right).

The transition state has been characterised by one dominant negative eigenvalue and was constructed, again through chemical intuition. Once again the dominant imaginary frequency is associated with a hydrogen atom stretch from the peroxide to the OR ligand. The calculated vibrational frequencies for the Ti-η^1[O(H)OH] transition state are shown below, taken from the DGauss output.

Infrared Vibrational Intensities

Mode	Freq	Intens-au.
1	-218.24	0.1328
2	-46.17	0.0022
8	0.13	0.0001
9	10.18	0.0001
10	20.12	0.0011

One can clearly see that there is just one dominant negative wavenumber, which is two magnitudes greater in intensity than the other negative mode. The fact that there is only one other negative vibration arising from the constraints placed on the Si ions suggests there to be little strain on the silanol bonds in the transition state. This is unsurprising as the peroxide molecule does not significantly distort the metal cluster, either in the reactant or the transition state, figure 4.23.

4.4.6 Conclusions

The aim of this section was to explore the energetics of formation of two Ti-peroxo species proposed in the literature, a side-bonded or Ti-η^2(OOH) complex and the other a 5 membered ring Ti-η^1(OOH) complex. In addition, the effect of R groups on all the calculated reaction pathways was also explored. Complete reaction profiles for the interaction of H_2O_2 with a Ti-OR dehydrated tripodal cluster to form the η^2 and, separately, the η^1 product have been calculated using the BP86/DZVP recipe. Furthermore, while exploring the effect that peroxidic proton transfer may have on the stability of the two aforementioned Ti-peroxo clusters, we have isolated a new, stable and undocumented Ti-peroxo complex, referred to as Ti-η^1[O(H)OH]. The reaction profile for the formation of such a cluster has also been calculated for a number of R groups. Table 4.5 shows the actual calculated peroxide binding energies and activation barriers for each of the three stable Ti-peroxo complexes considered.

R	Peroxide Binding Energy / kJmol^{-1}			Activation Energy / kJmol^{-1}		
	Ti-η^2(OOH)	Ti-η^1(OOH)	Ti-η^1[O(H)OH]	Ti-η^2(OOH)	Ti-η^1(OOH)	Ti-η^1[O(H)OH]
H	-37	-22	-38	46	38	19
CH_3	-37	-12	-26	53	34	10
CH_2F	-36	-20	-21	55	44	12
CF_3	-40	-29	-18	55	68	2
Iso-butyl	-42	-20	-21	60	38	16
Tert-butyl	-19	-19	-39	43	-	-
SiH_3	-30	-8	-18	55		4
SnH_3	-39	-15	-20	55	38	-
GeH_3	-30	-8	-20	52	37	7

Table 4.5 BP86/DZVP calculated energies for the formation of three structurally distinct Ti-peroxo complexes for a number of R groups.

For all three mechanisms the interaction of peroxide with the tripodal Ti cluster is a energetically favourable process, as shown by the negative binding energies and the activation barriers are reachable under reaction conditions. The activation barriers for the η^2 mechanism compare reasonably well with previous estimates of 56 kJmol^{-1} for a tripodal Ti-OH cluster and H_2O_2 [41]. However, the activation barrier of the η^1 mechanism is considerably lower than estimates in the literature of > 100 kJmol^{-1} [38], and this is, to the best of my knowledge, the first time the transition state for the five membered ring complex has been isolated.

By calculating the intrinsic reaction coordinate of each mechanism the progress of the interaction of H_2O_2 with the tripodal cluster, to the transition state and down hill to the desired product has been charted. IRC calculations are very time consuming, but ensuring that the transition structure is indeed the true and desired transition state is imperative in obtaining meaningful reaction energies.

I therefore, suggest that the Ti-η^2(OOH), Ti-η^1(OOH) and Ti-η^1[O(H)OH] complexes will all form in the pores of titanosilicates under reaction conditions with H_2O_2 and will be stable. However, turning to R group effects, the nature of R groups does not have an appreciable effect on the energetics of the η^2 complex. This is

because the OR ligand is only weakly coordinated to the Ti centre and within bonding distance of the peroxide moiety. Considering that R groups are known to effect epoxidation kinetics, I suggest that either,

- the formation of Ti-peroxo species is not the rate determining step or
- Ti-η^1(OOH) and Ti-η^1[O(H)OH] complexes and *not* Ti-η^2(OOH) species are the oxygen-donating agents for catalysis.

The initial aim of this work was to explore just two Ti-peroxo models proposed in the literature. This study is now expanded to include a number of other possible Ti-peroxo representations proposed in the literature.

4.4.7 Other Ti-peroxo species

Ti-$\eta^2(O_2)$ radicals are observed in a number of discrete, Ti-$\eta^2(O_2)(L_4)$ molecules, where L = Ligand, and have subsequently been suggested as representative of the oxygen-donating species in titanosilicates [46]. The anionic analogues of the Ti-η^2(OOH) and Ti-η^1(OOH) complexes extensively discussed previously are also possible models of the oxygen-donating agents in titanosilicates. However, considering the activation barrier for removal of a peroxidic hydrogen atom and subsequent transfer to the adjacent peroxide oxygen atom on the η^1 structure was calculated to be 155 kJmol^{-1} in section 4.3.3, the stability of a Ti-$\eta^1(OO^-)$ anion is unlikely. The Ti-$\eta^2(O_2)$ radical and Ti-$\eta^2(OO^-)$ and Ti-η^1(OO-) anions are shown schematically in figure 4.24. It should be noted that in this section only the R = H clusters are considered.

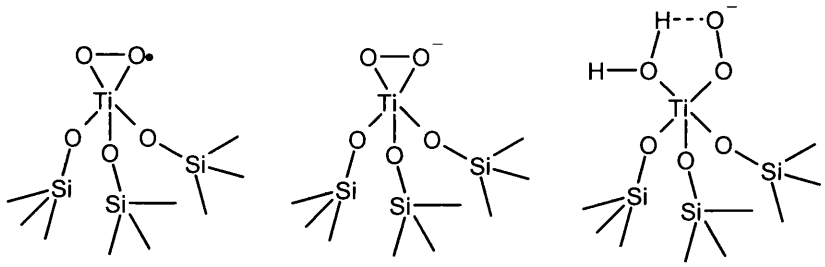

Figure 4.24: Radical and anion Ti-peroxo complexes suggested as models of the oxygen-donating species in titanosilicates.

The reader will note that for all three structures in figure 4.24 the titanium is five coordinate as indeed it is in the Ti-η^1(OOH) model (section 4.4.3) and the Ti-η^1[O(H)OH] model (section 4.4.5). As has been previously shown in section 4.3, titanium sites do expand their coordination sphere to six in the presence of water, through weak H_2O binding to the metal cluster. Thus, in a similar approach to that presented in section 4.3, all of the Ti-peroxo clusters mentioned thus far (except for the Ti-η^2(OOH) model, the reason which will be explained later) have been optimised with one molecule of water within bonding distance of the Ti centre. Using chemical intuition, one molecule of water has been docked at a 2Å from the Ti centre, with the H_2O oxygen orientated closest to the metal with the hydrogen atoms pointing away from the centre of the cluster. The water molecule was then rotated so as to eliminate any hydrogen bonding interactions in the starting geometry that could influence the course of optimisation.

In the case of the Ti-η^2(OOH) model (section 4.4.2) the Ti is already in octahedral coordination due to the side-bonding of the peroxide to the metal, thus in this case we have removed the O(H)R ligand, where R = H to explore the stability of this structure in a dehydrated environment (see figure 4.25).

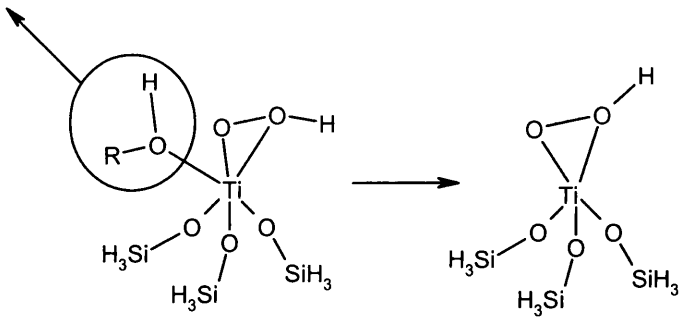

Figure 4.25: Modelling the Ti-η^2(OOH) cluster in dehydrated conditions, i.e. where the Ti ions are five coordinate.

The BP86/DZVP energy minimised geometries for the following structures have been calculated.

- Ti-$\eta^2(O_2)$ radical, Ti-$\eta^1(OO^-)$ anion and the Ti-$\eta^2(OO^-)$ anion, figure 4.24, both with and without one molecule of water.
- Ti-η^2(OOH) cluster with removal of the O(H)R ligand, figure 4.25.
- Ti-η^1(OOH) and Ti-η^1[O(H)OH] complexes with one molecule of water, figure 4.19 and figure 4.21 respectively, but with R = H.

The reaction energy for the formation of each cluster from the interaction between H_2O_2 and a tripodal Ti-OH cluster have been calculated for all the combinations described above. Thus the reaction energy (ΔE) for the formation of a hydrated Ti-$\eta^2(O_2)$ radical species from attack of H_2O_2 to a tripodal Ti-OH was calculated as follows:

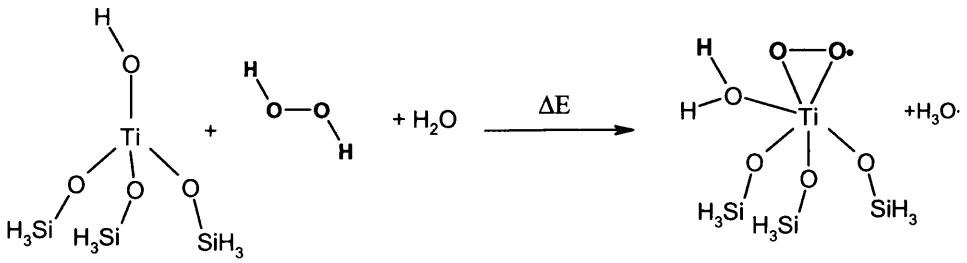

All calculated ΔE have been compared to the analogous reaction energies for the 6 coordinate Ti-η^2(OOH) cluster discussed in section 4.4.2, the five coordinate Ti-

η^1(OOH), discussed in section 4.4.3 and the five coordinate Ti-η^1[O(H)OH] cluster, analysed in section 4.4.5 and the results are shown in figure 4.26.

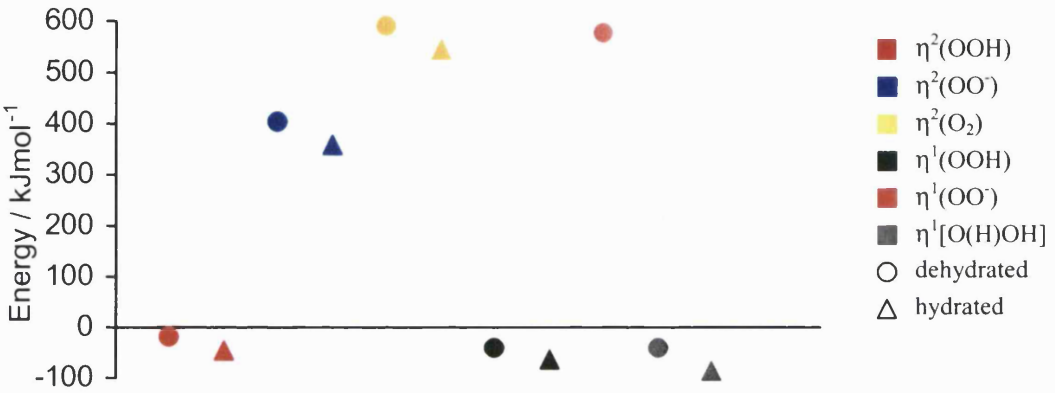

Figure 4.26. BP86/DZVP optimised reaction energies for the formation of a number of Ti-peroxo complexes, calculated with and without one molecule of water.

The x axis, positioned at 0 kJmol^{-1} in figure 4.26 represents the energy of the reactants. Thus any point above the x axis shows a Ti-peroxo species which is less stable than the reactants (an endothermic process) and any point above the x axis represents a Ti-peroxo complex which is more stable than the reactants (an exothermic process)

There are a number of points of interest shown in figure 4.26:

1) Regardless of the degree of hydration the DFT calculated Ti-η^2(O_2) radical, the Ti-η^1(OO^-) anion and Ti-η^2(OO^-) anion are > 300 kJmol^{-1} higher in energy than the reactants; a tripodal Ti-OH cluster, H_2O_2 and H_2O.
2) Again regardless of the degree of hydration, the BP86/DZVP optimised Ti-η^2(OOH), Ti-η^1(OOH), Ti-η^1[O(HOH] are lower in energy than the reactants.
3) For all Ti-peroxo models studied, the hydrated or 6 coordinate analogue is the most stable.
4) The binding energies of water to each cluster (calculated by subtracting the energy of the hydrated cluster from the sum of the dehydrated counterpart and isolated water) are < 50 kJmol^{-1}.

Turning to point 1, the Ti-η^1(OO-) anion was correctly surmised to be unstable with respect to the reactants due to the large 155 kJmol^{-1} activation barrier calculated for proton transfer within the cluster η^1(OOH). Formation of this anion requires +576 kJmol^{-1}. The fact that formation of the hydrated and dehydrated Ti-η^2(O_2) radical model is +357 kJmol^{-1} and +403 kJmol^{-1} respectively more unstable than the reactants give rise to considerable doubt with respect to a number of early epoxidation mechanisms reported [46]. Interestingly, Ti-η^2(O_2) radicals are known to be stable in the liquid phase.

The binding energies of water to all the models are small (table 4.6) with a magnitude which is again indicative of physisorption. The introduction of water to the metal-peroxo complexes does not significantly distort the geometry. Indeed, just as was observed for unreacted Ti sites in section 4.3, water weakly binds to the Ti centres, the interaction being stabilised through hydrogen bonds with the other ligands.

Model	Binding Energy of Water / kJmol^{-1}
Ti-η^2(O_2)	25
Ti-η^2(OOH)	45
Ti-η^2(OO^-)	46
Ti-η^1(OOH)	24
Ti-η^1(OO^-)	45
Ti-η^1[O(H)OH]	45

Table 4.6 BP86/DZVP calculated binding energies of water to a number of Ti-peroxo complexes.

4.4.8 Conclusion

DFT cluster calculations on six different representations of Ti-peroxo species in H_2O_2/titanosilicate mixtures, five proposed of which are in the literature and one documented here for the first time, strongly suggest that Ti-η^2(OOH), Ti-η^1(OOH)

and Ti-η^1(O(H)OH) will form in the pores of Ti molecular sieves with H_2O_2, with a preferential coordination number of 6. Water, however, will only weakly coordinate to the metal centre and, consistent with our work on the hydration of pre-reacted Ti centres, can be considered as mobile with fluctional hydrogen bonds to the peroxide and OR ligands. Calculation of a number of other Ti-peroxo representations, a Ti-η^2(O_2) radical, Ti-η^2(OO^-) and Ti-η^1(OO^-) anion, show their formation to be over 300 $kJmol^{-1}$ higher in energy than their reactants. Thus I suggest that these models are relatively poor representatives of the oxygen-donating species in titanosilicates.

Ti-η^2(OOH), Ti-η^1(OOH) and Ti-η^1[O(H)OH] complexes are proposed to form in the pores of titanosilicates and in the case of the latter two, will expand their coordination number to 6 in the presence of water. All three models have been shown to be between 19 $kJmol^{-1}$ and 87 $kJmol^{-1}$ more stable than the reactants (H_2O_2 + H_2O + tripodal Ti-OH site) and the activation barriers for formation are < 60 $kJmol^{-1}$. In order to test this hypothesis, the models have been compared to Extended X-ray Absorption Fine Structure (EXAFS) analysis of a TBHP/Ti-MCM41 catalyst.

4.4.9 TBHP/Ti-MCM41 EXAFS

The stationary point structures of all Ti-peroxo models discussed in the last section have been used, in turn, as starting point for the refinement of Ti K-edge EXAFS of Ti-MCM41 exposed to tert butyl hydroperoxide (TBHP). The data were collected and analysis performed by Dr G. Sankar and Dr. D. Gleeson of the Royal Institution of Great Britain. The R factor is a measure of how close a theoretical model is to the experimental data: the lower the value the closer the fit. The R factors of each Ti-peroxo model employed in the experimental analysis is shown in table 4.7.

	Dehydrated	Hydrated
Ti-η^2(OOH)	25	16
Ti-η^1(OOH)	21	16
Ti-η^1[O(H)OH]	26	26
Ti-η^2(O_2^-)	19	19
Ti-η^2(OO^-)	28	27
Ti-η^1(OO^-)	21	-

Table 4.7: EXAFS R factors for a number of different Ti-peroxo DFT optimised structures.

Full multiple scattering calculations were performed for each of the 12 structures. The 6 coordinate DFT calculated Ti-η^2(OOH) complex and the 6 coordinate Ti-η^1(OOH) species are in excellent agreement with the experimental data, indicated by the small R factor of 16. The respective Fourier transforms for theory and experiment for the 6 coordinate Ti(η^2-OOH) cluster are shown in figure 4.27.

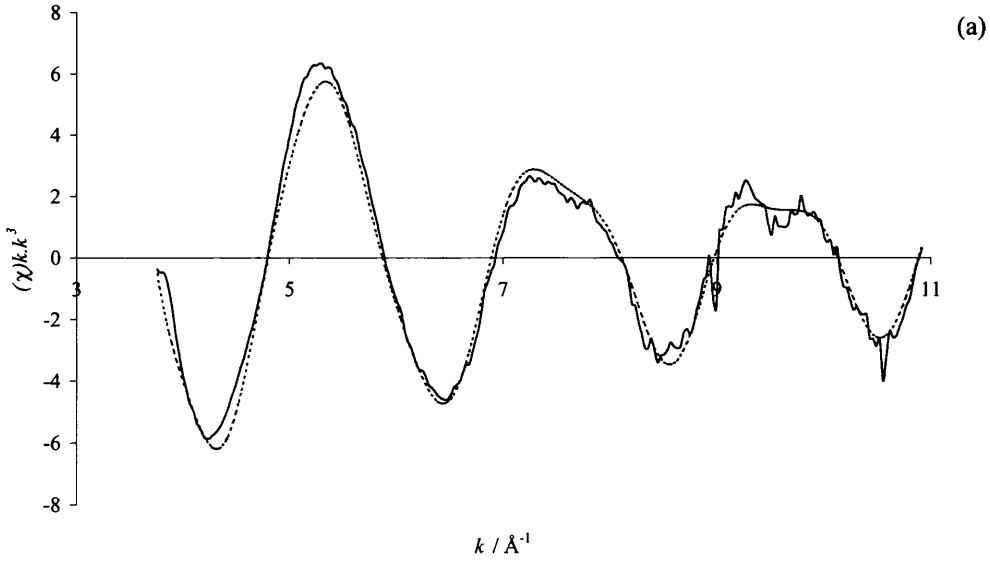

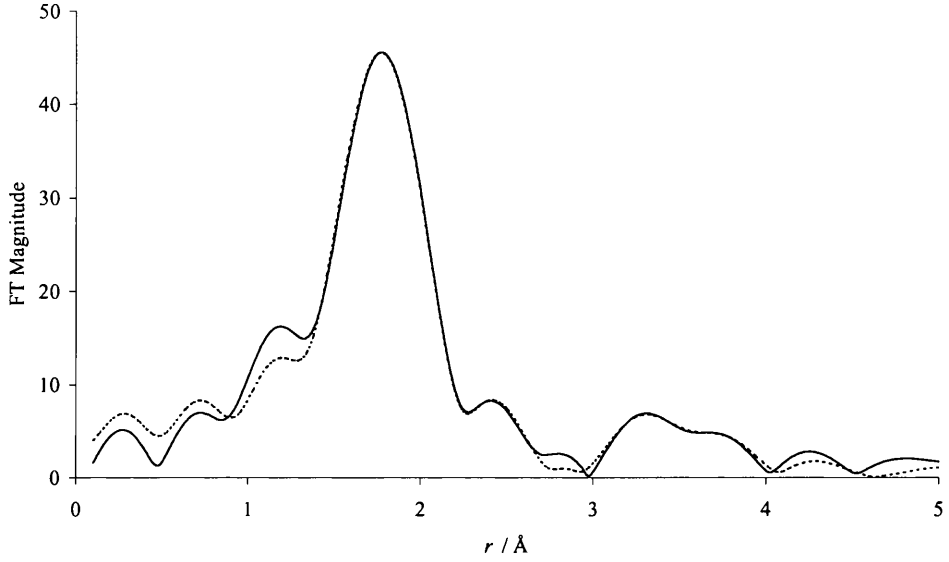

Figure 4.27. Ti-K edge EXAFS best fit (a) and associated Fourier Transform (b) for Ti-MCM41 catalyst using the DFT optimised Ti-η^2(OOH) model as the starting structure for refinement.

The favourable fit to experiment for both the 6 coordinate η^1 and η^2 Ti-OOH species is highly significant, since it strongly suggests that these two models are representative of Ti-peroxo in Ti-MCM41. This finding is entirely consistent with the theoretical prediction that 6 coordinate Ti(η^2-OOH) and Ti-η^1(OOH) species are likely to exist in titanosilicates under reaction conditions. The DFT optimised geometries and select theoretical and experimental geometrical parameters for both oxygen-donating species observed by EXAFS is shown in figure 4.28.

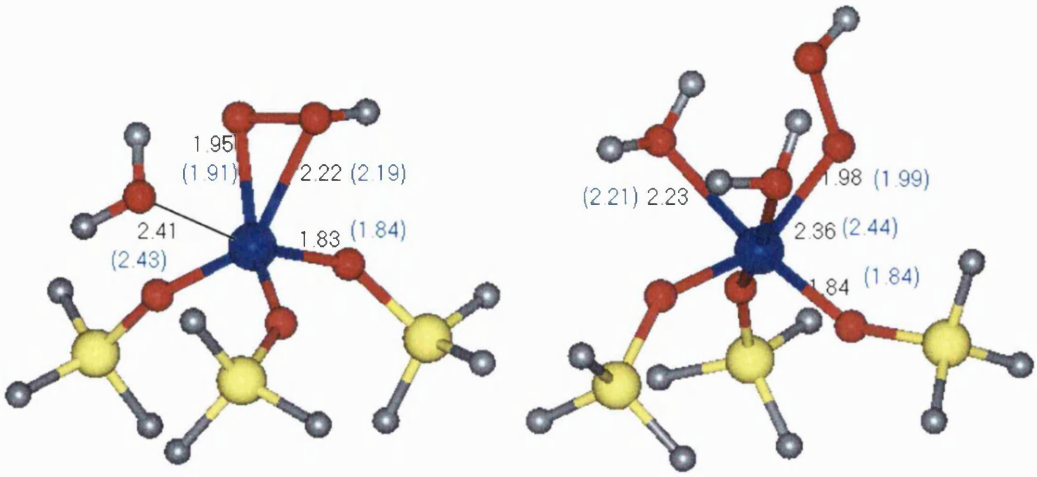

Figure 4.28: BP86/DZVP optimised geometries (in black) and experimentally derived parameters (in blue), for 6-coordinate Ti-η^2(OOH), shown left and Ti-η^1(OOH), shown right, complexes.

Of particular interest in table 4.7 is the observation that both the *5 coordinate* analogue of the Ti-η^2(OOH) complex and the Ti-η^1(OOH) species compares unfavourably with the experimental data (R-factors of 25 and 21 respectively). Even though our DFT calculations predict these structures to be stable, they are not found in the active catalyst, which is consistent with the widely held view, strongly supported by this work, that Ti centres will be six coordinate in a hydrated or peroxide rich medium.

Moving on to the remaining eight Ti-peroxo models studied. Consistent with our theoretical predictions, analysis of the experimental data shows that both 5 and 6 coordinate Ti-η^2(O_2) radical, Ti-η^2(OO^-) anion and Ti-η^1(OO^-) complexes are not found in TBHP/Ti↑MCM-41 catalysts, indicated by the high R factors. Note that the R factor is used as a measure of how good a theoretical model fits to the experiment data. For example, the latter three models aforementioned, resulted in a large discrepancy between the experimental and DFT calculated spectra and yielded unphysical structural parameters, in particular with regard to Debye-Waller factors and bond angles.

Finally, the Ti-η^1[O(H)OH] complex, which was predicted to exist in titanosilicate/peroxide mixtures and be stable, was found to fit unsuccessfully to the

experimental data, with R factors of 26 for both the hydrated and dehydrated species. The reader will recall that, in this model, the peroxide molecule remained intact upon binding to the metal cluster and we surmise that in reaction conditions the peroxide will be mobile and no stable interaction as we suggested in section 4.4.5 will actually form. This result highlights the limitations of the cluster approach in modelling complex systems and mechanisms.

4.4.9.1 DFT models with TBHP

In comparing the small BP86/DZVP cluster models with experimental EXAFS data of a TBHP exposed Ti-MCM41 catalysts two assumptions have been made.

1. The tert-butyl substituent in the experimental system does not influence the geometry of the oxygen-donating species.
2. The geometry of DFT models is not unduly distorted by the constraints imposed on the Si ions.

In order to achieve a more realistic comparison of our BP86/DZVP optimised models with experiment, the 5 and 6 coordinate Ti-η^2(OOH), Ti-η^1(OOH) and Ti-η^1[O(H)OH] complexes have been calculated employing TBHP as the peroxide. For each species the peroxidic hydrogen atom (which it will be recalled from section 4.4.2 and 4.4.3 was found not to within bonding distance to the OR ligand) has been replaced by a tert-butyl functionality and the resultant geometry optimised using the BP86/DZVP recipe. These six particular Ti-peroxo species were chosen since the peroxide substitutent is an integral part of the complex.

In agreement with our previous studies employing H_2O_2 as the sacrificial oxidant, only the 6 coordinate Ti(η^2-OO^{t}Bu) and Ti(η^1-OO^{t}Bu) clusters fit well to the experimental data, with R factors of 16 and 15 respectively. Little difference, both energetically as well as structurally, was found between the DFT calculated Ti-peroxo complexes, considered when employing the computationally expensive TBHP as the sacrificial oxidant, and those using H_2O_2.

4.4.9.2 Extending the model

EXAFS spectroscopy probes the local structure around the Ti centres and is accurate for the 1st and 2nd coordination shell. In order to verify that the constraints imposed throughout this work on the 2nd coordination shell Si ions do not affect the comparison of the DFT calculated models to experiment, the 6 coordinate Ti(η^1-OOH) and Ti(η^2-OOH), observed by experiment, have been calculated using a larger cluster size, extending to the 3rd coordination shell from the central metal ion. Only two of the complexes considered were re-optimised with an extended cluster size due to the computationally demanding nature of the calculations involved. Further details regarding the theoretical approach adopted here can be found in section 4.2.

The BP86/DNP optimised extended 6 coordinate Ti(η^1-OOH) and Ti(η^2-OOH) were optimised and the resultant geometry used as the starting models for refinement of the EXAFS data. Minimal change in either the structure or fit to experiment was found when employing the extended cluster model compared with the more computationally efficient clusters, which encompass just the first two coordination spheres around the central Ti ion. Thus I conclude that inclusion of the third shell of oxygens around Ti centres is not necessary when comparing cluster models to titanosilicate EXAFS data `

4.5 Summary

In this chapter the structure and stability of a number of Ti^{4+} configurations, which have been proposed in the literature as representative of Ti sites in zeolites has been explored. The effect of water on the stability, geometry and electronic configuration of these metal centres has also been discussed. The findings were as follows,

- The monopodal, bipodal, tripodal and tetrapodal models are of similar energy (when hydrogen bonding between the Ti-OH ligands and the zeolite framework is taken into account). However the titanyl model was 74 $kJmol^{-1}$ – 191 $kJmol^{-1}$ higher in energy than the other four models (section 4.3.1).

- The introduction of water was favourable with binding energies of 15 – 59 kJmol^{-1}. This was accountable due to hydrogen bonding with the Ti ligands but inclusion of water had little effect on the Ti site geometry or electronic configuration (section 4.3.2).

Due to the representation of water being static, where as in fact it would be mobile, I suggest that inclusion of water would be more computationally expensive and would lead to errors in reaction energies. Thus, a dehydrated tripodal model was chosen for all further work presented here. Tripodal because the monopodal model seems unlikely with only one framework anchoring bond and the tetrapodal is thought not to form in grafted Ti molecular sieves. The bipodal cluster is a very plausible model but since it only has two anchoring bonds and the tripodal complex has three, the latter was favoured. Furthermore, mechanistic studies regarding the epoxidation of alkenes employing the bipodal cluster, have been reported elsewhere [41].

Using the dehydrated tripodal model of Ti sites in zeolites the oxidation of titanosilicates with hydrogen peroxide has been explored, with specific regard to the effect that R groups have on reaction pathways.

- Formation of side-bonded Ti-η^2(OOH) (section 4.4.2) and five-membered ring Ti-η^2(OOH) (section 4.4.3) complexes as proposed in the literature and a Ti-η^1[O(H)OH] complex (section 4.4.5) isolated by this work is favourable with activation barriers of < 50 kJmol^{-1}, < 60 kJmol^{-1} and < 30 kJmol^{-1} respectively.
- 6 coordinate Ti-η^2(OOH) and Ti-η^1(OOH) were indeed found to exist in Ti-MCM41/TBHP mixtures as shown by EXAFS (section 4.4.9).
- All Ti-peroxo studied are more stable when 6 coordinate, by the inclusion of water (section 4.4.7).
- Formation of Ti-η^2(O_2) complexes was shown require > 300 kJmol^{-1} in energy and no evidence for there existence were found in the EXAFS analysis (section 4.4.7).
- The nature of R groups influenced the reaction pathway energetics for the formation of the Ti-η^1(OOH) model but not the Ti-η^2(OOH).
- Sterically bulky ligands such as iso-butyl did not inhibit access to the Ti centres.

Using a relatively simple cluster model approach the presence of Ti-η^2(OOH) and Ti-η^1(OOH) complexes, shown in figure 4.28, has been correctly predicted. Since R groups were found to effect reaction kinetics in the formation profile of the Ti-η^1(OOH) complex and not the Ti-η^2(OOH) cluster (the R group-activity relationship is a well observed phenomena) we predict that the η^1 Ti-peroxo cluster is the oxygen-donating specie in titanosilicates.

In Chapter 5 the reaction between alkenes (ethene and propene will both be examined) and the Ti-η^2(OOH) and Ti-η^1(OOH) species, shown to exist in this chapter, to form epoxides, will be explored. Again the affect that R groups have on reaction kinetics and the ability for the epoxidation mechanism to regenerate the original catalyst will be discussed in detail.

4.6 References

(1) Sankar, G.; Thomas, J. M.; Catlow, C. R. A.; Barker, C. M.; Glesson, D.; Kaltsoyannis, N. *J. Phys. Chem. B* **2001**, *105*, 9028 - 9030.

(2) Barker, C. M.; D.Gleeson; Sankar, G.; Kaltsoyannis, N.; Catlow, C. R. A.; Thomas, J. M. *Accepted in Phys. Chem. Chem. Phys.* **2001**.

(3) DGauss; Oxford Molecular Inc In; 4.1 ed.: Cambridge.

(4) DMol; Molecular Simulations Inc In; 4.2 ed.: San Diego.

(5) Cerius2; Molecular Simulations Inc. In; 4.2 ed.: San Diego.

(6) Sinclair, P. E. In *Department of Chemistry*; University College London: London, 1997.

(7) Becke, A. *Phys. Rev. A* **1988**, *38*, 3098.

(8) Perdew, J.; Wang, Y. *Phys. Rev. B.* **1986**, *33*, 8800.

(9) Vosko, S.; Wilk, L.; Nusair, W. *Can. J. Phys.* **1980**, *58*, 1200.

(10) Alonso, J.; Balbas, L.; Rubio, A. *Int. J. Quant. Chem.* **1995**, *56*, 697.

(11) Pudzianowski, A. *J. Phys. Chem.* **1990**, *100*, 4781.

(12) Hertwig, R.; Koch, W. *Int. J. Quant. Chem.* **1995**, *56*, 576.

(13) Kieninger, M.; Suhai, S. *Int. J. Quant. Chem.* **1994**, *52*.

(14) Allinger, N.; Sakakibara, K.; Labanowski, J. *J. Phys. Chem.* **1995**, *99*, 9603.

(15) Bizzarri, A.; Stolte, S.; Reuss, J.; Rijdt, J. v. D.-v. d.; Duijneveldt, F. v. *Chemical Physics* **1990**, *143*, 423.

(16) Hehre, W.; Radom, L.; Schleyer, P.; Pople, J. *Ab-Initio Molecular Orbital Theory*; John Wiley and Sons:, 1986.

(17) Serrallach, A.; Meyer, R.; Gunthard, H. *J. Mol. Spect.* **1974**, *52*, 94.

(18) Barnes, A.; Hallam, H. *J. Chem. Soc., Faraday Trans.* **1970**, *108*, 1920.

(19) Huisken, F.; Kulcke, A.; Laush, C.; Lisy, M. *J. Chem. Phys.* **1991**, *95*, 3924.

(20) Jentys, A.; Catlow, C. R. A. *Catal. Lett.* **1993**, *22*, 251.

(21) Sheldon, R. A. *J. Mol. Catal.* **1980**, *7*, 107-126.

(22) Man, A. J. M. d.; Sauer, J. *J. Phys. Chem.* **1996**, *100*, 5025-5034.

(23) Ricchiardi, G.; Andres, d. M.; Sauer, J. *Phys. Chem. Chem. Phys* **2000**, *2*, 2195-2204.

(24) Allen, M. P.; Tildesley, D. J. *Computer Simulation of Liquids*; Claredon Press: Oxford, 1994.

(25) Tossel, J. *J. magn. Reson.* **1991**, *94*, 301.

(26) Millini, R.; Perego, G.; Seiti, K. *Studies in Surface Science and catalysis* **1994**, *84*, 2123-2129.

(27) Lamberti, C.; Bordiga, S.; Arduino, D.; Zecchina, A.; Spano, G.; Genoni, F.; Petrini, G.; Carati, A.; Villain, F.; Vlaic, G. *J. Phys. Chem. B* **1998**, *102*, 6382-6390.

(28) Sinclair, P. E.; Sankar, G.; Catlow, C. R. A.; Thomas, J. M.; Maschmeyer, T. *J. Phys. Chem. B* **1997**, *101*, 4232-4237.

(29) Maschmeyer, T.; Rey, F.; Sankar, G.; Thomas, J. M. *Nature* **1995**, *378*, 159-162.

(30) Oldroyd, R. D.; Thomas, J. M.; Sankar, G. *J. Chem. Soc., Chem. Commun* **1997**, 2025-2026.

(31) Sankar, G.; Rey, F.; Thomas, J. M.; Greaves, G. N.; Corma, A.; Dobson, B. R.; Dent, A. J. *J. Chem. Soc., Chem. Commun.* **1994**, 2279-2280.

(32) Oldroyd, R. D.; Sankar, G.; Thomas, J. M.; Ozkaya, D. *J. Phys. Chem. B* **1998**, *102*, 1849-1855.

(33) Bellussi, G.; Fatore, V. *Stud. Surf. Sci. Catal.* **1991**, *69*, 79.

(34) Pei, S.; Zajak, G. W.; Kaduck, J. A.; Faber, J.; Boyanov, B. I.; Duck, D.; Fazzini, D.; Morrison, T. I.; Yang, D. S. *Catal. Lett.* **1993**, *21*, 333.

(35) Bordiga, S.; Coluccia, S.; Lamberti, C.; Marchese, L.; Zecchina, A.; Boscherini, F.; Buffa, F.; Genomi, F.; Leofanti, G.; Petrini, G.; Vlaic, G. *J. Phys. Chem.* **1994**, *98*, 4125.

(36) Davis, R. J.; Liu, Z.; Tabora, J. E.; Wieland, W. S. *Catalysis Letters* **1995**, *34*, 101-113.

(37) Vayssilov, G. N.; Santen, R. A. v. *Journal of Catalysis* **1998**, *175*, 170-174.

(38) Neurock, M.; Manzer, L. E. *J. Chem. Soc., Chem. Commun.* **1996**, 1133-1134.

(39) Zecchina, A.; Bordiga, S.; Lamberti, C.; Ricchiardi, G.; Scarano, D.; Petrini, G.; Leofanti, G.; Mantegazza, M. *Catalysis Today* **1996**, *32*, 97-106.

(40) Roberts, M. A.; Sankar, G.; Thomas, J. M.; Jones, R. H.; Du, H.; Chen, J.; Pang, W.; Xu, R. *Nature* **1996**, *381*, 401-404.

(41) Sinclair, P. E.; Catlow, C. R. A. *J. Phys. Chem. B.* **1999**, *103*, 1084-1095.

(42) Zicovich-Wilson, C. M.; Dovesi, R.; Corma, A. *J. Phys. Chem. B* **1999**, *103*, 988.

(43) Zhanpeisov, N. U.; Matsuoka, M.; Yamashita, H.; Anpo, M. *J. Phys. Chem. B.* **1998**, *102*.

(44) Geobaldo, F.; Bordiga, S.; Zeccina, A.; Giamello, E.; Leofanti, G.; Petrini, G. *Catalysis Letters* **1992**, *16*, 109-115.

(45) UniChem; Oxford Molecular Inc In; 4.1 ed.: Cambridge.

(46) Notari, B. *Stud. Surf. Sci. Catal.*, **1988**, *37*, 413.

Chapter 5

Epoxidation of alkenes by Titanium molecular sieves

5.1 Introduction

In this chapter, gradient corrected density functional theory calculations on the mechanism of the epoxidation of alkenes catalysed by Ti-peroxo complexes, the oxidising agents in peroxide doped Ti molecular sieve catalysts, are reported.

Firstly, the electron distribution of η^1 and η^2 Ti-peroxo complexes which have been found to exist in Ti substituted molecular sieves (see Chapter 4) are examined to gain insight into the most likely point of attack by two alkenes, namely ethene and propene. The effect that different R groups (attached to the Ti centres *via* oxygen bridges), with varied functionalities, have on the charge distribution of the oxygen-donating Ti-peroxo complexes is a focal point of this work.

Secondly, a molecular orbital theory approach has been used to adjudge favourable initial orientations of ethene and propene to the oxygen-donating Ti-peroxo complexes. Favourable and unfavourable binding sites of the alkene to the Ti-peroxo oxidising agent are distinguished and a number of plausible mechanisms are given in terms of the reaction profile energetics, product and by-product selection and ease of renewal of the original catalyst.

5.2 Methodological details

An identical approach to that discussed in section 4.2 has been employed, using BP86/DZVP non-local density functional theory within the cluster approximation for all geometry optimisation and total energy calculations. In accordance with work reported in the previous chapter, all silicon atoms are fixed in space to represent the rigidity of the molecular sieve framework. All effective partial charges were calculated using the widely utilised Mulliken population analysis approach. Calculation and visualisation of all molecular orbitals was performed using DGauss[1] and Unichem[2] respectively.

Ethene and propene have been chosen as model substrates because they are the smallest and consequently least computationally expensive of the alkene. Furthemore, ethene and propene also display quite different epoxidation kinetics, propene is readily converted to propene oxide by Ti substituted molecular sieves with hydrogen peroxide but ethene is fairly inert.

It is considered that the catalytic epoxidation of propene to propene oxide is potentially one of the most lucrative industrial applications of Ti molecular sieves. Propene oxide (or propylene oxide as it is often termed) is currently mass produced by homogeneous hydrogen peroxide/Ti-silica mixtures (where Ti is supported on a bed of silica). However, the necessary use of concentrated H_2O_2 due to the hydrophilicity of the silica support has put a question mark over the longevity of this process. Evidently the environmentally friendly hydrophobicity Ti substituted molecular sieves are a viable alternative.

Two distinct oxygen-donating Ti-peroxo complexes, shown to exist in tert-butyl hydroperoxide doped Ti grafted MCM-41 silicas (section 4.4.9) and which I suggest are also present in other porous titanosilicates, are employed in this section. The Ti-peroxo complexes, used are shown in figure 5.1 with the peroxide molecule emphasised in grey. Consistent with the previous chapter the structures in the figure below will be referred to as η^1 and η^2 Ti-peroxo complexes (species a and b respectively), a direct reference to the number of bonds between the Ti atom and the peroxide moiety.

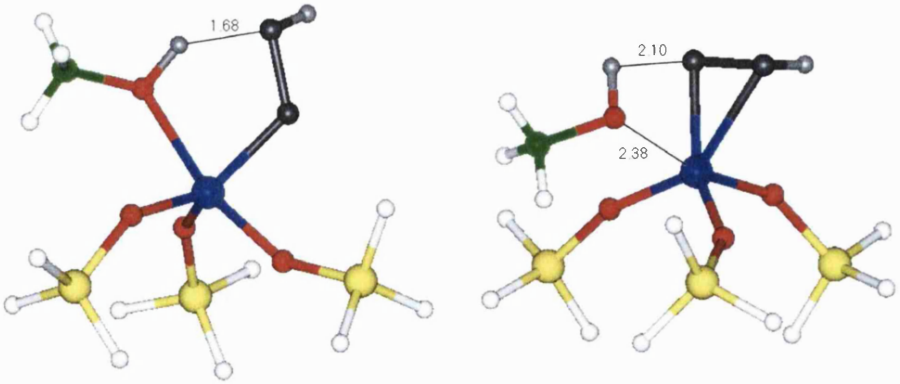

(a) (b)

Figure 5.1 DFT optimised η^1 (a) and η^2 (b) Ti-peroxo complexes, suggested to exist in Ti molecular sieves. The peroxide oxygen atoms are in dark grey and the peroxide hydrogen atoms are shown in light grey. Distances are in Å. Here the R group is CH_3.

5.3 Which oxygen is donated to the alkene?

The first step in determining the mechanism of epoxidations within Ti molecular sieves is to predict which oxygen in each of the Ti-peroxo complexes is most likely to be donated to the alkene. It has been suggested by a number of groups [3] [4-10] that the alkene will bind to one of the peroxidic oxygen atoms but there is debate about which one will be donated to form the epoxide. Since the interaction of an electron-rich alkene double bond with a nucleophilic peroxidic oxygen atom is a repulsive interaction it is thought that the *most electrophilic* peroxidic oxygen will form the epoxide.

A Mulliken population analysis of the peroxidic oxygens in the energy minimised R derivatised η^1 and η^2 Ti-peroxo clusters, for a number of different R groups has been performed. The calculated partial charge of the peroxidic oxygen closest to the Ti centre is highlighted in red and the peroxidic oxygen furthest away from the metal centre is highlighted in blue, figure 5.2. An identical methodology has been used for analysis of all the R derivatised Ti-peroxo complexes, therefore any random errors due to the choice of charge analysis scheme would be expected to be small in comparison to the trends. The reader

should be concerned with the trends shown in figure 5.2 rather than the absolute magnitude of the actual calculated partial charges.

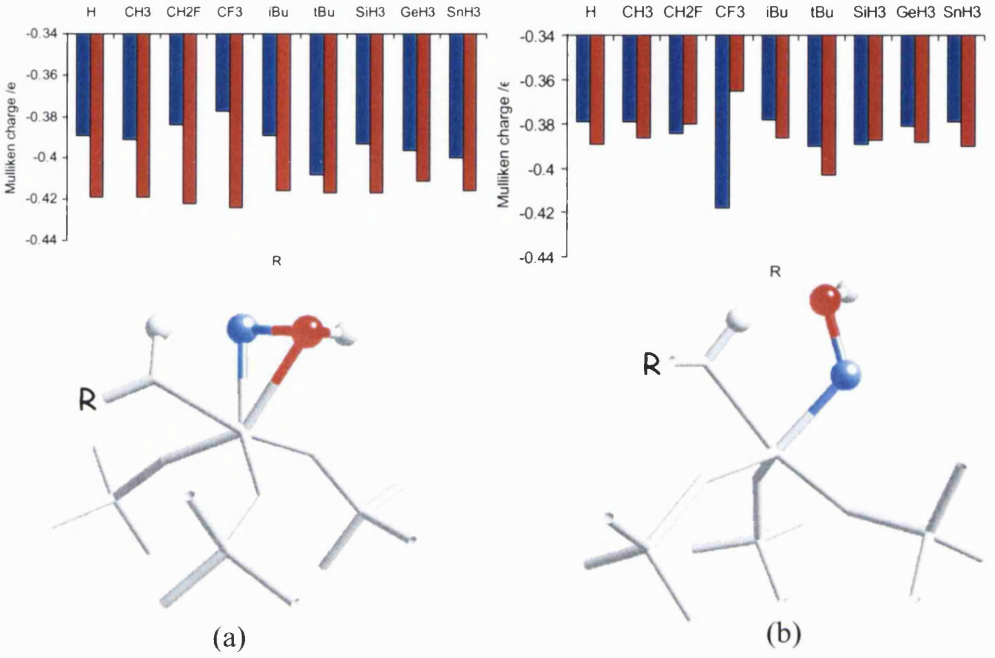

Figure 5.2 Mulliken partial charge of the peroxidic oxygen closest to Ti (in blue) and the peroxidic oxygen furthest way from the metal (in red) for different η^2 (a) and η^1 (b) R derivatised Ti-peroxo complexes.

It is clear from the result of the Mulliken charge analysis that for both Ti-peroxo complexes, the peroxide oxygen closest to the Ti centre, shown in blue, is for almost all the R groups the more electropositive. There are only two instances were the converse is true, for the electron-withdrawing CF_3 and CH_2F groups in the Ti-η^1(peroxo) cluster (figure 5.2b). Here the electron-withdrawing functionalities cause the -OR ligand to move away from the Ti centre and thus the electron density on the metal is no longer shared between five nearest neighbour oxygens but just four. Figure 5.3 clearly illustrates this argument by showing the difference in geometries between the R=CF_3 Ti-η^1(peroxo) complex and the similar sized R=CH_3 Ti-η^1(peroxo) cluster.

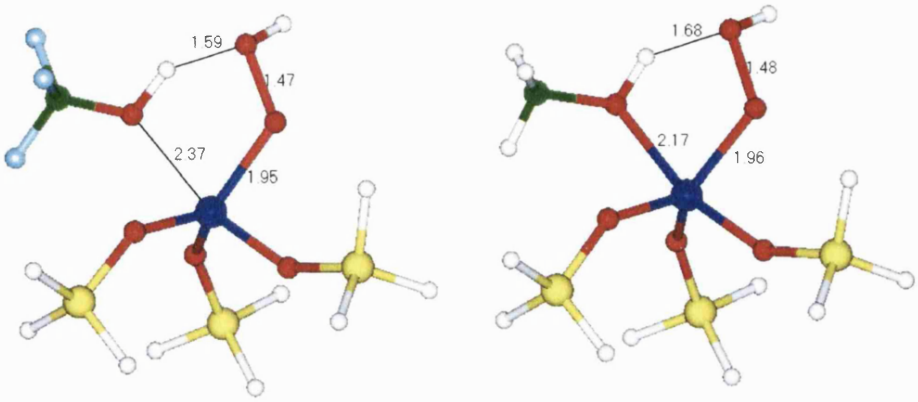

(a) (b)

Figure 5.3 BP86/DZVP optimised geometries of Ti-η^1(peroxo) complexes. Structure (a) contains a CF_3 R group whilst (b) contains a CH_3 group. All bond distance are in Å.

Figure 5.3 also illustrates that the hydrogen bond between the –OR ligand and the peroxide fragment is appreciable shorter and thus stronger in the R=CF_3 cluster (1.6Å compared to 1.7Å). Withdrawal of electron density from the -OR oxygen by the CF_3 R group results in an increase in the electron population on the –O(R)H hydrogen which is subsequently donated to the nearest neighbour peroxide oxygen.

The first aim of this chapter was to gain insight into the most likely point of attack of an alkene to η^1 and η^2 Ti-peroxo complexes. For the majority of R derivatised metal complexes the peroxidic oxygen closest to the metal centre was found to be the more electropositive. The presence of electron-withdrawing R groups on the η^1 structure result in the peroxidic oxygen furthest away from the Ti centre being more electropositive. Since electron-withdrawing groups are known to retard epoxidation reaction rates it is proposed that an electron-rich alkene double bond will preferentially bind to the nearest neighbour peroxide oxygen atom to the Ti centre. Whether it is the η^1 or the η^2 structure that is in fact the oxygen-donating catalytic species, will be discussed later in the chapter.

5.4 R group effects

The reader will recall that in chapter 4, the η^1 peroxo complex was proposed as the oxygen-donating species, on the basis that the nature of R groups was found to affect the energetics of its formation. R groups are known to affect epoxidation reaction rates, but no such R group effects were observed for the η^2 Ti-peroxo cluster.

However, if formation of the Ti-peroxo complex is not the rate-determining step (in epoxidation reactions) then any R dependent changes in the reaction profile of this process will not be transferred to differences in reaction rates. Thus, surely if the η^2 model is to be considered as representative of the oxygen-donating species;

1. Oxygen transfer from the Ti-peroxo complex to the alkene must be assumed to be the rate determining step.
2. R groups must be shown to have an influence on the aforementioned mechanistic step.

Electron-withdrawing groups are known to retard epoxidation reaction rates. Figure 5.3 clearly indicates that the presence of electron-withdrawing groups in the η^1 cluster does indeed affect the electronic configuration of the peroxide oxygen atoms. However, the presence of electron-withdrawing groups in the η^2 model does not appreciably change the partial charges of the peroxide oxygen atoms, which are assumed to be transferred to the alkene. This again instils doubt in the proposal that η^2 type Ti-peroxo complexes are the oxygen-donating species.

In conclusion, different R groups do affect the electronic configuration of the peroxidic oxygens in η^1 Ti-peroxo structures but do not appreciably change the electron populations of the oxygen atoms in η^2 Ti-peroxo sites. Therefore, the proposal remains that the η^1 complex is most likely to be the oxygen-donating catalytic species, as the presence of electron-withdrawing CF_3 functionalities was found to affect the partial charges of the peroxide fragment in the η^1 model but

not in the η^2 cluster. Focus now turns to actually modelling the reaction of ethene and propene to the peroxidic oxygens atoms in the η^1 and η^2 Ti-peroxo structures.

5.5 Orbital analysis

A frontier orbital approach has been used to assist in the orientation of the starting geometries for the modelling of the interaction of alkenes with the peroxidic oxygens in the Ti-η^1(peroxo) cluster and in the Ti-η^2(peroxo) cluster. A bond results from overlap of orbitals, which must occupy the same space and be of the same phase. The idea that the course of a reaction can be controlled by orbital symmetry is a fundamental concept in chemical theory. Woodward, Hoffmann and Fukui, the originators of this approach, were awarded the Nobel Prize for their work.

For bond formation to occur the highest occupied molecular orbital (HOMO) of reactant A must overlap with the lowest occupied molecular orbital (LUMO) or vice versa; the overlap must be sterically allowable and the lobes must be of identical phases [11]. Using the cycloaddition of 1,3 butadiene and ethene as an example, interaction between the HOMO of butadiene to the LUMO of ethene and the LUMO of butadiene and the HOMO of ethene are both symmetry allowed interactions, figure 5.4.

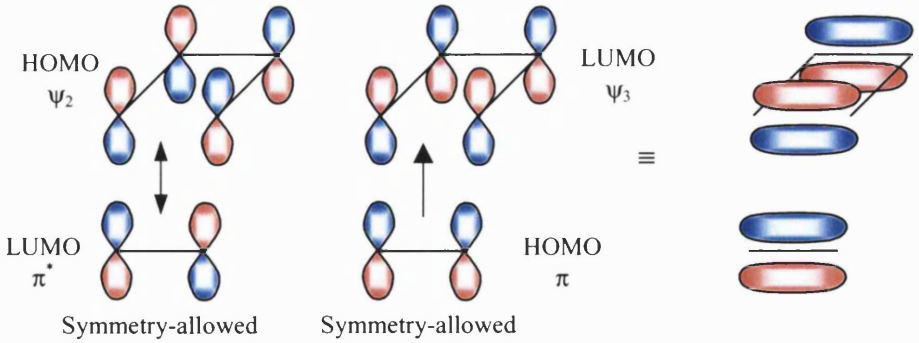

Figure 5.4 Symmetry allowed cycloaddition of 1,3 butadiene and ethene. Overlap of (a) the HOMO of butadiene and the LUMO of ethene and (b) the HOMO of

ethene and the LUMO of butadiene. Interaction (b) has been represented schematically in two ways.

The highest molecular orbital (HOMO) and lowest molecular orbital (LUMO) of each Ti-peroxo model, ethene and propene are shown in figure 5.5. Calculation of all orbitals has been performed on stationary point structures, described in sections 4.4.2 and 4.4.3.

	HOMO	LUMO
Ethene	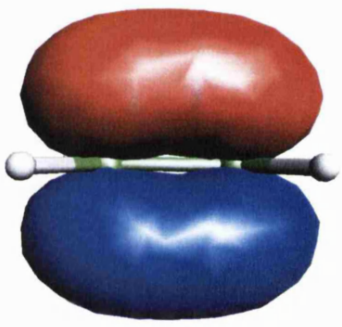	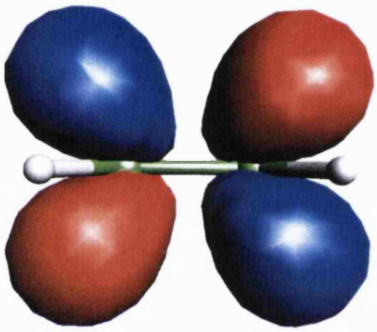
Propene	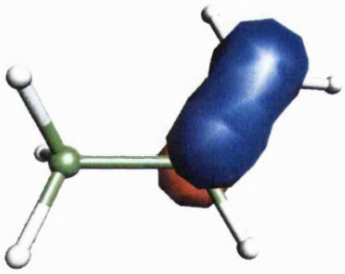	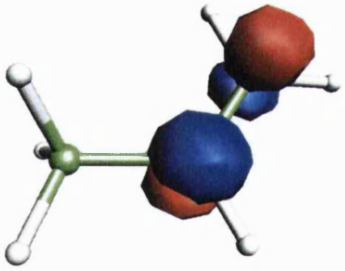
η^1 Ti-peroxo	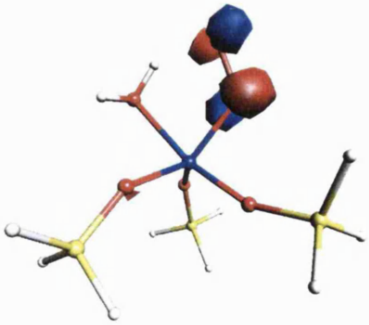	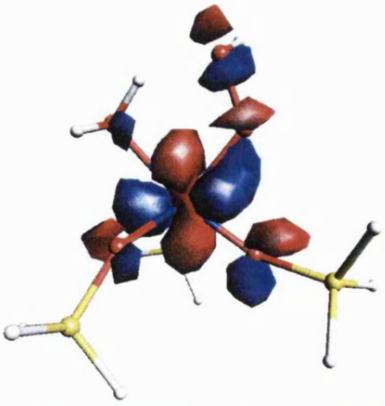

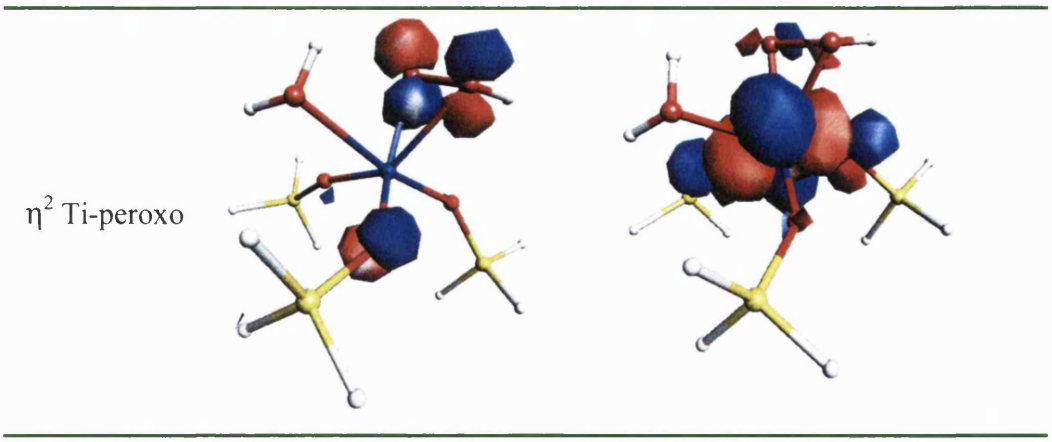

Figure 5.5 Calculated HOMOs and LUMOs of ethene, propene and the η^1 and η^2 Ti-peroxo complexes. Red and blue indicate orbitals of alternate phase.

The HOMO of ethene and propene is clearly the carbon-carbon double bond σ orbital and the LUMO is the π^* orbital of each of the sp^2 carbons. The most dominant contribution to the HOMO of both the Ti clusters is clearly the π orbitals on the peroxidic oxygens. The most dominant LUMO of each Ti cluster is the d orbital of the Ti, however, access to such a sterically hindered atom by an alkene, even one as small as ethene, is very diffcult. For epoxidation reactions the π^* orbitals on the peroxidic oxygen atoms, which are part of the LUMO for both clusters, have been targeted.

5.5.1 HOMO-LUMO gap

For a reaction to occur, favourable, sterically uninhibited HOMO-LUMO overlap must be feasible. In addition the energetic gap between the orbitals must be small enough to enable population of the unoccupied orbital. Figure 5.6 shows the HOMO-LUMO gap for both possible bonding combinations of ethene to a number of R derivatised η^1 Ti-peroxo clusters (graph a) and both possible bonding combinations of ethene to a number of R derivatised η^2 Ti-peroxo catalysts (graph b). The two possible bonding combinations are;

- LUMO of the Ti-peroxo catalytic species and the HOMO of ethene, shown in red.
- HOMO of the Ti-peroxo catalytic species and the LUMO of ethene, shown in blue.

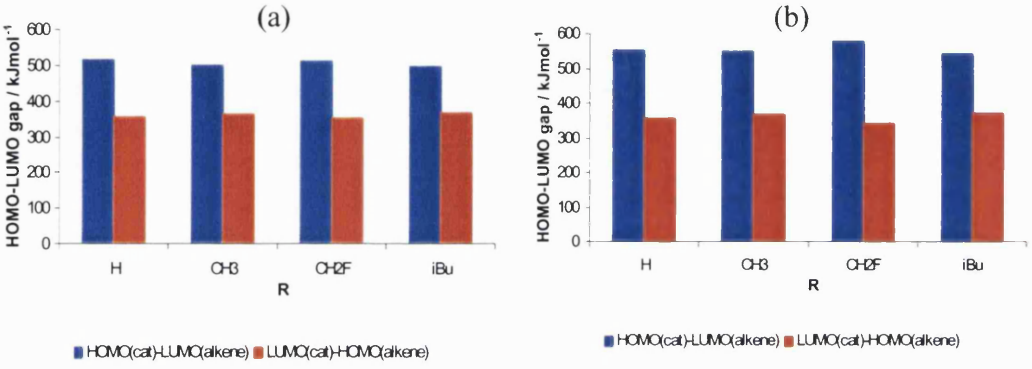

Figure 5.6 HOMO-LUMO gap of (a) ethene and a number of R derivatised Ti-η^1(peroxo) complexes and (b) ethene and a number of R derivatised Ti-η^2(peroxo) complexes (n.b. 'cat' denotes catalyst).

The figure above shows that for both the η^1 and η^2 structures and for all R groups, the interaction between the LUMO of the catalyst and the HOMO of the alkene is ~200 kJmol^{-1} smaller than the converse interaction (the HOMO of the catalyst and the LUMO of the alkene). This is consistent with a number of studies[12]. Note that there is no substantial difference between the magnitude of the HOMO-LUMO gap in the η^1 and the η^2 mechanism. On the basis of these figures, reaction between the LUMO of the catalyst and the HOMO of ethene is the favoured mechanism for epoxidation transformations.

Extending this study to consider propene, again the energy difference between the LUMO of the catalyst and the HOMO of propene is smallest, between 190 and 300 kJmol^{-1} less than the energy gap between the HOMO of the catalyst and the LUMO of propene. Again, note that there is no appreciable difference between the η^1 and η^2 mechanism. As found in the case of ethene, the HOMO-LUMO gap is essentially insensitive to the presence of R groups.

Focusing upon the most energetically favourable interaction (the LUMO(catalyst)-HOMO(alkene)), the LUMO-HOMO gap with propene is about 50 $kJmol^{-1}$ systematically smaller than for ethene, regardless of Ti-peroxo structure or the nature of the R functionality, figure 5.7.

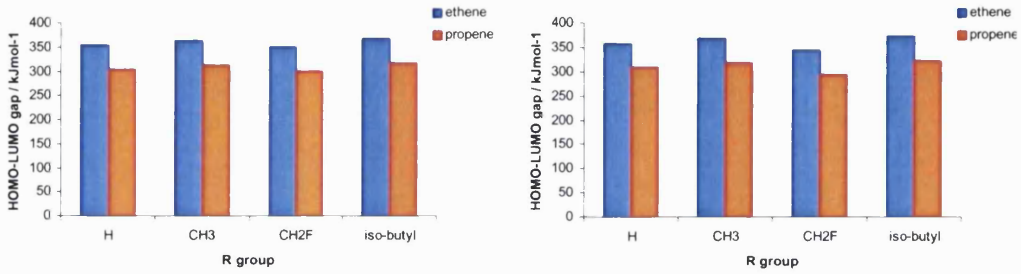

η^1 Ti-peroxo species η^2 Ti-peroxo species

Figure 5.7 Energy difference in $kJmol^{-1}$ between the LUMO of the catalytic species (η^1 on the left and η^2 on the right) and the HOMO of an alkene (ethene in blue and propene in orange).

The lower HOMO-LUMO gap in the presence of propene is consistent with (and indicative of) the fact that propene is readily oxidised to the epoxide in Ti substituted molecular sieves and ethene is not.

5.5.2 Summary

Insight has been gained of the most likely point of attack of alkenes to η^1 and η^2 peroxo complexes by analysis of electron populations (section 5.3) and the calculation of the frontier orbitals of the catalytic species and the substrates (section 5.5). Based on the findings of these investigations, predictions into the Ti molecular sieve catalysed epoxidations of alkenes are as follows:

- Alkenes will preferentially bind to the peroxidic oxygen closest to the Ti centre in the η^1 and η^2 Ti-peroxo complexes.

- The η^1 cluster will be the oxygen-donating species since R groups affect the electron populations of the peroxidic oxygens. No such effects are observed for the η^2 cluster.
- Overlap between the HOMO of the alkene to the LUMO of the η^1 or η^2 catalytic species will be the most favourable interaction (HOMO-LUMO gap is ~ 200 $kJmol^{-1}$ smaller than LUMO(alkene)-HOMO(catalyst) overlap).
- Epoxidation of propene will be more energetically favourable than epoxidation of ethene ((the HOMO(alkene)-LUMO(catalyst) gap for propene is ~50 $kJmol^{-1}$ smaller than for ethene).

The next section describes the systematic modelling of ethene and propene interacting with the peroxidic oxygens in η^1 and η^2 catalytic species.

5.6 Interaction of alkenes with Ti-peroxo stuctures

Using the molecular orbitals shown in table 5.5 as a guide, starting structures for the interaction of ethene to each of the peroxidic oxygens (in turn) in η^1 and η^2 complexes have been configured. Firstly, I will describe how the starting models for investigation into the binding of ethene and propene to the η^1 catalytic species were constructed and what insights the optimisation of these models afforded. Discussion of alkene binding to the η^2 catalytic species will be presented in section 5.6.2.

5.6.1 Epoxidation *via* the η^1 Ti-peroxo complex

Firstly, let us consider overlap between the HOMO of the η^1 catalyst and the LUMO of ethene. The energy minimised ethene molecule was manually orientated so as to overlap the alkenes sp^2 carbon π^* orbitals (the LUMO) with the HOMO π of the peroxidic oxygens on the energy minimised η^1 complex. The most symmetrically favourable orientation is shown in figure 5.8.

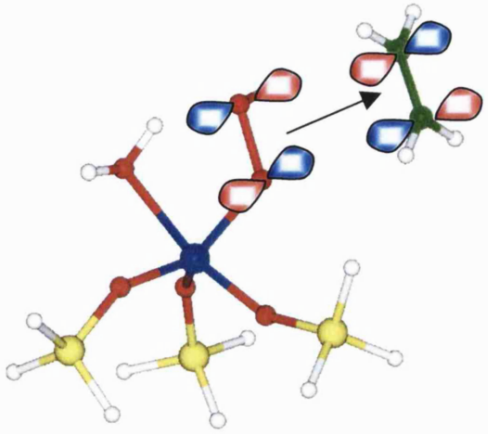

Figure 5.8 Starting structure for modelling the interaction of ethene to an η^1 Ti-peroxo cluster. Part of the HOMO of the Ti cluster and the LUMO of ethene are superimposed over the structure.

In the resultant starting structure, each carbon to peroxidic oxygen bond distance was 1.6Å. Relaxation of this geometry using the BP86/DZVP DFT recipe resulted in the ethene being repelled from the active site, with no epoxide formed. This is accordance with the conclusion presented in section 5.5.2, that the HOMO of the catalyst to the LUMO of the alkene will be the least favourable interaction.

This strategy was employed again for propene, which again resulted in no oxygen transfer or alkene binding. Note that when modelling the propene cluster, the CH_3 substituent on the olefin was orientated so as to bend away from the complex, minimising potential hydrogen bonding interactions between the hydrogen atoms on the methyl substituent and the silanol oxygen or reaction between the methyl carbon and the Ti centre.

Now, let us turn to the interaction between the HOMO of ethene and the LUMO of the η^1 catalyst. Two orientations of the organic substrate orbitals to the catalyst orbitals were symmetrically favourable. The first orientation is where the alkene is orientated towards the peroxide oxygen closest to the Ti centre and in the second the alkene is orientated towards the adjacent peroxidic oxygen, shown in figure 5.9.

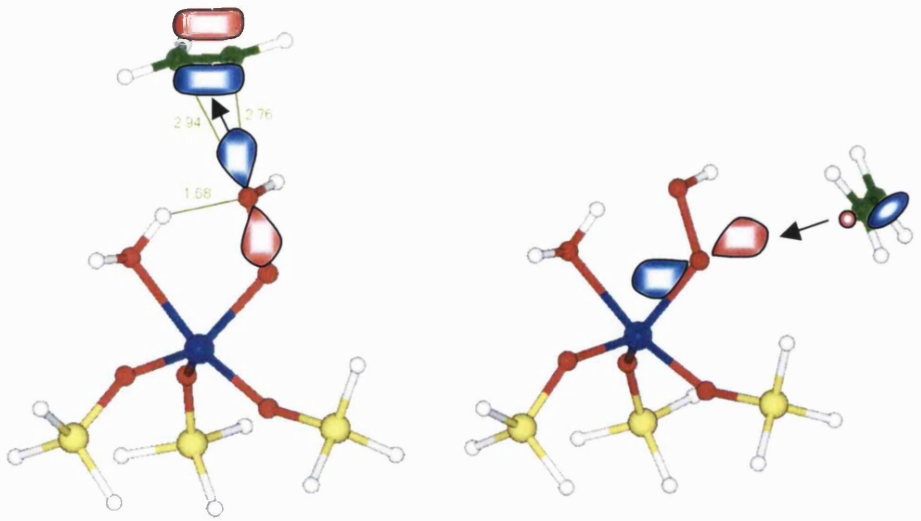

Figure 5.9 (a) BP86 optimised geometry for the interaction of ethene to the peroxidic oxygen furthest from the Ti centre and (b) the starting geometry for ethene attack of the peroxidic oxygen closest to the Ti centre in a η^1 Ti-peroxo complex. Distances are in Å.

As figure 5.9(a) shows, overlap of the HOMO of ethene with the LUMO of the peroxidic oxygen not directly bonded to the metal centre is not a bonding interaction. Both ethene and propene were repelled out of the coordination sphere and away from the active site during energy minimsation. Again, this is consistent with the prediction stated in section 5.5.2 that the alkene would not preferentially bind to the peroxidic oxygen furthest from the Ti atom. This rules out one of the suggested mechanisms of Clerici and Ingallina in their visionary work of 1993 [6] shown in figure 3.12.

Turning now to attack of the alkene to the oxygen closest to the Ti centre in the η^1 catalytic species, figure 5.9(b). The reader will recall that Mulliken population analysis of this Ti cluster showed the oxygen closest to the metal centre to be the most electrophilic (least negative). On the basis of the partial charge analysis, I proposed that the alkene would preferentially attack this oxygen due to lower repulsion between the electron-rich carbon-carbon double bond and the oxygen. Energy minimisation of the structure (b), figure 5.9, where ethene is

positioned 1.6Å away from the peroxidic oxygen closest to the titanium centre did result in spontaneous formation of the epoxide, expulsion of water and regeneration of the original catalyst as shown in figure 5.10.

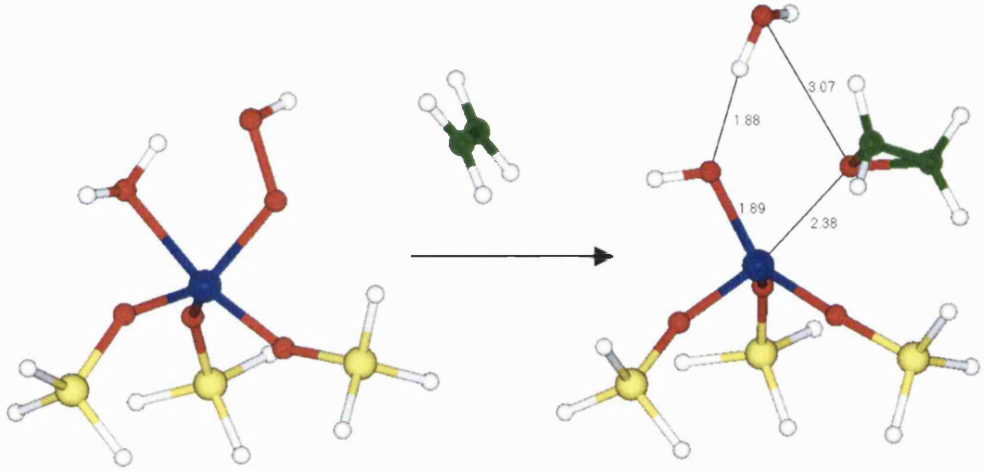

(a) (b)

Figure 5.10 (a) Starting configuration and (b) the BP86/DZVP optimised geometry for the attack of ethene to the peroxidic oxygen closest to the Ti centre of an η^1 Ti-peroxo complex. Distances are in Å.

Figure5.10 (b) shows that the water molecule remains bound to the complex through hydrogen bonding to the OR ligand (where in this instance R=H). At no point does the alkene interfere with the anchoring silanol bonds. This is consistent with the unusually low amount of Ti leaching observed for these catalysts. The favourable binding of ethene to the oxygen closest to the metal centre is consistent with the hypothesis (section 5.3) that the peroxidic oxygen closest to the metal centre will be preferentially donated to the alkene, due to it being the most electrophilic oxygen donor. Furthermore, it is the reaction between the LUMO (specifically the π^* orbital on the peroxidic oxygen) of the Ti-η^1(peroxo) catalytic species and the HOMO (the π carbon sp^2) of the alkene that gives rise to epoxide formation.

I would like to stress that the structure shown in figure 5.10 (b) has been previously reported by Neurock and Manzer [3] who examined the attack of ethene

to the peroxidic oxygen atoms in an η^1 complex, a reaction first hypothesised by Clerici and Ingallina [6]. The bond distances shown in figure 5.10 are in reasonable agreement with those reported in the Neurock and Manzer paper. However the energetics of this epoxidation process were not discussed by the aforementioned authors and thus we address this in the next section.

5.6.1.1 Energetics of η^1 mediated epoxidation

I now consider the energetics of ethene and propene epoxidations mediated by Ti-η^1(peroxo) complexes; are they affected by the choice of alkene (i.e. is the reaction profile more energetically favourable when employing ethene or propene?) or by the choice of R group?

Figure 5.11 shows the BP86/DZVP reaction pathway for the formation of ethene oxide from the interaction of ethene to a number of R derivatised η^1 Ti-peroxo complexes. Starting from the left-hand side of the reaction scheme in figure 5.11, the initial interaction of ethene with the η^1 catalyst is an unfavourable one, indicated by the increase in energy. As has been commented on previously, the interaction between an electron-rich alkene double bond and a nucleophilic oxygen atom is a repulsive one. So it is perhaps unsurprising that there is an energy cost incurred in initial alkene binding. However, the height of the reaction barrier is relatively small, < 15 $kJmol^{-1}$. It is notable that the activation barrier is highest for the R-CH_2F complex. This is consistent with the targeted peroxidic oxygen being more nucleophilic with electron-withdrawing groups; consequently there is a greater repulsion between the oxygen and the alkene.

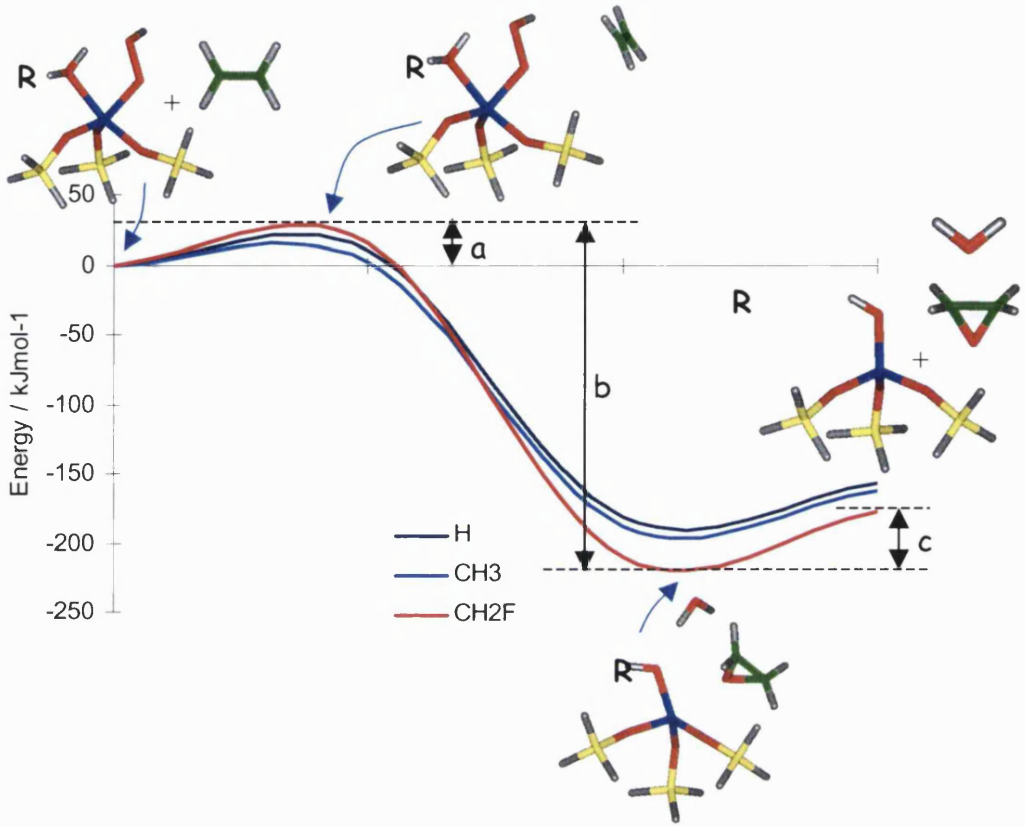

Figure 5.11 BP86/DZVP optimised reaction pathway for the epoxidation of ethene, by reaction with a number of R derivatised η^1 Ti-peroxo complex.

For all of the R groups studied, the formation of the epoxide is a highly exothermic process; around 200 $kJmol^{-1}$ more stable than the isolated reactant species, the Ti-η^1(peroxo) complex and ethene. The presence of the electron-withdrawing CH_2F R group gives rise to the lowest energy epoxide intermediate by 20 $kJmol^{-1}$ however, differences in the geometry and electronic configuration of the CH_2F lowest energy structure and the similar sized CH_3 species are too subtle to explain why this is the case. Modelling of the more highly electron-withdrawing CF_3 functionality could be used to probe the apparent trend however, due to time constraints it is beyond the scope of this thesis.

Due to the high computational expense of calculating iso-butyl or tert-butyl derivatised clusters, the reaction profile in figure 5.11 with sterically bulky iso-butyl and tert-butyl R ligands has not been modelled. However, judging by the fact that the –H, $-CH_3$ and $-CH_2F$ R groups stay bent back away from the peroxide ligand, I predict that counter to some arguments put forward in the

literature, large -OR ligands *will not* impede alkene access to the catalytically active sites.

In section 4.3 the HOMO(alkene)-LUMO(catalyst) gap for propene was found to be around 50kJmol^{-1} smaller than for ethene. Table 5.1 gives the BP86/DZVP calculated reaction energies (a, b and c) for the reaction pathway shown in figure 5.11 for ethene and for propene.

R	a^* / kJmol^{-1}		b^* / kJmol^{-1}		c^* kJmol^{-1}	
	Ethene	Propene	Ethene	Propene	Ethene	Propene
H	10	4	-181	-212	-25	-44
CH_3	2	-1	-188	-213	-26	-30
CH_2F	16	5	-211	-225	-34	-40

Table 5.1 Reaction energies for the epoxidation of ethene and propene *via* R derivatised η^1 Ti-peroxo complexes. The epoxidation of ethene is shown schematically in figure 5.11. *See figure 5.11 for definition of reaction energies.

The reader will observe in table 5.1 that the reaction kinetics for epoxidation *via* an η^1 catalytic site are more favourable when propene is employed. The initial binding of propene to the Ti-peroxo complex is marginally more favourable than for ethene by between 3 and 11 kJmol^{-1} (reaction energy (a)). Furthermore, the resultant epoxidation intermediate is more stable with respect to the reactants for propene than for ethene, for example for the R=H cluster, -212 kJmol^{-1} compared to –181 kJmol^{-1} respectively (reaction energy (b)). I suggest that the more favourable epoxidation kinetics for propene may be due to the inductive effect of the alkene CH_3 substituent; the electron population of the alkene double bond will be enhanced resulting in stronger binding to the targeted peroxidic oxygen.

The epoxidation mechanism shown in figure 5.11 is very plausible, not only because of the large decrease in energy upon forming the products, but due to the original Ti-OR active site being regenerated. This is entirely consistent with the strong R group effects that have been observed by a number of experimental studies on Ti-silsesquioxanes [13,14], the molecular analogues of Ti

molecular sieves. However, the activation barrier associated with this process is necessary to ascertain the true viability of this mechanism.

5.6.1.2 The transition state

Unfortunately, after much effort, I have been unable to locate the actual transition state for the epoxidation reaction pathway shown in figure 5.11. Simple chemical intuition, LST and QST procedures coupled with mode following algorithms (see section 2.5.1 and references [15,16]) have all failed to find a starting geometry that is within the quadratic region of the transition structure saddle point. The presence of constraints on the Si ions severely inhibits the ability to follow a negative eigenvalue up the potential energy surface to give the transition state stationary point [17]. As mentioned in Chapter 4, geometrical constraints also give rise to negative eigenvalues and most mode (eigenvalue) following algorithms rely on only one imaginary frequency being present in the Hessian.

Earlier in section 5.6, I described the formation of epoxide and the expulsion of water as spontaneous. If the alkene is initially placed at a distance of 3Å away from the peroxidic oxygen bound to the Ti atom of the energy minimised Ti-η^1(peroxo) structure and the resultant geometry minimised, then the alkene moves away from the catalytic species with no epoxide formation. This indicates that the energy barrier for this process is associated with the electron-electron repulsion barrier between the alkene double bond and the peroxidic oxygen. In order to gain insight into the nature of the transition state and the magnitude of the activation barrier, I have analysed the output from three separate optimisations of the η^1 cluster with ethene.

The first optimisation was the initial attempt at modelling the interaction of ethene to the oxygen directly bonded to the titanium in a η^1 Ti-peroxo complex. The starting geometry for this calculation was generated by positioning the carbon atoms in ethene at a 2Å distance from the targeted peroxidic oxygen. Minimisation of the resultant cluster showed the alkene to be repelled from the catalyst with no epoxide formation or reaction of any kind. This is of course counter to the results presented in section 5.6.1.

In the second attempt, I brought the alkene in closer to the catalytic species for construction of a second starting geometry. Here the carbon-peroxidic oxygen starting bond distance was 1.7Å but optimisation of the resultant geometry again showed there to be no reaction and the alkene was observed to move away from the Ti-peroxo cluster.

Finally, the third starting geometry was constructed where the starting carbon-peroxidic oxygen bond length was selected to be 1.6Å. Optimisation of this structure did result in epoxide formation as shown in figure 5.10. Evidently, the first two starting geometries were on the reactant side of the potential energy surface and the third structure was on the product side.

This assertion is supported by considering the single point energies of all the intermediate structures for all three optimisation calculations as a function of sp^2 carbon - peroxidic oxygen bond distance. The results are shown in figure 5.12.

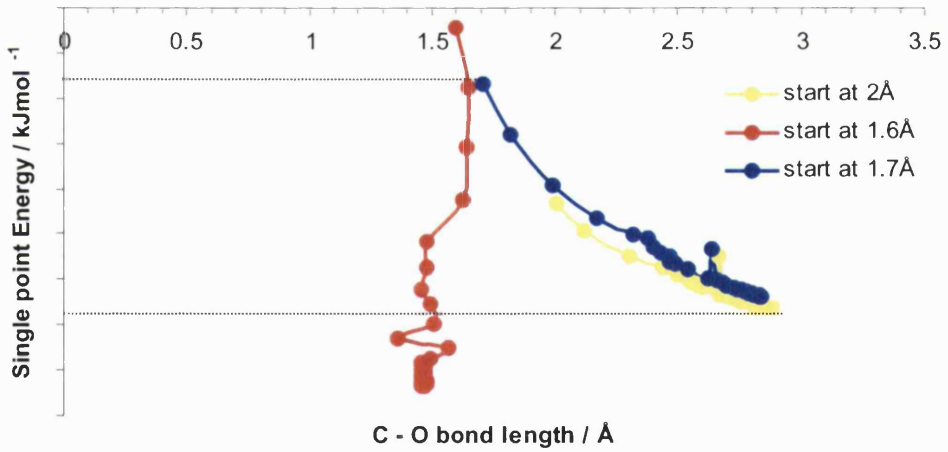

Figure 5.12 Single point energies of intermediate structures in the optimisation of a Ti-η^1(peroxo) complex with ethene in close proximity. The three series differ only in the initial positioning of ethene to the stationary point η^1 complex with an sp^2 carbon – peroxidic oxygen bond distance of 2Å, 1.7Å and 1.6Å respectively. Each increment on the y-axis represents 100 $kJmol^{-1}$.

It is clear from the graph above that in the *transition state* for the η^1 catalysed epoxidation of ethene, the alkene will reside between 1.6 Å and 1.7 Å away from the peroxidic oxygen bound to the titanium centre. Reading from the graph in figure 5.12, the upper bound for the activation barrier associated with the reaction of ethene to the peroxidic oxygen in a η^1 Ti-peroxo catalytic species is 500 kJmol^{-1}. However, each data point in the graph is not an optimised structure of course and in reality the activation barrier will be much lower than the figure just quoted. Indeed, the reader will see in figure 5.12 that the optimisation pathway for the "start at 1.6Å" cluster is extremely steep with each of the initial optimisation steps dropping by ~ 100 kJmol^{-1} (one increment on the y-axis). This indicates that the transition state is likely to be much lower in energy than the "1.6Å" or "1.7Å" starting geometries which were very high energy structures.

In conclusion, a viable mechanism for the epoxidation of ethene and propene from donation of the peroxidic oxygen bound to the titanium atom in a Ti-η^1(peroxo) catalytic species has been presented. Overlap between the HOMO of the alkene and the LUMO of the catalyst is the most favourable with the resultant product about 20 kJmol^{-1} more stable when propene is used. The transition state for this process will contain the alkene at a 1.6Å – 1.7Å distance from the peroxidic oxygen donor. I now turn to investigation of the η^2 catalytic species.

5.6.2 Epoxidation *via* the η^2 Ti-peroxo complex

Consistent with the previous section, interaction between the HOMO of the Ti-peroxo complex with the LUMO of ethene will be considered first. An energy minimised ethene molecule was positioned so that the alkene sp^2 carbon atoms and the peroxidic oxygens in the stationary point η^2 Ti-peroxo structure were at a 1.6Å distance from each other. For symmetrical overlap of the HOMO orbitals of the olefin to the LUMO orbitals of the catalyst (see figure 5.5), the alkene double bond was positioned parallel to the peroxide O-O bond, figure 5.13. Optimisation of this starting geometry resulted in the each of the alkene carbons bonding to the nearest peroxidic oxygen and subsequently causing the peroxide O-O bond to

break, see figure 5.13. No epoxide was formed, however breakage of one of the metal-peroxidic oxygen bonds results in formation of an alcohol type functionality which remains bound to the Ti *via* the remaining peroxidic oxygen.

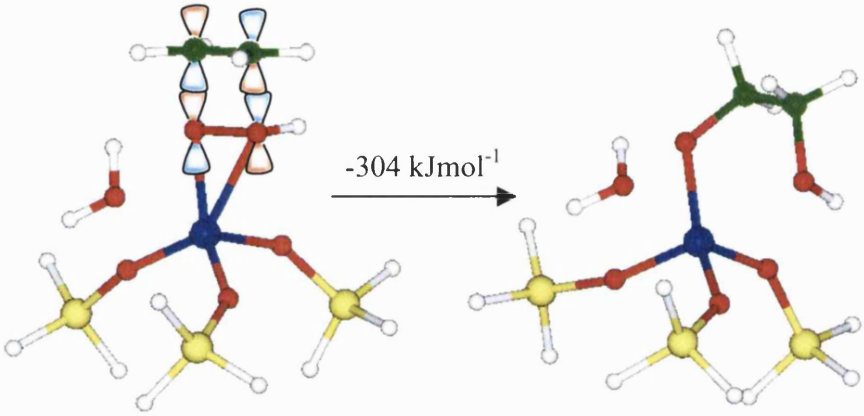

Figure 5.13 Starting configuration (left) and BP86/DZVP optimised geometry (right) for the interaction of the LUMO of ethene with the HOMO of an η^2 Ti-peroxo complex. The orbitals have been superimposed onto the structure.

One can see that the complex shown on the right of figure 5.13 could easily rearrange to form the diol, which is, in fact a known by-product of Ti substituted molecular sieve catalysed epoxidations [18,19]. Based on these results, a suggested mechanism for diol formation *via* the η^2 Ti-peroxo catalytic species is shown in figure 5.14.

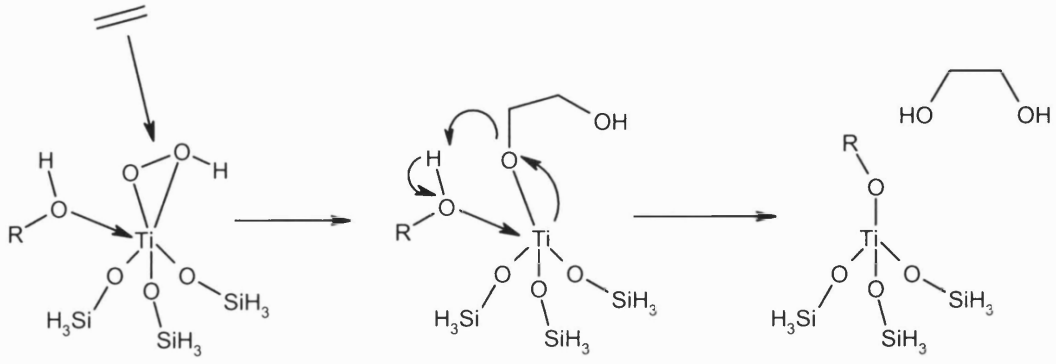

Figure 5.14 Suggested mechanism for diol formation by the side-on attack of ethene to a Ti-η^2(peroxo) catalytic species.

It was previously proposed in section 5.4 that interaction of the LUMO of the alkene to the HOMO of the Ti-η^2(peroxo) complex would not give rise to the epoxide, since the HOMO-LUMO gap is ~ 200 kJmol^{-1} larger than the converse LUMO(catalyst)-HOMO(alkene) arrangement. Indeed it doesn't, however I suggest that the formation of a diol could be feasible given that this process is highly exothermic, calculated to be around 300 kJmol^{-1}. I believe this to be the first mechanistic explanation of how diol by-products are produced in titanium molecular sieve catalysed alkene epoxidations with peroxide.

The alternative mechanism, overlap of the HOMO of ethene with the LUMO of the η^2 Ti-peroxo complex, is now discussed. Ethene has been brought to within a 1.6Å distance of each of the peroxidic oxygen atoms in turn so as to maximise the overlap between the π C=C orbital and the π^* orbital on the oxygen. In both instances, optimisation of the resultant geometry, which is shown in figure 5.15, repelled ethene away from the active site without any binding to the Ti cluster or epoxide formation.

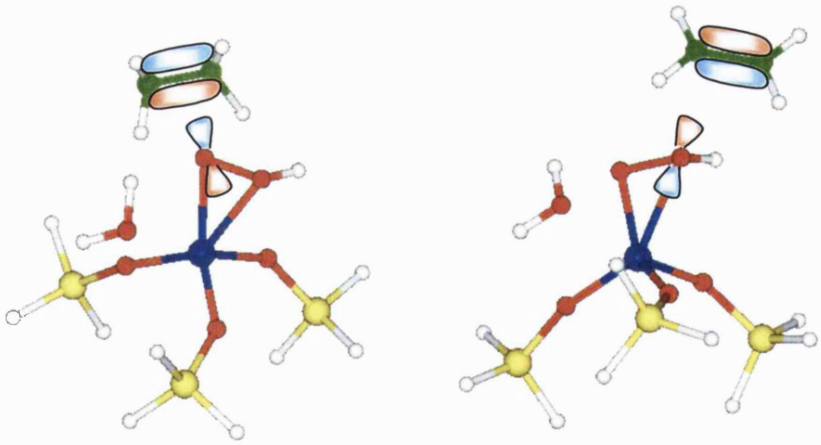

(a) (b)

Figure 5.15 Modelling the interaction between the HOMO of ethene and the LUMO of a Ti-η^2(peroxo) complex, directed (a) towards the peroxidic oxygen closest to the Ti centre and (b) the peroxidic oxygen furthest away from the Ti centre.

In section 5.3, I proposed that the peroxidic oxygen closest to the metal would preferentially coordinate to the incoming alkene, given that it is the most

electrophilic. However, this effect was not observed in the calculations presented. The reason for this discrepancy can be attributed to the fact that maximal overlap between the HOMO of ethene and the LUMO of this oxygen could not be achieved, due to steric inhibition by the weakly coordinated -O(H)R group (where R in the figure above is H).

EXAFS analysis of a TBHP doped titanium grafted MCM-41 catalysts, presented in the preceding chapter showed that the η^2 cluster is 6 coordinate and the η^2 structure with the –O(R)H group removed gave a very poor fit to experiment. However, in the real catalytic system, the O(R)H group is likely to fluctuate between states of an isolated species (water when R=H or an alcohol when R is an organic moiety) and being bound to the Ti centre. This will be dependent on the nature of the R group, the nature of the solvent and the reaction conditions. The methodology employed here cannot be routinely used to directly model such mobile or fluctuant effects. Thus, in order to investigate whether ethene will bind to the peroxidic oxygen closest to the metal centre, when the sterically inhibiting O(R)H group is not bonded to the Ti-peroxo complex, the following strategy was implemented.

Firstly the O(R)H ligand was removed from the stationary point Ti-η^2(peroxo) complex and the resultant structure optimised using the BP86/DZVP recipe. One molecule of ethene was then brought to a 1.6Å distance from the peroxidic oxygen closest to the metal centre, figure 5.16.

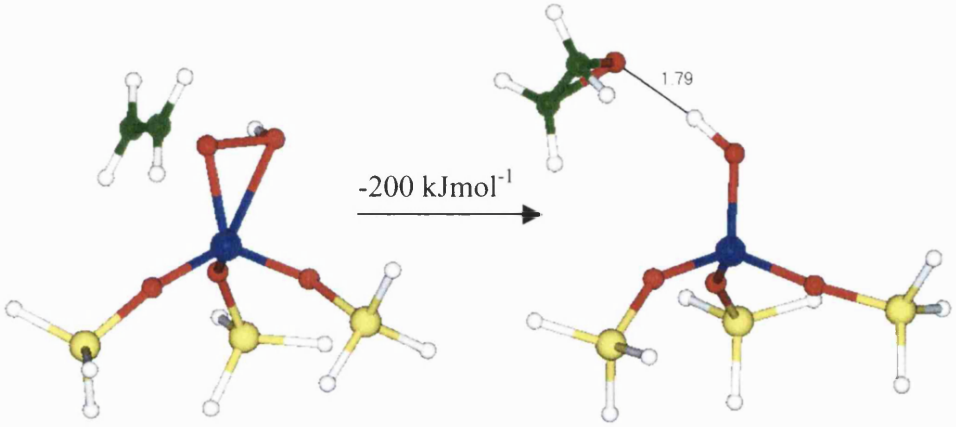

Figure 5.16 Starting geometry (left) and BP86/DZVP resultant optimised structure (right) for attack of ethene to a 5 coordinate Ti-η^2(peroxo) complex.

As figure 5.16 shows, optimisation of the resultant structure gives rise to epoxide formation, a process that is energtically favourable by ~ 200 kJmol^{-1}. The reader will note that on the basis of the Mulliken partial charge analysis in section 5.3, the oxygen closest to the Ti centre was predicted to be the preferred oxygen donor. In addition, overlap between the HOMO of the olefin and the LUMO of the catalyst was found be the most favourable interaction. The epoxidation reaction shown in figure 5.16 is therefore consistent with the predictions outlined earlier in this chapter. Furthermore, the epoxidation product is found to be more stable with propene than with ethene (176 kJmol^{-1} compared to 200 kJmol^{-1} respectively). This result is consistent with the suggestion put forward in section 5.5, that oxidation of propene will be more energetically favourable than ethene. A similar mechanism to this has been postulated before by Sinclair and Catlow [9] with ethene and an η^2 bipodal model which was also five-coordinate, the reader is referred to section 3.9.

Of course, the original tripodal Ti-OR catalyst is not regenerated because the –OR ligand has been removed and replaced by an –OR' group, where R' is the peroxide substitutent, figure 5.17.

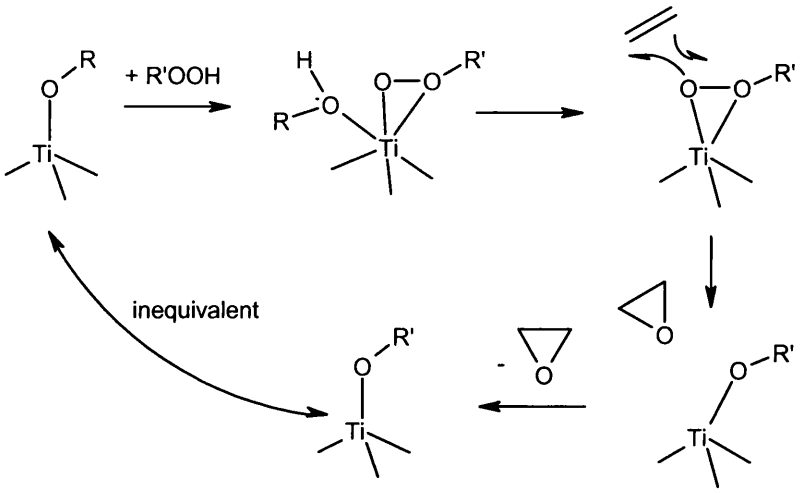

Figure 5.17 Problems concerning the regeneration of the catalyst for η^2 mediated epoxidations.

The removal of the ligand containing the R group is necessary to facilitate the production of epoxide and therefore this places a question mark over this particular mechanism. As I have mentioned previously, R groups are known to affect reaction rates for epoxidation transformations. Even though η^2 Ti-peroxo complexes have been shown to exist in titanium doped molecular sieves I suggest that they are not the predominant oxygen-donating species for epoxidations.

Thus far, mechanistic aspects regarding the epoxidation of alkenes *via* η^1 and η^2 Ti-peroxo complexes, the structures of which have been shown to exist in a TBHP doped Ti-MCM41 catalyst, have been presented. The reader will recall that in chapter 4 the isolation of a new and stable Ti-peroxo complex was presented, named 'Ti-η^1[O(H)OH]'. This was of particular interest as the activation barrier for its formation was the smallest of the three mechanism considered, < 20 kJmol^{-1}. EXAFS of a TBHP/Ti-MCM41 catalyst failed to find evidence for its existence. However, because the peroxide remains intact upon binding with the titanium site, and is stabilised by a hydrogen bond between the peroxide molecule and the hydroxyl ligand, under reaction conditions it is possible that Ti-η^1[O(H)OH] complexes could have a short lifetime, figure 5.18.

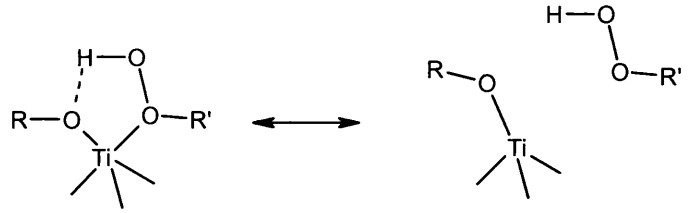

Figure 5.18 Possible dissociation of the Ti-η^1[O(H)OH] complex

If this is the case, Ti-η^1[O(H)OH] complexes could exist long enough to react with alkenes and to facilitate epoxidation production. The EXAFS study that the Ti-peroxo structures were compared to (described in section 4.4.9), was conducted on a titanium catalyst which had *not* been reacted with an alkene, just a peroxide. Therefore, Ti-η^1[O(H)OH] complexes may not have lived long enough to be captured by the spectroscopic technique but in the presence of unsaturated olefins could live long enough to be the oxygen-donating species. The interaction of ethene and propene to a Ti-η^1[O(H)OH] cluster is now described.

5.7 Interaction of alkenes with a Ti-η^1[O(H)OH] complex

Earlier in the chapter, I described how for both the η^1 and η^2 clusters, the alkene preferentially binds to the peroxidic oxygen that is not protonated, which is, incidentally the peroxidic oxygen atom closest to the titanium centre. Thus for the Ti-η^1[O(H)OH] complex only the peroxidic oxygen which is not protonated is targeted in this investigation, figure 5.19.

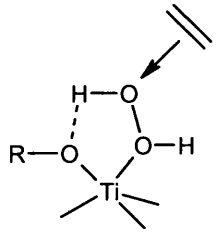

Figure 5.19 Modelling the interaction of alkene with a Ti-η^1[O(H)OH] complex.

The starting geometry used to model this interaction is shown in figure 5.20, species (a). For both ethene and propene the alkene was positioned so that the double bond carbon atoms were 1.6Å away from the targeted peroxidic oxygen. Energy minimisation of the structure using the BP86/DZVP recipe resulted in epoxide formation, as shown in figure 5.20, species (b).

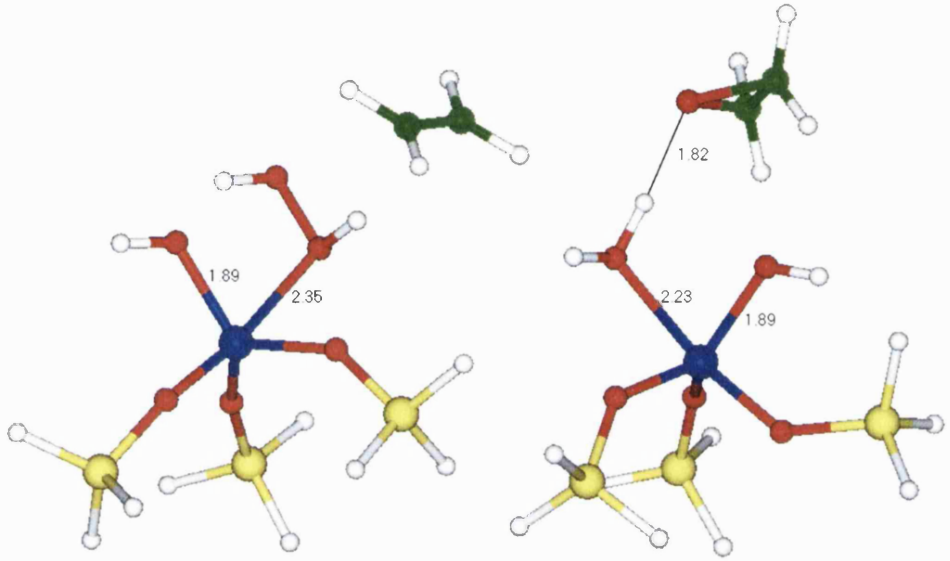

(a) (b)

Figure 5.20 (a) Starting model and (b) resultant BP86/DZVP optimised geometry the interaction of ethene with a Ti-η^1[O(H)OH] complex. The peroxidic oxygen furthest from the Ti centre has been targeted.

The hydrogen originally attached to the donated oxygen migrates to the OR ligand (R in figure 5.20 is simply a hydrogen atom) and forms a hydrogen bond with the epoxide oxygen. This mechanism for epoxide formation has not been reported elsewhere. The mechanism and reaction energetics for this process with ethene and propene are displayed in figure 5.21.

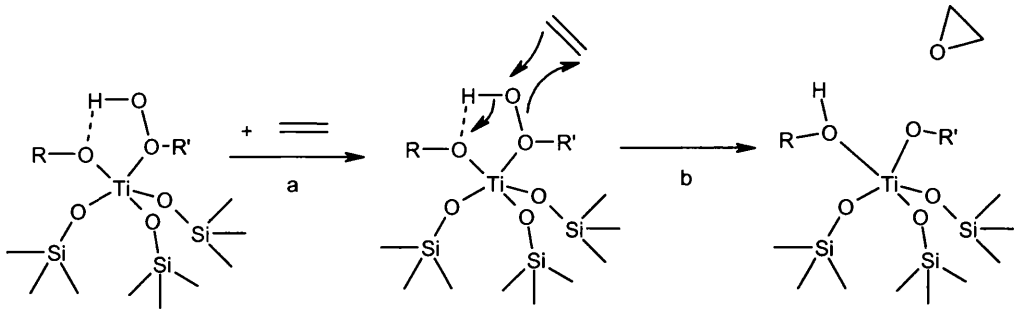

R	Ethene		Propene	
	a / kJmol^{-1}	b / kJmol^{-1}	a / kJmol^{-1}	b / kJmol^{-1}
H	-14	-197	-23	-216
CH_3	-24	-198	-30	-207
CH_2F	-26	-200	-6	-239

Figure 5.21 Proposed mechanism and BP86/DZVP calculated reaction energies for the epoxidation of alkenes *via* a R derivatised Ti-η^1[O(H)OH] complex. R' is the peroxide substituent.

It is clear that the formation of the epoxide is more energetically favourable for propene than for ethene with the propene reaction product consistently lower in energy (for example 239 kJmol^{-1} compared to 200 kJmol^{-1} for the R=CH_2F catalyst). Considering that formation of the epoxide in the above mechanism is of the same order of magnitude than the η^1 and η^2 mechanisms, discussed in sections 5.6.1 and 5.6.2 respectively, and that formation of the Ti-η^1[O(H)OH] catalytic species in the first instance has the lowest associated activation barrier, < 20 kJmol^{-1} this new mechanism is very plausible.

Furthermore, R groups do seem to affect the reaction energetics, consistent with experimental observations. For example, initial interaction of propene is –30 kJmol^{-1} for the CH_3 R groups and only –6 kJmol^{-1} for the CH_2F R functionality. However, the mechanism in figure 5.21 also highlights the need for more work to be conducted into the catalytic step concerned with the regeneration of the original catalyst. Depending on the relative binding strength of the R group, the

R' peroxidic substituent and the protic environment, proton transfer from the OR group to the OR' ligand could occur resulting in the expulsion of the R'OH alcohol and regeneration of the original catalyst, figure 5.22.

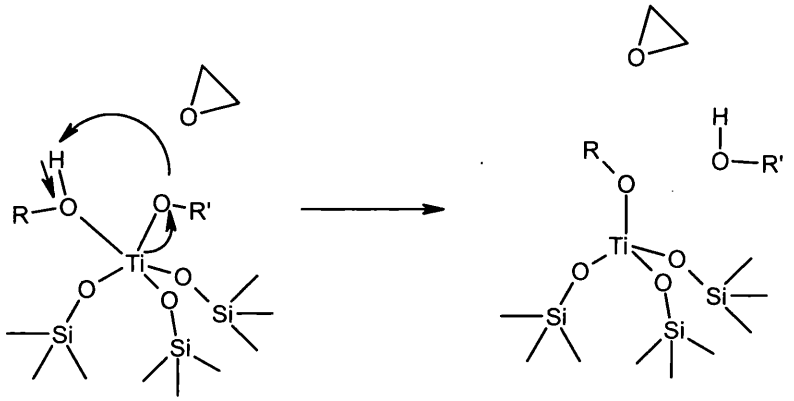

Figure 5.22 Suggested mechanism for the regeneration of the Ti active site post Ti-η^1[O(H)OH] catalysed epoxidation.

The proton transfer step shown in the figure above is quite plausible, given that hydrogen peroxide is the sacrificial oxidant. Clearly, H_2O would be expelled and an electron-donating R group would bind strongly to the metal centre. I propose that Ti-η^1[O(H)OH] complexes are plausible oxygen-donating species for the epoxidation of alkenes.

5.8 Summary

Although many studies into titanium molecular sieve epoxidation catalysts have been presented in the literature, this is the first time a systematic and quantitative study of all viable catalytic species and mechanisms has been carried out. As I have noted at certain points within this chapter, some of the structures and mechanisms presented here have been previously reported by other groups (albeit with a different computational methodology), however others are unique to this piece of work.

This study is unique in its use of R group effects as a tool in relating changes in theoretically derived reaction energies to experimental observations. The effect that electron-withdrawing groups have on the reaction pathways presented in this chapter have been used to rationalise the most viable oxidation mechanism. Due to the limitations in the quantum mechanical code DGauss in treating large systems, it has not been possible to study the Ti-peroxo – alkene systems with sterically bulky R groups. However, all indications from chapter 4 are that sterically bulky groups would not inhibit the pathway of the incoming alkene to the titanium oxygen-donating species, as the R groups were found to bend back away from the peroxidic ligand in isolated (in the absence of alkene) Ti-peroxo clusters.

The work presented here has used η^1, η^2 and Ti-η^1[O(H)OH] Ti-peroxo complexes defined in sections 4.4.3, 4.4.2 and 4.4.5 respectively, as models of the oxygen-donating catalytic species. Both ethene and propene have been modelled as the reactant species.

The work presented in this chapter is summarised as follows:

1. Prediction of which oxygen in the η^1 and η^2 Ti-peroxo models will be preferentially donated to the ethene and propene.
2. Analysis of the frontier orbitals of the Ti-peroxo catalytic species and ethene and propene to aid orientation of the starting geometries.

3. Modelling the interaction of ethene and propene to η^1, η^2 and Ti-η^1[O(H)OH] Ti-peroxo complexes.

In conclusion:

- It is the unprotonated peroxidic oxygen that is donated to the alkene, for each of the three Ti-peroxo models studied. For η^1 and η^2 Ti-peroxo complexes this is the peroxidic oxygen closest to the titanium centre. This was predicted correctly by a Mulliken partial charge analysis of the peroxidic oxygens, which found the peroxidic oxygen closest to the titanium centre in η^1 and η^2 species to be the most electropositive, thus minimising electron-electron repulsion with the alkene double bond.
- R groups do affect the electron populations on the peroxidic oxygen atoms in the η^1 Ti-peroxo model but not in the η^2 complex. The peroxidic oxygen closest to the metal centre in the η^1 model is more nucleophilic and thus more replusive to the alkene with the electron-withdrawing CH_2F R groups.
- Overlap between the LUMO of the oxygen-donating catalytic species and the HOMO of the alkene is the most favourable route to epoxidation since the LUMO-HOMO gap is over 200 $kJmol^{-1}$ smaller than the reverse HOMO-LUMO interaction.
- The experimental observation that propene epoxidises readily in titanium molecular sieves and ethene is relatively labile, can be rationalised by the fact that the LUMO-HOMO gap for propene is ~ 50 $kJmol^{-1}$ smaller than ethene, for all R derivatised η^1 and η^2 Ti-peroxo catalytic species.

Moving on to the modelling of ethene and propene to Ti-peroxo complexes, both the literature proposed η^1 and η^2 Ti-peroxo catalytic species were found to act as oxygen-donating agents to ethene and propene. Both mechanisms involved *overlap between the HOMO of the alkene and the LUMO of the catalyst and donation of the peroxidic oxygen closest to the titanium centre.*

Epoxidation of alkenes catalysed by η^1 intermediates is found to be very plausible. The reaction energy is ~ -200 $kJmol^{-1}$ and due to the spontaneous

production of the epoxide and water, the original titanium active site is formed, i.e. the catalyst is regenerated. This is important because the R group must remain on the titanium site to explain the pronounced R group effects observed by experiment. I therefore propose that epoxidation of alkenes *via* the 'η^1 mechanism' shown in figure 5.11 does occur in the pores of alkene doped Ti molecular sieves with peroxide.

The O(R)H ligand on the η^2 catalytic site was found to hinder the pathway of the alkene towards the targeted peroxidic oxygen and thus, the O(R)H group must be removed for the alkenes to interact favourably with the η^2 cluster. It is quite conceivable that the ROH group could be expelled under reaction conditions since it is only weakly coordinated to the metal centre. However, the removal of the R group clearly discounts the observed R group effects. I therefore predict, that η^2 complexes are not the oxygen donating species for epoxidations, however they do explain diol formation *via* overlap of the π^* LUMO of the alkene to the peroxidic oxygen atoms π HOMO. Diols are a common by-product of titanosilicate catalysed epoxidations. The overlap of the HOMO of the alkene to the LUMO of the catalyst is the most favourable interaction. This could be interpreted as indicative of the fact that high epoxide selectivities are observed for these systems.

Finally, I turn to Ti-η^1[O(H)OH] complexes, postulated for the first time in this work. Epoxidation of ethene and propene is facilitated by donation of the non-protonated peroxidic oxygen, which in this case is furthest from the titanium centre. The process is energetically favourable by ~ 200 kJmol^{-1} and the R group remains attached to the Ti atom and is thus capable of explaining R group effects. Regeneration of the original catalyst is suggested through proton transfer of a hydrogen atom from the OR ligand to the OR' group resulting in the expulsion of an R'OH alcohol. Considering that the activation barrier for the formation of Ti-η^1[O(H)OH] complexes is < 20 kJmol^{-1}, which is the least for the three mechanism studied, and that the energetics of epoxidation are also favourable, Ti-η^1[O(H)OH] complexes are a new and viable route to epoxidations.

I suggest that both Ti-η^1[O(H)OH] and η^1 complexes are the oxygen-donating species in titanium molecular sieve catalysts and the η^2 species are present but give rise to diol formation depending on the reaction conditions.

5.9 References

(1) DGauss; Oxford Molecular Inc In; 4.1 ed.: Cambridge.

(2) UniChem; Oxford Molecular Inc In; 4.1 ed.: Cambridge.

(3) Neurock, M.; Manzer, L. E. *J. Chem. Soc., Chem. Commun.* **1996**, 1133-1134.

(4) Notari, B. *Catalysis Today* **1993**, *18*, 163-172.

(5) Karlsen, E.; Schoffel, K. *Catalysis Today* **1996**, *32*, 107-114.

(6) Clerici, M. G.; Ingallina, P. *J. Catal* **1993**, *140*, 71-83.

(7) Khouw, C. B.; Dartt, C. B.; Labinger, J. A.; Davis, M. E. *Journal of Catalysis* **1994**, *149*, 195-205.

(8) Bellussi, G.; Carati, A.; Clerici, M. G.; Maddinelli, G.; Millini, R. *Journal of Catalysis* **1992**, *133*, 220-230.

(9) Sinclair, P. E.; Catlow, C. R. A. *J. Phys. Chem. B.* **1999**, *103*, 1084-1095.

(10) Tantanak, D.; Vincent, M. A.; Hillier, I. H. *J. Chem. Soc., Chem. Commun.* **1998**, 1031-1032.

(11) Santen, R. A. v. *Catal. Lett.* **1992**, *16*, 59 - 69.

(12) Wu, Y.; Lai, D. *J. Org. Chem.* **1995**, *60*.

(13) Crocker, M.; Herold, R. H. M.; Orpen, A. G. *Chem. Commun.* **1997**, 2411 - 4212.

(14) Maschmeyer, T.; Klunduk, M. C.; Martin, C. M.; Shephard, D. S.; Thomas, J. M.; Johnson, B. F. G. *Chem. Commun.* **1997**, 1847 - 1848.

(15) Roothan, C. C. J. *Rev. Mod. Phys.* **1951**, *23*, 69.

(16) Halgren, T. A.; Lipscomb, W. N. *Chem. Phys. Lett.* **1977**, *49*, 225 - 231.

(17) Schlegel, H. B. In *Ab Initio Methods in Quantum Chemistry I*; Lawley, K. P., Ed.; John Wiley & Sons Ltd., 1987; pp 249 - 285.

(18) Bhaumik, A.; Tatsumi, T. *Journal of Catalysis* **1998**, *176*, 305-309.

(19) Clerici, M. G.; Bellussi, G.; Romano, U. *Journal of Catalysis* **1991**, *129*, 159-167.

Chapter 6

Summary and Conclusions

6.1 Overview

Despite extensive experimental studies, there is only limited understanding of the mechanism of the epoxidation of alkenes catalysed by titanium molecular sieves with a hydroperoxide. A number of groups have used theoretical techniques to explore the mechanism of Ti molecular sieve catalysed oxidations. However, most of these studies have not quantitatively investigated the viability of the particular Ti-peroxo complex suggested. Surely, elucidation of the titanium lead epoxidation mechanism can only be achieved if the nature of the Ti-peroxo key catalytic species is known? A major part of this work has been the determination of Ti-peroxo complexes, which was discussed in detail in chapter four. With detailed knowledge of the key catalytic species (the Ti-peroxo functionality) one can systematically model the epoxidation of alkenes catalysed by Ti embedded or grafted molecular sieves, which was presented in chapter five. The full catalytic mechanism for the epoxidation of alkenes by titanium molecular sieves with a hydroperoxide based on this work is presented in figure 6.1 at the end of this chapter.

Preceding the work on the epoxidation mechanism (chapters four and five), is discussion concerning the area of molecular sieve science and the principles of molecular modelling. Furthermore, a detailed Ti molecular sieve literature review is also presented. In chapter one the nature of molecular sieves was discussed and why they are used so widely as industrial catalysts. A brief appraisal of experimental methods that have been applied to problems in molecular sieve science was also presented leading onto theoretical techniques in chapter two, an approach which has been used for the work described in this thesis. Chapter two showed why, at the time this work was started, using density functional theory and a cluster approach was the most appropriate technique to investigate reaction mechanisms in transition metal substituted molecular sieves*.

The majority of this thesis has conveyed the results and discussion of the modelling of catalytic processes in porous transition metal silicates. Indeed, chapters four and five report a large number of calculations and hypotheses and these have been split into three broad areas.

1. The nature of Titanium atoms in molecular sieve frameworks
2. Mechanistic studies on the reaction of peroxide to the Ti sites.
3. Mechanistic studies on the reaction of alkenes to peroxide bound titanium complexes.

6.2 Conclusions

6.2.1 The Ti active site

I firstly investigated the most appropriate model of the Ti active site using five potential structures. When taking into account the hydrogen bond energies which are likely to arise after hydrolysis of the Ti-O-Si bonds (see section 4.3.1), it was found that the monopodal, bipodal, tripodal and tetrapodal are all of similar

* C.R.A. Catlow, C.M. Barker, R.G. Bell, S.T. Bromley, D.S. Coombes, F. Corá, S. French, B. Slater, A.A. Sokol, L. Whitmore, S.M. Woodley, "Computer modelling of catalysts and catalysis", *NATO ASI series*, **2000** *560*, 3-60.

energy. However, the titanyl (Ti=O) is found to be 74-191 $kJmol^{-1}$ higher in energy than the aforementioned species and therefore is rejected. The monopodal model is unlikely to be important in the catalytic cycle, since there is only a single bond that anchors the metal to the zeolite framework and minimal metal leaching is observed, therefore this model was rejected. The tetrapodal model is thought unlikely in surface grafted molecular seives because after calcination the cyclopentadienyl ring is transformed to a hydroxyl group. To generate the four-fold model, requires this group to be converted to a silanol group *via* migration of siliceous species from the framework, a process that is highly unlikely. It is clear that of the two remaining structures, the triopodal model posesses an additional anchoring bond in comparison with the bipodal model. In reaction conditions, it would be expected that the tripodal model would be more robust and I therefore propose the *tripodal* model is the most accurate representation of the metal in *dehydrated* molecular seives.

To assess the accuracy of the model in a *hydrated* molecular seive, each of the five potential models were optimised in vacuuo, in the presence of one water molecule and finally, with two water molecules. Aside from the titanyl species, the binding energies of water to the cluster were found to be similar and their magnitude was indicative of physisorption. These energies can be accounted for, by considering the hydrogen bonds between the water and the oxygen containing Ti ligands. However, the absorption of water has negligible effect on either the geometry or the electronic configuration of the cluster. Since the effect of water has no influence on the chemistry of the model, it was neglected in the remaining work. Including explicit water molecules in the calculation would incur a severe computational penalty, and potentially introduce systematic errors into the reaction energetics, since of course in the real system, the hydrogen bonding network provided by the water would be mobile.

6.2.2 The Ti-peroxo species

Using a dehydrated, tripodal cluster, the oxidation of porous titanosilicates with hydrogen peroxide was investigated. In total, five Ti-peroxo models from the

literature were assessed two of which were found to be more stable than the reactants, one molecule of hydrogen peroxide and the tripodal Ti site. In the first structure, both peroxide oxygen atoms are bound directly to the metal (η^2). In the second model, only one of the peroxidic oxygen atoms is bonded to the metal centre(η^1). The activation energies of formation for the aforementioned species was less than 60 kJ mol^{-1} and 50 kJ mol^{-1} respectively, which could easily be traversed under mild reaction conditions. A new, stable Ti-peroxo complex was also isolated where the H_2O_2 molecule stays intact upon binding to the metal centre, referred to in the text as Ti-η^1[O(H)OH], section 4.4.4. The activation barrier for the formation of this complex was < 20 $kJmol^{-1}$. Using all six Ti-peroxo complexes considered in this work as starting geometries for the analysis of EXAFS data of a TBHP doped Ti-MCM-41 catalyst, both the Ti-η^2(OOH) and Ti-η^1(OOH) were confirmed to exist in the pores of titanosilicates [†]. Furthermore, their geometry is six coordinate where any under coordination is addressed by the binding of a water molecule to the metal centre.

6.2.3. The Epoxidation of alkenes

Finally, in chapter five, the interaction of alkenes to Ti-peroxo complexes has been examined. Interaction of ethene or propene to Ti-η^1 species (see figure 6.1) gives rise to the corresponding epoxide *via* movement of electron density from the π HOMO of the alkene double bond to the π^* LUMO of the peroxidic oxygen which is directly bonded to the Ti atom. This process results in the original catalyst being spontaneously regenerated and water (if H_2O_2 was employed) or an alcohol (where the carbon backbone is the substitutent on the organoperoxide) being released. For example if tert-butyl hydroperoxide is the sacrificial oxidant then tert-butanol would be released upon epoxidation.

A viable mechanism for the epoxidation of alkenes *via* a Ti-η^1[O(H)OH] complex has also been determined. The Ti-η^1[O(H)OH] model, isolated for the

[†] C.M. Barker, D. Gleeson, G. Sankar, N. Kaltsoyannis, C.R.A. Catlow, J.M. Thomas, accepted to Phys. Chem. Chem. Phys., **2001**. G. Sankar, J.M. Thomas, C.R.A. Catlow, C.M. Barker, D. Gleeson, N. Kaltsoyannis, J. Phys. Chem. B, **2001**, *105*, 9028.

first time in this work, is a very plausible model for the oxygen-donating species in titanosilicate catalysts. The activation barrier for its formation is the lowest of all three mechanisms (< 20 $kJmol^{-1}$) and attack of ethene or propene results in epoxide formation, a pathway which is ~ 200 $kJmol^{-1}$ energetically favourable. A highly plausible mechanism has been suggested for the regeneration of the original catalyst involving proton transfer from the OR ligand to the OR' ligand. However this step has not been directly examined in this thesis and has been marked with a question mark on figure 6.1. Common to the η^1 mechanism the R group stays bound to the metal centre *via* an oxygen bridge throughout the course of the reaction pathway. Thus, the Ti-η^1[O(H)OH] complex can account for the R group dependence on reaction kinetics.

In agreement with the comprehensive work of Sinclair and Catlow[‡] the η^2 Ti-peroxo is also found to facilitate alkene epoxidations. However, the η^2 mechanism does not explain the experimentally observed effect that R groups have on the reaction kinetics, since for ethene or propene to be epoxidised by the η^2 complex, the ligand containing the R group has to leave due to sterically inhibitingh the alkene pathway. However, η^2 complexes do promote the formation of diols, a common by-product in epoxidation reactions, the mechanism of which is outlined in chapter five. Thus, I propose that Ti-η^2(OOR') species are the oxygen donating species in diol formation (under appropriate reaction conditions) but are not the oxygen donating species for epoxidations.

6.2.4 R group effects

How R groups affect the reaction energetics of the interaction of peroxide to Ti sites and the interaction of alkenes to Ti-peroxo complexes has been a focal point of this work. Electron-withdrawing R groups such as CF_3 and CH_2F are found to give slightly higher activation barriers and to increase the electron population on the peroxidic oxygen donor thus resulting in a more repulsive alkene-oxygen interaction. This is consistent with the experimental observations that electron-

withdrawing R groups retard the reaction kinetics of titanosiliacte catalysed epoxidations. Sterically bulky R moieties such as iso-butyl and tert-butyl do not inhibit the Ti centre during peroxide binding or the peroxidic oxygens during alkene binding at any point. It was thought previously that sterically bulky groups would inhibit peroxide and/or alkene access to the titanium centres, however this work shows that this is not the case.

6.3 Concluding Remarks

The work presented in this thesis has focused upon the *chemistry* of catalytic processes using proven approximations and computational recipes. This work has shown that theoretical techniques provide reliable, complimentary and supplementary information to experimental techniques. Furthermore, in areas where experimental techniques have severe limitations, such as reaction mechanisms, theoretical approaches are essential predictive tools.

This work has shown that through a combination of theoretical and experimental techniques evidence of detailed key catalytic structures in molecular sieve porous solids can be obtained. I predict that the future applications of titanium molecular sieve oxidation catalysts will be with R derivatised solids, tailor made to deliver specific selectivities, yields or stereospecificites.

I will finish with my proposal for the complete catalytic cycle for alkene epoxidation reactions promoted by Titanium substituted molecular sieve porous solids with peroxide, based on all of the results presented in this thesis.

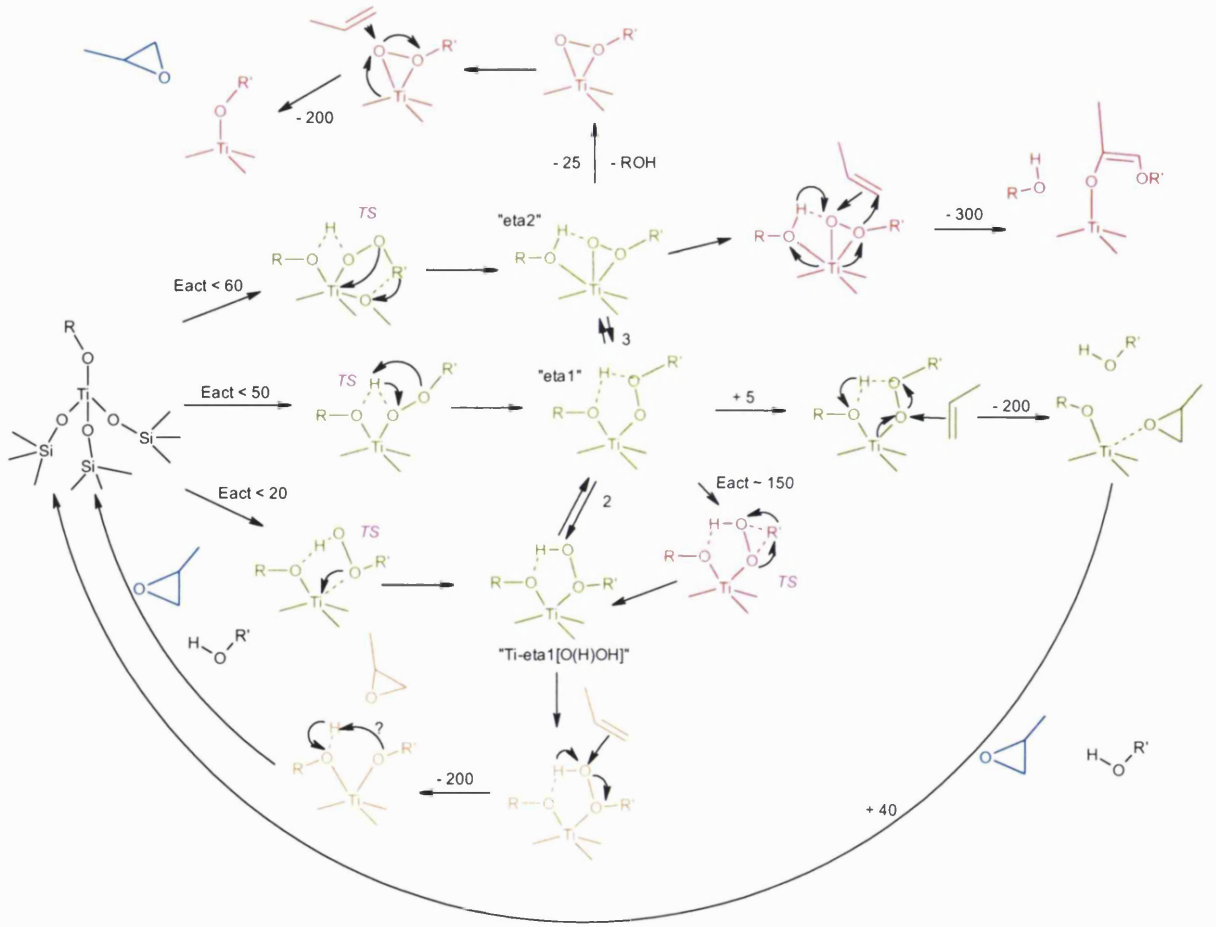

Figure 6.1 Proposed catalytic cycle for the epoxidation of alkenes. Green signifies favourable and red unfavourable pathways for epoxide formation. Amber indicates a suggested favourable pathway but that needs further work to verify its viability. Blue emphasises the epoxide product. Energies are in $kJmol^{-1}$.

Appendix

The xyz cartesian coordinates in Å for all energy minimised structures presented pictorially in this thesis are shown below. The format is atomic symbol, x coordinate, y coordinate, z coordinate.

1) Figure 2.4

```
O    0.831228   1.904964 -0.730874
O    0.829893  -1.830506 -0.731517
O   -2.183539   0.044876 -0.672619
O   -1.628539  -2.468523 -0.419694
O   -1.629259   2.551511 -0.435606
O    2.403729   0.037874 -0.426927
Si   2.507780   1.631556 -0.840558
Si   2.494705  -1.563938 -0.842098
Si  -0.220939  -3.152161 -0.840781
Si  -2.876970  -1.523013 -0.831232
Si  -2.883056   1.601808 -0.837714
Si  -0.222887   3.235504 -0.847270
O    3.038274   1.750568 -2.382742
O    3.191235   2.446732  0.403827
O    3.037244  -1.675362 -2.383840
O    3.187614  -2.374911  0.403959
O   -0.311876  -3.620630 -2.398767
O    0.233606  -4.111971  0.397622
O   -3.263199  -1.876201 -2.387594
O   -3.954685  -1.647501  0.389867
O   -3.259014   1.939990 -2.394672
O   -3.962018   1.719953  0.377463
O   -0.304427   3.700019 -2.400780
O    0.234025   4.179797  0.395688
H    3.626801   2.447710 -2.719932
H    4.117889   2.744330  0.400477
H    3.515424  -2.438480 -2.750132
H    4.121768  -2.645725  0.390358
H   -0.110053  -4.505645 -2.743773
H   -0.050488  -5.039030  0.471346
H   -4.137793  -1.706404 -2.778119
H   -4.611131  -2.364893  0.422363
H   -4.141722   1.830170 -2.786652
H   -4.602697   2.449578  0.432529
H    0.086646   4.507546 -2.773139
H   -0.126778   5.070447  0.547010
Ni  -0.011900   0.097803 -0.012448
C    1.390045  -1.167845  3.287150
H    2.007663  -1.970136  3.682361
C    1.852419   0.167802  3.344344
H    2.815102   0.383172  3.801352
C    1.076009   1.207663  2.836525
H    1.418163   2.237946  2.895586
C   -0.199403   0.924103  2.283934
```

2) Figure 4.1, left

```
Ti -0.629279   0.077093 -0.448025
O  -2.402605   0.041885 -0.049341
O  -0.083308   1.799847 -0.279145
O  -0.398108  -0.361667 -2.197570
O   0.353848  -0.959196  0.669946
Si -3.676040   0.991039 -0.610283
Si  0.381432   2.775854  1.012583
H   1.683302   2.259071  1.533827
H  -0.654265   2.707799  2.096893
H   0.526916   4.187674  0.535013
Si  1.396875  -2.217544  1.046657
H   1.967989  -2.785521 -0.218681
H   0.638798  -3.275400  1.789005
H   2.512455  -1.699953  1.905590
Si  0.713750   0.184097 -3.346582
H   0.447496  -0.511086 -4.644807
H   2.110255  -0.119291 -2.883368
H   0.572123   1.667384 -3.521031
H  -3.841001   0.783634 -2.088094
H  -3.383565   2.440877 -0.346893
H  -4.924588   0.584277  0.105951
```

```
H  -0.872451  1.746409  2.042065
C  -0.682932 -0.418447  2.268629
H  -1.723067 -0.613445  2.010578
C   0.128386 -1.463138  2.760035
H  -0.241297 -2.484715  2.755925
```

3) Figure 4.1, right

```
H   0.342654  1.071082 -2.964727
H  -0.441403 -2.724561 -3.102834
H   2.880411 -0.512768 -3.371132
H   3.376740 -1.494984  0.331640
H   0.071589  4.347180 -1.358797
H   1.605015  2.851092  1.690019
H   1.516059 -2.605946  3.474772
H   3.254965  0.400146  3.616440
H  -1.829585  3.296507  1.507233
H  -3.730291 -0.470748  2.041502
H  -3.358823 -3.092113 -0.174758
H  -3.784508  0.052718 -1.884282
O   0.325248  0.185482 -3.365970
O   0.457397 -2.395418 -3.228131
Si  0.924128 -1.065322 -2.514137
Ti -0.024285 -0.388620  0.357102
Si  2.210248 -0.966862  2.204959
Si -0.077779  2.794730  0.222258
O   2.513657 -0.958738 -2.596450
O   0.580272 -1.430487 -0.955949
O   0.620962 -0.812000  1.941490
O   3.370598 -0.881128  1.082518
O   0.317238  3.430981 -1.169781
O   0.835808  3.359381  1.395698
O   0.358616  1.276140 -0.127337
O   2.271383 -2.363607  2.924039
O   2.379508  0.205352  3.253258
O  -1.710824 -0.565120  0.819481
O  -1.584862  3.259881  0.571318
Si -3.055207 -0.898754  0.005392
O  -4.055561 -0.843327  1.213718
O  -3.184612 -2.319828 -0.732201
O  -3.334771  0.253082 -1.053391
```

4) Table 4.5, far left – top row

```
Ti -0.097844 -0.241866 -0.021208
O  -0.364972 -1.122628 -1.375679
O  -0.191225 -1.228760  1.524227
O  -0.955938  1.381262  0.006006
Si -1.795053  2.596881  0.793307
H  -1.598924  2.495784  2.280104
H  -3.259647  2.512643  0.484720
H  -1.246403  3.910416  0.319270
Si -0.726400 -1.235059  3.112257
H  -2.201520 -1.506242  3.137600
H  -0.459023  0.089892  3.771399
H   0.002300 -2.307445  3.864733
```

5) Table 4.5, 2nd left – top row

```
Ti -0.009572  0.008326  0.012102
O  -0.579901 -0.975324 -1.415850
O   1.810350 -0.027659  0.013429
O  -0.710856 -0.697046  1.529422
O  -0.554141  1.748001 -0.048349
H  -1.500847 -1.278950 -1.555714
H  -1.265211  2.173160  0.472173
Si -0.720830 -1.238123  3.115247
H  -2.092565 -1.754107  3.433083
H  -0.395652 -0.094140  4.032986
H   2.329771  0.755985  0.293248
H   0.286467 -2.332229  3.309036
```

6) Table 4.5, middle – top row

```
Ti  0.006530 -0.005923  0.005134
O  -0.564735 -0.952361 -1.444503
O   1.825610 -0.004287  0.003483
O  -0.693406 -0.722123  1.516819
O  -0.608612  1.708635  0.006694
H  -1.475250 -1.296395 -1.560965
Si -1.795053  2.596881  0.793307
H  -1.737375  2.343892  2.271777
H  -3.152148  2.208878  0.279636
H  -1.566619  4.055015  0.529522
Si -0.726400 -1.235059  3.112257
H  -2.103667 -1.745558  3.415684
H  -0.405867 -0.088021  4.025279
H   0.275734 -2.331724  3.320173
H   2.354330  0.751041  0.338446
```

7) Table 4.5, 2nd right – top row

```
O  -0.943531  1.462772  1.073492
O  -0.355152  0.265836 -1.531491
O  -0.266853 -1.425831  0.910371
Si  0.241451  2.550487  1.540217
H   1.604085  1.921425  1.449557
H  -0.010043  2.976970  2.955229
H   0.200552  3.750914  0.639693
Si  0.863083 -2.566498  1.376962
H   2.045673 -2.516789  0.453264
H   0.235783 -3.927094  1.308996
H   1.315413 -2.288107  2.779415
Si  0.627593  0.039950 -2.869037
H  -0.037343 -0.922189 -3.809173
H   1.956385 -0.511372 -2.443892
H   0.825818  1.358587 -3.554594
Ti -1.110730 -0.057812  0.081057
O  -2.871887 -0.480967 -0.158254
H  -3.388088 -0.121315 -0.910489
```

8) Table 4.5, far right – top row

See (1)

9) Table 4.5, far left – middle row

```
Ti -0.288456 -0.145611 -0.059853
O  -1.404923 -1.048002 -0.865606
O  -0.054140 -0.683380  1.693667
O  -0.711063  1.654204 -0.060908
Si -1.795053  2.596882  0.793308
H  -1.627064  2.383322  2.271601
H  -3.210492  2.259587  0.418734
H  -1.542129  4.045623  0.486502
Si -0.726400 -1.235059  3.112257
H  -2.195612 -1.502583  2.962829
H  -0.513396 -0.221897  4.199498
H  -0.036133 -2.512474  3.514441
O   1.598938 -1.051901 -0.619097
H   1.909720 -1.433673  0.234214
H   1.479707 -1.808359 -1.234224
```

10) Table 4.5, 2nd left – middle row

```
Ti -0.408193  0.133651  0.086834
O  -0.864829 -1.293400 -1.024734
O   1.440968  0.340389  0.280501
O  -0.892492 -0.422511  1.746732
O  -1.373159  1.665806 -0.157486
H  -1.391453 -2.015709 -0.622241
Si -0.858685 -1.124456  3.270200
H  -2.226136 -1.631763  3.610596
H  -0.424924 -0.105987  4.282138
H   0.113037 -2.268802  3.262900
H   1.814565  0.251567  1.180335
O   0.457870  0.654509 -2.046636
H   1.387633  0.601590 -1.722432
H   0.255740 -0.221211 -2.448028
H  -1.223148  2.108423 -1.021675
```

11) Table 4.5, middle – middle row

```
Ti -0.160210  0.094905  0.076232
O  -1.109760 -1.165989 -0.924199
O   1.683180 -0.086498  0.257249
O  -0.730830 -0.413739  1.735072
O  -0.729594  1.827049  0.083582
H  -1.801020 -1.647977 -0.423368
Si -1.902742  2.679181  0.910203
H  -1.797005  2.413938  2.385505
H  -3.273628  2.276876  0.444678
H  -1.712854  4.146530  0.662541
Si -0.834088 -1.152758  3.229154
H  -2.233493 -1.651180  3.437341
H  -0.492174 -0.165514  4.309405
H   0.116569 -2.312220  3.305480
H   2.080810  0.128696  1.126840
O   0.612472  0.317767 -2.062388
```

12) Table 4.5, 2nd right – middle row

```
Ti -0.588407 -0.070584 -0.075766
O  -2.359027 -0.334448  0.465484
O  -0.379142  1.674590  0.385880
O  -0.328744 -0.049506 -1.892641
O   0.748629 -0.876665  0.858528
H  -2.808307  0.419009  0.902468
Si  0.521498  2.834826  1.189468
H   1.987242  2.654614  0.920107
H   0.267709  2.738864  2.665029
H   0.087241  4.185227  0.700056
Si  1.688544 -2.257199  0.981643
H   2.176928 -2.679348 -0.372662
H   0.906695 -3.371335  1.607724
H   2.874654 -1.940354  1.843167
Si  0.792024  0.366221 -3.056790
H   0.246900 -0.034422 -4.396912
```

```
H   1.548621  0.042040 -1.946446
H   0.142375 -0.430933 -2.493378
```

```
H   2.091891 -0.350355 -2.829966
H   1.038967  1.846790 -3.046157
O  -1.198256 -2.307673 -0.602289
H  -2.100033 -2.181291 -0.221340
H  -1.313493 -2.274577 -1.575293
```

13) Table 4.5, far right – middle row

```
Ti -0.482893 -0.053120 -0.177389
O  -2.335872 -0.152506  0.118314
O  -0.301086  1.691016  0.290131
O  -0.332010 -0.063297 -1.985567
O   1.039916 -0.775700  0.545606
Si -3.288264  1.036551 -0.607809
Si  0.521498  2.834826  1.189468
H   2.002099  2.675677  1.002527
H   0.185820  2.673093  2.641629
H   0.103263  4.200308  0.732819
Si  1.688544 -2.257199  0.981643
H   1.849126 -3.138117 -0.224805
H   0.833354 -2.953376  1.997613
H   3.042612 -2.001367  1.572049
Si  0.834263  0.384871 -3.090993
H   0.444037 -0.151097 -4.435889
H   2.168948 -0.178997 -2.698708
H   0.935792  1.879656 -3.161973
O  -1.078504 -2.349557 -0.384960
H  -2.026397 -2.084016 -0.291142
H  -0.949330 -2.547496 -1.336640
H  -2.871903  1.273449 -2.030068
H  -3.214646  2.325668  0.153461
H  -4.700982  0.533393 -0.592598
```

14) Table 4.5, far left – bottom row

```
Ti -0.260979 -0.151677 -0.116751
O  -1.456598 -1.007865 -0.867904
O  -0.102740 -0.681262  1.673862
O  -0.695832  1.680061 -0.063138
Si -1.795053  2.596882  0.793308
H  -1.635875  2.388539  2.274150
H  -3.210718  2.259796  0.413433
H  -1.555696  4.050119  0.491045
Si -0.726400 -1.235059  3.112257
H  -2.194660 -1.542931  3.031878
H  -0.502750 -0.219177  4.196057
H  -0.002138 -2.499287  3.497416
O   0.551554  0.404512 -2.172465
H  -0.289842  0.192321 -2.638601
H   0.559882  1.386430 -2.099808
O   1.615052 -1.271912 -0.301938
H   1.589446 -1.842445  0.499006
H   1.720283 -1.850715 -1.086222
```

15) Table 4.5, 2nd left – bottom row

```
Ti -0.143716  0.015432  0.126957
O  -1.206184 -1.000388 -1.086321
O   1.593939  0.547036  0.678307
O  -0.842398 -0.776577  1.647989
O  -0.950442  1.658062  0.088610
O  -1.931009 -1.488291 -0.640464
Si -0.858684 -1.124455  3.270201
H  -2.232075 -1.575068  3.677031
H  -0.462920  0.060255  4.102236
H   0.105590 -2.249374  3.555411
H   1.669701  1.515247  0.820654
O   0.784454  0.202586 -1.962833
H   1.655258 -0.231032 -1.840565
H   0.185504 -0.487350 -2.341797
O   1.336318 -1.854594 -0.004244
H   1.962024 -1.413845  0.620679
H   0.905748 -2.581176  0.491872
H  -1.710684  1.752016 -0.521141
```

16) Table 4.5, middle – bottom row

```
Ti -0.092395  0.032542  0.099174
O  -1.257960 -0.919758 -1.088115
O   1.740653  0.334216  0.567782
O  -0.832011 -0.691240  1.631587
O  -0.704272  1.748580  0.207969
H  -2.100366 -1.169295 -0.651380
Si -1.902741  2.679181  0.910204
H  -1.906457  2.479442  2.398946
H  -3.249883  2.298436  0.363150
H  -1.645173  4.125673  0.609837
Si -0.834088 -1.152759  3.229154
H  -2.196823 -1.662236  3.599070
H  -0.470445 -0.010907  4.133919
H   0.162236 -2.264051  3.439459
H   1.896192  1.264673  0.836901
O   0.760920  0.219744 -1.969273
H   1.606906 -0.274688 -1.909519
H   0.110660 -0.384032 -2.406482
O   1.185664 -1.983826 -0.137645
H   1.857621 -1.701979  0.526051
H   0.661273 -2.708719  0.262040
```

17) Table 4.5, 2nd right – bottom row

18) Table 4.5, far right – bottom row

```
Ti -0.538282 -0.103284 -0.102699
O  -2.484429 -0.207444  0.141807
O  -0.318982  1.648214  0.380203
O  -0.393379 -0.007142 -1.934340
O   1.085325 -0.810800  0.380556
H  -2.958791  0.526667 -0.300559
Si  0.521498  2.834827  1.189467
H   2.001950  2.700860  0.983329
H   0.237167  2.724232  2.666867
H   0.061055  4.177862  0.709189
Si  1.688544 -2.257198  0.981644
H   2.395086 -2.989319 -0.123119
H   0.606448 -3.122691  1.544948
H   2.682213 -1.945524  2.065497
Si  0.792023  0.366222 -3.056789
H   0.303701 -0.007589 -4.425313
H   2.054020 -0.392217 -2.764156
H   1.076198  1.840285 -3.025573
O  -1.217368 -2.318126 -0.504620
H  -2.148214 -1.979649 -0.409828
H  -1.073133 -2.379702 -1.473381
O  -1.022327 -0.649176  2.143926
H  -1.959944 -0.370902  1.969058
H  -0.631862  0.032162  2.730210
```

19) Figure 4.9, left

See (16)

```
Ti -0.438752 -0.078840 -0.098121
O  -2.368582 -0.177629  0.084598
O  -0.275404  1.708062  0.262681
O  -0.268614 -0.084784 -1.924384
O   1.171980 -0.756502  0.457108
Si -3.288264  1.036551 -0.607809
Si  0.521498  2.834826  1.189468
H   2.011441  2.703603  1.079256
H   0.128658  2.612734  2.632666
H   0.095852  4.213133  0.785478
Si  1.688544 -2.257199  0.981643
H   1.857442 -3.182966 -0.189814
H   0.753351 -2.867126  1.977147
H   3.034110 -2.073397  1.629402
Si  0.834263  0.384871 -3.090993
H   0.384978 -0.152661 -4.418518
H   2.206519 -0.141326 -2.784116
H   0.885274  1.882800 -3.161525
O  -1.021221 -2.346731 -0.366043
H  -1.972651 -2.085758 -0.282269
H  -0.862908 -2.440074 -1.330254
O  -0.941298 -0.443110  2.182161
H  -1.882238 -0.181100  2.038664
H  -0.541886  0.235341  2.765992
H  -2.906619  1.302174 -2.035133
H  -3.162650  2.311866  0.178526
H  -4.727434  0.600214 -0.562770
```

20) Figure 4.9, right

See (17)

21) Figure 4.11

See (7)

22) Figure 4.13, Far left R=H

See (7)

23) Figure 4.13 Far left R=CH_3

```
O  -0.958022  1.479635  1.081630
O  -0.327166  0.277828 -1.518824
O  -0.271487 -1.432809  0.913019
Si  0.241451  2.550487  1.540217
H   1.594621  1.900710  1.447202
H   0.006870  2.987904  2.955743
H   0.219895  3.752736  0.640822
Si  0.863083 -2.566498  1.376962
H   2.045557 -2.514593  0.452826
H   0.241266 -3.930625  1.307696
H   1.323378 -2.297814  2.779261
Si  0.627593  0.039950 -2.869037
H  -0.047244 -0.922641 -3.802480
H   1.959327 -0.518658 -2.459757
H   0.827701  1.354163 -3.563576
Ti -1.099783 -0.045778  0.086619
O  -2.828788 -0.432410 -0.246767
C  -3.723643 -0.021105 -1.280607
H  -4.383899 -0.868741 -1.540568
H  -4.343889  0.822353 -0.925471
H  -3.167560  0.292968 -2.183834
```

24) Figure 4.13 Far left R=CF_3

```
O  -0.912639  1.408278  1.096506
O  -0.197709  0.182995 -1.409345
O  -0.344373 -1.471035  0.961492
Si  0.241451  2.550487  1.540217
H   1.609093  1.936599  1.457159
H  -0.030115  2.990597  2.944774
H   0.160218  3.721227  0.608426
Si  0.863083 -2.566498  1.376962
H   2.005424 -2.443459  0.412605
H   0.278155 -3.943065  1.306698
H   1.341250 -2.277419  2.766981
22  0.627593  0.039950 -2.869037
H  -0.111808 -0.899582 -3.768933
H   2.000161 -0.492441 -2.585023
H   0.722590  1.399820 -3.487537
Ti -1.099683 -0.083022  0.104025
O  -2.900888 -0.447413 -0.290429
C  -3.782681 -0.072606 -1.220437
F  -4.636649 -1.089886 -1.531008
F  -4.546872  0.985896 -0.810700
F  -3.179199  0.314223 -2.398164
```

25) Figure 4.13, Far left R=iso-but

O	-0.926805	1.393393	1.165654
O	-0.321903	0.243447	-1.481832
O	-0.394042	-1.556194	0.875372
Si	0.216492	2.552254	1.550217
H	1.605998	1.988985	1.436925
H	-0.011907	3.012049	2.959449
H	0.091635	3.722164	0.617293
Si	0.838124	-2.564731	1.386962
H	2.027663	-2.433508	0.479664
H	0.351850	-3.983759	1.357680
H	1.244372	-2.205661	2.786147
Si	0.602634	0.041718	-2.859037
H	-0.108624	-0.879815	-3.807052
H	1.937547	-0.543865	-2.503182
H	0.798482	1.375913	-3.515278
Ti	-1.136801	-0.078670	0.102083
O	-2.885626	-0.336771	-0.277162
C	-3.612283	-0.289449	-1.514605
H	-4.120911	0.693032	-1.574102
H	-2.896540	-0.352808	-2.359305
C	-4.651407	-1.419369	-1.629647
C	-4.034549	-2.797511	-1.339884
C	-5.282564	-1.361237	-3.034716
H	-4.529442	-1.583650	-3.814108
H	-5.711660	-0.366725	-3.254721
H	-6.092388	-2.105347	-3.134017
H	-3.572695	-2.818381	-0.339095
H	-3.253342	-3.050588	-2.081649
H	-4.805748	-3.587232	-1.380380
H	-5.439068	-1.224334	-0.876120

26) Figure 4.13, Far left R=GeH_3

O	-0.951795	1.472268	1.082416
O	-0.338009	0.253406	-1.523104
O	-0.267770	-1.429856	0.920390
Si	0.241451	2.550487	1.540217
H	1.601449	1.915389	1.449260
H	-0.004079	2.981389	2.955824
H	0.207885	3.752506	0.640937
Si	0.863083	-2.566498	1.376962
H	2.049215	-2.520665	0.457150
H	0.242115	-3.931350	1.311272
H	1.315448	-2.292138	2.781330
Si	0.627593	0.039950	-2.869037
H	-0.040493	-0.910251	-3.820240
H	1.963241	-0.516446	-2.470906
H	0.821329	1.365601	-3.544416
Ti	-1.110078	-0.053911	0.091250
O	-2.852869	-0.435202	-0.165366
Ge	-4.066107	0.019153	-1.453322
H	-4.908525	-1.254162	-1.708430
H	-4.915074	1.178676	-0.875929
H	-3.272968	0.452573	-2.713387

27) Figure 4.13, η^2 Reactant R=H

O	-0.192791	1.554715	0.760868
Si	0.687342	2.776686	1.496004
H	2.127701	2.371656	1.613694
H	0.125544	3.025164	2.863134
H	0.589146	4.024225	0.669836
Si	1.308975	-2.340299	1.332748
H	2.316439	-2.099147	0.249635
H	1.007847	-3.806022	1.433340
H	1.855207	-1.855481	2.642480
Si	1.073484	0.266150	-2.913251
H	0.278509	-0.518894	-3.918022
H	2.531272	-0.041205	-3.073158
H	0.836960	1.731136	-3.143274
O	-0.134536	-1.534079	0.993799
Ti	-0.604293	-0.027259	-0.008342
O	0.585440	-0.151911	-1.370954
O	-2.177965	-0.031782	-1.032542
O	-2.468545	-0.196536	1.445789
O	-2.599852	-1.520571	2.075847
H	-3.126804	-0.263718	0.705071
H	-1.689363	-1.872443	1.845320
H	-2.111712	0.040298	-2.007807

28) Figure 4.13, η^2 Reactant R=CH_3

O	-0.136760	1.606277	0.621492
Si	0.687342	2.776686	1.496004
H	2.120644	2.367010	1.669285
H	0.048196	2.940938	2.841681
H	0.627553	4.072793	0.744154
Si	1.308975	-2.340299	1.332748
H	2.295973	-2.117683	0.226772
H	0.970065	-3.798568	1.426928
H	1.902387	-1.884449	2.632327
Si	1.073484	0.266150	-2.913251
H	0.545273	-0.586601	-4.029129
H	2.568890	0.152334	-2.874940
H	0.687199	1.695733	-3.162057
O	-0.115913	-1.484681	1.047102
Ti	-0.632674	-0.023137	-0.011052
O	0.439314	-0.259963	-1.459859
O	-2.263148	-0.066601	-0.901147
O	-2.364641	-0.053015	1.631037
O	-2.435726	-1.302373	2.406104
H	-3.070096	-0.198219	0.947435
H	-1.566255	-1.699675	2.102084
C	-2.627257	0.051728	-2.275649
H	-1.742305	-0.010958	-2.936918

29) Figure 4.13, η^2 Reactant R=CF_3

O	-0.109645	1.590097	0.594689
Si	0.687343	2.776686	1.496004
H	2.121126	2.373564	1.668546
H	0.021971	2.893154	2.831524
H	0.604053	4.069427	0.746714
Si	1.308975	-2.340300	1.332749
H	2.280237	-2.144048	0.210405
H	0.875887	-3.772330	1.410380
H	1.943256	-1.932856	2.628321
Si	1.073485	0.266150	-2.913251
H	0.710450	-0.703285	-3.988987
H	2.564346	0.296478	-2.751827
H	0.574536	1.644107	-3.211590
O	-0.072384	-1.388194	1.087076
Ti	-0.631500	-0.010764	-0.024402
O	0.426729	-0.276232	-1.444175
O	-2.333936	-0.065358	-0.954493
O	-2.367263	-0.008946	1.571680
O	2.274092	-1.037068	2.619658
H	-3.158615	-0.307713	1.058203
H	-1.427716	-1.472525	2.305452
C	-2.851127	0.045206	-2.171456
F	-1.908919	0.086579	-3.179255
F	-3.601041	1.185042	-2.310570
F	-3.677680	-1.007967	-2.464513

30) Figure 4.13, η^2 Reactant R=iBu

O	-0.465165	1.458472	0.477736
Si	0.241451	2.550486	1.540218
H	1.266956	1.856314	2.387217
H	-0.803223	3.174756	2.414633
H	0.918387	3.613756	0.726601
Si	0.863084	-2.566498	1.376961
H	1.238281	-3.232157	0.085339
H	0.513749	-3.609356	2.395708
H	2.022169	-1.752470	1.870876
Si	0.627592	0.039950	-2.869038
H	0.010179	-0.537088	-4.107707
H	2.055584	-0.406406	-2.772091
H	0.569248	1.537417	-2.939831
O	-0.489833	-1.586910	1.162906
Ti	-1.076004	-0.198161	0.046407
O	-0.225615	-0.517430	-1.531895
O	-2.830617	-0.311666	-0.497032
O	-2.471335	0.114239	2.053941
O	-2.383516	-1.003158	3.009467
H	-3.315578	-0.094698	1.580347
H	-1.649119	-1.511037	2.553356
C	-3.479781	-0.296785	-1.777862
C	-4.052588	-1.672080	-2.168940
H	-3.206184	-2.386362	-2.165315
C	-4.621981	-1.598968	-3.599788
C	-5.115582	-2.162902	-1.171072
H	-2.759740	0.036312	-2.549995
H	-4.296557	0.451888	-1.727618
H	-3.855617	-1.289613	-4.332630
H	-5.461272	-0.881063	-3.661376
H	-5.007715	-2.584825	-3.914400
H	-5.478417	-3.168934	-1.446787
H	-5.990215	-1.484653	-1.158514
H	-4.712199	-2.220165	-0.146525

31) Figure 4.13, η^2 Reactant R=GeH_3

O	-0.486399	1.362881	0.609081
Si	0.216492	2.552254	1.550217
H	1.682503	2.261830	1.695743
H	-0.414853	2.590321	2.910740
H	0.037174	3.879036	0.875265
Si	0.838125	-2.564731	1.386962
H	1.834259	-2.378872	0.281351
H	0.370016	-3.990292	1.412044
H	1.476963	-2.229627	2.702132
Si	0.602634	0.041718	-2.859037
H	-0.131803	-0.622068	-3.988180
H	2.068161	-0.254673	-2.999977
H	0.386245	1.525750	-2.955333
O	-0.492258	-1.564848	1.157674
Ti	-1.043172	-0.252060	0.038195
O	0.067894	-0.545082	-1.393943
O	-2.644973	-0.516826	-1.219802

32) Figure 4.13, η^2 TS R=H

O	-0.121427	1.615540	0.589372
Si	0.687342	2.776686	1.496004
H	2.130844	2.389022	1.621622
H	0.063100	2.868731	2.854629
H	0.574603	4.089512	0.783920
Si	1.308975	-2.340299	1.332748
H	2.324309	-2.146721	0.246023
H	0.835609	-3.763517	1.338386
H	1.925785	-2.017159	2.661123
Si	1.073484	0.266150	-2.913251
H	0.470643	-0.455781	-4.084137
H	2.549408	0.003937	-2.876403
H	0.826291	1.738798	-3.056090
O	-0.020743	-1.337214	1.096323
Ti	-0.631077	0.009235	-0.012312
O	0.380967	-0.312612	-1.499562
O	-2.295485	0.333238	-1.194844
H	-3.134757	1.019162	-2.449305
H	-3.318642	-0.769753	-2.541252

O	-2.959129	-0.056152	0.960377
O	-3.328866	1.240884	1.539410
H	-3.260880	-0.220835	-0.250798
H	-3.440609	0.960599	2.477258
Ge	-3.033035	-1.807770	-2.472678
H	-1.677347	-2.334854	-2.988103
H	-3.854526	-1.104407	-3.580379
H	-3.852470	-2.908834	-1.754936

O	-2.491867	-0.188931	1.038794
O	-2.755259	-1.635625	1.146626
H	-2.818163	0.032393	-0.152076
H	-1.914186	-1.914411	1.594750
H	-2.470119	-0.225842	-1.979789

33) Figure 4.13, η^2 TS R=CH_3

O	0.228860	1.656605	0.865237
Si	1.091159	2.770476	1.778371
H	2.516546	2.318583	1.902497
H	0.474755	2.882193	3.139492
H	1.041000	4.095113	1.080358
Si	1.712792	-2.346509	1.615116
H	2.793744	-2.215839	0.582340
H	1.170525	-3.745615	1.604891
H	2.276952	-2.044074	2.971303
Si	1.477301	0.259940	-2.630883
H	1.006704	-0.468252	-3.856282
H	2.909410	-0.101526	-2.365329
H	1.372230	1.739001	-2.863317
O	0.450385	-1.284861	1.302664
Ti	-0.314667	0.051912	0.272888
O	0.539455	-0.199274	-1.325200
O	-2.073064	0.386121	-0.701549
C	-2.624115	0.096808	-1.994772
O	-2.055585	-0.208993	1.497025
O	-2.280104	-1.667225	1.522330
H	-2.520685	0.078319	0.349335
H	-1.410498	-1.950148	1.907549
H	-3.218846	0.962209	-2.339830
H	-3.270101	-0.797917	-1.945234
H	-1.800242	-0.087097	-2.704121

34) Figure 4.13, η^2 TS R=CF_3

O	0.261245	1.692834	0.781255
Si	1.091160	2.770476	1.778372
H	2.500788	2.291562	1.956965
H	0.408338	2.854992	3.109218
H	1.084838	4.109468	1.109117
Si	1.712792	-2.346509	1.615116
H	2.694826	-2.363182	0.483286
H	0.872102	-3.591565	1.573515
H	2.428002	-2.277858	2.929626
Si	1.477302	0.259940	-2.630884
H	1.004914	-0.516149	-3.818096
H	2.949895	0.049486	-2.442227
H	1.195413	1.720461	-2.801709
O	0.697571	-1.010344	1.490914
Ti	-0.197121	0.029263	0.284573
O	0.690913	-0.317397	-1.247090
O	-2.013778	0.747214	-0.906817
C	-2.659382	0.400738	-2.026577
O	-2.106952	-0.082295	1.255436
O	-1.884364	-1.444915	0.687635
H	-2.453262	0.409282	0.182582
H	-1.602878	-1.920523	1.508314
F	-3.699694	1.248959	-2.295595
F	-3.199065	-0.863964	-1.971568
F	-1.825215	0.430701	-3.109387

35) Figure 4.13, η^2 TS R=iso-butyl

O	-0.636635	1.490165	0.578174
Si	0.241451	2.550486	1.540218
H	1.661170	2.074857	1.642897
H	-0.370029	2.614885	2.906528
H	0.208313	3.903467	0.898046
Si	0.863083	-2.566498	1.376961
H	1.964979	-2.476832	0.362106
H	0.283243	-3.950165	1.376938
H	1.411170	-2.257385	2.737579
Si	0.627592	0.039950	-2.869038
H	0.190765	-0.697041	-4.100781
H	2.037976	-0.350696	-2.536746
H	0.567194	1.516816	-3.128313
O	-0.366620	-1.479059	1.023710
Ti	-1.171116	-0.137094	0.037261
O	-0.375030	-0.371480	-1.592840
O	-2.998415	0.057507	-0.834445
C	-3.612760	-0.213094	-2.111116
O	-2.811680	-0.362075	1.387014
O	-3.037817	-1.782638	1.697844

36) Figure 4.13, η^2 TS R=GeH_3

O	-0.620848	1.436616	0.627083
Si	0.241451	2.550486	1.540218
H	1.666837	2.098593	1 664343
H	-0.374953	2.662203	2.901338
H	0.191291	3.875123	0.842205
Si	0.863083	-2.566498	1.376961
H	1.944035	-2.435828	0.344185
H	0.320818	-3.965604	1.366737
H	1.427244	-2.264064	2.733148
Si	0.627593	0.039950	-2.869038
H	0.156996	-0.688241	-4.094437
H	2.059701	-0.321515	-2.603484
H	0.522520	1.519011	-3.101471
O	-0.399322	-1.504851	1.064509
Ti	-1.164376	-0.168077	0.034734
O	-0.310253	-0.419263	1.563353
O	-2.840378	0.183096	-0.760921
Ge	-3.481011	-0.130165	-2.248962
O	-2.905293	-0.428983	1.258871
O	-3.129812	-1.887215	1.284177

H	-3.379817	-0.203082	0.235117
H	-2.100804	-2.055917	1.878392
C	-3.901862	-1.704617	-2.346644
H	-2.920973	0.171075	-2.880560
H	-4.547451	0.380083	-2.157489
C	-4.903078	-2.274766	-1.325984
H	-2.935887	-2.235467	-2.234211
C	-4.402951	-1.905364	-3.789975
H	-4.550955	-2.159384	-0.287304
H	-5.058798	-3.354665	-1.497286
H	-5.887340	-1.777273	-1.419277
H	-5.379911	-1.411072	-3.946250
H	-4.537719	-2.979474	-4.006942
H	-3.693324	-1.499423	-4.532766
H	-3.370393	-0.141671	0.111181
H	-2.260206	-2.170137	1.669396
H	-4.336390	1.024950	-2.676481
H	-4.306920	-1.378583	2.177621
H	-2.358184	-0.317047	-3.224738

37) Figure 4.13, η^2 Product R=H

O	0.001212	-0.572793	-1.551320
O	-0.476745	-1.538225	1.063939
Si	0.628038	0.051381	-2.966540
H	1.548333	1.197581	-2.645360
H	-0.452875	0.544533	-3.882419
H	1.419589	-1.012433	-3.670294
Si	0.251570	2.460985	1.577542
H	1.510178	1.889199	2.158002
H	-0.665147	2.895375	2.683798
H	0.594482	3.649577	0.725646
Si	0.852518	-2.488427	1.437139
H	0.474771	-3.395782	2.570451
H	2.008580	-1.629699	1.860653
H	1.256320	-3.316543	0.252225
Ti	-1.074207	-0.251951	-0.096062
O	-0.535955	1.327945	0.635841
O	-2.965086	-0.350746	0.378926
O	-2.841678	-1.536502	-0.510098
H	-2.749303	-2.262582	0.157087
O	-2.230200	1.174773	-1.662978
H	-3.097362	1.083315	-1.203137
H	-1.920063	2.082254	-1.456102

38) Figure 4.13, η^2 Product R=CH_3

O	0.004576	-0.477217	-1.518983
O	-0.484911	-1.553921	1.047666
Si	0.628038	0.051381	-2.966540
H	1.533258	1.229566	-2.729465
H	-0.459951	0.471066	-3.914781
H	1.427666	-1.046880	-3.605008
Si	0.251570	2.460985	1.577542
H	1.494646	1.854405	2.159486
H	-0.593629	3.027196	2.681035
H	0.637659	3.570248	0.640946
Si	0.852518	-2.488427	1.437139
H	0.454885	-3.443217	2.523766
H	1.980156	-1.628227	1.928656
H	1.310857	-3.268537	0.238903
Ti	-1.110764	-0.232754	-0.074026
O	-0.631878	1.316547	0.749221
O	-2.998245	-0.444811	0.331583
O	-2.819991	-1.589777	-0.595094
H	-2.705522	-2.335270	0.047093
O	-2.307497	1.154315	-1.588347
C	-2.032329	2.551875	-1.840410
H	-1.866027	3.105407	-0.898843
H	-2.862133	3.006874	-2.410753
H	-1.118539	2.594484	-2.451328
H	-3.165592	1.067767	-1.112414

39) Figure 4.13, η^2 Product R=CF_3

O	-0.060350	-0.636630	-1.612743
O	-0.550751	-1.615734	1.158298
Si	0.622993	0.076361	-2.979861
H	1.289041	1.366305	-2.607996
H	-0.440172	0.314524	-4.004720
H	1.645493	-0.882128	-3.512211
Si	0.250513	2.456572	1.580014
H	1.434789	1.906363	2.316062
H	-0.803114	2.877971	2.558187
H	0.669678	3.622833	0.740586
Si	0.868704	-2.489699	1.407435
H	0.619562	-3.458899	2.521556
H	1.980481	-1.559410	1.792644
H	1.251260	-3.234081	0.163100

40) Figure 4.13, η^2 Product R=iBu

O	-0.049657	-0.546642	-1.572928
O	-0.487827	-1.571885	1.027469
Si	0.628038	0.051381	-2.966540
H	1.380771	1.320655	-2.675211
H	-0.410752	0.347176	-4.012499
H	1.587325	-0.957439	-3.529994
Si	0.251570	2.460985	1.577542
H	1.489916	1.914735	2.224513
H	-0.686610	2.974005	2.631402
H	0.632665	3.596681	0.670845
Si	0.852518	-2.488427	1.437139
H	0.470461	-3.402199	2.564316
H	1.982909	-1.608089	1.885514
H	1.305019	-3.313460	0.266900

```
Ti -0.937518 -0.321078 -0.067208
O  -0.361324  1.254780  0.581470
O  -2.797530  0.090014 -0.223046
O  -2.874025 -1.334649 -0.612415
H  -3.242902 -1.741459  0.210247
O  -2.542080  1.880035 -2.351950
C  -2.846599  3.181017 -2.157457
F  -3.226749  3.440802 -0.864873
F  -3.870069  3.609289 -2.954273
F  -1.772464  3.961497 -2.445408
H  -2.919093  1.310051 -1.625681
```

41) Figure 4.13, η^2 Product R=GeH_3

```
Ti -1.105857 -0.248226 -0.090109
O  -0.513056  1.278648  0.689223
O  -2.972558 -0.337854  0.458820
O  -2.900295 -1.511729 -0.450579
H  -2.776031 -2.245961  0.202863
O  -2.324181  1.153384 -1.574850
C  -1.922440  2.479225 -2.019252
H  -1.299327  2.955622 -1.237314
H  -1.293237  2.308765 -2.907493
H  -3.116151  1.229005 -0.994863
C  -3.112978  3.381318 -2.375456
C  -3.891052  3.814564 -1.117529
C  -2.604089  4.602268 -3.167104
H  -3.786611  2.794167 -3.029851
H  -4.241092  2.956448 -0.513618
H  -4.786872  4.399462 -1.388094
H  -3.259057  4.444642 -0.464110
H  -2.202923  4.302927 -4.151135
H  -3.418319  5.327523 -3.339775
H  -1.800116  5.128855 -2.619857
```

42) Figure 4.14, left

See (32)

```
O  -0.024424 -0.483050 -1.511531
O  -0.511605 -1.562325  1.046586
Si  0.603080  0.053148 -2.956540
H   1.506813  1.230322 -2.712012
H  -0.473585  0.461927 -3.919341
H   1.415259 -1.046762 -3.579841
Si  0.226612  2.462753  1.587542
H   1.468254  1.857587  2.175957
H  -0.620342  3.039867  2.683676
H   0.624386  3.563164  0.647698
Si  0.827559 -2.486660  1.447139
H   0.437934 -3.441416  2.536477
H   1.945031 -1.614224  1.940050
H   1.299636 -3.267899  0.254651
Ti -1.139508 -0.240128 -0.067538
O  -0.639585  1.302701  0.758677
O  -3.030622 -0.463621  0.369323
O  -2.851104 -1.600931 -0.569284
H  -2.732635 -2.350723  0.066993
O  -2.326409  1.130171 -1.566332
Ge -2.004914  2.922153 -1.892273
H  -1.840644  3.666377 -0.547242
H  -3.219195  3.450335 -2.696113
H  -0.709538  2.909896 -2.724801
H  -3.193820  0.995491 -1.114673
```

43) Figure 4.14, right

See (34)

44) Figure 4.15, left

See (27)

45) Figure 4.15, right

See (28)

46) Figure 4.17, η^1, far left R=H

See (7)

47) Figure 4.17, η^1, far left R=CH_3

48) Figure 4.17, η^1, far left R=CF_3

See (23)

49) Figure 4.17, η^1, far left R=iBu

See (25)

51) Figure 4.17, η^1, Reactant R=H

O	-0.544986	1.478429	0.520875
Si	0.241451	2.550486	1.540217
H	1.702437	2.207692	1.612532
H	-0.340542	2.491319	2.921369
H	0.087081	3.936032	0.988366
Si	0.863084	-2.566498	1.376962
H	1.870240	-2.390114	0.280044
H	0.355873	-3.979197	1.369003
H	1.513021	-2.285540	2.700495
Si	0.627592	0.039951	-2.869037
H	-0.230258	-0.608284	-3.920607
H	2.064013	-0.307567	-3.123634
H	0.448834	1.528609	-2.943318
O	-0.430049	-1.513661	1.178163
Ti	-0.966387	-0.217281	0.013289
O	0.177928	-0.545740	-1.370038
O	-2.570054	-0.479193	-0.962577
O	-2.921925	0.008577	1.407882
O	-3.257665	1.317953	1.983769
H	-3.500772	-0.027516	0.595843
H	-3.596705	1.021366	2.860717
H	-2.513374	-0.964077	-1.812543

53) Figure 4.17, η^1, Reactant R=CF_3

O	-0.654854	1.533864	0.539793
Si	0.239953	2.546456	1.542951
H	1.701005	2.271059	1.333280
H	-0.102887	2.310753	2.982178
H	-0.063587	3.964002	1.167361
Si	0.879355	-2.567194	1.347072
H	1.867695	-2.439338	0.227009
H	0.200594	-3.901647	1.293243
H	1.576359	-2.406499	2.663915
Si	0.622902	0.063973	-2.882435
H	0.107835	-0.807789	-3.983269
H	2.107084	-0.104746	-2.745476
H	0.298194	1.502027	-3.154089
O	-0.296587	-1.360579	1.217239
Ti	-1.038574	-0.169848	0.073762
O	-0.079766	-0.415191	-1.424624
O	-2.802642	-0.551071	-0.697843
O	-2.821322	0.038996	1.698159
O	-2.867864	1.204718	2.588969
H	-3.601191	0.193715	1.106969
H	-2.970417	0.740698	3.452778

See (24)

50) Figure 4.17, η^1, far left R=GeH_3

See (26)

52) Figure 4.17, η^1, Reactant R=CH_3

O	-0.540041	1.426156	0.575328
Si	0.241451	2.550486	1.540217
H	1.705700	2.223155	1.615857
H	-0.328388	2.561972	2.926755
H	0.073037	3.905559	0.918158
Si	0.863084	-2.566498	1.376962
H	1.865456	-2.373458	0.277619
H	0.417850	-4.000031	1.400694
H	1.498838	-2.227867	2.693562
Si	0.627592	0.039951	-2.869037
H	-0.072267	-0.679245	-3.985408
H	2.104058	-0.199764	-3.001268
H	0.350726	1.511241	-2.989832
O	-0.473585	-1.577967	1.143951
Ti	-1.004819	-0.244009	0.012304
O	0.112887	-0.553965	-1.398376
O	-2.599265	-0.446952	-0.972906
O	-2.952176	0.004969	1.405657
O	-3.204471	1.306029	2.042309
H	-3.491253	0.057329	0.565289
H	-3.629557	0.992273	2.874716
C	-2.866685	-1.061023	-2.233835
H	-1.935811	-1.416371	-2.712288
H	-3.355701	-0.328472	-2.904539
H	-3.542615	-1.925734	-2.095247

54) Figure 4.17, η^1, Reactant R=iBu

O	-0.465165	1.458472	0.477736
Si	0.241451	2.550486	1.540218
H	1.266956	1.856314	2.387217
H	-0.803223	3.174756	2.414633
H	0.918387	3.613756	0.726601
Si	0.863084	-2.566498	1.376961
H	1.238281	-3.232157	0.085339
H	0.513749	-3.609356	2.395708
H	2.022169	-1.752470	1.870876
Si	0.627592	0.039950	-2.869038
H	0.010179	-0.537088	-4.107707
H	2.055584	-0.406406	-2.772091
H	0.569248	1.537417	-2.939831
O	-0.489833	-1.586910	1.162906
Ti	-1.076004	-0.198161	0.046407
O	-0.225615	-0.517430	-1.531895
O	-2.830617	-0.311666	-0.497032
O	-2.471335	0.114239	2.053941
O	-2.383516	-1.003158	3.009467
H	-3.315578	-0.094698	1.580347
H	-1.649119	-1.511037	2.553356

C	-3.177268	-1.160199	-1.816881
F	-2.525055	-2.352856	-2.030583
F	-2.956576	-0.393122	-2.939815
F	-4.518535	-1.443737	-1.799377

C	-3.479781	-0.296785	-1.777862
C	-4.052588	-1.672080	-2.168940
H	-3.206184	-2.386362	-2.165315
C	-4.621981	-1.598968	-3.599788
C	-5.115582	-2.162902	-1.171072
H	-2.759740	0.036312	-2.549995
H	-4.296557	0.451888	-1.727618
H	-3.855617	-1.289613	-4.332630
H	-5.461272	-0.881063	-3.661376
H	-5.007715	-2.584825	-3.914400
H	-5.478417	-3.168934	-1.446787
H	-5.990215	-1.484653	-1.158514
H	-4.712199	-2.220165	-0.146525

55) Figure 4.17, η^1, Reactant R=GeH_3

O	-0.556569	1.433561	0.560923
Si	0.216492	2.552254	1.550217
H	1.684384	2.240405	1.609920
H	-0.348522	2.514367	2.937654
H	0.024420	3.919352	0.964966
Si	0.838125	-2.564731	1.386962
H	1.853688	-2.375792	0.299000
H	0.380656	-3.993836	1.405141
H	1.461803	-2.230782	2.710683
Si	0.602634	0.041718	-2.859037
H	-0.028934	-0.701767	-3.997784
H	2.091035	-0.144669	-2.938749
H	0.279105	1.502707	-2.993726
O	-0.486249	-1.560022	1.148436
Ti	-1.038203	-0.240433	0.020864
O	0.050257	-0.558992	-1.406530
O	-2.677685	-0.477508	-0.857095
O	-2.948076	0.013620	1.563594
O	-3.216178	1.325885	2.172994
H	-3.504577	0.039791	0.734911
H	-3.611119	1.022930	3.023258
Ge	-3.150030	-1.303347	-2.416356
H	-1.900717	-1.974817	-3.035672
H	-3.721665	-0.195906	-3.340524
H	-4.230325	-2.357623	-2.063671

56) Figure 4.17, η^1, TS R=H

O	-0.567319	1.389341	0.633586
Si	0.241451	2.550486	1.540217
H	1.684953	2.162822	1.665835
H	-0.382791	2.642531	2.898842
H	0.128711	3.863313	0.828133
Si	0.863084	-2.566498	1.376962
H	1.878418	-2.372920	0.290235
H	0.389719	-3.989716	1.382598
H	1.479895	-2.243358	2.705336
Si	0.627592	0.039951	-2.869037
H	0.024751	-0.681979	-4.039924
H	2.103517	-0.222261	-2.832189
H	0.380399	1.512599	-3.011877
O	-0.466635	-1.563414	1.140537
Ti	-1.076968	-0.216964	0.031901
O	-0.064923	-0.538811	-1.455348
O	-2.741377	0.107039	-1.150631
O	-2.937759	-0.415130	1.083007
O	-3.201151	-1.861825	1.190840
H	-3.264054	-0.193806	-0.107863
H	-2.360077	-2.140611	1.638963
H	-2.916011	-0.452042	-1.935576

57) Figure 4.17, η^1, TS R=CH_3

O	-0.440753	1.382537	0.556667
Si	0.241451	2.550486	1.540217
H	1.703654	2.258388	1.716479
H	-0.423568	2.560886	2.884824
H	0.075819	3.888853	0.884762
Si	0.863084	-2.566498	1.376962
H	1.868319	-2.389615	0.279294
H	0.387669	-3.989593	1.403058
H	1.495281	-2.231400	2.696011
Si	0.627592	0.039951	-2.869037
H	-0.116043	-0.625429	-3.993788
H	2.092993	-0.244775	-3.028546
H	0.398370	1.522176	-2.947555
O	-0.463074	-1.559838	1.149315
Ti	-0.995817	-0.246288	0.018415

58) Figure 4.17, η^1, TS R=CF_3

O	-0.446735	1.309542	0.647798
Si	0.239953	2.546456	1.542951
H	1.715017	2.295393	1.657345
H	-0.370740	2.583094	2.911789
H	-0.003760	3.846390	0.839295
Si	0.879355	-2.567194	1.347072
H	1.853995	-2.360685	0.227962
H	0.403840	-3.988163	1.365489
H	1.530203	-2.233813	2.656400
Si	0.622902	0.063973	-2.882435
H	-0.093833	-0.620642	-4.004397
H	2.093583	-0.217198	-2.979307
H	0.393331	1.545766	-2.968799
O	-0.458965	-1.560421	1.154243
Ti	-1.006666	-0.270332	0.028166

O	0.113501	-0.582398	-1.408422
O	-2.587268	-0.460830	-1.257933
O	-2.934054	-0.049586	0.913958
O	-3.319029	1.229967	1.519268
H	-3.233387	-0.208072	-0.293615
H	-3.468580	0.923479	2.443447
C	-2.876004	-1.502506	-2.206499
H	-1.927953	-1.849777	-2.649703
H	-3.523016	-1.097687	-3.004876
H	-3.382557	-2.352056	-1.713949

59) Figure 4.17, η^1, TS R=iBu

O	-2.317253	3.284059	0.849355
Si	1.575507	3.893353	1.820038
H	3.030866	3.703951	2.105769
H	0.854379	3.996693	3.116049
H	1.381583	5.105346	0.992382
Si	2.613743	-1.112549	2.498003
H	3.752631	-0.986918	1.559071
H	2.268754	-2.543195	2.669012
H	3.003601	-0.548009	3.813068
Si	2.877502	0.878920	-2.067303
H	2.417233	0.077509	-3.228864
H	4.345302	0.713221	-1.928466
H	2.584083	2.310853	-2.338090
O	1.281830	-0.176978	1.921346
Ti	0.683815	0.940277	0.574718
O	2.091474	0.563664	-0.598134
O	-0.618399	0.270942	-0.766917
O	-1.622742	0.843841	1.230531
O	-2.429727	2.268935	1.529475
H	-1.524682	0.776404	0.176270
H	-2.057834	2.431225	2.416509
C	-0.897083	-0.822129	-1.681273
H	0.031103	-1.073477	-2.212672
H	-1.618429	-0.427920	-2.412946
C	-1.488689	-2.089374	-1.012373
C	-2.603340	-1.766346	-0.000012
C	-1.998111	-3.035376	-2.122238
H	-2.834343	-2.570425	-2.662672
H	-2.361907	-3.977373	-1.692097
H	-1.214441	-3.275977	-2.852398
H	-3.395101	-1.158788	-0.460665
H	-2.226605	-1.214021	0.864050
H	-3.062958	-2.687148	0.377965
H	-0.671811	-2.592511	-0.474962

60) Figure 4.17, η^1, TS R=GeH_3

O	-0.486399	1.362881	0.609081
Si	0.216492	2.552254	1.550217
H	1.682503	2.261830	1.695743
H	-0.414853	2.590321	2.910740
H	0.037174	3.879036	0.875265
Si	0.838125	-2.564731	1.386962
H	1.834259	-2.378872	0.281351
H	0.370016	-3.990292	1.412044
H	1.476963	-2.229627	2.702132
Si	0.602634	0.041718	-2.859037
H	-0.131803	-0.622068	-3.988180
H	2.068161	-0.254673	-2.999977
H	0.386245	1.525750	-2.955333
O	-0.492258	-1.564848	1.157674
Ti	-1.043172	-0.252060	0.038195
O	0.067894	-0.545082	-1.393943
O	-2.644973	-0.516826	-1.219802
O	-2.959129	-0.056152	0.960377
O	-3.328866	1.240884	1.539410
H	-3.260880	-0.220835	-0.250798
H	-3.440609	0.960599	2.477258
Ge	-3.033035	-1.807770	-2.472678
H	-1.677347	-2.334854	-2.988103
H	-3.854526	-1.104407	-3.580379
H	-3.852470	-2.908834	-1.754936

61) Figure 4.17, η^1, Product R=H

O	-0.881593	1.511778	0.850385
Si	0.241451	2.550487	1.540217
H	1.611197	1.937172	1.510280
H	-0.156165	2.824067	2.960872
H	0.254782	3.836840	0.769085
Si	0.863084	-2.566498	1.376961
H	2.028751	-2.891149	0.487761
H	-0.162587	-3.653290	1.271590
H	1.340544	-2.446174	2.793247

62) Figure 4.17, η^1, Product R=CH_3

O	-0.747604	1.525616	0.669824
Si	0.241451	2.550487	1.540217
H	1.636797	1.999481	1.619727
H	-0.295093	2.739135	2.929982
H	0.275843	3.879765	0.843965
Si	0.863084	-2.566498	1.376961
H	2.045147	-2.972235	0.544508
H	-0.201949	-3.614988	1.270341
H	1.298625	-2.424491	2.805351

Si	0.627592	0.039950	-2.869037
H	0.215747	-0.735043	-4.087621
H	1.966024	-0.451060	-2.398531
H	0.738190	1.492982	-3.232412
O	0.218187	-1.096835	0.880272
Ti	-1.090770	-0.117172	0.080604
O	-0.548092	-0.159693	-1.694986
O	-2.950886	0.500289	-0.881257
H	-2.835839	0.270455	-1.828150
O	-2.340992	-1.319823	0.990607
O	-3.788005	-1.314514	0.694319
H	-3.635721	-0.120033	-0.479947
H	-4.144503	-1.026958	1.567080

Si	0.627592	0.039950	-2.869037
H	0.296465	-0.680284	-4.143678
H	1.963005	-0.424851	-2.365134
H	0.701106	1.514561	-3.152791
O	0.286908	-1.091236	0.818030
Ti	-1.053703	-0.144620	0.014657
O	-0.585479	-0.269276	-1.760454
O	-2.977445	0.569492	-0.689060
C	-3.345239	0.998449	-2.019691
O	-2.250482	-1.369284	0.966348
O	-3.706012	-1.411548	0.709796
H	-3.643287	-0.077225	-0.306007
H	-4.037541	-1.272473	1.626869
H	-4.285809	1.575124	-1.970106
H	-3.455838	0.136748	-2.700876
H	-2.536448	1.645693	-2.385102

63) Figure 4.17, η^1, Product R=CF_3

O	-0.723374	1.551476	0.599236
Si	0.239953	2.546456	1.542952
H	1.627888	1.983217	1.635255
H	-0.345364	2.664191	2.919809
H	0.287425	3.901216	0.903673
Si	0.879355	-2.567193	1.347072
H	2.039252	-2.991583	0.496256
H	-0.245381	-3.544292	1.196159
H	1.311064	-2.497180	2.780553
Si	0.622902	0.063972	-2.882435
H	0.273258	-0.640926	-4.157296
H	1.967412	-0.397134	-2.399199
H	0.661556	1.545389	-3.114440
O	0.380723	-1.030839	0.863766
Ti	-0.956590	-0.146549	0.023006
O	-0.541635	-0.333368	-1.735948
O	-3.039245	0.668756	-0.752515
C	-3.482025	1.029332	-1.994315
O	-2.240577	-1.274323	0.963648
O	-3.668079	-1.342836	0.599582
H	-3.635386	-0.048198	-0.323707
H	-4.076754	-1.245881	1.492229
F	-4.756805	1.517261	-1.933649
F	-3.500422	-0.015548	-2.869429
F	-2.682645	1.990719	-2.491265

64) Figure 4.17, η^1, Product R=iBu

O	-0.694236	1.543047	0.585033
Si	0.241450	2.550487	1.540218
H	1.638193	2.015279	1.669148
H	-0.369351	2.676041	2.906045
H	0.285781	3.904641	0.896157
Si	0.863084	-2.566498	1.376961
H	2.061831	-2.974878	0.570101
H	-0.195477	-3.619657	1.255159
H	1.271354	-2.417682	2.813004
Si	0.627593	0.039950	-2.869038
H	0.284850	-0.612392	-4.177443
H	1.962114	-0.467497	-2.404546
H	0.717225	1.525561	-3.080353
O	0.310175	-1.087085	0.804233
Ti	-1.043271	-0.148709	0.010229
O	-0.573137	-0.322600	-1.765763
O	-2.996002	0.422168	-0.684651
C	-3.537364	0.857765	-1.964253
O	-2.178558	-1.318107	1.114843
O	-3.653489	-1.346741	0.991979
H	-3.644770	-0.149772	-0.175260
H	-3.900611	-1.102627	1.913855
H	-4.545166	1.273766	-1.767449
C	-3.594599	-0.241018	-3.038561
H	-2.886081	1.683143	-2.291849
C	-4.368092	-1.488552	-2.576530
C	-4.210501	0.350348	-4.322021
H	-4.119444	-0.362693	-5.159772
H	-3.712168	1.288264	-4.627100
H	-5.286626	0.566494	-4.185078
H	-2.550632	-0.538697	-3.242650
H	-4.323968	-2.274034	-3.350788
H	-5.435921	-1.259817	-2.394397
H	-3.947069	-1.922219	-1.654055

65) Figure 4.17, η^1, Product R=GeH_3

O	-0.748444	1.526438	0.656050
Si	0.216492	2.552254	1.550217

66) Figure 4.18, η^1TS R=CH_2F

O	-0.431373	1.375581	0.552977
Si	0.241451	2.550486	1.540217

H	1.614579	2.010680	1.645729
H	-0.343451	2.724785	2.932850
H	0.251564	3.888184	0.867188
Si	0.838125	-2.564731	1.386961
H	2.021929	-2.970501	0.557659
H	-0.224154	-3.616399	1.284789
H	1.271816	-2.418987	2.815683
Si	0.602634	0.041718	-2.859037
H	0.278295	-0.672936	-4.138519
H	1.935675	-0.424674	-2.350649
H	0.678492	1.517087	-3.136986
O	0.263787	-1.090161	0.821501
Ti	-1.084522	-0.145544	0.021873
O	-0.622568	-0.271514	-1.762961
O	-2.999412	0.561303	-0.669546
Ge	-3.453520	1.113687	-2.376834
O	-2.259629	-1.374505	0.998525
O	-3.714774	-1.425822	0.738562
H	-3.659387	-0.074780	-0.253926
H	-4.050419	-1.280440	1.653264
H	-4.792142	1.881816	-2.214141
H	-3.616795	-0.138454	-3.268048
H	-2.300826	2.036661	-2.806661

67) Figure 4.18, η^2TS R=CH_2F

O	-0.652242	1.456004	0.622878
Si	0.241450	2.550487	1.540217
H	1.659042	2.071244	1.636600
H	-0.359194	2.651117	2.908279
H	0.196603	3.879298	0.852195
Si	0.863084	-2.566498	1.376961
H	1.976173	-2.476407	0.375308
H	0.253089	-3.936861	1.336786
H	1.398704	-2.300508	2.751825
Si	0.627592	0.039951	-2.869038
H	0.204417	-0.726620	-4.087080
H	2.042222	-0.319597	-2.521043
H	0.538042	1.511108	-3.145178
O	-0.336335	-1.442252	1.042997
Ti	-1.172858	-0.150927	0.033891
O	-0.376906	-0.378257	-1.594272
O	-2.998061	0.135354	-0.936097
C	-3.554893	-0.131068	-2.190849
O	-2.891968	-0.466533	1.256142
O	-3.077701	-1.929885	1.246744
H	-3.410290	-0.173905	0.121774
H	-2.236217	-2.198331	1.695415
F	-4.241545	0.996263	-2.654696
H	-4.288200	-0.955613	-2.123662
H	-2.743340	-0.350737	-2.905649

68) Figure 4.19, right

See (63)

H	1.705665	2.266546	1.707561
H	-0.422653	2.540471	2.884788
H	0.057603	3.887430	0.889208
Si	0.863084	-2.566498	1.376962
H	1.863773	-2.393423	0.274777
H	0.366508	-3.981802	1.396039
H	1.500212	-2.242001	2.695343
Si	0.627592	0.039951	-2.869037
H	-0.102339	-0.616462	-4.005941
H	2.092631	-0.259602	-2.993130
H	0.410612	1.523679	-2.933445
O	-0.453875	-1.542611	1.158013
Ti	-1.003974	-0.244153	0.025399
O	0.074969	-0.584877	-1.418841
O	-2.634938	-0.542789	-1.263864
O	-2.927633	-0.057373	0.897011
O	-3.319917	1.214820	1.506064
H	-3.269386	-0.269074	-0.316154
H	-3.488740	0.901210	2.425268
C	-2.930837	-1.539577	-2.203895
H	-1.985332	-1.899259	-2.645789
F	-3.708533	-1.000396	-3.231149
H	-3.517280	-2.356397	-1.743587

68) Figure 4.19, left

See (62)

69) Figure 4.21

O	-0.831001	1.375922	1.047594
Si	0.238539	2.572520	1.553428
H	1.640016	2.035138	1.578834
H	-0.156643	3.004895	2.932534
H	0.167717	3.740149	0.616235

Si	0.863278	-2.563563	1.347628
H	2.021813	-2.586966	0.394232
H	0.361585	-3.962858	1.554925
H	1.314518	-1.998916	2.662468
Si	0.630309	0.014980	-2.852915
H	-0.105800	-0.815958	-3.863454
H	1.936756	-0.642269	-2.517780
H	0.888202	1.379193	-3.420883
O	-0.392467	-1.644032	0.725147
Ti	-1.195572	-0.105452	0.075061
O	-0.283782	0.180617	-1.464192
O	-2.922104	-0.107275	-0.691533
H	-3.015408	0.239933	-1.601841
O	-2.661398	-0.949460	1.725574
O	-4.094074	-1.029793	1.405238
H	-4.035657	-0.667093	0.463687
H	-2.387273	-1.897984	1.688425

70) Figure 4.22, Ti-η^1(OOH)

See (61)

71) Figure 4.22, TS

O	-0.263859	1.494938	1.048549
Si	0.806851	2.695841	1.533738
H	2.213532	2.172531	1.535343
H	0.436525	3.142402	2.914910
H	0.707396	3.856088	0.587721
Si	1.469623	-2.436400	1.352500
H	2.661584	-2.542444	0.445425
H	0.883956	-3.801907	1.560096
H	1.901236	-1.871757	2.674532
Si	1.154156	0.112050	-2.861004
H	0.430172	-0.746257	-3.859590
H	2.446923	-0.550977	-2.485815
H	1.443608	1.448296	-3.480576
O	0.340900	-1.435001	0.642673
Ti	-0.628206	0.010498	0.083974
O	0.201950	0.343267	-1.509953
O	-2.413637	0.028123	-0.698090
H	-2.567778	0.444363	-1.569806
O	-1.864853	-0.899633	1.603264
O	-3.449028	-0.615353	1.396492
H	-3.312259	-0.269610	0.383667
H	-2.853529	-1.606207	1.405381

72) Figure 4.22, Tiη^1[O(H)OH]

See (69)

73) Figure 4.23, far left R=H

See (7)

74) Figure 4.23, far left R=CH_3

See (23)

75) Figure 4.23, far left R=CF_3

See (24)

76) Figure 4.23, far left R=iBu

See (25)

77) Figure 4.23, far left R=GeH_3

See (26)

78) Figure 4.23, reactant R=H

O	-1.000801	1.506213	1.075317

79) Figure 4.23, reactant R=CH_3

O	-1.015126	1.508693	1.107230

O	-0.389816	0.231922	-1.550005
O	-0.236030	-1.394439	0.914461
Si	0.241451	2.550487	1.540217
H	1.568209	1.858645	1.432351
H	-0.001027	2.960424	2.960517
H	0.228914	3.757015	0.651444
Si	0.863083	-2.566498	1.376962
H	2.057456	-2.533549	0.468902
H	0.208974	-3.913290	1.294893
H	1.300885	-2.301707	2.786874
Si	0.627593	0.039950	-2.869037
H	0.009558	-0.909980	-3.850694
H	1.949552	-0.504343	-2.411472
H	0.835943	1.376299	-3.516057
Ti	-1.122800	-0.054569	0.087504
O	-2.883929	-0.434512	0.002870
H	-3.546491	0.303500	0.137280
O	-3.619684	2.504742	1.713822
O	-4.458273	1.798455	0.717065
H	-2.728282	2.098862	1.516370
H	-5.184915	1.494979	1.308934

80) Figure 4.23, Reactant R=CF_3

O	-0.972882	1.438090	1.124762
O	-0.191350	0.191154	-1.399283
O	-0.342809	-1.456211	0.979549
Si	0.241451	2.550487	1.540217
H	1.579513	1.882336	1.417677
H	0.008414	2.982787	2.951071
H	0.168071	3.716094	0.604085
Si	0.863083	-2.566498	1.376962
H	2.001917	-2.423923	0.412266
H	0.282908	-3.943454	1.290198
H	1.332494	-2.281955	2.769995
Si	0.627593	0.039950	-2.869037
H	-0.119245	-0.922873	-3.736473
H	2.007924	-0.470268	-2.587360
H	0.693294	1.392412	-3.505727
Ti	-1.094577	-0.075106	0.111233
O	-2.897345	-0.441934	-0.240572
C	-3.782110	-0.360312	-1.239568
O	-3.397187	2.271736	2.594947
O	-4.385160	2.818622	1.646883
H	-2.679711	1.992249	1.968776
H	-5.042776	2.084150	1.639203
F	-4.398760	-1.558645	-1.458624
F	-4.762049	0.553908	-0.968880
F	-3.205266	0.015373	-2.430553

81) Figure 4.23, Reactant R=iBu

O	-0.291631	0.299699	-1.495619
O	-0.273945	-1.433108	0.904212
Si	0.241451	2.550487	1.540217
H	1.559944	1.838954	1.430476
H	0.028402	2.988279	2.956358
H	0.241997	3.742469	0.631889
Si	0.863086	-2.566498	1.376962
H	2.052147	-2.510075	0.463146
H	0.247502	-3.932402	1.310726
H	1.303772	-2.279995	2.781891
Si	0.627593	0.039950	-2.869037
H	-0.083328	-0.916654	-3.780276
H	1.959925	-0.533624	-2.486003
H	0.823943	1.352561	-3.566573
Ti	-1.092892	-0.038058	0.085561
O	-2.808158	-0.424838	-0.264583
C	-3.737939	-0.023306	-1.278445
O	-3.510904	2.705469	1.977605
O	-4.631713	2.229321	1.143448
H	-2.753107	2.185071	1.592975
H	-5.096700	1.657630	1.797485
H	-4.396185	-0.879513	-1.512114
H	-4.339227	0.821094	-0.897906
H	-3.204826	0.285086	-2.197071

O	-1.041929	1.506562	1.140883
O	-0.286142	0.257622	-1.455730
O	-0.329534	-1.443468	0.965858
Si	0.216492	2.552254	1.550217
H	1.533452	1.835558	1.452610
H	0.006901	3.020993	2.956960
H	0.219908	3.723937	0.615527
Si	0.838124	-2.564731	1.386962
H	2.009206	-2.464898	0.452880
H	0.252252	-3.942760	1.301175
H	1.297630	-2.298976	2.789664
Si	0.602634	0.041718	-2.859037
H	-0.130663	-0.894880	-3.773119
H	1.947817	-0.532792	-2.527822
H	0.769976	1.372858	-3.527698
Ti	-1.117664	-0.040946	0.119443
O	-2.838868	-0.400910	-0.252052
C	-3.609725	-0.275773	-1.461491
O	-3.547474	2.638105	2.011587
O	-4.593917	2.238230	1.052198
H	-2.755612	2.170519	1.629042
H	-5.075562	1.574601	1.597333
H	-4.118825	0.705789	-1.433230
H	-2.915716	-0.282044	-2.325739
C	-4.644448	-1.405895	-1.617293
C	-4.042438	-2.794002	-1.343582
C	-5.242787	-1.317326	-3.034957
H	-4.467433	-1.519792	-3.798189
H	-5.669171	-0.319606	-3.243956
H	-6.045854	-2.062511	-3.172169
H	-3.593422	-2.838661	-0.337787
H	-3.255658	-3.044520	-2.080196

82) Figure 4.23, TS, R=H

O	-0.617813	1.129913	1.255924
O	-0.328520	0.178221	-1.503360
O	-0.430013	-1.759714	0.670753
Si	0.241451	2.550487	1.540218
H	1.707023	2.222947	1.505263
H	-0.123172	3.074392	2.893900
H	-0.061322	3.569927	0.485452
Si	0.863084	-2.566499	1.376962
H	2.072457	-2.436611	0.496740
H	0.503810	-4.014291	1.517435
H	1.163786	-1.984445	2.726471
Si	0.627593	0.039951	-2.869038
H	-0.031985	-0.890812	-3.844151
H	1.975767	-0.501395	-2.492879
H	0.781191	1.396507	-3.487823
Ti	-1.075086	-0.164653	0.098467
O	-2.915023	-0.260008	-0.118158
O	-3.613955	2.618184	1.385499
O	-4.651315	1.711468	0.813687
H	-4.212066	3.344634	1.667593
H	-4.044437	0.975606	0.515368
H	-3.274987	-0.753579	-0.886337

83) Figure 4.23, TS, R=CH_3

O	-0.633741	1.144423	1.242550
O	-0.327159	0.172074	-1.505628
O	-0.444068	-1.758278	0.693525
Si	0.241451	2.550487	1.540218
H	1.706093	2.220272	1.507130
H	-0.121631	3.069459	2.896735
H	-0.051435	3.584836	0.495578
Si	0.863084	-2.566499	1.376962
H	2.062487	-2.431756	0.485006
H	0.501553	-4.015461	1.508888
H	1.177752	-1.997939	2.728609
Si	0.627593	0.039951	-2.869038
H	-0.030097	-0.890152	-3.847215
H	1.978569	-0.499707	-2.500451
H	0.776455	1.397111	-3.488416
Ti	-1.091023	-0.166209	0.091147
O	-2.903010	-0.242876	-0.232034
C	-3.560859	-0.690553	-1.432302
O	-3.600722	2.574462	1.394031
O	-4.639874	1.686051	0.798866
H	-4.184384	3.328251	1.631043
H	-4.032695	0.944139	0.518903
H	-4.220567	-1.543117	-1.191738
H	-4.168957	0.138139	-1.839531
H	-2.829472	-1.003670	-2.199214

84) Figure 4.23, TS, R=CF_3

O	-0.625044	1.106797	1.311599
O	-0.258833	0.306704	-1.463152
O	-0.392886	-1.740389	0.618040
Si	0.241451	2.550487	1.540218
H	1.707359	2.241764	1.462849
H	-0.100336	3.083616	2.891649
H	-0.129229	3.526502	0.465312
Si	0.863084	-2.566499	1.376962
H	2.085144	-2.493387	0.510897
H	0.445998	-3.993520	1.553420
H	1.147847	-1.941196	2.708786
Si	0.627593	0.039951	-2.869038
H	-0.110489	-0.907268	-3.757474
H	1.967694	-0.525490	-2.500585
H	0.804838	1.366470	-3.543858
Ti	-1.029570	-0.144654	0.082060
O	-2.899018	-0.212329	-0.265200
C	-3.573493	-0.755602	-1.292902
O	-3.630271	2.759118	1.521456
O	-4.640681	1.830034	0.959193
H	-4.247956	3.447253	1.850172
H	-4.027030	1.158975	0.569429
F	-4.310175	-1.833823	-0.904006
F	-4.429323	0.141973	-1.852395
F	-2.741150	-1.197138	-2.294587

85) Figure 4.23, TS, R=iBu

O	-0.633741	1.144423	1.242550
O	-0.327158	0.172074	-1.505627
O	-0.444068	-1.758278	0.693525
Si	0.241450	2.550487	1.540217
H	1.706092	2.220272	1.507130
H	-0.121630	3.069458	2.896734
H	-0.051435	3.584836	0.495577
Si	0.863084	-2.566498	1.376961
H	2.062486	-2.431756	0.485006
H	0.501552	-4.015460	1.508888
H	1.177752	-1.997938	2.728609
Si	0.627592	0.039951	-2.869038
H	-0.030097	-0.890151	-3.847214
H	1.978569	-0.499707	-2.500451
H	0.776454	1.397111	-3.488415
Ti	-1.091022	-0.166208	0.091146
O	-3.070403	-0.112125	-0.251418
C	-3.188347	-0.891449	-1.273026
O	-3.600722	2.574461	1.394031
O	-4.639873	1.686051	0.798865
H	-4.184383	3.328250	1.631042
H	-4.032694	0.944139	0.518903
C	-4.257020	-1.783642	-1.180231
H	-3.212088	-0.402901	-2.088135
H	-2.403646	-1.425337	-1.266529
C	-5.505233	-1.200632	-1.462997
H	-4.822727	-3.573200	-1.406598
H	-5.450337	-1.226242	-0.878704

```
C  -3.988794 -2.788961 -2.104547
H  -4.260307 -2.171000 -0.315427
H  -3.966708 -2.420843 -2.978260
H  -4.668488 -3.455469 -2.057069
H  -3.149227 -3.179917 -1.901983
H  -5.498205 -0.853861 -2.330168
H  -5.691146 -0.519949 -0.833082
H  -6.196068 -1.879226 -1.397854
```

86) Figure 4.23, Product, R=H

87) Figure 4.23, Product, R=CH_3

87) Figure 4.23, Product, R=CF_3

```
O  -0.689148  1.214509  1.156080
Si  0.236970  2.568710  1.555785
H   1.686553  2.188235  1.577346
H  -0.196203  3.037971  2.908883
H   0.001047  3.641040  0.535329
Si  0.879418 -2.563819  1.318278
H   1.957797 -2.448922  0.283720
H   0.509402 -4.002169  1.518998
H   1.353034 -1.975705  2.613863
Si  0.625823  0.038344 -2.866475
H  -0.106080 -0.920620 -3.753323
H   2.044429 -0.417777 -2.697503
H   0.594110  1.422772 -3.433636
O  -0.504918 -1.759188  0.793813
Ti -1.115491 -0.171273  0.100816
O  -0.060356  0.054366 -1.325229
O  -2.839504 -0.027930 -0.821743
C  -3.322407  0.429396 -1.975091
O  -2.700707 -0.837942  1.686816
O  -4.141306 -0.748876  1.424128
H  -4.095684 -0.464386  0.466879
H  -2.555489 -1.813580  1.738707
F  -2.354434  0.813752 -2.872710
F  -4.134386  1.519008 -1.790159
F  -4.082285 -0.522472 -2.606742
```

88) Figure 4.24, left

```
See (78)
```

88) Figure 4.24, left

```
O  -0.775032  1.315173  1.094718
Si  0.238539  2.572520  1.553428
H   1.663657  2.100072  1.568007
H  -0.143560  3.046233  2.921755
H   0.100753  3.702861  0.575303
Si  0.863278 -2.563563  1.347628
H   1.933007 -2.542008  0.294983
H   0.499045 -3.984242  1.660563
H   1.380910 -1.899775  2.590835
Si  0.630309  0.014981 -2.852915
H  -0.138715 -0.857566 -3.802058
H   2.018489 -0.530073 -2.696531
H   0.699468  1.406780 -3.409017
O  -0.518808 -1.767938  0.818838
Ti -1.150901 -0.168697  0.115900
O  -0.116464  0.054722 -1.358519
O  -2.817423 -0.181505 -0.743592
C  -3.199219  0.240255 -2.066422
O  -2.667369 -0.722723  1.852130
O  -4.091974 -0.657960  1.502508
H  -3.969742 -0.428744  0.526397
H  -2.505589 -1.696247  1.909522
C  -4.087395 -0.794199 -2.785562
H  -3.584696 -1.775225 -2.679514
C  -5.493865 -0.888938 -2.167823
C  -4.167171 -0.446490 -4.286175
H  -2.283111  0.415276 -2.660380
H  -3.734853  1.207787 -1.980910
H  -4.817606 -1.162788 -4.818987
H  -3.172849 -0.475829 -4.765847
H  -4.591183  0.562896 -4.444504
H  -6.090322 -1.672467 -2.668031
H  -6.038720  0.067695 -2.279879
H  -5.459321 -1.139295 -1.093795
```

89) Figure 4.24, left

```
See (81)
```

90) Figure 4.28, left

```
See (37)
```

91) Figure 4.28, left

```
O  -0.737331  1.443002  0.776957
Si  0.241450  2.550487  1.540217
H   1.655425  2.044246  1.600990
H  -0.252070  2.797914  2.936988
```

```
H   0.219471  3.846967  0.783125
Si  0.863083 -2.566498  1.376961
H   2.041214 -3.010278  0.558773
H  -0.200785 -3.625787  1.326754
H   1.303835 -2.383071  2.799136
Si  0.627593  0.039950 -2.869037
H   0.210608 -0.801837 -4.048636
H   1.902949 -0.525572 -2.312807
H   0.889147  1.434030 -3.365707
O   0.290705 -1.121345  0.759273
Ti -1.099209 -0.177928  0.045258
O  -0.622241  0.035626 -1.771248
O  -2.993536  0.683723 -0.790630
H  -2.953345  0.629692 -1.768084
O  -2.439442 -0.843164  1.330991
O  -3.759858 -1.253632  0.798321
H  -3.726441  0.103961 -0.453014
H  -4.285680 -1.195930  1.628335
O  -1.858494 -2.178759 -0.934970
H  -2.712277 -2.455960 -0.530291
H  -1.998323 -2.064513 -1.897519
```

92) Figure 5.1 (a)

```
See (62)
```

93) Figure 5.1 (b)

```
See (38)
```

94) Figure 5.2 (a) R=H

```
See (37)
```

95) Figure 5.2 (a) R=CH_3

```
See (38)
```

96) Figure 5.2 (a) R=CH_2F

```
O  -0.035649 -0.578448 -1.567571
O  -0.503954 -1.564348  1.095869
Si  0.628039  0.051380 -2.966541
H   1.524354  1.208620 -2.622724
H  -0.444281  0.526728 -3.901259
H   1.446105 -1.007919 -3.643097
Si  0.251570  2.460985  1.577543
H   1.510457  1.919639  2.185764
H  -0.693775  2.895850  2.658054
H   0.586897  3.635569  0.705189
Si  0.852518 -2.488427  1.437139
H   0.507034 -3.411010  2.568035
H   1.998025 -1.609327  1.845833
H   1.246471 -3.295054  0.234849
Ti -1.046536 -0.279985 -0.074355
O  -0.489670  1.286186  0.647537
O  -2.947009 -0.233240  0.292692
O  -2.863691 -1.482257 -0.510089
H  -2.880622 -2.167520  0.204810
O  -2.335511  1.314539 -1.800263
C  -1.998478  2.673088 -1.888797
H  -1.825788  3.130975 -0.897601
H  -1.106631  2.739931 -2.532325
H  -3.088453  1.199840 -1.169896
F  -3.032487  3.397239 -2.498692
```

97) Figure 5.2 (a) R=CF_3

```
See (39)
```

98) Figure 5.2 (a) R=iBu

99) Figure 5.2 (a) R=tBu

See (40)

O	-0.595679	1.547585	0.474121
Si	0.216492	2.552254	1.550217
H	1.620949	2.060781	1.741241
H	-0.490552	2.579995	2.872821
H	0.243911	3.932613	0.967158
Si	0.838125	-2.564731	1.386961
H	1.918396	-2.725280	0.356919
H	-0.045933	-3.783504	1.358417
H	1.456839	-2.454977	2.748773
Si	0.602634	0.041718	-2.859037
H	0.319361	-0.765166	-4.094547
H	2.032243	-0.184520	-2.457999
H	0.413054	1.496263	-3.179818
O	-0.082040	-1.205698	1.095911
Ti	-1.158995	-0.125251	0.053264
O	-0.432569	-0.444753	-1.638350
O	-3.046978	0.401843	-1.120983
C	-3.822257	-0.034684	-2.307205
O	-2.679218	-0.116615	1.319407
O	-2.771665	-1.518083	0.829045
H	-3.636424	0.388858	-0.325978
H	-2.296938	-1.996253	1.555251
C	-3.831918	-1.571037	-2.380725
C	-3.125160	0.582478	-3.523614
C	-5.245875	0.524566	-2.142513
H	-4.323241	-2.009314	-1.495272
H	-2.801998	-1.959606	-2.437864
H	-4.380855	-1.903177	-3.280059
H	-2.122812	0.147026	-3.656903
H	-3.022379	1.672823	-3.395879
H	-3.710557	0.385653	-4.438418
H	-5.859786	0.276880	-3.025469
H	-5.225435	1.622348	-2.032408
H	-5.746601	0.089043	-1.257881

100) Figure 5.2 (a) R=SiH_3

O	0.067282	-1.351781	-0.648058
O	2.232274	-0.318272	0.867317
Si	-0.943510	-1.945066	-1.835093
H	-1.248424	-0.859236	-2.828005
H	-2.228721	-2.463266	-1.260998
H	-0.243819	-3.064521	-2.552240
Si	0.085272	2.936176	-0.526773
H	1.342358	3.060608	-1.337215
H	0.031397	4.031756	0.496476
H	-1.099676	3.052749	-1.438510
Si	3.613899	-0.556227	-0.047756
H	4.802079	-0.481181	0.864744
H	3.739246	0.505801	-1.101082
H	3.582584	-1.904996	-0.706677
Ti	0.403486	-0.247016	0.777240
O	0.055407	1.452202	0.242821
O	0.071000	-0.266518	2.704733
O	0.366209	-1.705216	2.486193
H	1.316662	-1.745798	2.763621
O	-1.976309	-0.423679	1.112144
S	-3.203782	0.504252	0.381205

101) Figure 5.2 (a) R=GeH_3

See (41)

```
H  -2.932306  1.972988  0.495656
H  -4.511633  0.184595  1.037183
H  -3.208487  0.089311 -1.050595
H  -1.861751 -0.326070  2.088305
```

102) Figure 5.2 (a) R=SnH_3

```
O   0.008567 -0.496726 -1.523909
O  -0.480753 -1.556600  1.029717
S   0.628038  0.051381 -2.966540
H   1.526248  1.232121 -2.714524
H  -0.452003  0.466794 -3.923737
H   1.446259 -1.035016 -3.604036
Si  0.251570  2.460985  1.577542
H   1.476880  1.846704  2.188848
H  -0.611564  3.049952  2.654061
H   0.679464  3.557047  0.644268
Si  0.852518 -2.488427  1.437139
H   0.458445 -3.439387  2.528607
H   1.967720 -1.614848  1.934824
H   1.333515 -3.273947  0.251236
Ti -1.119868 -0.236700 -0.090334
O  -0.611166  1.318745  0.720559
O  -3.007343 -0.476987  0.360720
O  -2.819931 -1.625838 -0.561388
H  -2.687733 -2.363579  0.085730
O  -2.279097  1.094000 -1.578707
Si -1.967282  3.108302 -1.901047
H  -1.858006  3.937489 -0.369749
H  -3.358991  3.635641 -2.822760
H  -0.489779  3.157167 -2.818808
H  -3.171243  0.918502 -1.195168
```

103) Figure 5.2 (b) R=H

See (61)

104) Figure 5.2 (b) R=CH_3

See(62)

105) Figure 5.2 (b) R=CH_2F

```
O  -0.740333  1.550076  0.621624
Si  0.241451  2.550487  1.540217
H   1.637057  2.002097  1.609485
H  -0.309463  2.684758  2.930043
H   0.270609  3.902958  0.891135
Si  0.863084 -2.566498  1.376961
H   2.020292 -2.966157  0.509509
H  -0.216298 -3.600715  1.282232
H   1.331405 -2.438044  2.795965
Si  0.627592  0.039950 -2.869037
H   0.315016 -0.715856 -4.125219
H   1.984874 -0.354396 -2.361768
H   0.635548  1.512500 -3.173831
O   0.276771 -1.075663  0.863546
Ti -1.041025 -0.145744  0.021797
O  -0.549965 -0.302292 -1.732717
O  -2.984601  0.549496 -0.771944
C  -3.369558  1.136282 -1.989961
O  -2.293406 -1.298740  0.987441
O  -3.736274 -1.357092  0.675790
H  -3.677776 -0.068953 -0.375844
H  -4.104546 -1.213365  1.578482
H  -4.312829  1.697253 -1.862308
F  -3.598217  0.169882 -2.970751
```

```
H  -2.539470  1.779209 -2.318598
```

106) Figure 5.2 (b) R=CF_3

See (63)

107) Figure 5.2 (b) R=iBu

See (64)

108) Figure 5.2 (b) R=SiH_3

```
O  -0.749337  1.526658  0.653680
S   0.216492  2.552254  1.550217
H   1.613379  2.009005  1.646225
H  -0.348482  2.719084  2.931310
H   0.250741  3.888371  0.868753
Si  0.838125 -2.564731  1.386961
H   2.020102 -2.974243  0.557054
H  -0.232444 -3.606613  1.279794
H   1.270587 -2.423977  2.816583
Si  0.602634  0.041718 -2.859037
H   0.275377 -0.676058 -4.134864
H   1.932654 -0.427191 -2.345724
H   0.676987  1.516783 -3.132359
O   0.280954 -1.081609  0.828695
Ti -1.065716 -0.148944  0.028427
O  -0.620178 -0.274528 -1.754965
O  -3.007484  0.544826 -0.672693
Si -3.426270  1.073367 -2.242234
O  -2.248039 -1.369560  1.011873
O  -3.702991 -1.415410  0.745994
H  -3.643960 -0.087986 -0.204460
H  -4.043797 -1.285064  1.661660
H  -4.723291  1.819712 -2.132211
H  -3.600527 -0.094737 -3.160054
H  -2.337293  1.981296 -2.696893
```

109) Figure 5.2 (b) R=GeH_3

See (65)

110) Figure 5.2 (b) R=SnH_3

```
O  -0.587048  1.354367  0.724478
S   0.241451  2.550487  1.540217
H   1.696238  2.194146  1.643427
H  -0.332964  2.706482  2.918694
H   0.104146  3.845936  0.795515
Si  0.863084 -2.566498  1.376961
H   2.120513 -3.057884  0.722568
H  -0.076445 -3.716002  1.584100
H   1.204871 -1.957492  2.705469
Si  0.627592  0.039950 -2.869037
H   0.310087 -0.555455 -4.211488
H   1.719408 -0.746773 -2.214784
H   1.083045  1.455307 -3.070901
O   0.158434 -1.400272  0.394767
Ti -1.130221 -0.183571 -0.059705
O  -0.780067  0.002534 -1.949204
O  -2.930941  0.472571 -0.851014
Si -3.070447  0.585662 -2.933920
O  -2.319426 -1.213742  1.063967
O  -3.776185 -1.078497  1.015556
H  -3.707538  0.115339 -0.344459
H  -3.956854 -0.783218  1.936813
H  -4.809740  0.888427 -2.930810
```

111) Figure 5.3 (a)

See (63)

```
H  -2.774726 -0.920728 -3.763876
H  -2.230997  1.996131 -3.518507
```

112) Figure 5.3 (b)

See (62)

113) Figure 5.5 ethene

```
C  -2.24496  -2.95071  0.33800
C  -2.88991  -2.06466 -0.43751
H  -3.70710  -1.44306 -0.04820
H  -2.62406  -1.92842 -1.49492
H  -2.50548  -3.08838  1.39592
H  -1.42807  -3.56980 -0.05694
```

114) Figure 5.5 propene

```
C  -3.960993  2.011619 -0.051185
C  -2.519669  2.294390 -0.438961
C  -1.766484  3.276814  0.086027
H  -4.058718  1.896283  1.042650
H  -4.630323  2.836107 -0.358033
H  -4.330964  1.087673 -0.525675
H  -2.069978  1.632510 -1.195076H
-0.722713  3.424500 -0.217056
H  -2.172825  3.969671  0.836798
```

115) Figure 5.5 η^1-peroxo

See (61)

116) Figure 5.5 η^2-peroxo

See (37)

117) Figure 5.9 (a)

```
O  -0.008230  1.736132  1.086584
Si  1.114815  2.774840  1.776416
H   2.484561  2.161525  1.746479
H   0.717198  3.048421  3.197071
H   1.128147  4.061193  1.005283
Si  1.736447 -2.342146  1.613161
H   2.902115 -2.666797  0.723961
H   0.710775 -3.428937  1.507790
H   2.213907 -2.221821  3.029447
Si  1.500957  0.264303 -2.632839
H   1.089111 -0.510692 -3.851423
H   2.839388 -0.226709 -2.162333
H   1.611555  1.717335 -2.996214
O   1.091551 -0.872483  1.116471
Ti -0.217407  0.107181  0.316803
O   0.325271  0.064659 -1.458788
O  -2.077523  0.724643 -0.645059
H  -1.962475  0.494808 -1.591952
O  -1.467629 -1.095470  1.226806
O  -2.914642 -1.090161  0.930518
H  -2.762358  0.104320 -0.243749
H  -3.271140 -0.802605  1.803279
C  -5.455191 -1.949346  0.265626
C  -5.632649 -0.671518 -0.110541
H  -6.063445  0.079796  0.563883
H  -5.349779 -0.323692 -1.113114
H  -5.721164 -2.303340  1.270176
H  -4.993315 -2.687399 -0.401641
```

118) Figure 5.10 (b)

```
O  -0.012588  1.632954  1.263306
Si  1.114815  2.774840  1.776416
```

119) Figure 5.11, far left, R=H

See (61)

```
H   2.499931  2.197654  1.734559
H   0.776092  3.152509  3.187127
H   1.055075  3.989133  0.900432
Si  1.736447 -2.342146  1.613161
H   3.047861 -2.469130  0.893427
H   1.052479 -3.682510  1.608872
H   1.990881 -1.945333  3.039917
Si  1.500957  0.264303 -2.632839
H   0.822317 -0.601260 -3.653659
H   2.785881 -0.383605 -2.206361
H   1.794863  1.607678 -3.234308
O   0.773940 -1.227231  0.848031
Ti -0.319580  0.143056  0.269457
O   0.500350  0.499018 -1.314910
O  -2.056631  0.130959 -0.475127
H  -2.061987  0.532291 -1.371108
O  -1.812848 -0.975708  1.743980
O  -4.610262 -0.736658  0.505605
H  -3.766554 -0.408531  0.097488
H  -4.616599 -0.289249  1.375287
C  -2.106788 -2.366312  1.353227
C  -1.673006 -2.041626  2.728246
H  -0.644530 -2.259083  3.040437
H  -2.418520 -1.986768  3.530338
H  -1.366617 -2.792336  0.664634
H  -3.166155 -2.513353  1.112013
```

120) Figure 5.11, far left, R=CH_3

See (62)

121) Figure 5.11, far left, R=CH_2F

See (105)

122) Figure 5.11, 2nd left, R=H

```
O   0.078678  1.742804  0.959608
Si  1.114815  2.774840  1.776416
H   2.499965  2.197220  1.823697
H   0.614319  2.985765  3.175979
H   1.148375  4.090717  1.058063
Si  1.736447 -2.342146  1.613161
H   2.965213 -2.707736  0.830530
H   0.709847 -3.416372  1.442230
H   2.103194 -2.201873  3.060230
Si  1.500957  0.264303 -2.632839
H   1.184353 -0.445909 -3.917043
H   2.820783 -0.221232 -2.105960
H   1.599240  1.738483 -2.906176
O   1.154537 -0.875482  1.035368
Ti -0.176987  0.091683  0.249757
O   0.261705 -0.034845 -1.549981
O  -2.056315  0.782019 -0.652892
H  -1.963097  0.522254 -1.595238
O  -1.409023 -1.106091  1.158778
O  -2.862408 -1.068775  0.916839
H  -2.747196  0.187587 -0.231415
H  -3.177128 -0.882963  1.831778
C  -1.748289 -4.070467  3.216140
C  -2.093411 -3.154335  4.133260
H  -1.390817 -2.817671  4.905846
H  -3.094317 -2.703116  4.148229
```

123) Figure 5.11, 2nd left, R=CH_3

```
O   0.124110  1.754456  0.883614
Si  1.114815  2.774840  1.776416
H   2.504179  2.211119  1.854044
H   0.567239  2.950208  3.162244
H   1.159508  4.110384  1.093279
Si  1.736447 -2.342146  1.613161
H   2.973037 -2.703221  0.843154
H   0.710849 -3.416331  1.426982
H   2.082722 -2.217491  3.067650
Si  1.500957  0.264303 -2.632839
H   1.172456 -0.434291 -3.921049
H   2.843412 -0.208253 -2.150238
H   1.574111  1.743036 -2.891203
O   1.167068 -0.865277  1.057538
Ti -0.168926  0.074172  0.242058
O   0.311787 -0.079373 -1.521983
O  -2.096517  0.768674 -0.627562
C  -2.521616  0.756688 -2.013315
O  -1.394834 -1.062330  1.215339
O  -2.842020 -1.074983  0.971392
H  -2.761549  0.262521 -0.080400
H  -3.161335 -0.952048  1.893720
C  -1.758122 -4.086058  3.248310
C  -2.127499 -3.175741  4.162086
H  -1.428599 -2.804341  4.923001
H  -3.144806 -2.761912  4.186183
```

H	-0.748124	-4.520900	3.204668
H	-2.440334	-4.393447	2.428832

H	-0.740853	-4.496111	3.226964
H	-2.445261	-4.442329	2.470013
H	-1.622183	0.724598	-2.644445
H	-3.096812	1.675003	-2.225757
H	-3.136177	-0.135858	-2.227139

124) Figure 5.11, 2nd left, R=CH_2F

O	0.143400	1.762530	0.854267
Si	1.114815	2.774840	1.776416
H	2.504704	2.217573	1.879546
H	0.535407	2.926788	3.152548
H	1.163031	4.116981	1.109549
Si	1.736447	-2.342146	1.613161
H	2.989328	-2.700417	0.867779
H	0.711575	-3.411795	1.400491
H	2.053247	-2.217569	3.073607
Si	1.500957	0.264303	-2.632839
H	1.184112	-0.413900	-3.933580
H	2.832971	-0.214983	-2.131695
H	1.575173	1.747725	-2.868236
O	1.172410	-0.866393	1.038728
Ti	-0.163173	0.076375	0.236620
O	0.282161	-0.080484	-1.545429
O	-2.103494	0.739223	-0.622017
C	-2.517703	0.808854	-1.972403
O	-1.395645	-1.021760	1.252974
O	-2.852945	-1.001764	1.037750
H	-2.801576	0.283736	-0.053532
H	-3.147507	-0.943607	1.975837
C	-1.790545	-4.094006	3.281706
C	-2.172259	-3.198182	4.205562
H	-1.473147	-2.813426	4.958388
H	-3.201118	-2.817203	4.247744
H	-0.763438	-4.476732	3.245322
H	-2.480682	-4.468677	2.516073
H	-1.608067	0.919826	-2.579464
H	-3.239008	1.634692	-2.107763
F	-3.164644	-0.368446	-2.345870

125) Figure 5.11, 2nd right, R=H

See (118)

126) Figure 5.11, 2nd right, R=CH_3

O	0.119478	1.459640	1.446277
Si	1.114815	2.774840	1.776416
H	2.557126	2.366182	1.705723
H	0.809332	3.272667	3.156890
H	0.860960	3.871068	0.782808
Si	1.736447	-2.342146	1.613161
H	3.088430	-2.408191	0.965592
H	1.206926	-3.739325	1.778407
H	1.880915	-1.725386	2.976800
Si	1.500957	0.264303	-2.632839
H	0.651145	-0.561879	-3.553997
H	2.762048	-0.486533	-2.317497
H	1.846740	1.557243	-3.310027
O	0.679501	-1.468664	0.663926
Ti	-0.236259	0.098091	0.278634
O	0.676269	0.606528	-1.216589
O	-1.908235	0.098777	-0.546896

127) Figure 5.11, 2nd right, R=CH_2F

O	0.186909	1.403388	1.468594
Si	1.114815	2.774840	1.776416
H	2.571850	2.422334	1.721902
H	0.772720	3.275459	3.146312
H	0.818137	3.838902	0.761571
Si	1.736447	-2.342146	1.613161
H	3.055711	-2.357735	0.898893
H	1.271230	-3.753656	1.824057
H	1.913473	-1.687982	2.955092
Si	1.500957	0.264303	-2.632839
H	0.636418	-0.524195	-3.567767
H	2.764414	-0.492879	-2.345503
H	1.840164	1.585848	-3.254221
O	0.594435	-1.527489	0.702800
Ti	-0.243124	0.071370	0.307242
O	0.681292	0.541252	-1.190072
O	-1.947950	0.208061	-0.527615

```
C  -2.321445  0.458013 -1.870854
O  -1.750900 -0.800350  1.868546
O  -4.588198 -0.521260  0.351666
H  -3.650506 -0.310141  0.110017
H  -4.775568  0.091177  1.090520
C  -2.218269 -2.165916  1.592624
C  -1.632491 -1.818420  2.905409
H  -0.607802 -2.130631  3.141161
H  -2.287941 -1.637098  3.765442
H  -1.590544 -2.702133  0.870525
H  -3.303875 -2.221136  1.452014
H  -1.450255  0.683824 -2.511321
H  -2.977654  1.347027 -1.826444
H  -2.893492 -0.378682 -2.313937
```

128) Figure 5.11, far right, R=H

See (7)

```
C  -2.278848  0.488012 -1.846923
O  -1.778980 -0.713637  1.866527
O  -4.630645 -0.332243  0.541334
H  -3.697026 -0.178442  0.252606
H  -4.806244  0.400141  1.164439
C  -2.284847 -2.084956  1.690741
C  -1.629926 -1.675816  2.952641
H  -0.599208 -1.990602  3.154950
H  -2.239871 -1.431029  3.829780
H  -1.703698 -2.675519  0.972759
H  -3.376983 -2.120894  1.610956
H  -1.455080  1.006887 -2.372105
H  -3.221013  1.068046 -1.878390
F  -2.518781 -0.707587 -2.554058
```

129) Figure 5.11, far right, R=CH_3

See (23)

130) Figure 5.11, far right, R=CH_2F

```
O  -0.848442  1.374348  1.171589
O  -0.384173  0.292997 -1.496636
O  -0.288098 -1.544471  0.821253
Si  0.232824  2.608123  1.510558
H   1.646865  2.109262  1.414077
H  -0.025967  3.101335  2.902100
H   0.042291  3.730829  0.532818
Si  0.887885 -2.631632  1.316373
H   2.070589 -2.546984  0.396811
H   0.312727 -4.014984  1.270007
H   1.318339 -2.306730  2.715706
Si  0.621501  0.066744 -2.819344
H  -0.033696 -0.879154 -3.780616
H   1.936321 -0.497503 -2.369906
H   0.840542  1.393811 -3.481734
Ti -1.097128 -0.087112  0.117151
O  -2.887032 -0.347494 -0.163772
C  -3.767213 -0.022710 -1.191372
F  -4.412631 -1.179942 -1.647703
H  -4.551251  0.656903 -0.807196
H  -3.234463  0.412010 -2.060353
```

131) Figure 5.11, far right, ethene oxide

132) Figure 5.11, far right, water

```
O   0.000000  0.053077  2.080000
H   0.771850  0.653023  2.080002
H  -0.771850  0.653023  2.079998
```

132) Figure 5.11, far right, ethene oxide

```
O   0.235894  1.706125  0.620618
C  -0.076048  0.342716  0.235339
C   0.345703  0.668686  1.618532
H   1.372332  0.432914  1.934726
H  -0.403465  0.697406  2.423035
H   0.646166 -0.115283 -0.455140
H  -1.136238  0.154992  0.011675
```

133) Figure 5.13, right

```
O  -0.320049 -1.446949 -0.613831
O   1.800588 -0.308321  0.927046
Si -1.392082 -1.861317 -1.816095
H  -1.627555 -0.690524 -2.734356
```

134) Figure 5.16, right

```
O  -0.774184 -1.168863 -1.351130
O   1.850479 -0.306973 -0.145654
Si -1.235231 -2.355309 -2.439534
H  -1.379470 -1.735489 -3.799247
```

```
H  -2.719529 -2.282893 -1.253933
H  -0.830540 -2.992772 -2.625394
Si -0.363300  3.019925 -0.507775
H   0.798763  3.455248 -1.348175
H  -0.384911  3.816625  0.765107
H  -1.635291  3.285901 -1.262802
Si  3.165327 -0.472478 -0.028758
H   4.367714 -0.323374  0.857332
H   3.215661  0.571478 -1.104081
H   3.196750 -1.836549 -0.659695
Ti -0.033768 -0.193985  0.713537
O  -0.259499  1.387089 -0.178720
O  -0.556075  0.358603  2.474835
O   0.145280 -2.157625  2.058204
H   1.128782 -2.121688  2.058709
O  -2.445983 -0.248909  0.856834
H  -2.308173  0.246308  1.704147
H  -2.861412  0.380023  0.231065
C  -0.328825 -1.839286  3.391431
C  -0.126792 -0.336527  3.632907
H  -0.713260 -0.012077  4.516060
H   0.943060 -0.110978  3.829918
H  -1.401576 -2.090217  3.374020
H   0.175282 -2.468596  4.149792
```

```
H  -2.555092 -2.918825 -2.004799
H  -0.214370 -3.452023 -2.501763
Si -0.762553  2.908255 -1.041129
H   0.336430  3.110580 -2.046231
H  -0.817713  4.099450 -0.131502
H  -2.072604  2.774225 -1.759790
Si  3.322654 -0.887461 -0.694524
H   4.407173 -0.512610  0.271803
H   3.630779 -0.293685 -2.038317
H   3.260310 -2.381255 -0.824881
Ti  0.032869 -0.216256 -0.036109
O  -0.467992  1.546874 -0.106579
O  -0.313488  0.470418  3.972484
O  -0.526971 -0.869304  1.543826
H  -0.378121 -0.480035  2.454323
C   0.059427  1.867659  3.757104
C  -1.353987  1.485994  3.980498
H  -1.812541  1.652547  4.963716
H  -2.041851  1.448120  3.125951
H   0.644410  2.298313  4.579581
H   0.399997  2.097126  2.739193
```

135) Figure 5.20, (b)

```
O  -0.094908  1.359372  1.074391
Si  0.806851  2.695841  1.533738
H   2.259343  2.331891  1.646914
H   0.313206  3.175153  2.866807
H   0.651170  3.794851  0.524155
Si  1.469623 -2.436400  1.352500
H   2.746187 -3.081077  0.900697
H   0.368846 -3.467498  1.244862
H   1.589299 -2.050053  2.799370
Si  1.154156  0.112050 -2.861004
H   0.741515 -0.646924 -4.089326
H   2.384964 -0.516338 -2.278140
H   1.455470  1.530761 -3.248713
O   1.116466 -1.121091  0.403215
Ti -0.401290 -0.123974  0.057876
O  -0.115480  0.096350 -1.759423
O  -2.448203  0.588867 -0.452227
H  -2.570463  0.477573 -1.418347
O  -1.541180 -1.430504  0.813047
O  -4.561449 -0.570807  0.989661
H  -3.159572  0.040733  0.001848
H  -1.100056 -2.267963  1.081634
C  -4.460664 -1.715321  1.890966
C  -4.319903 -0.335959  2.408852
H  -3.554357 -2.313592  1.745822
H  -3.316098  0.037828  2.644463
H  -5.159026  0.137973  2.933759
H  -5.406958 -2.253736  2.032807
```

136) isolated H_2O_2

```
O  -3.625504  2.548667  1.704907
O  -4.499653  1.908839  0.700157
H  -2.789218  2.056597  1.535067
H  -5.132557  1.450114  1.299826
```